

HYDRAULIC FRACTURING INDUCED CONTAMINANT PATHWAYS IN
GROUNDWATER

A Thesis

Presented to

the Faculty of the Department of Environmental Engineering

University of Houston

In Partial Fulfillment

of the Requirements for the Degree

Master of Science

In Environmental Engineering

By

Taylor Burton

May 2015

HYDRAULIC FRACTURING INDUCED CONTAMINANT PATHWAYS IN
GROUNDWATER

Taylor Burton

Approved:

Dr. Hanadi Rifai, Professor & Chair
Civil and Environmental Engineering
University of Houston

Committee Members:

Dr. Bill Rixey, Associate Professor
Civil and Environmental Engineering
University of Houston

Dr. Thomas Holley, Professor &
Director
Petroleum Engineering,
University of Houston

Dr. Kevin Schug, Associate Professor
Department of Chemistry & Biochemistry
University of Texas Arlington

Dr. Suresh K. Khator, Associate Dean,
Cullen College of Engineering

Dr. Hanadi Rifai, Director,
Environmental Engineering Graduate
Program

ACKNOWLEDGEMENTS

I would like to thank my thesis advisor Dr. Rifai who has supported me throughout my time at UH and encouraged me to write this master's thesis. When I was considering a non-thesis degree plan, she propelled me to achieve new heights and I have learned so much throughout this entire process! Also, I would like to thank Dr. Rixey and Dr. Holley who have both taken time to help me in the development of the research methods in this thesis. Many thanks to Dr. Schug and the UTA research team who shared their data sets for use in this work. Thanks to everyone in the Rifai Lab: Dan, Amin, Aparna, Emily, Rose, and Maria. The final result of this research would not be what it is without the input and support of this team. Thanks to my family, friends, and church community for their encouragement and prayers.

HYDRAULIC FRACTURING INDUCED CONTAMINANT PATHWAYS IN
GROUNDWATER

An Abstract

of a

Thesis

Presented to

the Faculty of the Department of Environmental Engineering

University of Houston

In Partial Fulfillment

of the Requirements for the Degree

Master of Science

In Environmental Engineering

By

Taylor Burton

May 2015

ABSTRACT

Hydraulic fracturing in areas of natural gas production has been viewed as the cause of several environmental issues; notably among them is groundwater contamination. Proponents of hydraulic fracturing argue the improbability of induced contaminant pathways in groundwater since gas well annuli are sealed and the reservoirs lay thousands of feet below the water table, but opponents have cited a change in ground water quality over time. An ArcGIS model is created in this thesis to analyze groundwater quality data with respect to the relative proximity of gas wells, knowledge of the reservoir pressure gradient, gas well characteristics and fracture treatment data in order to explore the relationships, if any, between groundwater quality changes and hydraulic fracturing operations. Results indicate that elevated concentrations of certain groundwater constituents are related to natural gas production in the study area.

TABLE OF CONTENTS

	ACKNOWLEDGEMENTS.....	iv
	ABSTRACT.....	vi
	TABLE OF CONTENTS.....	vii
	LIST OF FIGURES.....	ix
	LIST OF TABLES.....	xxiii
1	INTRODUCTION	1
2	BACKGROUND	5
3	STUDY AREA & DATA DESCRIPTIONS.....	15
	3.1 THE BARNETT SHALE	15
	3.2 THE TRINITY AQUIFER	23
	3.3 DATA SET DESCRIPTIONS.....	32
	3.3.1 GAS WELL LOCATIONS.....	32
	3.3.2 GAS WELL BOTTOM HOLE PRESSURES	33
	3.3.3 WELL DESIGN AND HYDRAULIC FRACTURING TREATMENT DATA	36
	3.3.4 GROUNDWATER DATA	37
	3.4 PRELIMINARY DATA ANALYSIS	45
	3.4.1 BOTTOM HOLE PRESSURE DATA	45
	3.4.2 GROUNDWATER DATA	52
4	METHODS.....	64
	4.1 VISUAL CORRELATIONS OF GROUNDWATER CHANGE	64
	4.1.1 CONTOURING CONStituent CHANGES	66

4.2	NONPARAMETRIC TEST FOR EVALUATING GROUNDWATER QUALITY	70
4.3	MODEL ANALYSIS OF WATER CONSTITUENT PREDICTIONS, BOTTOM HOLE PRESSURE, AND GAS WELL DENSITY	74
4.3.1	EVALUATION OF SUBGROUP 1 VERSUS SUBGROUP 6.....	76
4.3.2	CONSTITUENT CORRELATIONS.....	78
4.4	CLUSTER ANALYSIS FOR UNDERSTANDING CONTAMINANT PATHWAYS IN HYDRAULICALLY FRACTURED WELL	78
5	<i>RESULTS.....</i>	<i>84</i>
5.1	VISUAL CORRELATIONS OF GROUNDWATER QUALITY CHANGE.	84
5.2	NONPARAMETRIC TEST FOR EVALUATING WATER QUALITY	87
5.3	MODEL ANALYSIS OF WATER CONSTITUENT PREDICTIONS, BOTTOM HOLE PRESSURE, AND GAS WELL DENSITY	91
5.3.1	MANN-WHITNEY U-TEST FOR SUBGROUP 1 and SUBGROUP 6.....	93
5.3.2	R-SQUARED VALUES between CONSTITUENTS	96
5.4	CLUSTER ANALYSIS FOR UNDERSTANDING CONTAMINANT PATHWAYS IN HYDRAULICALLY FRACTURED WELLS.....	103
6	<i>DISCUSSION & CONCLUSIONS</i>	<i>113</i>
	<i>REFERENCES.....</i>	<i>114</i>
	<i>APPENDIX A.....</i>	<i>121</i>
	<i>APPENDIX B.....</i>	<i>136</i>
	<i>APPENDIX C.....</i>	<i>152</i>
	<i>APPENDIX D.....</i>	<i>192</i>

LIST OF FIGURES

Fig. 2-1: Patterns of Defects and Pathways in a Cement Sheath (adapted from Deremble, Loizzo, Huet, Lecampion & Quesada, 2010).....12

Fig. 3-1: Stratigraphic Section of the Fort Worth Basin adapted from Jarvie, 2004 16

Fig. 3-2: The Barnett Shale Region and Major Geological Features (Bruner & Smosna, 2011)17

Fig. 3-3: Study Area as displayed in ArcGIS18

Fig. 3-4: Active Well Extraction Sites in the Barnett Shale (<https://www.tceq.texas.gov/airquality/barnettshale/bshale-maps>, 10-24-14) 19

Fig. 3-5: New Well Completions in Barnett Shale Region per Year (data sourced from Drillinginfo.com)20

Fig. 3-6: Barnett Shale Depth Profile displayed in ArcGIS22

Fig. 3-7: Extent of Trinity and Woodbine Aquifers (TWDB, 3-31-14) and Fault Line Locations (USGS, 7-29-13) displayed in ArcGIS24

Fig. 3-8: Relative lateral extent of Trinity Aquifer sandstones (adapted from Harden et al., 2004).....25

Fig. 3-9: Cross Section of Trinity Aquifer in the North-South Direction (adapted from Harden, 2004).....26

Fig. 3-10: Depth Profile of the Paluxy Sandstone and well locations with Aquifer ID references Antlers, Twin Mountains, and Paluxy.....27

Fig. 3-11: Gas Wells Color Coded to Represent Relative Thickness between the Barnett Shale and Trinity Aquifer.....28

Fig. 3-12: Shallowest and deepest Paluxy Aquifer depths shown in ArcGIS30

Fig. 3-13: Cross Section of Paluxy Aquifer Depth shallowest and deepest points.....31

Fig. 3-14: Map of Drilled Gas Well Locations 2001-201433

Fig. 3-15: Texas Railroad Commission Districts Encompassing the Barnett Shale (http://www.rrc.state.tx.us/oil-gas/major-oil-gas-formations/barnett-shale-information/countyproducing , 12-9-14).....	34
Fig. 3-16: Map of Gas Wells with recorded BHP (a total of 2056 wells shown)	35
Fig. 3-17: Map of Gas Wells with recorded Wellbore Completions Data	37
Fig. 3-18: Map of Water Well Locations from Texas Water Development Board Data Set	38
Fig. 3-19: Map of Water Well Locations from University of Texas Arlington Data Set	42
Fig. 3-20: Contour Plot of Flowing BHP Data.....	47
Fig. 3-21: Grid of Data Points to create model of RPG	50
Fig. 3-22: Map of Barnett Shale Reservoir Pressure Gradient over Study Region	51
Fig. 3-23: Water samples locations denoted by relative measurements in Dissolved Alpha (pc/L)	52
Fig. 3-24: Sample of Dissolved Alpha from 1988-2011 in Denton, Johnson, Somervell, Parker, Tarrant, and Wise counties.....	53
Fig. 3-25: Sample of Dissolved Aluminum from 1988-2011 in Denton, Johnson, Somervell, Parker, Tarrant, and Wise counties	54
Fig. 3-26: Samples of Total Arsenic from 1985-2011 in Denton, Johnson, Somervell, Parker, Tarrant, and Wise counties.....	54
Fig. 3-27: Samples of Total Barium from 1985-2011 in Denton, Johnson, Somervell, Parker, Tarrant, and Wise counties.....	55
Fig. 3-28: Samples of Total Beryllium from 1985-2011 in Denton, Johnson, Somervell, Parker, Tarrant, and Wise counties.....	55
Fig. 3-29: Samples of Dissolved Boron from 1988-2011 in Denton, Johnson, Somervell, Parker, Tarrant, and Wise counties.....	56

Fig. 3-30: Samples of Dissolved Bromide from 1988-2011 in Denton, Johnson, Somervell, Parker, Tarrant, and Wise counties	56
Fig. 3-31: Samples of Total Copper from 1988-2011 in Denton, Johnson, Somervell, Parker, Tarrant, and Wise counties	57
Fig. 3-32: Samples of Dissolved Iron from 1986-2011 in Denton, Johnson, Somervell, Parker, Tarrant, and Wise counties	57
Fig. 3-33: Samples of Dissolved Molybdenum from 1986-2011 in Denton, Johnson, Somervell, Parker, Tarrant, and Wise counties	58
Fig. 3-34: Samples of Total Nickel from 1990-2011 in Denton, Johnson, Somervell, Parker, Tarrant, and Wise counties	58
Fig. 3-35: Samples of Total Nitrate from 1990-2011 in Denton, Johnson, Somervell, Parker, Tarrant, and Wise counties	59
Fig. 3-36: Samples of Oxidation Reduction Potential from 1990-2011 in Denton, Johnson, Somervell, Parker, Tarrant, and Wise counties	59
Fig. 3-37: Samples of Dissolved Oxygen from 1988-2011 in Denton, Johnson, Somervell, Parker, Tarrant, and Wise counties	60
Fig. 3-38: Samples of Dissolved Radium 226 from 1988-2011 in Denton, Johnson, Somervell, Parker, Tarrant, and Wise counties	60
Fig. 3-39: Samples of Dissolved Radium 228 from 1988-2011 in Denton, Johnson, Somervell, Parker, Tarrant, and Wise counties	61
Fig. 3-40: Samples of Total Selenium from 1985-2011 in Denton, Johnson, Somervell, Parker, Tarrant, and Wise counties	61
Fig. 3-41: Samples of Water Temperature from 1987-2011 in Denton, Johnson, Somervell, Parker, Tarrant, and Wise counties	62
Fig. 4-1: Contours of the Reservoir Pressure Gradient in the Study Region	65
Fig. 4-2: Locations of Extraction Points.....	69

Fig. 4-3: Locations of Control Group Samples and Test Group Samples	72
Fig. 4-4: Raster of Relative Gas Well Density per raster cell.....	74
Fig. 4-5: Grid of Data Points overlaying raster cells	75
Fig. 5-1: Change in Dissolved Alpha (pc/L) in study region and gas well locations	84
Fig. 5-2: Change in Dissolved Alpha (pc/L) in study region and contour of RPG (psi/ft) .	86
Fig. 5-3: ArcGIS Cluster Analysis of Surface Casing Values.....	104
Fig. 5-4: ArcGIS Cluster Analysis of Bottom Hole Casing Values	104
Fig. 5-5: ArcGIS Cluster Analysis of Injected Fluid Values.....	105
Fig. 5-6: ArcGIS Cluster Analysis of Injected Sand Values	105
Fig. 5-7: ArcGIS Cluster Analysis of Injected Nitrogen Values	106
Fig. 5-8: ArcGIS Cluster Analysis of Total Vertical Depth Values.....	106
Fig. 5-9: ArcGIS Cluster Analysis of Lateral Length Values	107
Fig. 5-10: ArcGIS Cluster Analysis of Aquifer to Perforation Thickness Values.....	107
Fig. 5-11: ArcGIS Cluster Analysis of Azimuth Direction Values	108
Fig. 5-12: ArcGIS Cluster Analysis Number of Surrounding Gas Wells (1 Mile) Values	108
Fig. 5-13: ArcGIS Cluster Analysis of Bottom Hole Pressure	109
Fig. A- 1: Sample locations of Dissolved Alpha denoted by relative measurements in concentration (pc/L)	122
Fig. A- 2: Sample locations of Dissolved Aluminum denoted by relative measurements in concentration (ppb).....	122
Fig. A- 3: Sample locations of Total Arsenic denoted by relative measurements in concentration (ppb).....	123
Fig. A- 4: Sample locations of Total Barium denoted by relative measurements in concentration (ppb).....	123

Fig. A- 5: Sample locations of Total Benzene denoted by relative measurements in concentration (mg/L)	124
Fig. A- 6: Sample locations of Total Beryllium denoted by relative measurements in concentration (ppb)	124
Fig. A- 7: Sample locations of Dissolved Boron denoted by relative measurements in concentration (ppb)	125
Fig. A- 8: Sample locations of Total Bromide denoted by relative measurements in concentration (mg/L)	125
Fig. A- 9: Sample locations of Dissolved Bromide denoted by relative measurements in concentration (mg/L)	126
Fig. A- 10: Sample locations of Total Chloride denoted by relative measurements in concentration (mg/L)	126
Fig. A- 11: Sample locations of Total Copper denoted by relative measurements in concentration (ppb)	127
Fig. A- 12: Sample locations of Dissolved Oxygen denoted by relative measurements in concentration (mg/L)	127
Fig. A- 13: Sample locations of Total Ethanol denoted by relative measurements in concentration (mg/L)	128
Fig. A- 14: Sample locations of Total Iron denoted by relative measurements in concentration (ppb)	128
Fig. A- 15: Sample locations of Total Methanol denoted by relative measurements in concentration (mg/L)	129
Fig. A- 16: Sample locations of Dissolved Molybdenum denoted by relative measurements in concentration (ppb)	129
Fig. A- 17: Sample locations of Total Molybdenum denoted by relative measurements in concentration (ppb)	130

Fig. A- 18: Sample locations of Total Nickel denoted by relative measurements in concentration (ppb).....	130
Fig. A- 19: Sample locations of Total Nitrate denoted by relative measurements in concentration (mg/L).....	131
Fig. A- 20: Sample locations denoted by relative measurements of pH	131
Fig. A- 21: Sample locations of Dissolved Phosphorus denoted by relative measurements in concentration (mg/L)	132
Fig. A- 22: Sample locations of Dissolved Radium 226 denoted by relative measurements in concentration (pc/L)	132
Fig. A- 23: Sample locations of Dissolved Radium 228 denoted by relative measurements in concentration (pc/L)	133
Fig. A- 24: Sample locations of Total Selenium denoted by relative measurements in concentration (ppb).....	133
Fig. A- 25: Sample locations of Total Sulfate denoted by relative measurements in concentration (mg/L).....	134
Fig. A- 26: Sample locations of Total Dissolved Solids denoted by relative measurements in concentration (mg/L)	134
Fig. A- 27: Sample locations of Water Temperature denoted by relative measurements in concentration ($^{\circ}\text{C}$).....	135
Fig. A- 28: Sample locations of Dissolved Vanadium denoted by relative measurements in concentration (ppb)	135
Fig. A- 29: Sample locations of Total Zinc denoted by relative measurements in concentration (ppb).....	136
Fig. B- 1: Contour plots of Dissolved Alpha concentration in study region prior to 2001 (left) and after 2011 (right)	137

Fig. B- 2: Contour plots of Dissolved Aluminum concentration in study region prior to 2001 (left) and after 2011 (right).....	137
Fig. B- 3: Contour plots of Total Arsenic concentration in study region prior to 2001 (left) and after 2011 (right)	138
Fig. B- 4: Contour plots of Total Barium concentration in study region prior to 2001 (left) and after 2011 (right)	138
Fig. B- 5: Contour plot of Total Benzene concentration in the study region after 2011 .	139
Fig. B- 6: Contour plots of Total Beryllium concentration in study region prior to 2001 (left) and after 2011 (right)	139
Fig. B- 7: Contour plots of Dissolved Boron concentration in study region prior to 2001 (left) and after 2011 (right)	140
Fig. B- 8: Contour plots of Dissolved Bromide concentration in study region prior to 2001 (left) and after 2011 (right)	140
Fig. B- 9: Contour plot of Total Bromide concentration in the study region after 2011..	141
Fig. B- 10: Contour plot of Total Chloride concentration in the study region after 2011	141
Fig. B- 11: Contour plots of Total Copper concentration in study region prior to 2001 (left) and after 2011 (right)	142
Fig. B- 12: Contour plots of Dissolved Oxygen concentration in study region prior to 2001 (left) and after 2011 (right)	142
Fig. B- 13: Contour plot of Total Ethanol concentration in the study region after 2011 .	143
Fig. B- 14: Contour plot of Total Ethyl Benzene concentration in the study region after 2011.....	143
Fig. B- 15: Contour plots of Total Iron concentration in study region prior to 2001 (left) and after 2011 (right)	144
Fig. B- 16: Contour plot of Total Methanol concentration in the study region after 2011	144

Fig. B- 17: Contour plot of Total Molybdenum concentration in the study region after 2011.....	145
Fig. B- 18: Contour plots of Dissolved Molybdenum concentration in study region prior to 2001 (left) and after 2011 (right).....	145
Fig. B- 19: Contour plots of Total Nickel concentration in study region prior to 2001 (left) and after 2011 (right)	146
Fig. B- 20: Contour plot of Total Nitrate concentration in the study region after 2011...	146
Fig. B- 21: Contour plots of Oxidation-Reduction Potential in study region prior to 2001 (left) and after 2011 (right)	147
Fig. B- 22: Contour plot of pH in the study region after 2011	147
Fig. B- 23 Contour plots of Dissolved Phosphorus concentration in study region prior to 2001 (left) and after 2011 (right).....	148
Fig. B- 24: Contour plots of Dissolved Radium 226 concentration in study region prior to 2001 (left) and after 2011 (right).....	148
Fig. B- 25: Contour plots of Dissolved Radium 228 concentration in study region prior to 2001 (left) and after 2011 (right).....	149
Fig. B- 26: Contour plots of Total Selenium concentration in study region prior to 2001 (left) and after 2011 (right)	149
Fig. B- 27: Contour plots of Total Sulfate concentration in study region after 2011	150
Fig. B- 28: Contour plots of Total Dissolved Solids concentration in study region after 2011.....	150
Fig. B- 29: Contour plots of Water Temperature in study region prior to 2001 (left) and after 2011 (right)	151
Fig. B- 30: Contour plots of Dissolved Vanadium concentration in study region prior to 2001 (left) and after 2011 (right).....	151

Fig. B- 31: Contour plots of Total Zinc concentration in study region prior to 2001 (left) and after 2011 (right)	152
Fig. C- 1: Contour Plot of change in groundwater Dissolved Aluminum concentrations and gas well locations in the study region	153
Fig. C- 2: Contour Plot of change in groundwater Total Arsenic concentrations and gas well locations in the study region.....	154
Fig. C- 3: Contour Plot of change in groundwater Total Barium concentrations and gas well locations in the study region.....	155
Fig. C- 4: Contour Plot of change in groundwater Total Beryllium concentrations and gas well locations in the study region.....	156
Fig. C- 5: Contour Plot of change in groundwater Dissolved Boron concentrations and gas well locations in the study region.....	157
Fig. C- 6: Contour Plot of change in groundwater Dissolved Bromide concentrations and gas well locations in the study region.....	158
Fig. C- 7: Contour Plot of change in groundwater Total Copper concentrations and gas well locations in the study region.....	159
Fig. C- 8: Contour Plot of change in groundwater Dissolved Oxygen concentrations and gas well locations in the study region.....	160
Fig. C- 9: Contour Plot of change in groundwater Total Iron concentrations and gas well locations in the study region.....	161
Fig. C- 10: Contour Plot of change in groundwater Dissolved Molybdenum concentrations and gas well locations in the study region	162
Fig. C- 11: Contour Plot of change in groundwater Total Nickel concentrations and gas well locations in the study region.....	163

Fig. C- 12: Contour Plot of change in groundwater Total Nitrate concentrations and gas well locations in the study region.....	164
Fig. C- 13: Contour Plot of change in groundwater Oxidation-Reduction Potential and gas well locations in the study region.....	165
Fig. C- 14: Contour Plot of change in groundwater Dissolved Phosphorus concentrations and gas well locations in the study region	166
Fig. C- 15: Contour Plot of change in groundwater Dissolved Radium 226 concentrations and gas well locations in the study region	167
Fig. C- 16: Contour Plot of change in groundwater Dissolved Radium 228 concentrations and gas well locations in the study region	168
Fig. C- 17: Contour Plot of change in groundwater Total Selenium concentrations and gas well locations in the study region.....	169
Fig. C- 18: Contour Plot of change in groundwater Temperature and gas well locations in the study region	170
Fig. C- 19: Contour Plot of change in groundwater Dissolved Vanadium concentrations and gas well locations in the study region	171
Fig. C- 20: Contour Plot of change in groundwater Total Zinc concentrations and gas well locations in the study region.....	172
Fig. C- 21: Contour Plot of change in groundwater Total Zinc concentrations and Barnett Reservoir Pressure Gradient in the study region.....	173
Fig. C- 22: Contour Plot of change in groundwater Total Arsenic concentrations and Barnett Reservoir Pressure Gradient in the study region.....	174
Fig. C- 23: Contour Plot of change in groundwater Total Barium concentrations and Barnett Reservoir Pressure Gradient in the study region.....	175
Fig. C- 24: Contour Plot of change in groundwater Total Beryllium concentrations and Barnett Reservoir Pressure Gradient in the study region.....	176

Fig. C- 25: Contour Plot of change in groundwater Total Boron concentrations and Barnett Reservoir Pressure Gradient in the study region.....	177
Fig. C- 26: Contour Plot of change in groundwater Dissolved Bromide concentrations and Barnett Reservoir Pressure Gradient in the study region.....	178
Fig. C- 27: Contour Plot of change in groundwater Total Copper concentrations and Barnett Reservoir Pressure Gradient in the study region.....	179
Fig. C- 28: Contour Plot of change in groundwater Dissolved Oxygen concentrations and Barnett Reservoir Pressure Gradient in the study region.....	180
Fig. C- 29: Contour Plot of change in groundwater Total Iron concentrations and Barnett Reservoir Pressure Gradient in the study region.....	181
Fig. C- 30: Contour Plot of change in groundwater Dissolved Molybdenum concentrations and Barnett Reservoir Pressure Gradient in the study region...	182
Fig. C- 31: Contour Plot of change in groundwater Total Nickel concentrations and Barnett Reservoir Pressure Gradient in the study region.....	183
Fig. C- 32: Contour Plot of change in groundwater Total Nitrate concentrations and Barnett Reservoir Pressure Gradient in the study region.....	184
Fig. C- 33: Contour Plot of change in groundwater Oxidation-Reduction Potential concentrations and Barnett Reservoir Pressure Gradient in the study region...	185
Fig. C- 34: Contour Plot of change in groundwater Dissolved Phosphorus concentrations and Barnett Reservoir Pressure Gradient in the study region.....	186
Fig. C- 35: Contour Plot of change in groundwater Dissolved Radium 226 concentrations and Barnett Reservoir Pressure Gradient in the study region.....	187
Fig. C- 36: Contour Plot of change in groundwater Dissolved Radium 228 concentrations and Barnett Reservoir Pressure Gradient in the study region.....	188
Fig. C- 37: Contour Plot of change in groundwater Total Selenium concentrations and Barnett Reservoir Pressure Gradient in the study region.....	189

Fig. C- 38: Contour Plot of change in groundwater Temperature concentrations and Barnett Reservoir Pressure Gradient in the study region.....	190
Fig. C- 39: Contour Plot of change in groundwater Dissolved Vanadium concentrations and Barnett Reservoir Pressure Gradient in the study region.....	191
Fig. C- 40: Contour Plot of change in groundwater Total Zinc concentrations and Barnett Reservoir Pressure Gradient in the study region.....	192
Fig. D- 1: Relative distribution of Dissolved Alpha concentrations detected in Subgroup 6 (left) and Subgroup 1 (right)	193
Fig. D- 2: Relative distribution of Dissolved Aluminum concentrations detected in Subgroup 6 (left) and Subgroup 1 (right).....	193
Fig. D- 3: Relative distribution of Total Arsenic concentrations detected in Subgroup 6 (left) and Subgroup 1 (right)	194
Fig. D- 4: Relative distribution of Total Barium concentrations detected in Subgroup 6 (left) and Subgroup 1 (right)	194
Fig. D- 5: Relative distribution of Total Benzene concentrations detected in Subgroup 6 (left) and Subgroup 1 (right)	195
Fig. D- 6: Relative distribution of Total Beryllium concentrations detected in Subgroup 6 (left) and Subgroup 1 (right)	195
Fig. D- 7: Relative distribution of Dissolved Boron concentrations detected in Subgroup 6 (left) and Subgroup 1 (right)	196
Fig. D- 8: Relative distribution of Dissolved Bromide concentrations detected in Subgroup 6 (left) and Subgroup 1 (right).....	196
Fig. D- 9: Relative distribution of Total Bromide concentrations detected in Subgroup 6 (left) and Subgroup 1 (right)	197

Fig. D- 10: Relative distribution of Total Chloride concentrations detected in Subgroup 6 (left) and Subgroup 1 (right)	197
Fig. D- 11: Relative distribution of Total Copper concentrations detected in Subgroup 6 (left) and Subgroup 1 (right)	198
Fig. D- 12: Relative distribution of Dissolved Oxygen concentrations detected in Subgroup 6 (left) and Subgroup 1 (right).....	198
Fig. D- 13: Relative distribution of Total Ethanol concentrations detected in Subgroup 6 (left) and Subgroup 1 (right)	199
Fig. D- 14: Relative distribution of Total Ethyl Benzene concentrations detected in Subgroup 6 (left) and Subgroup 1 (right).....	199
Fig. D- 15: Relative distribution of Total Iron concentrations detected in Subgroup 6 (left) and Subgroup 1 (right)	200
Fig. D- 16: Relative distribution of Total Methanol concentrations detected in Subgroup 6 (left) and Subgroup 1 (right)	200
Fig. D- 17: Relative distribution of Dissolved Molybdenum concentrations detected in Subgroup 6 (left) and Subgroup 1 (right).....	201
Fig. D- 18: Relative distribution of Total Molybdenum concentrations detected in Subgroup 6 (left) and Subgroup 1 (right).....	201
Fig. D- 19: Relative distribution of Total Nickel concentrations detected in Subgroup 6 (left) and Subgroup 1 (right)	202
Fig. D- 20: Relative distribution of Total Nitrate concentrations detected in Subgroup 6 (left) and Subgroup 1 (right)	202
Fig. D- 21: Relative distribution of Oxidation-Reduction Potential detected in Subgroup 6 (left) and Subgroup 1 (right)	203
Fig. D- 22: Relative distribution of pH detected in Subgroup 6 (left) and Subgroup 1 (right)	203

Fig. D- 23: Relative distribution of Dissolved Phosphorus concentrations detected in Subgroup 6 (left) and Subgroup 1 (right).....	204
Fig. D- 24: Relative distribution of Dissolved Radium 226 concentrations detected in Subgroup 6 (left) and Subgroup 1 (right).....	204
Fig. D- 25: Relative distribution of Dissolved Radium 228 concentrations detected in Subgroup 6 (left) and Subgroup 1 (right).....	205
Fig. D- 26: Relative distribution of Total Selenium concentrations detected in Subgroup 6 (left) and Subgroup 1 (right)	205
Fig. D- 27: Relative distribution of Total Sulfate concentrations detected in Subgroup 6 (left) and Subgroup 1 (right)	206
Fig. D- 28: Relative distribution of Total Dissolved Solids concentrations detected in Subgroup 6 (left) and Subgroup 1 (right).....	206
Fig. D- 29: Relative distribution of Water Temperature detected in Subgroup 6 (left) and Subgroup 1 (right).....	207
Fig. D- 30: Relative distribution of Dissolved Vanadium concentrations detected in Subgroup 6 (left) and Subgroup 1 (right).....	207
Fig. D- 31: Relative distribution of Total Zinc concentrations detected in Subgroup 6 (left) and Subgroup 1 (right)	208

LIST OF TABLES

Table 3-1: The Sandstone Reservoirs in the Trinity Aquifer (adapted from Harden, 2004)	23
Table 3-2: Average Hydraulic Conductivity Values of Trinity Group Sandstones (Adapted from Harden, 2004).....	29
Table 3-3: Seepage Velocity Calculations for the Paluxy Aquifer at Varying Porosities .31	
Table 3-4: Summary of Water Quality Data Set from Texas Water Development Board for Study Counties	37
Table 3-5: UTA Groundwater Samples taken in 2011	39
Table 3-6: UTA Groundwater Samples taken in 2014.....	40
Table 3-7: TWDB-UTA Combined Groundwater Data Set	43
Table 3-8: Flowing Bottom Hole Pressure as a function of depth for Pressure Gradients of 0.433 psi/ft, 0.520 pis/ft, and 1.000 psi/ft.	46
Table 3-9: Range of Fluid Velocities in a Micro-Annulus	49
Table 4-1: Summary of Data Used in Contour Plots	67
Table 4-2: Constituent Detection Limits	73
Table 4-3: Subgroup Descriptions	76
Table 4-4: Abbreviations Referenced in Analysis Results	77
Table 4-5: Description of Clusters Analyzed	81
Table 4-6: Cluster Descriptions of ArcGIS Cluster and Outlier Analysis (adapted from http://resources.arcgis.com/en/help/main/10.1/index.html#//005p00000012000000 0)	83
Table 5-1: P-Value Determinations of Mann-Whitney U-Test for when Non-Detects are included as Zero Values.....	88

Table 5-2: P-Value Determinations of Mann-Whitney U-Test for when Non-Detects are included as ½ the Detection Limit	89
Table 5-3: P-Value Determinations of Mann-Whitney U-Test for when Non-Detects are Excluded from analysis	90
Table 5-4: Distribution Values of Constituent Concentrations Detected in Subgroups 1-6	92
Table 5-5: Results of Mann-Whitney U-Test for Subgroups 1 and 6	94
Table 5-6: Statistically Significant Distribution Differences Between Subgroups 1 and 6	95
Table 5-7: R-Squared Values for Data Extracted in Subgroup 1	97
Table 5-8: R-Squared Values for Data Extracted in Subgroup 2	98
Table 5-9: R-Squared Values for Data Extracted in Subgroup 3	99
Table 5-10: R-Squared Values for Data Extracted in Subgroup 4	100
Table 5-11: R-Squared Values for Data Extracted in Subgroup 5	101
Table 5-12: R-Squared Values for Data Extracted in Subgroup 6	102
Table 5-13: Mann-Whitney U-Test Evaluation of HH and LL Clusters of Wellbore Parameters using Beryllium Tracer Concentrations	110

1 INTRODUCTION

Over the past decade, the application of hydraulic fracturing technologies to directionally drilled wells has become an industry standard practice in the development of natural gas resources. This new approach to hydraulic fracturing has expanded the natural gas market by enabling access to gas reserves existing in low-permeability shale reservoirs that in the past, have been considered non-productive. As a result, the energy industry has experienced a “gas boom” in the United States, as an abundance of shale-gas reserves exist in multiple regions of the country. The use of modern hydraulic fracturing techniques pioneered by the United States has expanded to other parts of the world seeking to develop their own natural gas resources.

As the presence of hydraulic fracturing operations has increased in the U. S., concerns have been raised regarding the strain on the infrastructure with land use changes (Eaton, 2013), high quantities of fresh water consumption (Fry, Hoeninghau, Ponette-Gonzalez, Thompson & LaPoint, 2012; Murray, 2013), and earthquakes possibly induced by the hydraulic fracturing process (Bowman, Urbancic, & Baig, 2012; Davies, Fougler, Bindley & Styles, 2013). Additionally, environmental concerns have been raised regarding air (Rich, Grover & Sattler, 2014; Rabinowitz, et al., 2015), soil (McBroom, Thomas & Zhang, 2012), and most notably, groundwater quality (Flewelling & Sharma, 2013; Gordalla, Ewers & Frimmel, 2013; Gross et al., 2013; R.B. Jackson et al., 2013; R.E. Jackson et al., 2013; Molofsky, Connor, Farhat, Wylie & Wagner, 2011; Molofsky, Conner, Wylie, Wagner & Farhat, 2013; Myers, 2012; Osborn, Vengosh, Warner & Jackson, 2011; Revesz, Breen, Baldassare & Burruss, 2012) in areas that are in proximity to hydraulic fracturing operations.

Unlike hydraulic fracturing treatments of the past, fracturing operations today are performed on a much larger scale where multiple zones are treated along the lateral section of a directional wellbore with high pressures and large quantities of fluid. As the presence of these large-scale operations has increased, it has been thought by some that hydraulic fracturing creates subsurface fractures extending from the gas reservoir to the water aquifer. This theory, however, does not correspond to generally accepted understandings of hydraulic fracturing concepts. Wellbore testing techniques through production logs have demonstrated that fracture growth is hindered by some property of the interface between formation layers, presumably the stress differences between rock formations (Gidley, 1989, p. 69). There are many stratigraphic layers separating the water table and the gas reservoir by several thousand feet, making the idea of such fracture extension highly improbable. However, the issue of potential groundwater contamination due to hydraulic fracturing operations remains in discussion.

In Pennsylvania, concerns over groundwater contamination began when residents noted the presence of methane in their water wells near hydraulic fracturing sites in the Marcellus Shale. Subsequent investigations have analyzed this issue by studying methane concentration and origin in groundwater samples. Because methane exists in groundwater naturally, confirming hydraulic fracturing as the source of methane present in the groundwater has ultimately led to conflicting conclusions among the associated studies. However, many studies presented on the topic indicate that groundwater quality may be impacted by hydraulic fracturing in some way, even if specific knowledge of the contaminant pathway is not known. A more current understanding of this issue, however, proposes that contaminant pathways are most likely formed through an unsealed wellbore annulus (Darrah, Vengosh, Jackson, Warner & Poreda, 2014), where methane and/or other contaminants are mobilized upwards to the water table as the pressure of compressed gas in the reservoir is released during the

hydraulic fracturing process. Overall, because no great depth of study on this subject exists, a consensus in understanding the relationship between hydraulic fracturing and changes in groundwater quality has yet to be reached. Additionally, the conclusions that can be drawn from scientific studies on this subject are primarily limited by a lack of historical water quality data in order to reference changes in groundwater quality, further impeding an understanding of this issue.

The purpose of this thesis is to explore the relationship, if any, between hydraulic fracturing and groundwater quality change in an area of significant natural gas extraction. In this study, groundwater quality changes in the Barnett Shale region are evaluated over a 10-year period from 2001 to 2011, a period that saw a steady flux of gas well completions in the region, with the hypothesis being that if some change in groundwater quality is related to hydraulic fracturing activities, a cumulative change in groundwater quality detected over the aforementioned time period can be shown to correlate hydraulic fracturing operational properties.

The analyses in this thesis evaluate the extent to which reservoir pressure and proximity to gas wells can be used as predictors of groundwater quality change, with the assumption that reservoir pressure is the mobilizing mechanism of groundwater contaminants, and that the wellbore annulus is the contaminant pathway. The thesis contends that groundwater contamination may be attributed to the hydraulic fracturing process in that the flow of fluid through a micro-annulus would not otherwise occur in a low-permeability shale well that was not hydraulically fractured. Also, a pre-existing micro-annulus in the wellbore could possibly be expanded by the hydraulic fracturing process. The in this thesis evaluates changes in groundwater quality in a spatial context as natural water quality, reservoir pressure, and relative thickness between the shale reservoir and the water aquifer vary across the region.

The research in this thesis develops a spatial model in ArcGIS that incorporates various data sets including historical groundwater samples, recent groundwater samples; gas well completions data, reservoir pressure, and geologic depths of the water aquifer and Barnett Shale in order to interpret the potential relationship between hydraulic fracturing of gas wells and groundwater quality changes. Additionally, specific data describing the wellbores and hydraulic fracturing treatments are analyzed using statistical methods to draw an inference about the potential origin of the contaminant pathway in the wellbore. The Fort Worth Basin, which embodies the Barnett Shale, was chosen as the study area for this thesis for three reasons:

1. The Barnett has a long-standing natural gas production history making it a good area for studying cumulative water quality change over an extended period of time;
2. Relatively substantial historical water data is publically available for this region from the Texas Water Development Board; and
3. Two additional ground water quality data sets from the University of Texas Arlington provide relatively recent and detailed groundwater data that provide additional rigor to the analyses.

2 BACKGROUND

The United States has pioneered the development of unconventional natural gas reserves through modern applications of hydraulic fracturing technologies in directionally drilled wells. In oil and gas extraction, hydraulic fracturing is the process of stimulating a wellbore in order to improve its productivity index by increasing the hydraulic conductivity of the wellbore and rate of flow in the subsurface rock formation. Low-permeability shale formations, although rich in natural gas, have historically been considered a non-productible resource (Murray, 2013). Since the 1980's, considerable research has been completed to improve hydraulic fracturing techniques that were initially developed as early as 1949 (Smith & Hannah, 1996). The evolution of low-permeability hydraulic fracturing has provided a viable solution for accessing shale gas resources. In 1992, the first hydraulic fracturing treatment in a horizontal wellbore was performed in the Barnett Shale; since then, fracturing has evolved into an industry standard practice in the development of low-permeability shale formations (Smith & Hannah, 1996). Advances in horizontal drilling technologies over the past decade have led to the undertaking of large-scale hydraulic fracturing operations where multiple zones are fractured along the lateral section of a wellbore in the target reservoir formation.

In the United States, significant investments have been made in the development of the Barnett, Marcellus, Haynesville, and Eagle Ford shales (Arthur, Bohm & Cornue, 2009). Hydraulic fracturing has been a source of significant economic growth to the oil and gas industry, a contrast to the state of the economy at large (Wang, Chen, Jha & Rogers, 2014). Proponents of hydraulic fracturing recognize the economic potential of developing this resource, as well as its impact on the future energy outlook. Natural gas supplies 22% of the nation's (United States) energy needs (Arthur, Bohm & Cornue, 2009). The United States has an estimated volume 348.8 tcf of technically recoverable

natural gas reserves in the United States (EIA, 2013). In 2014, the U.S. consumed 2.68 tcf of natural gas (EIA.gov); the U.S. could supply itself with natural gas for decades to come. Furthermore, natural gas is an attractive energy source, as it is a clean burning fuel. The United States has had the largest reduction in the world of CO₂ emissions from fossil fuels since 2006 (Finkel & Hays, 2013; Wang, Chen, Jha & Rogers, 2014).

Despite the positive aspects of unconventional gas development, hydraulic fracturing has become a source of controversy over the potential risks to human health and the environment (Arthur, Bohm & Cornue 2009; Coughlin & Arthur, 2011; Finkel & Hays, 2012; Rahm, 2011; Walton & Woocay, 2013; Ziemkiewicz, Quaranta, Darnell & Wise, 2014). Reports of water well contamination due methane migration have been attributed to natural gas extraction, primarily in the Marcellus shale in Pennsylvania (R.B. Jackson et al., 2013; Osborn, Vengosh & Warner, 2011; Revesz, Breen, Baldassare & Burruss 2012; Rozell & Reaven, 2012; Vidic, Brantley, Vandenbossche, Yoxheimer & Abad, 2013; Warner et al., 2012). This has incited public scrutiny into the process of hydraulic fracturing. Additionally, the large amount of fresh water consumed by these operations has led to public concern over the management of fresh water resources, especially in urban areas like Fort Worth, TX (Fry, Heoinghaus & Ponette-Gonzalez, 2012). Land disturbance from wellsite construction has contributed to soil erosion and to degraded surface water quality (McBroom, Thomas & Zhang, 2012; Eaton, 2013).

Hydraulic fracturing operations are not regulated under the Safe Drinking Water Act (SDWA); a proposal in the House called the Fracturing Responsibility and Awareness Act (FRAC ACT) would repeal this exemption, but it has yet to be passed (Garmezy, 2013). Developing a regulatory framework for hydraulic fracturing operations is complicated since there is limited data available for informative policy making (Eaton, 2013). Human health and environmental risks associated with hydraulic fracturing are not well understood to date. Public concerns over hydraulic fracturing have been brought

to the forefront in the past few years and investigations have attempted to address potential contaminants and their pathways in air, water and soil.

Hydraulic fracturing operations use industrial pumps to inject a “slurry” consisting of water, sand, and chemicals into a wellbore at pressures that exceed the in-situ reservoir pressure; this process effectively “fractures” the subsurface rock allowing fluid to flow. Horizontal gas wells use an average of 4.8 million gallons of water per well (Freyman, 2014). The injected slurry consists of approximately 90% water, 9% sand, and 1% chemicals (fracfocus.org). In the United States, mining activities, which include hydraulic fracturing, account for about 1.7% of total water consumption (USGS.gov). although this is a relatively small amount of overall water use, approximately 30% of the total water injected is recovered to the surface, creating a permanent removal of fresh water from the hydrologic cycle (Coughlin & Arthur, 2011), a serious concern for the long-term use of hydraulic fracturing technologies and its strain on fresh water resources. The wastewater that is recovered to the surface presents an added risk to human health and the environment because it contains high levels of total dissolved solids (TDS), and other contaminants such as treatment chemicals, volatile pollutants, bromide, heavy metals, and naturally occurring radioactive material (NORM) (Gordolla Ewers & Frimmel, 2013; Ternes, 2012; Arthur, Bohm & Cornue, 2009). The various pollutants in the flowback water consist of fracture treatment chemicals as well as constituents from the shale formation itself. Trace mineral elements including Antimony, Arsenic, Barium, Beryllium, Cadmium, Chromium, Cobalt, Copper, Lead, Molybdenum, Nickel, Scandium, Thorium, Uranium, Vanadium, and Zinc are naturally concentrated in shale reservoirs (Chermak & Schreiber, 2014). The drilling of natural gas has brought increased exposure to radioactive waste, where the decay products of Uranium, such as Radium-226, have high concentrations in shale reservoirs (Brown, 2014). Additionally, the fluids in shale reservoirs have high salinity, the cause of the mobilization of

radionuclides (Brown, 2014). The flowback water is characterized by its high Bromide and Chloride content which originate from the brine in the shale reservoir (Harkness et al., 2015).

Due to the high salinity of this wastewater, it is difficult to treat, making management a challenge (Lutz, Lewis & Doyle, 2013; Rahm et al., 2013). Operators may dispose of wastewater through re-injection into a disposal well, or else by flowing it back to a retention pit to evaporate before the remaining solids are discarded. There is no uniform regulatory standard for wastewater management; regulations in oil and gas extraction are determined by the state rather than the federal government (Rahm, 2011). The State of Pennsylvania requires wastewater to be flowed into tanks and disposed of, whereas Texas allows for open-pit disposal (Rahm, 2011). The disadvantage of open pit disposal is that a leak in the pit liner could release contaminants into groundwater through the soil, or else volatile emissions may be released into the atmosphere.

A recent study in the Barnett Shale shows that air contaminants are more heavily concentrated in proximity to oil and gas operations and are at levels that are considered carcinogenic to humans (Rich, Grover & Sattler, 2014). A study in Garfield County, Colorado indicates that residents in proximity to natural gas operations are more likely to experience health impacts from volatile emissions (McKenzie, Witter, Newman & Adgate, 2012). Hydraulic fracturing operations occur over broad regional areas, communities within proximity to wells and production facilities are at an increased risk for exposure to hazards and pollution, especially respiratory symptoms (Ziemkiewicz, Quaranta, Darnell & Wise 2014; Rabinowitz et al., 2015).

Overwhelmingly, the least understood aspect of hydraulic fracturing is related to the groundwater contamination pathways through the subsurface as there are various possibilities including inadequate (oil or gas) well construction, well site surface discharges, wastewater disposal, defective seals in existing water wells, fractured rock

above the shale allowing for upward migration from the aquifer, or dormant faults that are activated by hydraulic fracturing (Rozell & Reaven, 2012; Walton & Woocay, 2013). In other words, the subsurface migration pathways could be natural, hydraulic fracturing-induced, or both, however, this is not well understood (Fontenot et al., 2013; Rozell & Reaven, 2012; Rutqvist, Rinaldi, Cappa & Mordis, 2013). Wellbore communication occurs frequently in oil and gas development where wellbores in close proximity may produce fluid that was injected into a neighboring wellbore (R.E. Jackson et al., 2013). This wellbore communication occurs in the horizontal direction. Vertical wellbore communication is not presumed to be occurring, however, some studies suggest that hydraulic fracturing operations are capable of inducing seismic activity (Bowman, Urbancic & Baig, 2012; Zoback, Kohli, Das & McClure, 2012; Davies, Fougler, Bindley & Styles, 2013; Rutqvist, Rinaldi, Cappa & Moridis, 2013) which may indicate that what is occurring deep in the subsurface could be significant enough to impact near-surface aquifers by either compromising the integrity of the wellbore, or activating dormant faults. Hydraulic fracturing induced contaminant pathways may be created by causing preexisting fault zones to slip earlier than they would naturally (Davies, Foulger, Bindley & Styles, 2013). A MODFLOW simulation determined that advective transport time to surface aquifers could decrease to less than 10 years (Myers, 2012), although two repudiations to this study state that the geophysical characterizations in this model are “unconstrained by reality” (Saiers & Barth, 2012) and are based on a “subjective judgment” (Cohen, Parratt & Andrews, 2013).

The geophysical characteristics potentially contributing to gas migration in an aquifer are a permeable fault zone, low residual saturation and porosity, large volumes of mobilized gas, or a shallow gas reservoir (Kissinger et al., 2013). Developing a model for understanding hydrogeologic properties of the subsurface in conjunction with fracturing-induced contaminant pathways is critical for developing a comprehensive and

holistic risk assessment of groundwater contamination due to hydraulic fracturing operations. Current modeling capabilities, however, rely upon simplifying assumptions for hydrogeologic systems that in reality are complex and heterogeneous in porosity and permeability (Kissinger et al., 2013).

Many studies have attempted to analyze methane abundance in water wells in order to determine if hydraulic fracturing may be responsible for the creation of contaminant pathways to the water table. While methane occurs in drinking water naturally, the most common claims of groundwater contamination cite an elevated methane concentration. However, the fact that shale formations lay several thousands of feet below the water aquifer renders a connection between natural gas extraction and elevated methane concentration in groundwater improbable to some experts. A 2011 study in the Marcellus shale concludes that elevated methane concentrations in water wells are a direct correlation to the surface topography, where geologic conditions containing thermogenic gas coincide with the location of the water well samples (Molofsky, Conner, Farhat, Wylie & Wagner, 2011). Molofsky et al. (2011) further validates their analysis “that shale gas extraction has not resulted in regional impacts on groundwater quality” in a 2013 study analyzing the isotropic signatures of methane gas in water wells to determine their origin. The methane signatures were those of Upper Devonian shale formations located over 2000 ft above the Marcellus shale. The study concludes that there are subsurface migration pathways, although not necessarily hydraulic fracturing related (Molofsky, Connor, Wylie, Wagner & Farhat, 2013).

Other groundwater studies have contradicted these findings by demonstrating that drinking water wells in Pennsylvania containing brines correspond to the geochemical properties of the Marcellus shale (Warner et al., 2012), methane concentrations are an average of 17 times higher in wells in close proximity to natural gas wells (Osborn, Vengosh, Warner & Jackson, 2011), and carbon and hydrogen

isotopic signatures correlate to those in nearby storage field observation wells (Revesz, Breen, Baldassare & Burruss, 2012). The aforementioned studies suggest that elevated methane concentrations in water wells are due to hydraulic fracturing.

Two parallel studies in the Marcellus and Eagle Ford shales evaluated stray gas abundance in water well samples. The Fayetteville shale showed no water contamination, while the isotopic signatures of natural gas in the Marcellus were correlated to the proximity of hydraulic fracturing. While some may claim that contaminant pathways are occurring in the geophysically, the Marcellus study ultimately concluded that well contamination is due to poor well construction (R.B. Jackson et al., 2013). A study in Parker County, TX used natural gas and hydrocarbon tracers in water well samples to determine that stray gas abundance is hydraulic fracturing induced and concluded that leaks in the wellbore annulus and ruptured wellbore casing are the pathways of contamination (Darrah, Vengosh, Jackson, Warner & Poreda, 2014). This latter study may corroborate a 2010 study of gas migration pathways in CO₂ storage wells where poor cement jobs at the time of well construction were the source of a deficient cement barrier in the gas wellbore (Deremble, Loizzo, Huet, Lecampion & Quesada, 2010). The common leak pathways identified through the annulus are illustrated in Figure 2-1, where the highest risk areas are highlighted in red.

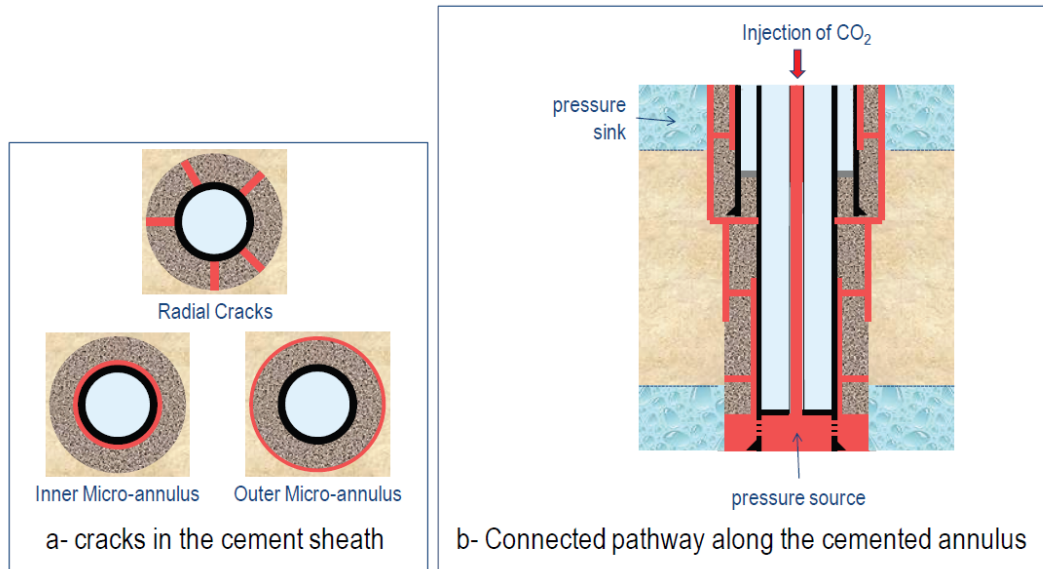


Fig. 2-1: Patterns of Defects and Pathways in a Cement Sheath (adapted from Deremble, Loizzo, Huet, Lecampion & Quesada, 2010)

Figure 2-1 depicts a vertical wellbore, however, a major problem in horizontal well completions is fluid loss during cement circulation as it is pumped around the “right-angle” of the wellbore causing a defective cement barrier and possible gas migration in the annulus. Certain additives to the cement mixture have shown a significant reduction in gas migration by allowing for improved cementation (Bexte, Willis, De Bruijn, Eitzen & Foulliard, 2008). However, even with improved completion practices, ruptured pipes during the fracturing operation can cause leakage in the wellbore (Gordalla, Ewers & Frimmel, 2013). Ultimately, a micro-annulus may be further impacted by the hydraulic fracturing process; the prospect of gas migration due to poor well completions or leaks, versus migration through the overburden geology, is generally supported by literature related to sedimentary basins which states that horizontal permeability is an order of magnitude higher than the vertical permeability; the notion of the existence of pre-existing fracture connections between shales and groundwater is contradictory (Flewelling & Sharma, 2013).

Overall, thorough scientific attempts to understand the correlation between hydraulic fracturing and groundwater contamination are generally limited by a lack of base-line data-sets for historical reference (Vidic, Brantley, Vandenbossche, Yoxtheimer & Abad, 2013), thus studies of groundwater quality and hydraulic fracturing have yielded conflicting conclusions. Accurate historical data sets, or baseline data sets prior to hydraulic fracturing, are necessary for a proper evaluation of contamination pathways (Lange et al., 2013, Gordalla, Ewers & Frimmel, 2013). In the Barnett Shale region, groundwater quality change over time was analyzed by the University of Texas Arlington (UTA) in a study comparing recent water sample data to historical base-line data collected from the Texas Water Development Board (TWDB). Various contaminants including total dissolved solids, methane, ethane, and heavy metal concentrations were measured from 100 water wells. The primary focus of the study was on the heavy metal concentrations of arsenic, selenium, strontium, and barium as these metals are known to occur at low-levels naturally in aquifers in the region (Fontenot et al., 2013).

The Fontenot et al. (2013) study used a Mann-Whitney pairwise U-test to interpret average changes over time of heavy metal constituents, arsenic, selenium, strontium, and barium from historical data samples (1989-1999) to 2011. Their results demonstrate a statistically significant median difference between their data set and historical data samples in areas near gas extraction activity citing elevated concentrations of heavy metals and Total Dissolved Solids (TDS), versus samples taken in areas without gas extraction, where a statistically significant change was not exhibited (Fontenot et al., 2013). The 2011 data set from Fontenot et al. (2013) was combined with data from the Texas Water Development Board and is used in this work, as will be seen later in the thesis.

Based upon the evidence cited in various studies, it can be assumed that groundwater quality is being impacted to some extent by hydraulic fracturing activities.

The specific pathway of the contamination and the extent of impact is undefined, therefore hydrogeologic research is necessary for identifying, characterizing, and monitoring aquifers that may be vulnerable to contamination by natural gas and other field-based contaminants since there is a “serious lack of scientific literature in this subject matter” (R.E. Jackson et al., 2013). This thesis uses a modeling-based approach to relate groundwater quality changes in the Barnett Shale region to hydraulic fracturing operations. The methods in this study use gas well proximity, gas well density, reservoir pressure of the shale formation, and thickness between the water aquifer and shale reservoir to evaluate and predict the extent to which water contamination may be occurring. Using more specific characterization of the wellbore environment, a relationship between hydraulic fracturing operations and groundwater quality changes may be better understood.

3 STUDY AREA & DATA DESCRIPTIONS

The model of the Barnett Shale region used in this thesis was created in ArcGIS using gas well and water well data for the Barnett Shale and Trinity aquifer, respectively. The data is sourced from Texas Water Development Board (TWDB), Texas Railroad Commission (RRC), Fracfocus.org, Drillinginfo.com, and the University of Texas at Arlington (UTA). In order to create a viable model for the analyses in this thesis, a study of the geologic stratigraphy was done to determine the necessary data.

3.1 THE BARNETT SHALE

The Barnett Shale is the Mississippian stratigraphic section of the Fort Worth Basin, which extends from central to northeast Texas with a changing stratigraphy from southwest to northeast (Montgomery, Jarvie, Bowker & Pollastro 2006). The Barnett Shale is described as multilayered, dense, organic-rich, soft, petroliferous, and fossiliferous limestone overlaid with shale (Bruner & Smosna, 2011). The Barnett is a hydrocarbon bearing formation characterized by its high gas content, making it a prime production target since the 1980's when viable production techniques allowed for gas extraction (Smith & Hannah, 1996). This gas reservoir is considered thermally mature, where the hydrocarbons in place have undergone thermal cracking for an extended period of time resulting in a methane content of 52% in some wells (Bowker, 2007; Jarvie, 2004). The gas content in the reservoir contributes to its above normal pressure gradient of 0.52 psi/ft, where pressure is defined in pounds per square inch (psi) and feet corresponds to vertical depth of the shale from the surface (Bowker, 2007).

The Barnett Shale extends from the Llano uplift, an outcrop found in central Texas, to the Texas Muenster Arch reverse thrust fault line in the northeastern part of the state (Lancaster, McKetta, Hill, Guidry & Jocen, 1992). The shallowest depth of the Barnett Shale is in Mills County around 1,000 ft and increases to 7,500 ft in the northeast

(Tian & Ayers, 2010). In the northeast section, the shale is intersected by the Forestburg Limestone formation, dividing it into upper and lower sections. The lower section of the Barnett Shale is the primary production target located within Denton, Parker, Tarrant, and Wise counties and has a thickness of 1,000 ft (Bruner & Smosna, 2011; Montgomery, Jarvie, Bowker & Pollastro, 2006; Tian & Ayers, 2010). The stratigraphic sections of the Fort Worth Basin are illustrated in Figure 3-1.

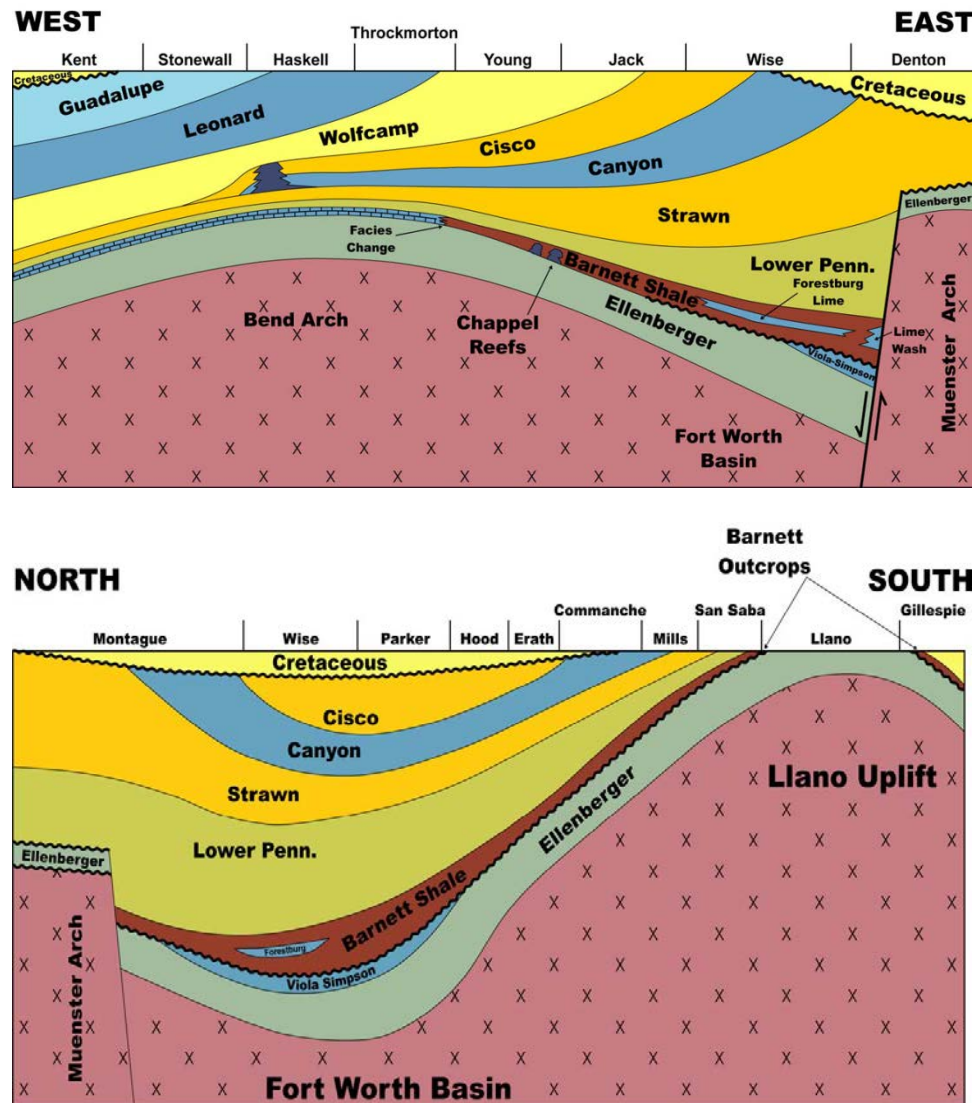
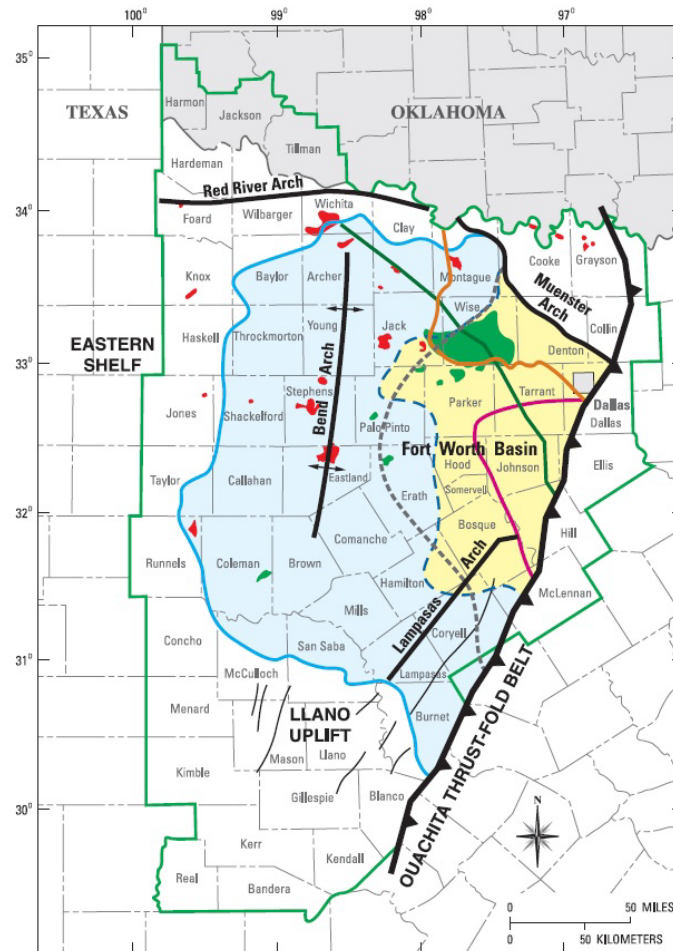


Fig. 3-1: Stratigraphic Section of the Fort Worth Basin adapted from Jarvie, 2004

As a shale deposit, the Barnett is considered both a reservoir rock and a source rock. Its orogenic process of deformation is similar to the Marcellus Shale where the convergence of tectonic plates resulted in a major fault line and arched structures (Bruner & Smosna, 2011). The greater Barnett Shale Region and its major geological features are shown in Figure 3-2.



Note: Forestburg limit modified from Givens and Zhao (2005); all others modified from Montgomery and others (2005); major oil and gas reserves from Galloway and others (1983) and Kosters and others (1989). The Major Gas and Oil Reserves refer to non-Barnett production.

EXPLANATION					
	USGS PROVINCE 45 BOUNDARY—BEND ARCH-FORT WORTH BASIN		MAJOR GAS RESERVES		VIOLA-SIMPSON FORMATION (absent west of this line)
	BARNETT SHALE EXTENT		MAJOR OIL RESERVES		MARBLE FALLS FORMATION (absent east of this line)
	GAS WINDOW AREA (Montgomery and others, 2005)		THRUST-FOLD BELT		FORESTBURG LIMESTONE (absent west of this line)
			GAS MATURATION LINE (Givens and Zhao, 2005)		

Fig. 3-2: The Barnett Shale Region and Major Geological Features (Bruner & Smosna, 2011)

The gas window area, denoted by the yellow shading, in Figure 3-3 is in the study area of this thesis. Gas well and water well data was obtained for the study area, that is the counties encompassing and bordering the gas window area, including Bosque, Clay, Collin, Cooke, Dallas, Denton, Ellis, Erath, Grayson, Hamilton, Hill, Hood, Hunt, Jack, Johnson, Kaufman, Montague, Palo Pinto, Parker, Rockwall, Somervell, Tarrant, and Wise which are shown in Figure 3-3.

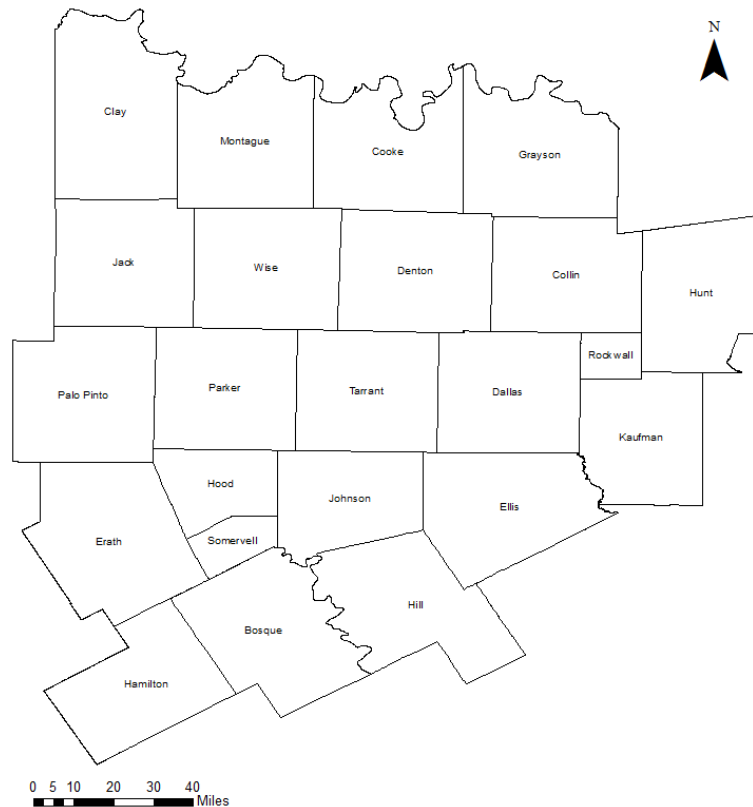


Fig. 3-3: Study Area as displayed in ArcGIS

Although the Barnett Shale is a valuable natural gas resource, the wells in this gas reservoir require hydraulic fracturing in order to be produced since the permeability of the reservoir rock in the production zone is very low, a range between 10^{-5} and 3.6×10^{-4} cm/s, with a porosity of 6% (Pratikno, Reese & Maguire, 2013). Since 2002, horizontal drilling has been successful in the Barnett Shale with lateral lengths varying between 500 and 3,500 ft (Montgomery, Jarvie, Bowker & Pollastro, 2006). The typical

reserves for a Barnett well are between 1.0 - 2.5 billion cubic feet (bcf), but range up to 7 bcf; maximized wellbore drainage has been achieved through horizontal drilling and the use of water based stimulation techniques (Montgomery, Jarvie, Bowker & Pollastro, 2006). Barnett shale wells are typically drilled between 6,500 and 8,000 ft in vertical depth (Lancaster, McKetta Hill, Guidry & Jochen, 1992). As of July 2012, over 13,000 horizontal wells have been completed in the Barnett Shale with a cumulative production totaling 12.4 trillion cubic feet (tcf) and 44.4 million barrels of oil (MMBO) (Pratikno, Reese & Maguire, 2013). The locations of active oil and gas wells in the Barnett Shale as of January 2014 are shown in Figure 3-4.

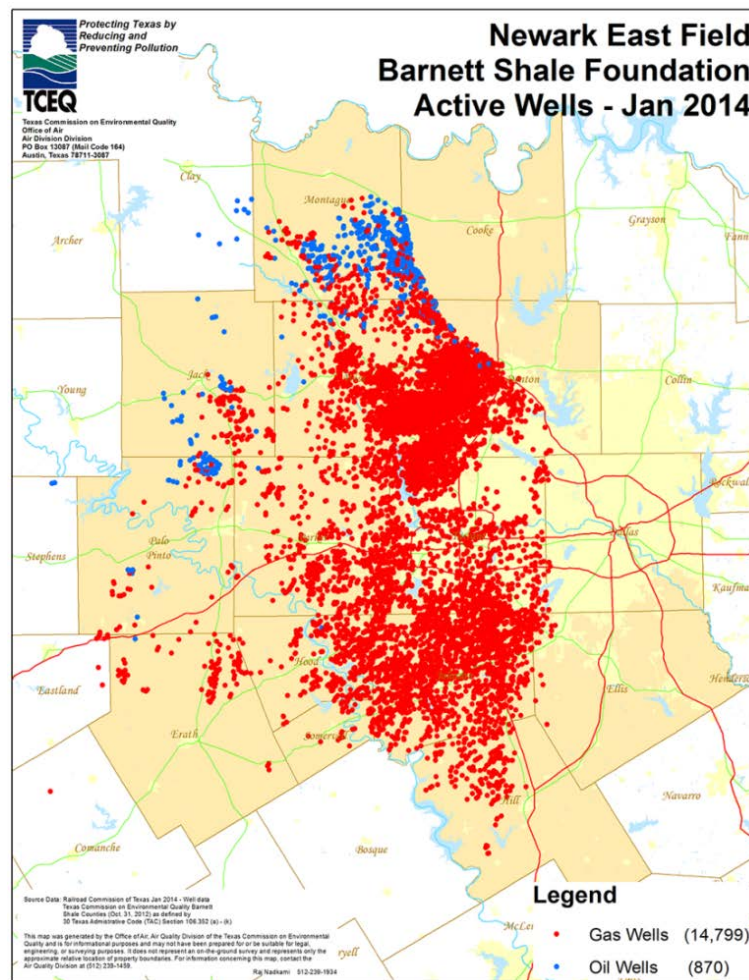


Fig. 3-4: Active Well Extraction Sites in the Barnett Shale
 (<https://www.tceq.texas.gov/airquality/barnettshale/bshale-maps>, 10-24-14)

Various chemicals are used in hydraulic fracturing operations and a list of them can be found from the U.S. House Committee of Energy and Commerce Report of 2011 (Waxman, Markey & Degette, 2011). Based upon this report, chemicals frequently contained in hydraulic fracturing products include compounds containing ammonia, benzene, chloride, ethanol, methanol, propanol, and sulfur. Some metal and metalloid constituents include aluminum, Borate, Copper, Magnesium, Silicon, Sodium, Titanium, and Zinc.

A search of gas well completions in the years between 2000-2014 was performed in Drillinginfo.com for the counties of the study area (Figure 3-5). A chart showing the count of new wells drilled per year is shown in Figure 3-5. The details of extracting the gas well data set used in this thesis are provided in Section 3.3.

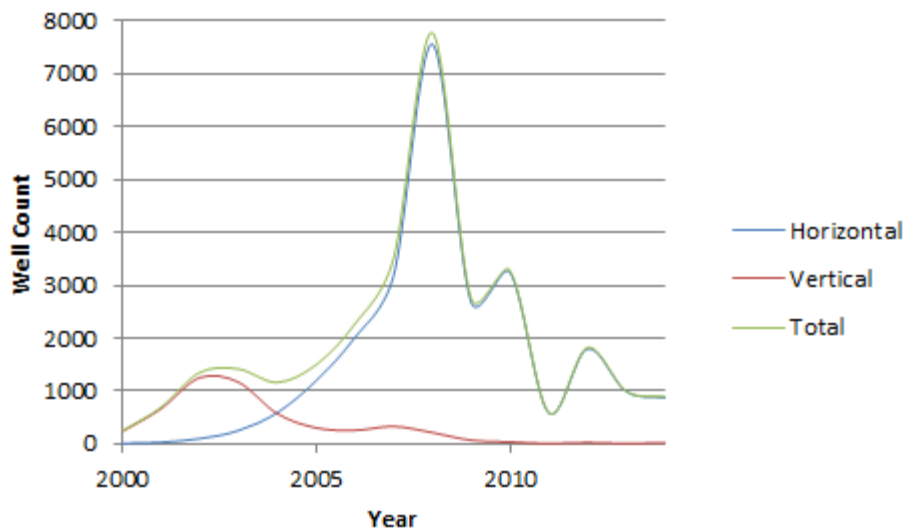


Fig. 3-5: New Well Completions in Barnett Shale Region per Year (data sourced from Drillinginfo.com)

The data in the figure above shows a significant increase in drilling activity since 2000 and peaking in 2008. This study examines the change in water quality before and after the peak production period for a 10-year timeframe, from 2001 to 2011. Because of

newly available groundwater data, samples used to characterize the groundwater after 2010, were taken from 2011-2014.

Vertical depths of gas wells drilled in the region were obtained from drillinginfo.com. This data was used to create a contour plot in ArcGIS of the vertical depth of the producing Barnett Shale formation. The total vertical depths (TVD) of wells in the Barnett Shale region were contoured using the Inverse Distance Weighting function in the ArcGIS under the Geostatistical Analyst toolbar. For the purpose of contouring, the latitude and the longitude of the well were rounded to two decimal places which explains why the locations appear in a grid-like arrangement in Figure 3-6, where multiple wells are represented in some locations denoted by the black dots. For multiple wells overlapping in a single location, the mean of the recorded TVD values for all of them was used in the contour function. The resulting contour plot of the Barnett Shale and the gas well locations are shown in Figure 3-6.

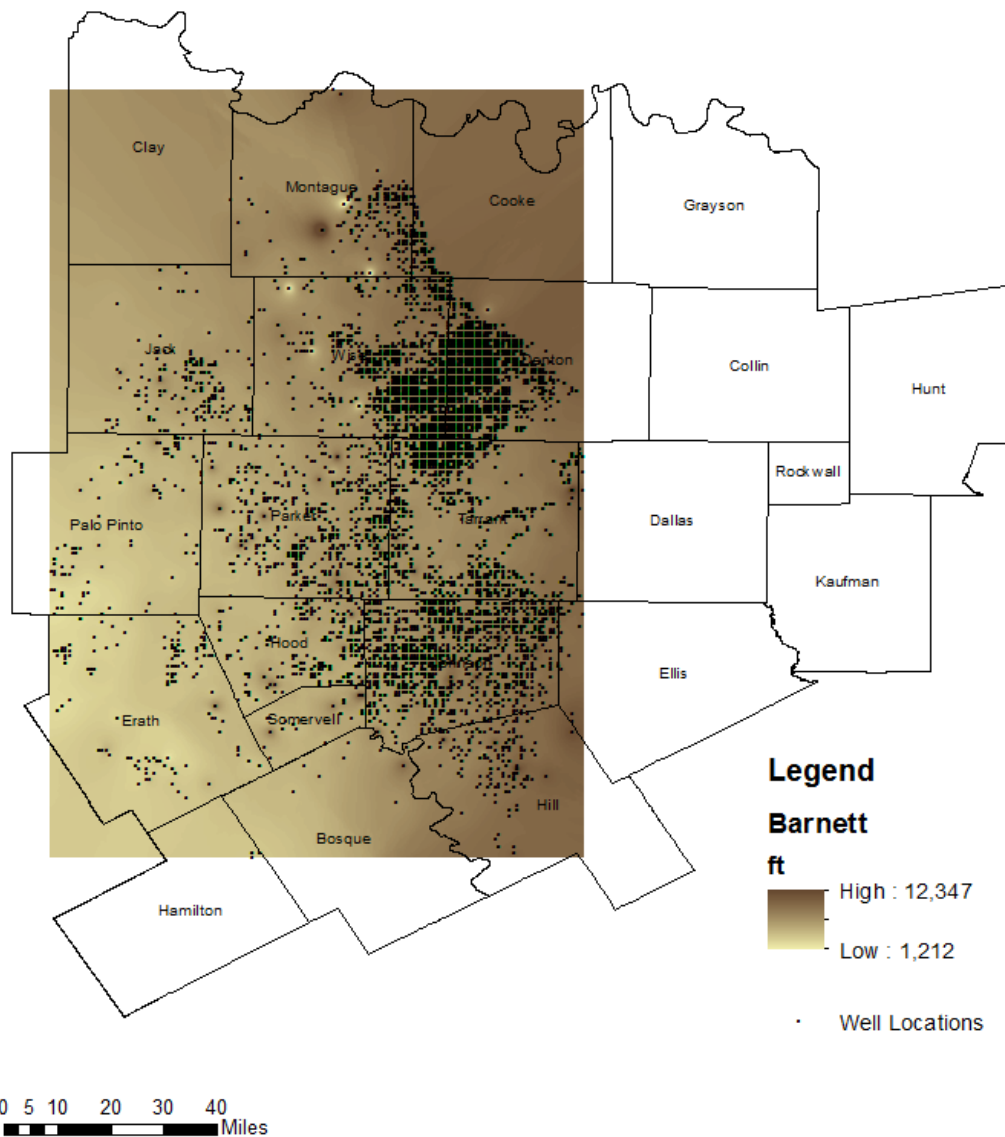


Fig. 3-6: Barnett Shale Depth Profile displayed in ArcGIS

Note that this plot denotes the producing zone over the region, based upon the Total Vertical Depth of gas wells in the region versus the upper vertical depth of the shale formation. As the plot shows, the shallowest vertical depth is 1,212 ft in the southwest and the deepest is 12,347 ft to the northeast. The average vertical well depth of the data used in this contour plot is 7,474 ft. It can also be seen that the wells are deeper in the northeast of the figure, particularly in Denton and Cooke counties.

3.2 THE TRINITY AQUIFER

The major water reservoir in the Fort Worth Basin is the Trinity Aquifer, which refers to a grouping of four sandstone formations separated by impermeable carbonate layers (see Table 3-1). These sandstone layers include the Woodbine, Hosston, Hensell, and Paluxy sands and their stratigraphy changes in the north-south direction (Harden, 2004).

Table 3-1: The Sandstone Reservoirs in the Trinity Aquifer (adapted from Harden, 2004)

Era	System	Groups	Formation					
			North		South			
			Sub-Group		Sub-Group			
Cenozoic	Quaternary							
	Tertiary							
		Woodbine						
		Washita						
		Fredericksburg						
		Trinity	Antlers	Paluxy Sand			Paluxy Sand	
				Glen Rose			Glen Rose	
				Twin Mountains	Hensell Sand			Hensell Sand
					Cow Creek			Cow Creek
				Travis Peak/Pearsall	Pine Island			Pine Island
					Hammett			Hammett
		Sycamore			Silgo			
		Hosston			Hosston			
Jurassic								
Triassic								
Paleozoic	Permian							
	Pennsylvanian							
	Mississippian							
		Barnett Shale		Barnett Shale				

In the northern part of the region, the Hensell and Hosston sand are differentiated appearing as a single sandstone layer called the Twin Mountains Formation. The Woodbine formation is the uppermost sandstone, however, it only partially extends over the basin (to the east of the Ouachita Thrust Fold Belt) and is considered a minor aquifer in the region (Harden, 2004). The Trinity aquifer group thickens in the south-southeast direction and the groundwater flows down-dip towards the Luling-Mexica-Talco fault

zone (Harden, 2004). The extents of the Trinity-Woodbine aquifers and the fault zones, shown in Figure 3-7, are mapped in ArcGIS using shapefiles downloaded from the Texas Water Development Board (<http://www.twdb.texas.gov/groundwater/data/gwdb rpt.asp>, 3-31-14) and the U.S. Geological Survey (<http://mrd data.usgs.gov/geology/state/state.php?state=TX>, 7-29-13) respectively.

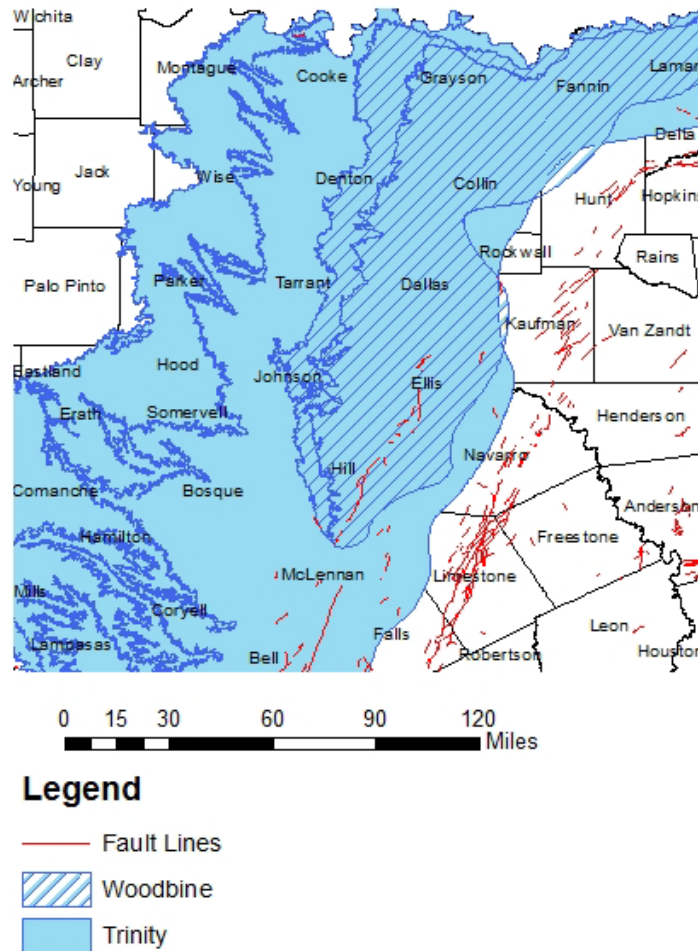


Fig. 3-7: Extent of Trinity and Woodbine Aquifers (TWDB, 3-31-14) and Fault Line Locations (USGS, 7-29-13) displayed in ArcGIS

The lateral extent of each sandstone layer in the Trinity group varies throughout the region. This is shown in Figure 3-8.

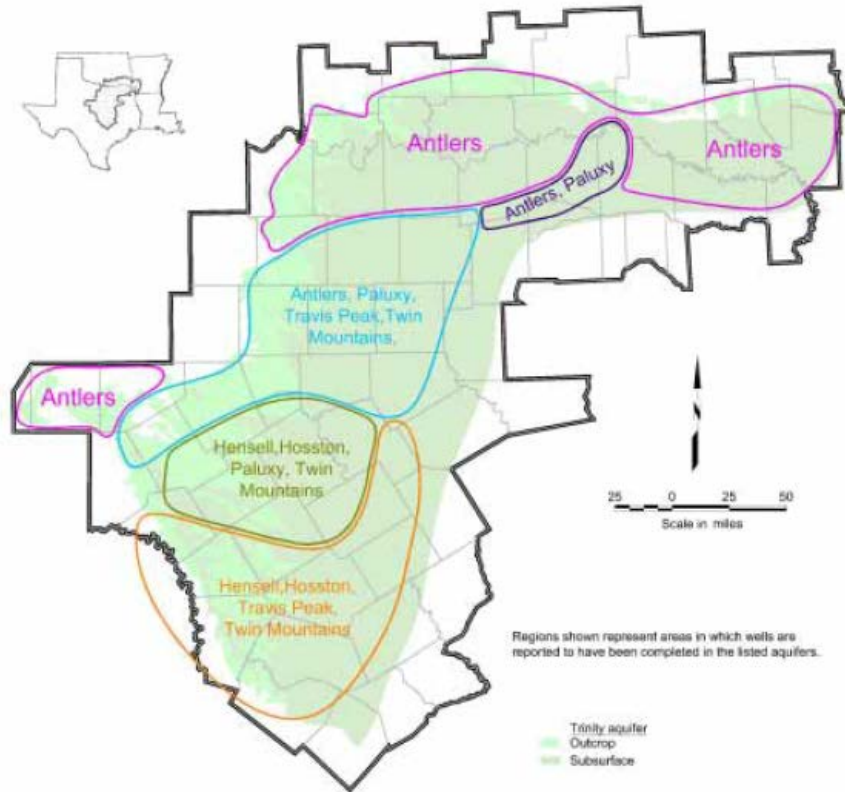


Fig. 3-8: Relative lateral extent of Trinity Aquifer sandstones (adapted from Harden et al., 2004)

As can be seen in Figure 3-8, the study counties of interest overlap with the Antlers, Paluxy, and Twin Mountains formations, but do not overlap as much with the Hensell, and Hosston formations (county boundaries shown in light gray). Therefore, it was determined to exclude water samples taken from these formations for the model used in this thesis and use only water samples taken in the Antlers, Paluxy, and Twin Mountains formations. Figure 3-9 shows a general stratigraphic cross-section of the remaining

sandstone layers in the north-south direction.

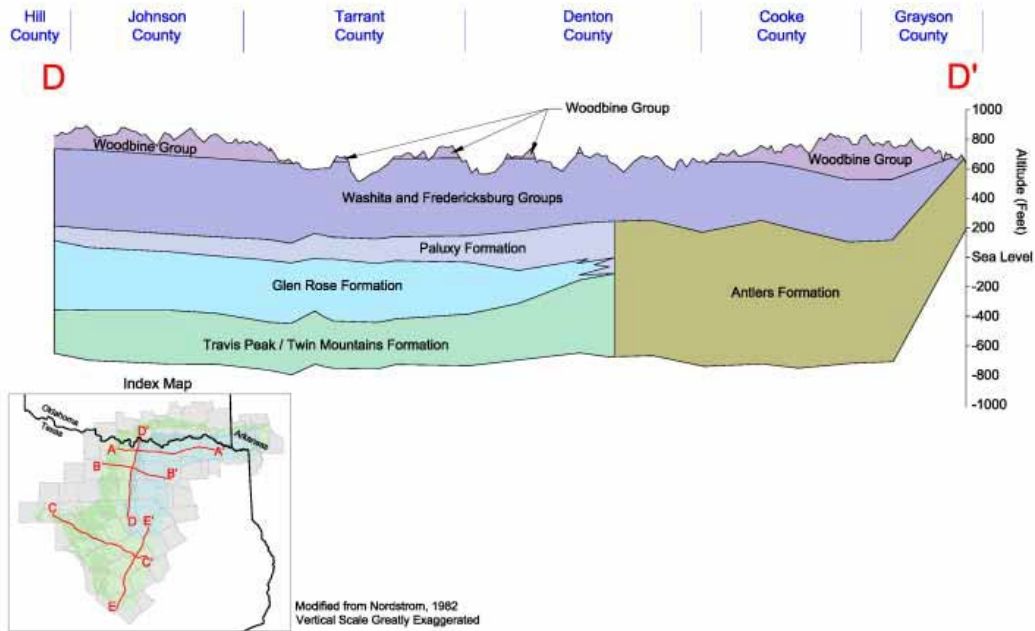


Fig. 3-9: Cross Section of Trinity Aquifer in the North-South Direction (adapted from Harden, 2004)

The Antlers formation is a continuous layer in the north, but in Denton County it is intersected by the Glen Rose formation, a low-permeability carbonate, dividing it into the Paluxy and Travis Peak/Twin Mountains formations. The Glen Rose, however, is not fully differentiated from the sandstones until further south in the region (Harden et al., 2004). The analysis methods in this study require that the water aquifer be modeled as a single stratigraphic layer. For the purpose of this thesis, water sample depths taken from the Antlers, Paluxy, and Travis Peak/Twin Mountains formations within the Trinity Aquifer group were combined to create a depth profile for a single stratigraphic layer that is referred to as the Paluxy Aquifer in this report (shown in Figure 3-10).

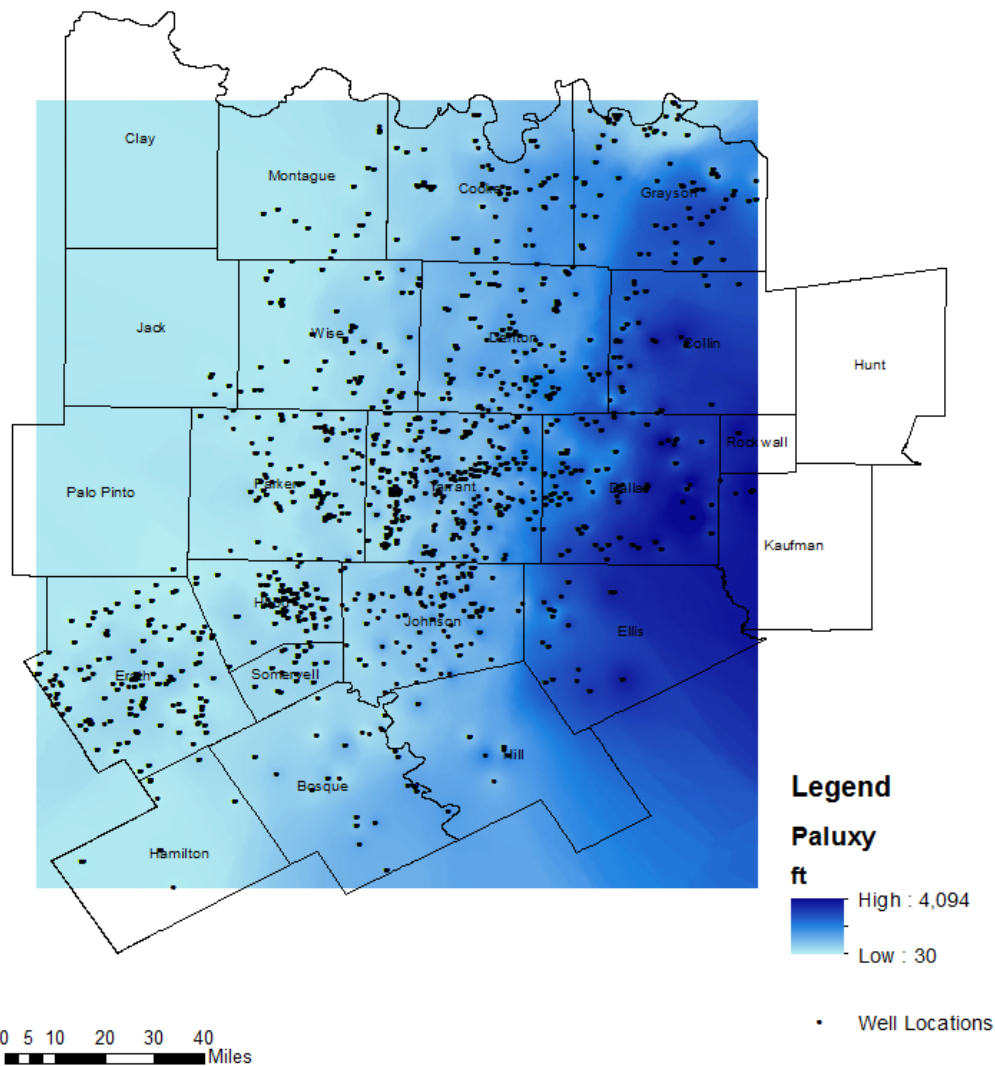


Fig. 3-10: Depth Profile of the Paluxy Sandstone and well locations with Aquifer ID references Antlers, Twin Mountains, and Paluxy

As can be seen from Figure 3-10, the model's shallowest water depth was found to be 30 ft, and the deepest depth is 4,094 ft. The deepest part of the aquifer is to the east of the Ouachita Thrust Fold Belt (see Figure 3-2) and is located outside the extent of the gas well locations (see Figure 3-8). Near Denton and Cooke counties, the counties with the deeper Barnett, the Paluxy water wells are approximately 2,000 ft deep. In order to verify the accuracy of this model, water samples were divided by Aquifer ID and plotted

separately. A comparison of the plots showed little distinction in aquifer depths between the Paluxy aquifer and Travis Peak/Twin Mountain contour plots.

The Trinity aquifer group is located vertically above the Barnett, thus, it is important to understand the relative depth separation between the Paluxy Aquifer layer and the Barnett Shale layer within the ArcGIS model. Using ArcGIS, the depths of the Paluxy Aquifer and the Barnett shale were extracted at gas well locations in the region. The difference between the depths was taken for each gas well and then re-plotted into ArcGIS. Using color coded symbology, the relative thickness was denoted using a color scale that shows the least thickness in blue and the greatest thickness in red as can be seen in Figure 3-11.

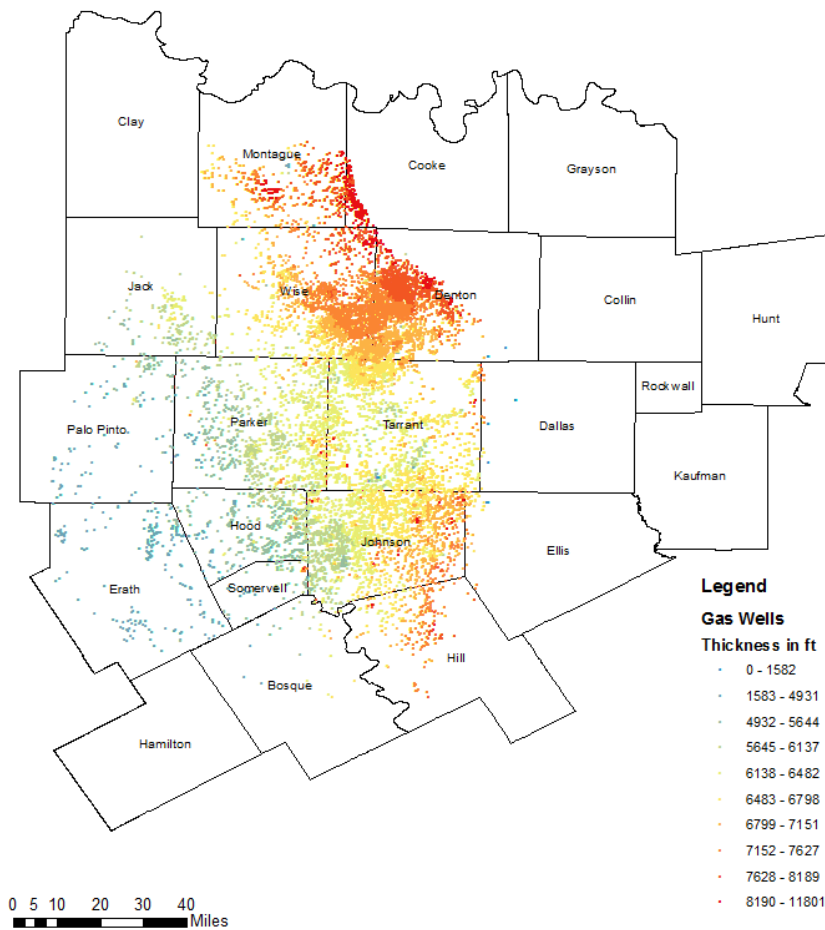


Fig. 3-11: Gas Wells Color Coded to Represent Relative Thickness between the Barnett Shale and Trinity Aquifer

At the gas well locations shown in Figure 3-11, the average depth of the Trinity Aquifer is 635 ft, and the average thickness between the Barnett Shale and Trinity aquifer is 6,740 ft (see section 4.1.1). The relevance of the separation between the Barnett and Trinity will be addressed in more detail in subsequent sections of the thesis, however, it is noted here that the areas that are most actively fracked exhibit the thickest separation between the Trinity and Barnett (e.g., Denton County).

In this study, it was also necessary to determine the extent to which groundwater flow velocities must be accounted for in understanding localized changes in water quality. The groundwater seepage velocity for the plot in Figure 3-11 was determined using Equation 3-1, where

$$\text{Seepage Velocity} = \frac{\text{Hydraulic Conductivity} \times \text{Reservoir Gradient}}{\text{Porosity}} \quad [3-1]$$

The hydraulic conductivities in the sandstone aquifer layers vary. These are summarized in Table 3-2 below.

Table 3-2: Average Hydraulic Conductivity Values of Trinity Group Sandstones (Adapted from Harden, 2004)

Formation	Hydraulic Conductivity (ft/day)
Woodbine	8.7
Paluxy	5.8
Hensell	13.3
Hosston	12.1

Average hydraulic conductivities were not specified in the Texas Water Development Board report for the Antlers and Twin Mountains formations. The seepage velocity calculated for this model uses the 5.8 ft/day from Table 3-2, the hydraulic conductivity of the Paluxy sandstone.

A gradient of the aquifer was determined from the ArcGIS model. The water flows from northwest to southeast. A grid of data points was overlaid in in the model to extract the shallowest depth from the northwest, and the deepest point in the southeast. These points are plotted in ArcGIS (see Figure 3-12).

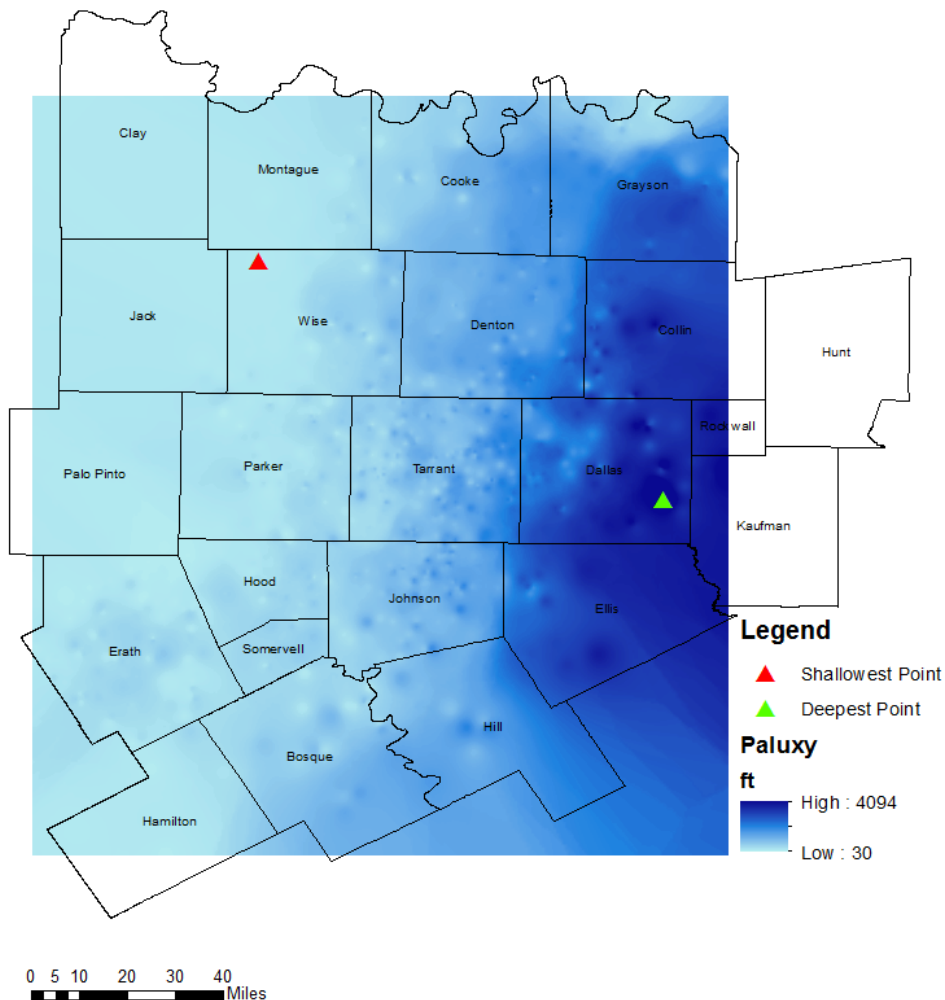


Fig. 3-12: Shallowest and deepest Paluxy Aquifer depths shown in ArcGIS

The depth of the shallowest point extracted in the northwest is 78 ft and the deepest depth extracted in the southeast is 4,083 ft. The distance between the data points is 86 miles. Data points in a line were created to connect the two points. At these data points the corresponding depths were extracted. The changing depth of the Paluxy Aquifer

between these two points was plotted in Excel to create a cross section of the aquifer, and a linear fit was applied to the data (Figure 3-13).

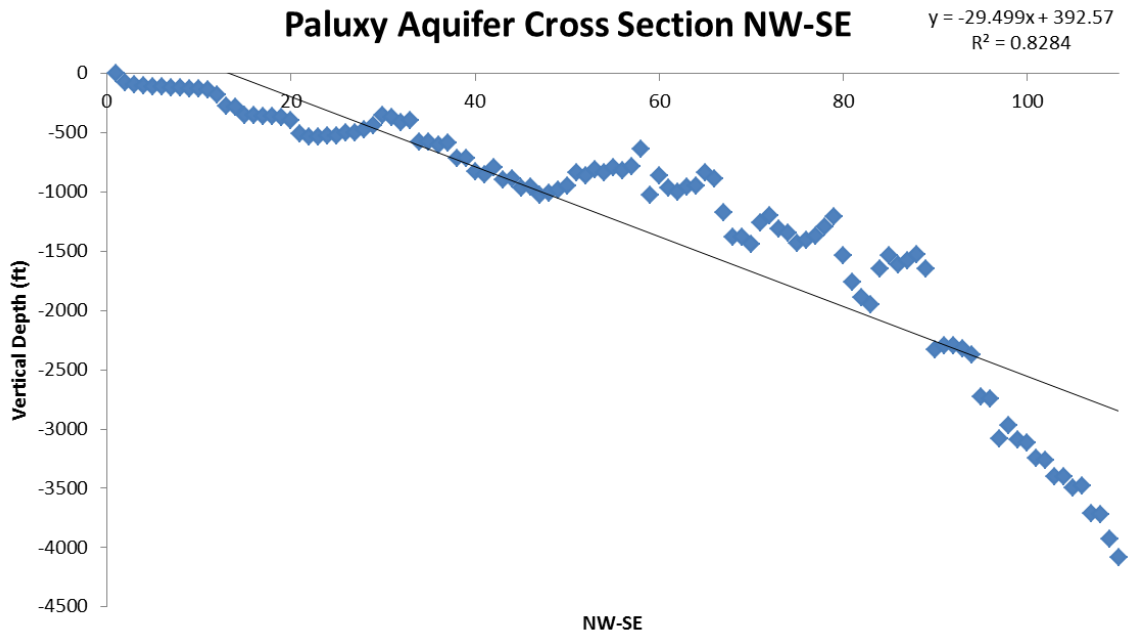


Fig. 3-13: Cross Section of Paluxy Aquifer Depth shallowest and deepest points

The distance between the points is 0.796 miles, and the changing depth between the points is -29.5 ft; this is equal to a gradient of -37.0 ft/mile. In the 86 miles between the points the total depth changes 4,006 ft, a gradient of 0.0088 mi/mi.

Using an average hydraulic conductivity of 5.8 ft/day, and an average gradient of 0.009, the estimated seepage velocity is shown at various porosities in Table 3-3:

Table 3-3: Seepage Velocity Calculations for the Paluxy Aquifer at Varying Porosities

Hydraulic Conductivity	Gradient	Porosity	Seepage Velocity	Seepage Velocity
<i>ft/day</i>			<i>ft/day</i>	<i>ft/10 years</i>
5.8	0.009	0.05	1.04	3,811
5.8	0.009	0.10	0.52	1,905
5.8	0.009	0.15	0.35	1,270
5.8	0.009	0.20	0.26	953
5.8	0.009	0.25	0.21	762
5.8	0.009	0.30	0.17	635

Paluxy Sandstone consists of sand, silt, and clay (Harden, 2004). These types of rocks generally have a high porosity, and a higher porosity rock will have a lower seepage velocity. In this model, the groundwater is assumed to have remained in close proximity to the sample location so the effect of groundwater flow is mostly negligible in the analysis in this thesis, otherwise, the analysis in this thesis assume a maximum flow distance of 1000 ft, based upon the range of distances calculated in Table 3-3. This flow distance, however, does not account for the retardation factors of the specific contaminants studied.

3.3 DATA SET DESCRIPTIONS

The analyses in this thesis are based upon the water well and gas well data available in the study region. Shapefiles (a Shapefile refers to an ArcGIS data layer type) were created in ArcGIS for gas well and water parameters at their corresponding coordinate locations. The combined gas well data was not sourced from a common location, so gas well locations were cross-referenced between gas well data sets. The water sample data provided by the University of Texas Arlington was not cross-referenced to the data set obtained from the Texas Water Development Board.

3.3.1 GAS WELL LOCATIONS

Well location coordinates and data were searched in Drillinginfo.com for gas wells completed in the study counties: Bosque, Collin, Cooke, Dallas, Denton, Ellis, Erath, Grayson, Hamilton, Hill, Hunt, Hood, Jack, Johnson, Kaufman, Montague, Palo Pinto, Parker, Rockwall, Somervell, Tarrant, and Wise counties. A well completions search was performed for each county per year from 2001 to 2014. The gas well coordinates are given in NAD27 coordinates. The well location data was exported to Excel, with each well being identified by both API number and State Gas Well ID Number. Well completions data retained in the spreadsheet included number operator,

well name, well number, type, completion date, measured depth, and name of reservoir as provided by Drillinginfo.com. This data was used to create a Shapefile of gas well locations. A total of 30,170 gas well locations are in this data set; 18,970 of these wells are in Denton, Tarrant, Parker, and Wise counties (see Figure 3-14).

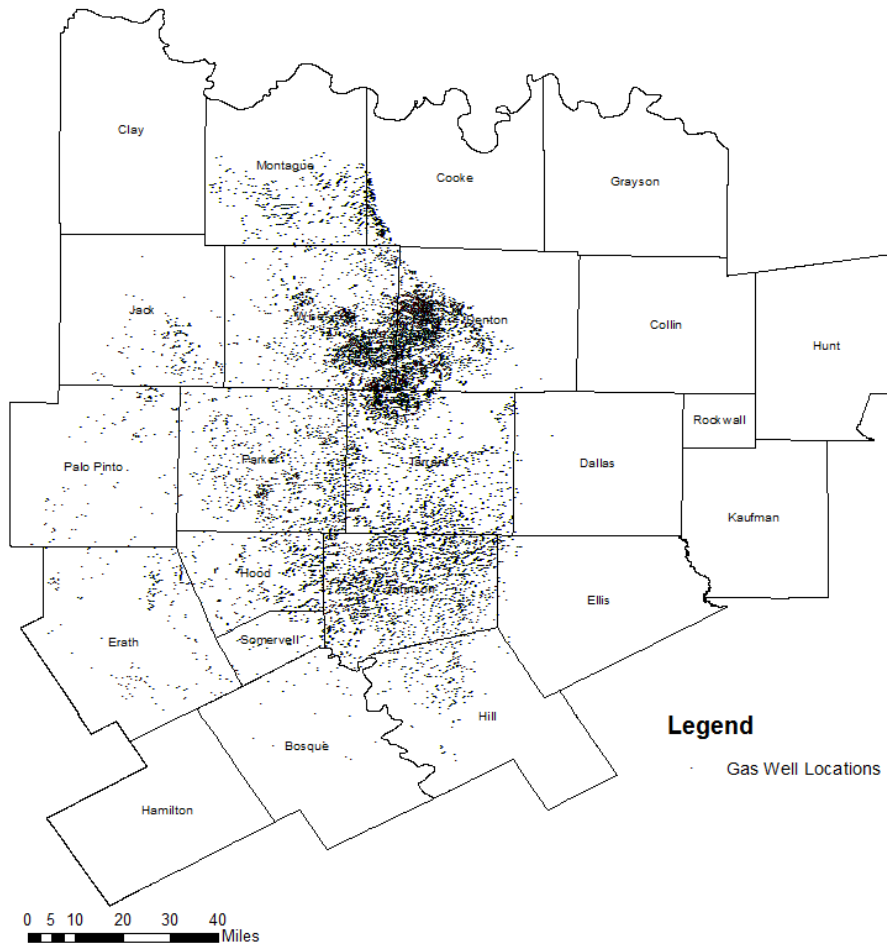


Fig. 3-14: Map of Drilled Gas Well Locations 2001-2014

3.3.2 GAS WELL BOTTOM HOLE PRESSURES

A model of the reservoir pressure over the region in the is model uses flowing Bottom Hole Pressure (BHP) from gas wells prior to production to determine the reservoir pressure exceeding the normal hydrostatic pressure for gas wells in the region.

G-10 completion forms from the Texas Railroad Commission (RRC) are the source of BHP data used in this analysis. G-10 forms are stored at the RRC office headquarters in Austin, TX where the filings are organized by District. The RRC Districts that include Barnett Shale wells are 9, 7B, and 5 (see Figure 3-15) so forms were searched for these districts only.

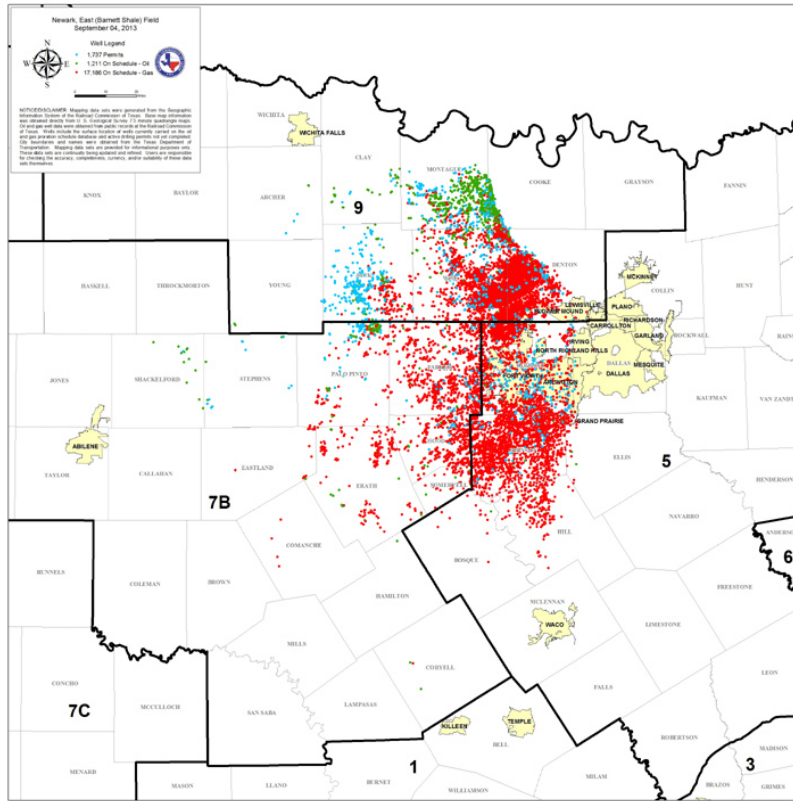


Fig. 3-15: Texas Railroad Commission Districts Encompassing the Barnett Shale
(<http://www.rrc.state.tx.us/oil-gas/major-oil-gas-formations/barnett-shale-information/countyproducing>, 12-9-14)

BHP data from the G-10 forms had to be manually obtained and copied for development of this information or use in this thesis. BHP values were recorded from G-10 forms that were filed for the Purpose of Survey, indicating the reservoir pressure prior to stimulation and production. The wells are identified on the form by the State Gas Well ID number. Since BHP is not a state-mandated field of entry on the G-10, data was not available for

every well. A total of 2,056 well entries were found and utilized in this study. The pressure values are recorded in units of psia (absolute pounds per square inch). The specific location data for the bottom hole pressures was not provided on the G-10 forms, so the locations were found by cross-referencing the State Gas Well ID number with the gas well data set found on Drillinginfo.com (Figure 3-15). A Shapefile of these gas well locations and corresponding BHP values was created in ArcGIS and is shown in Figure 3-16. Unfortunately, as can be seen in Figure 3-16, few wells in Denton County had BHP data, with none reported for Cooke County.

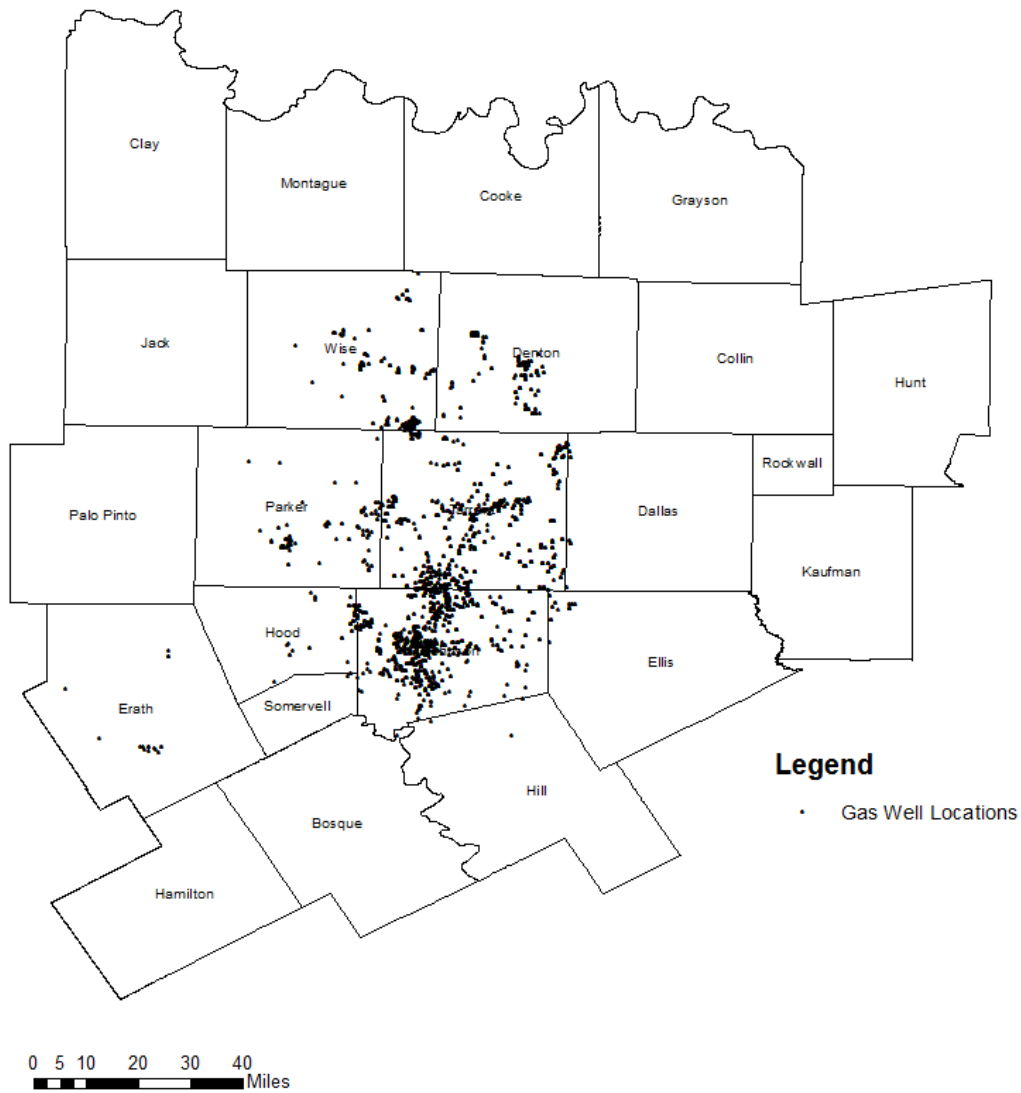


Fig. 3-16: Map of Gas Wells with recorded BHP (a total of 2056 wells shown)

3.3.3 WELL DESIGN AND HYDRAULIC FRACTURING TREATMENT DATA

The Texas Railroad Commission G-1 completion forms are the primary source of well design and hydraulic fracturing data in this study. G-1 forms are stored on the Texas Railroad Commission online servers; forms filed prior to 2010 (<http://www.rrc.state.tx.us/about-us/resource-center/research/online-research-queries/imaged-records-menu/>) are stored on a separate server than those filed after 2010 (<http://webapps.rrc.state.tx.us/CMPL/publicHomeAction.do>). The average directional azimuth (the direction of the lateral section of a wellbore measured in degrees) was recorded from Directional Surveys found on the Railroad Commission servers. Wells that were missing data related to fluid and sand volumes were searched on Fracfocus.org. Using these combined sources, an Excel spreadsheet was created to include wellbore completion data including, Completion Date, Average Directional Azimuth (deg), Intermediate Casing Size (in), Bottom Hole Casing Size (in), Fluid Volume (bbl), Weight of Sand (lbs), Volume of Nitrogen Gas (scf), Shallowest Perforation Depth (ft), Total Vertical Depth (ft), and Measured Depth (ft). Completions data was searched for 2,046 gas wells that are located in Denton, Parker, Tarrant, and Wise Counties. These gas wells were selected based upon their proximity to water well samples used in this study and have no relationship to the BHP data points described in Section 3.3.2. The use of this data set will be further explained in Section 4.3 of this thesis. The locations were cross-referenced from the drillinginfo.com data set. The well locations and corresponding data were plotted in ArcGIS to create a shapefile that was used in further analyses as will be discussed later in this thesis (Figure 3-17).

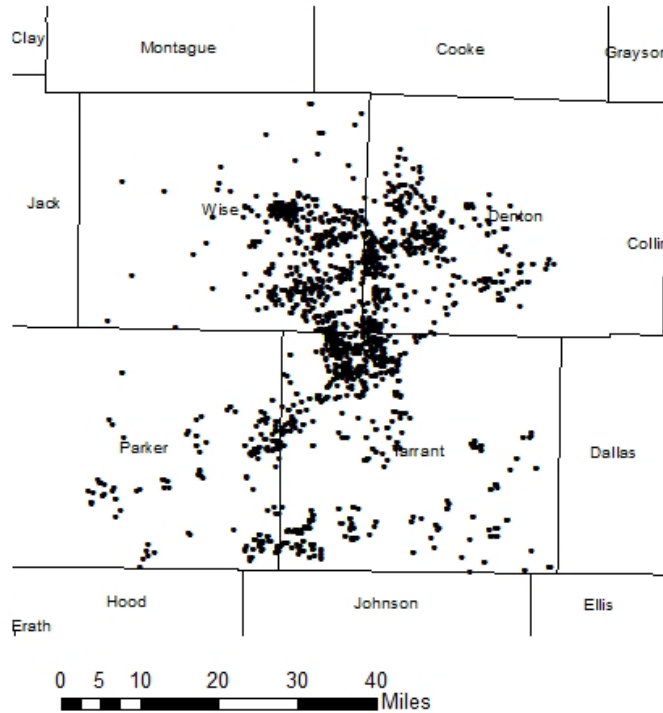


Fig. 3-17: Map of Gas Wells with recorded Wellbore Completions Data

3.3.4 GROUNDWATER DATA

This thesis uses groundwater sample data from two sources, the Texas Water Development Board and the University of Texas Arlington as mentioned earlier. Data was searched on the Texas Water Development Board Website (<http://www.twdb.texas.gov/groundwater/data/gwdb rpt.asp>, 10-7-14) for Bosque, Clay, Collin, Cooke, Dallas, Denton, Ellis, Erath, Grayson, Hamilton, Hill, Hood, Hunt, Jack, Johnson, Kaufman, Montague, Palo Pinto, Parker, Rockwall, Somervell, Tarrant, and Wise counties. This search returned a total of 52,398 groundwater samples (see Table 3-4 and Figure 3-18).

Table 3-4: Summary of Water Quality Data Set from Texas Water Development Board for Study Counties

SAMPLES	WELLS	CONSITUENTS	RANGE OF SAMPLE DATES
52,399	2,480	159	4/12/38 - 8/11/2011

The data set indicates that sampling frequency was not the same for all wells in the region, some wells have multiple samples and others did not. The location of the samples can be seen in Figure 3-18.

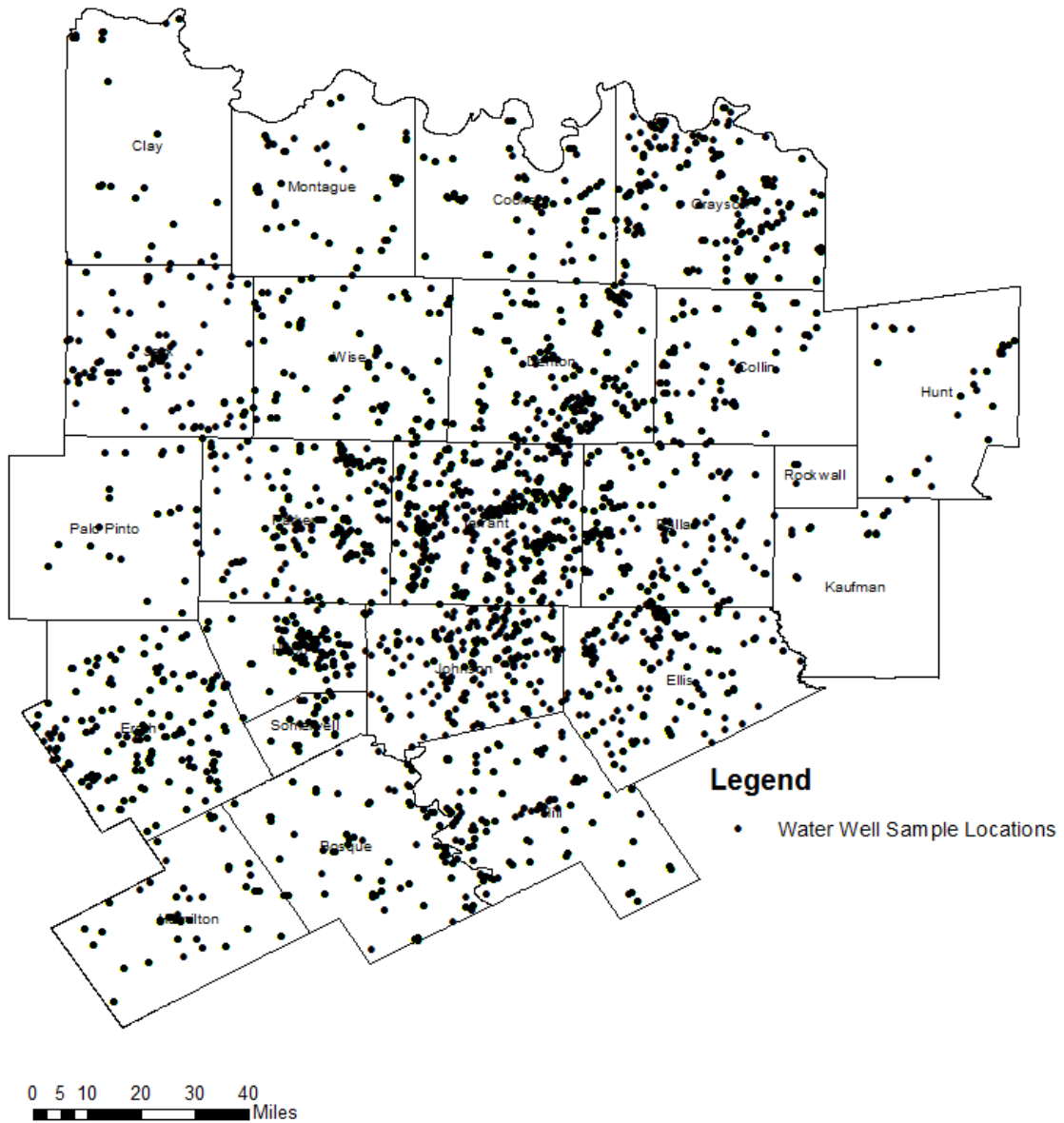


Fig. 3-18: Map of Water Well Locations from Texas Water Development Board Data Set

A selection of the constituent samples from this data was used based upon sample number, relatedness to hydraulic fracturing operations, and availability of historical

reference data. The constituents used in the methods of this thesis are listed in Table 3-7.

The second source of groundwater data, previously mentioned, is from a 2011 UTA study (Fontenot et al., 2013) which collected samples for 101 water wells in Bosque, Denton, Hamilton, Hood, Hunt, Jack, Johnson, Kaufman, Palo Pinto, Parker, Somervell, Tarrant, and Wise counties in 2011, placing a particular emphasis on heavy metal concentrations. A summary of this data set data set is shown in Table 3-5.

Table 3-5: UTA Groundwater Samples taken in 2011

Constituent	Number of Samples	Maximum Sample Value	Minimum Sample Value
DO (mg/L)	96	11.55	0.00
Water Temperature (°C)	100	33.63	20.35
pH	100	9.33	6.18
Conductivity (ms/cm)	100	2.97	0.49
Specific Conductance (ms/cm)	100	2.90	0.51
ORP (mV)	99	319.45	-916.80
Salinity (mg/L)	100	1.55	0.26
TDS (mg/L)	100	0.00	0.00
Methanol (mg/L)	35	328.99	0.76
Ethanol (mg/L)	23	11.26	0.15
Total Arsenic (ppb)	101	161.15	2.21
Total Selenium (ppb)	101	108.70	0.51
Total Strontium (ppb)	101	18,195.02	52.40
Total Barium (ppb)	101	173.69	2.87

The research team from UTA acquired more samples in the region in 2014. A data set was collected for 550 wells and 67 constituents in Collin, Dallas, Denton, Ellis, Hill, Hood, Johnson, Montague, Parker, Somervell, Tarrant, Wise counties. A summary of the constituents tested in this data set is shown in Table 3-6.

Table 3-6: UTA Groundwater Samples taken in 2014

Constituent	Maximum Sample Value	Minimum Sample Value
Temperature (°C)	56.5	6.1
DO (mg/L)	29.2	0.36
Specific Conductance (mS/cm)	5.13	0.24
TDS (mg/L)	3328	68.5
Salinity (mg/L)	8.51	0.11
pH	9.43	5.34
ORP (mV)	680	-269.4
Methanol (mg/L)	44.62	ND
Ethanol (mg/L)	394.19	0.2
Dichloromethane (mg/L)	2.94	0
n-Butanol (mg/L)	0	0
2-Ethyl Hexanol (mg/L)	0	0
1,2-Propanediol (mg/L)	0	0
EG Butyl Ether (mg/L)	0	0
Propargyl Alcohol (mg/L)	26.43	0.5
Isopropyl Alcohol (mg/L)	9.39	0.61
n-Propanol (mg/L)	0	0
Ethylene Glycol (mg/L)	0	0
Acetaldehyde (mg/L)	4.91	0.05
Chloroform (mg/L)	5.05	0.01
Cyclohexane (mg/L)	1.34	0.01
Benzene (mg/L) 0.005mg/L	0.09	0.02
Trichloroethylene (mg/L)	0.04	0.03
Toluene (mg/L) 1.0mg/L	0.52	0
Ethyl Benzene (mg/L) 0.7mg/L	0.03	0.01
1,2,3-Trimethyl Benzene (mg/L)	0	0
Cumene (mg/L)	0	0
m,p-Xylene (mg/L)	0.02	0
o-Xylene (mg/L)	0.05	0.01
Mesitylene (mg/L)	0	0
Benzyl Chloride (mg/L)	0	0
Formaldehyde (mg/L)	0	0
Glutaraldehyde (mg/L)	0	0
Dimethyl Formamide (mg/L)	0	0
Naphthalene (mg/L)	0	0

Table 3-6 Continued

1-Methyl Naphthalene (mg/L)	0	0
2-Methyl Naphthalene (mg/L)	0	0
1-Naphthol (mg/L)	0	0
2-Naphthol (mg/L)	0	0
Bisphenol A (mg/L)	0	0
d-Limonene (mg/L)	0	0
Acetophenone (mg/L)	0	0
Fluoride (mg/L)	5.1	0.03
Chloride (mg/L)	3373.78	0.96
Bromide (mg/L)	6.41	0.03
Nitrate (mg/L)	55.66	0.04
Sulfate (mg/L)	889.32	0.39
Acetate (mg/L)	6.95	0.09
Formate (mg/L)	0.46	0.05
Chlorate (mg/L)	8.92	0.12
Chromate (mg/L)	7.89	0.33
Perchlorate (mg/L)	0	0
Arsenic (mg/L)	0.11	0
Selenium (mg/L)	0.02	0
Barium (mg/L)	4.38	0.01
Beryllium (mg/L)	0.08	0
Cobalt (mg/L)	0.49	0.01
Chromium (mg/L)	0.34	0.34
Copper (mg/L)	1.37	0.01
Iron (mg/L)	12.31	0.01
Molybdenum (mg/L)	0.45	0
Nickel (mg/L)	0.55	0.01
Strontium (mg/L)	8.97	0.1
Titanium (mg/L)	5.35	0.1
Vanadium (mg/L)	0.7	0.1
Zinc (mg/L)	12.05	0.01
Zirconium (mg/L)	0.88	0.1

These water quality data sets enhance the analyses in this thesis as there are a large number of samples and constituents taken within a similar time frame with identical sampling procedures. The UTA water quality data does not include an Aquifer ID reference, but a majority of the samples included a water well depth. The samples

without a well depth were not used in this study. The samples with a water well depth were analyzed to determine if they fit within the confines of the Paluxy Aquifer Model (described in Section 3.2). Using the extract Multi-Values to Points function in ArcGIS, the associated vertical depths of the Paluxy, Woodbine, Hossten, and Hensell formations were extracted and cross-referenced to the vertical depth of the UTA samples. The samples that matched the depth of the Paluxy Aquifer model were retained for the analyses. The majority of the samples are within the most active region of the Barnett Shale. The well locations are given in World Geodetic System 1984 coordinates for latitude and longitude. The locations of the samples used from the UTA data sets are shown in Figure 3-19.

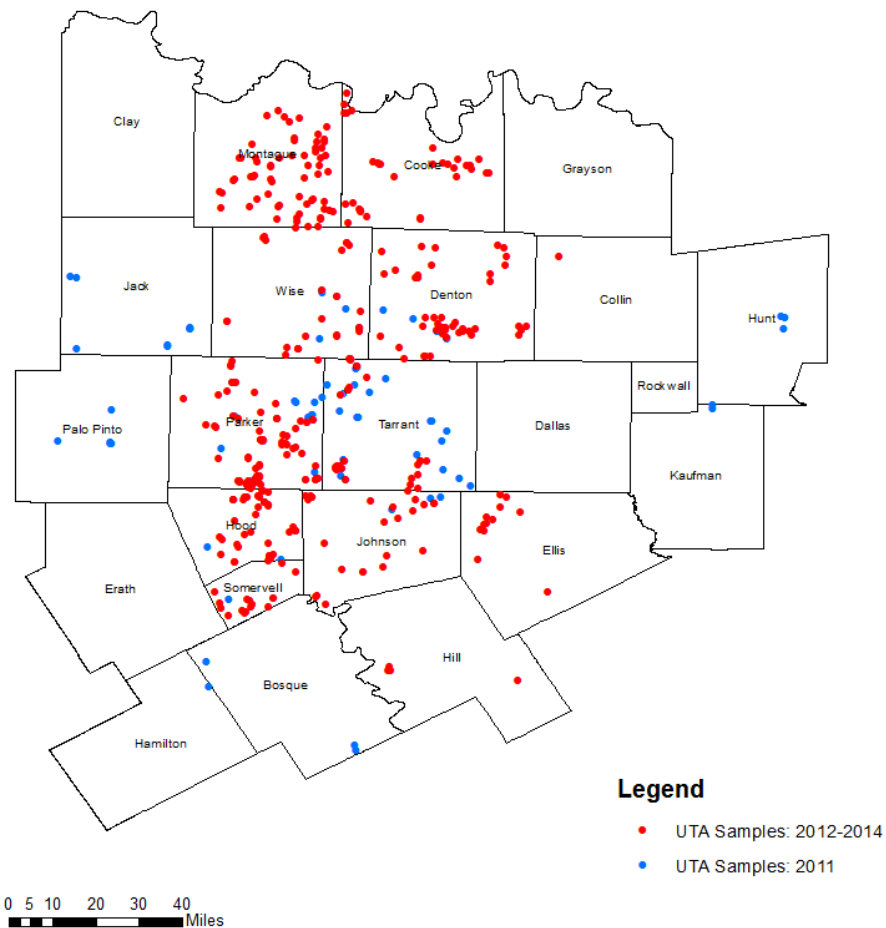


Fig. 3-19: Map of Water Well Locations from University of Texas Arlington Data Set

TWDB data were combined with data from the UTA water well data sets to form the water quality dataset for the study. It is important to note that the TWDB data did not have well identifiers that could be cross-referenced to the UTA dataset; thus it was not possible to determine which wells from the TWDB dataset had been sampled in the UTA study. The constituents serving as indicators in this thesis were chosen based upon sample number, relatedness to hydraulic fracturing operations, and availability of historical reference data. The US House Committee on Energy and Commerce Report of April 2011 (Waxman, Markey & DeGette, 2011) was used as a reference, but also constituents contained in flowback water. The flowback water contains heavy metals, halogens, and radioactive materials that are naturally occurring. It is presumed that some of the formation constituents found in flowback may affect the groundwater. The resulting water quality data set used in this thesis is summarized in Table 3-7.

Table 3-7: TWDB-UTA Combined Groundwater Data Set

CONSTITUENT NAME	TYPE	UNITS	SOURCE	DATE RANGE	NUMBER OF SAMPLES	NUMBER OF NON-DETECTS
Alpha	Dissolved	pc/L	TWDB	1976-2011	380	-
Aluminum	Dissolved	ppb	TWDB	1939-2011	786	-
Arsenic	Total	ppb	TWDB	1949-2007	116	-
	Total	ppb	UTA	2011	75	-
	Total	ppb	UTA	2012-2014	379	9
Barium	Total	ppb	TWDB	1985-2007	88	-
	Total	ppb	UTA	2011	75	-
	Total	ppb	UTA	2012-2014	379	8
Benzene	Total	mg/L	UTA	2012-2014	379	356
Beryllium	Total	ppb	TWDB	1994-2007	87	-
	Total	ppb	UTA	2012-2014	379	260
Boron	Dissolved	ppb	TWDB	1948-2011	756	-
Bromide	Total	mg/L	UTA	2012-2014	379	255
Bromide	Dissolved	mg/L	TWDB	1988-2011	738	-
Chloride	Total	mg/L	UTA	2012-2014	379	-
Copper	Total	ppb	TWDB	1980-2007	124	-
	Total	ppb	UTA	2012-2014	379	4

Table 3-7 Continued

Dissolved Oxygen	Dissolved	mg/L	TWDB	1983-2011	33	-
	Dissolved	mg/L	UTA	2011	73	-
	Dissolved	mg/L	UTA	2012-2014	358	-
Ethanol	Total	mg/L	UTA	2011	75	58
			UTA	2012-2014	379	200
Ethyl Benzene	Total	mg/L	UTA	2012-2014	379	361
Iron	Total	ppb	TWDB	1923-2007	1520	-
	Total	ppb	UTA	2012-2014	379	90
Methanol	Total	mg/L	UTA	2011	75	49
			UTA	2012-2014	379	358
Molybdenum	Total	ppb	UTA	2012-2014	379	22
Molybdenum	Dissolved	ppb	TWDB	1989-2011	756	-
Nickel	Total	ppb	TWDB	1994-2007	82	-
	Total	ppb	UTA	2012-2014	379	62
Nitrate	Total	mg/L	TWDB	1975-2007	161	-
	Total	mg/L	UTA	2012-2014	379	221
pH		pH	UTA	2011	73	-
		pH	UTA	2012-2014	379	-
Phosphorus	Dissolved	mg/L	TWDB	1952-2011	316	-
Radium 226	Dissolved	pc/L	TWDB	1977-2011	150	-
Radium 228	Dissolved	pc/L	TWDB	1988-2011	150	-
Redox Potential		mV	TWDB	1990-1999	269	-
		mV	UTA	2011	73	-
		mV	UTA	2012-2014	379	-
Selenium	Total	ppb	TWDB	1977-2007	106	-
	Total	ppb	UTA	2011	74	-
	Total	ppb	UTA	2012-2014	379	28
Sulfate	Total	mg/L	UTA	2012-2014	379	1
Temperature		°C	TWDB	1963-2011	715	-
		°C	UTA	2011	73	-
		°C	UTA	2012-2014	379	-
Total Dissolved Solids	Dissolved	mg/L	UTA	2011	73	-
	Dissolved	mg/L	UTA	2012-2014	379	-
Vanadium	Dissolved	ppb	TWDB	1989-2011	734	-
Zinc	Total	ppb	TWDB	1980-2007	135	-
	Total	ppb	UTA	2012-2014	379	182

3.4 PRELIMINARY DATA ANALYSIS

3.4.1 BOTTOM HOLE PRESSURE DATA

An analysis of the flowing bottom hole pressure (BHP) data was completed to determine if the recorded values fall in a range that would be expected based upon the literature descriptions of reservoir pressures in the region. As described in Section 3.3.2, the BHP values in question refer to the Flowing Bottom Hole Pressure that is the reservoir pressure in the Barnett Shale formation that exceeds a normal geopressure gradient. The normal geopressure gradient is based on density of a hydrostatic column shown in Equation 3-2 (adapted from http://www.engineeringtoolbox.com/hydrostatic-pressure-water-d_1632.html), where $P = \rho g h$, [3-2]

where P is the hydrostatic pressure, h is the height of the column, ρ is the density of the fluid, and g is the gravitational constant. The calculations of the hydrostatic gradient, per foot of depth, using Equation 3-2 is calculated as

$$0.433 \frac{\text{psi}}{\text{ft}} = \left[\left(1.940 \frac{\text{slugs}}{\text{ft}^3} \right) \left[\left(\frac{1 \text{ lb} \cdot \text{s}^2}{\text{ft}} \right) \times 1 \frac{\text{ft}^2}{144 \text{ in}^2} \right] \left(32.174 \frac{\text{ft}}{\text{s}^2} \right) \times 1 \text{ ft} \right] \frac{1}{\text{ft}}$$

The gradient for the total reservoir pressure gradient, that is the geopressure exceeding 0.433 psi/ft, is determined by adding the flowing bottom hole pressure to normal geopressure and dividing by the total vertical depth. This function is defined in Equation 3-3, where

$$\text{Reservoir Pressure Gradient} \left(\frac{\text{psi}}{\text{ft}} \right) = \frac{\text{Flowing BHP (psi)} + \left(0.433 \frac{\text{psi}}{\text{ft}} \times \text{Vertical Shale Depth (ft)} \right)}{\text{Vertical Shale Depth (ft)}}. \quad [3-3]$$

The excess pressure in the rock is due to the conversion of oil to gas over time, as gas is generated it will expand, but it is compressed as it is trapped in the reservoir rock (Barker, 1990). In gas bearing reservoirs, the pressure gradient may be close to a

normal hydrostatic pressure gradient, but in some cases the gradient could be as high as 1.0 psi/ft depending on the duration of thermal cracking and specific kerogen properties (Barker, 1990). In the Barnett Shale, the typical reservoir pressure gradient is 0.52 psi/ft (Bowker, 2007). For reference, Table 3-8 shows the flowing Bottom Hole Pressures that correspond to reservoir pressure gradients of 0.433 psi/f, 0.520 psi/ft, and 1.000 psi/ft at 6,500 ft and 8,000 ft of vertical depth (typical Barnett well depths).

Table 3-8: Flowing Bottom Hole Pressure as a function of depth for Pressure Gradients of 0.433 psi/ft, 0.520 psi/ft, and 1.000 psi/ft.

Pressure Gradient (psi/ft)	Depth (ft)	Reservoir Pressure (psi)	Flowing BHP (psi)	Depth (ft)	Reservoir Pressure (psi)	Flowing BHP (psi)
0.433	6,500	2,815	0	8,000	3,464	0
0.520	6,500	3,380	566	8,000	4,160	696
1.000	6,500	6,500	3,686	8,000	8,000	4,536

As Table 3-8 demonstrates, there is no BHP at a normal pressure gradient, but in a typical Barnett well with a gradient of 0.52 psi/ft pressure gradient, and a vertical depth between 6,500 ft and 8,000 ft, the expected flowing BHP is between 560 psi and 700 psi.

Using the data described in section 3.3.2, the local depth of the Barnett Shale at each BHP data point was extracted in ArcGIS from the Barnett Shale contour plot shown in Figure 3-4. By substituting these values for the data set into Equation 3-1, the highest reservoir pressure gradient calculated from the data points was 0.97 psi/ft at a vertical depth of 8,674, ft and BHP of 4,620. This well is an exception, however, as the average of the remaining data was 715 psi. The average vertical depth of these data points is 7,348 ft, and the average reservoir pressure gradient of the remaining data is 0.53 psi/ft, which corresponds to the literature references for reservoir pressure gradient in the region (Bowker, 2007). A contour of the BHP data was created in ArcGIS using the Radial Basis Function in ArcGIS. This contouring function excludes the outliers as can

be seen in Figure 3-20, where the maximum BHP calculated by the contour is 3,298 psi rather than 4,620 psi as mentioned.

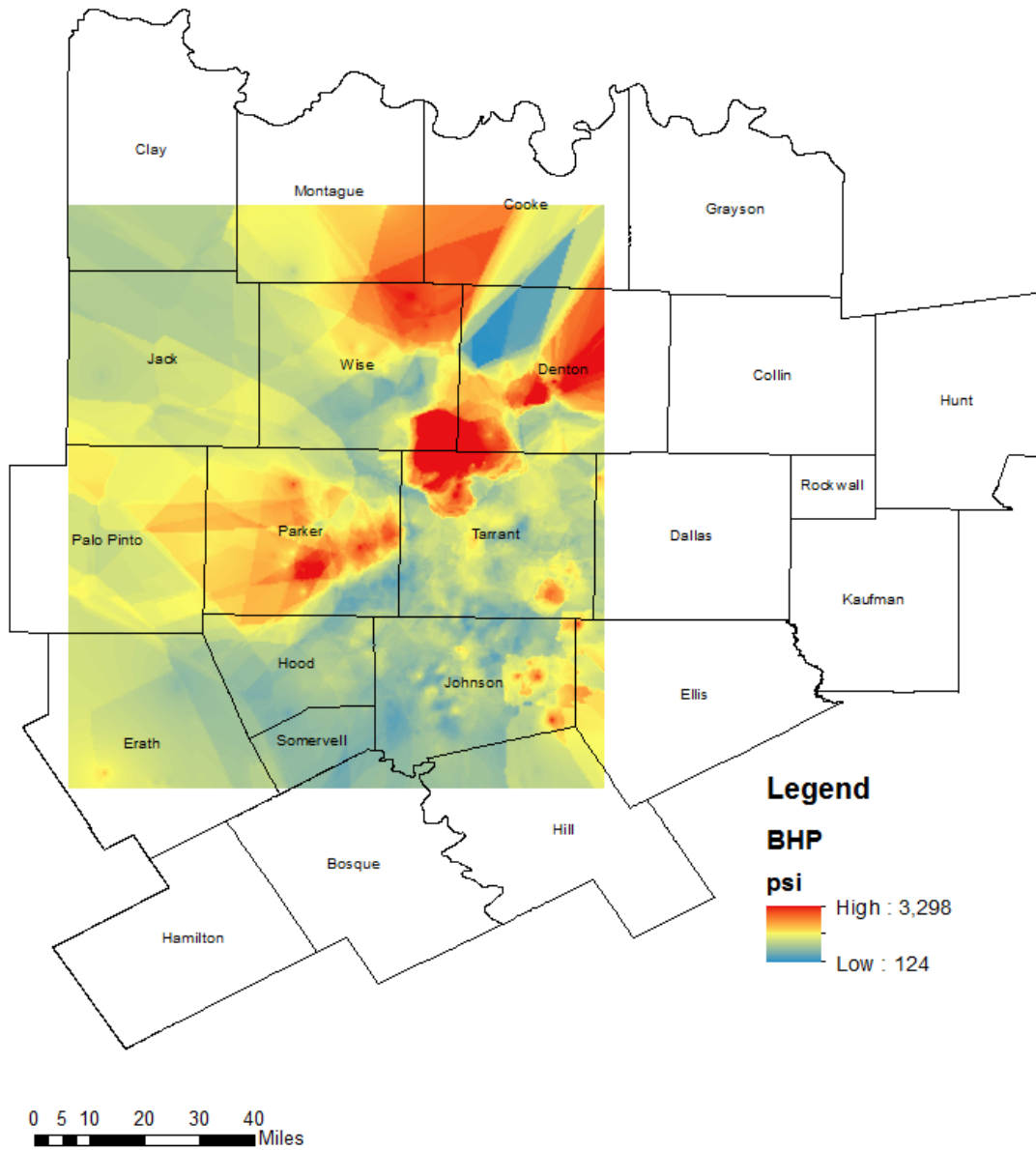


Fig. 3-20: Contour Plot of Flowing BHP Data

The analysis of the BHP data that was collected corroborates the expected reservoir pressure gradient for the region making it appropriate for modeling in this thesis.

The thesis proposes that the reservoir pressure of the Barnett Shale is the mobilizing mechanism of water contaminants, where stray gases lift contaminants to the

water aquifer through the annular section of the wellbore. An unsealed annulus could exist before the hydraulic fracturing treatment due to an insufficient cement job, or else the release of natural gas at high pressures due to hydraulic fracturing has caused a crack in the cement seal. In either scenario, the annular pathway may be narrow on the scale of nanometers (nm), and referred to as a micro-annulus. In order to determine that contaminant mobilization through a micro-annulus is possible, calculations were completed using a formula proposed by Deremble et al., 2010 to predict fluid flow velocity through a micro-annulus in a vertical wellbore, shown in Equation 3-4 (adapted

$$\text{from Deremble et al., 2010), } v_f = -\frac{w^2}{12\mu_f} \left(\frac{dP}{ds} + \rho g \cos(\alpha) \right), \quad [3-4]$$

where v_f is the mean fluid velocity, w is the width of the defect, μ_f is the effective fluid viscosity, $\frac{dP}{ds}$ is the change in reservoir pressure over a vertical well distance, ρ is the fluid density, g is the gravitational constant, and α is the angle of the wellbore.

This equation was applied to the average Barnett Shale well depth for the gas wells in the data set. Using the extract Multi-Values to Points function in ArcGIS, the depth of the Barnett shale was extracted at each gas well location from the plot in Figure 3-6, as well as the corresponding Paluxy Aquifer depth from the contour plot in Figure 3-10. The average Barnett well depth in the model is 7,375 ft and the average depth of the Paluxy Aquifer is 635 ft. The average thickness between them is 6,740 ft, this was used to calculate the pressure differential (dP/ds). The values in Equation 3-4 were calculated as follows:

$$\text{Average Reservoir Pressure of Barnett Shale} = (0.53 \text{ psi/ft}) \times (7,375 \text{ ft}) = 3,909 \text{ psi}$$

$$\text{Average Reservoir Pressure of Trinity Aquifer} = (0.433 \text{ psi/ft}) \times (635 \text{ ft}) = 275 \text{ psi}$$

$$dP = 275 \text{ psi} - 3,909 \text{ psi} = -3,634 \text{ psi}$$

$$\text{Average Thickness} = ds = 6,740 \text{ ft}$$

$$dP/ds = -3,634 \text{ psi} / 6,740 \text{ ft} = -0.54 \text{ psi/ft.}$$

For the purposes of this calculation, fluid properties of density and viscosity were derived for a theoretical dry gas containing 85% methane and 15% carbon dioxide. Values for fluid density and viscosity were taken from the Table 1.1 in the SPE Textbook Series Volume 5, Gas Reservoir Engineering (Lee & Wattenbarger, 1996, p. 2). The calculations are as follows:

$$\text{Gas Density of CO}_2 = 0.1160 \text{ lb/ft}^3$$

$$\text{Gas Density of Methane} = 0.04228 \text{ lb/ft}^3$$

$$\text{Gas Viscosity of CO}_2 = .01439 \text{ cP}$$

$$\text{Gas Viscosity of Methane} = 0.01078 \text{ cP}$$

$$\text{Density of Gas Mixture} = 0.85(0.04228 \text{ lb/ft}^3) + 0.15(0.1160 \text{ lb/ft}^3) = 0.053 \text{ lb/ft}^3$$

$$\text{Gas Viscosity} = 0.85(.01078 \text{ cP}) + 0.15(0.01439 \text{ cP}) = 0.0113 \text{ cP}.$$

The gravitational constant is 32.3 ft/s², and in a vertical well, $\alpha = 0$. According to Deremble et al. (2010), a defect width may be between 10-100 μm . Using Excel, the calculated values for gas density, gas viscosity, and corresponding conversion factors were substituted into Equation 3-4 and the fluid velocity was determined for 10 μm and 100 μm (see Table 3-9).

Table 3-9: Range of Fluid Velocities in a Micro-Annulus

Width of Defect	Velocity
μm	ft/day
10	81.4
100	8,137

These calculations show that gas migration through the micro-annulus from the shale to the water aquifer is on the scale of 1-10 days. The calculation is based upon the reservoir pressure prior to treatment, however, the added pressure effects due to the

hydraulic fracturing treatment process may increase the pressure differential, and possibly increase the initial fluid velocity through the micro-annulus. Thus, the aforementioned calculations demonstrate the potential for gas migration in the annular section of a wellbore and the potential for contamination of groundwater since natural gas contains contaminants that through contact with the water table may degrade the quality of the groundwater.

The analysis and calculations in the section above have demonstrated that the depth of the Barnett shale affects the value of the overall pressure gradient. The methods use a contour plot of the RPG, rather than the BHP values alone as was shown in Figure 3-20. A contour plot of the RPG was created by overlaying a grid of data points on the BHP plot as in Figure 3-21.

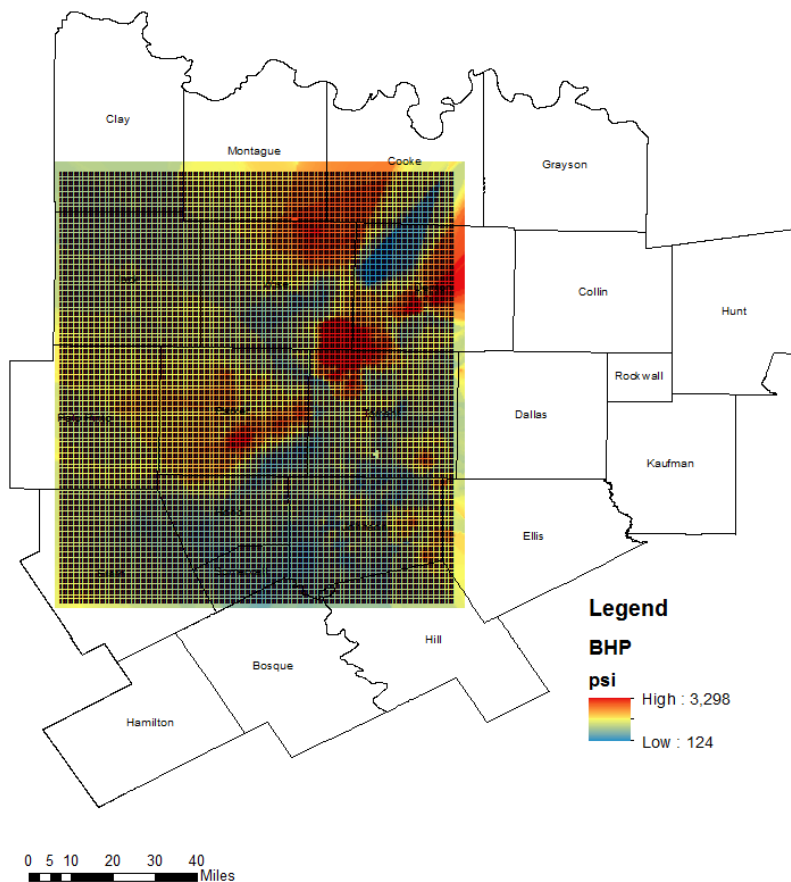


Fig. 3-21: Grid of Data Points to create model of RPG

At each data point, the corresponding BHP and Barnett Shale depth was extracted in order to calculate the RPG for each point using Equation 3-2. The RPG values in the grid were contoured in ArcGIS using the Inverse Distance Weighting function and the resulting contour plot of the RPG is shown in Figure 3-22.

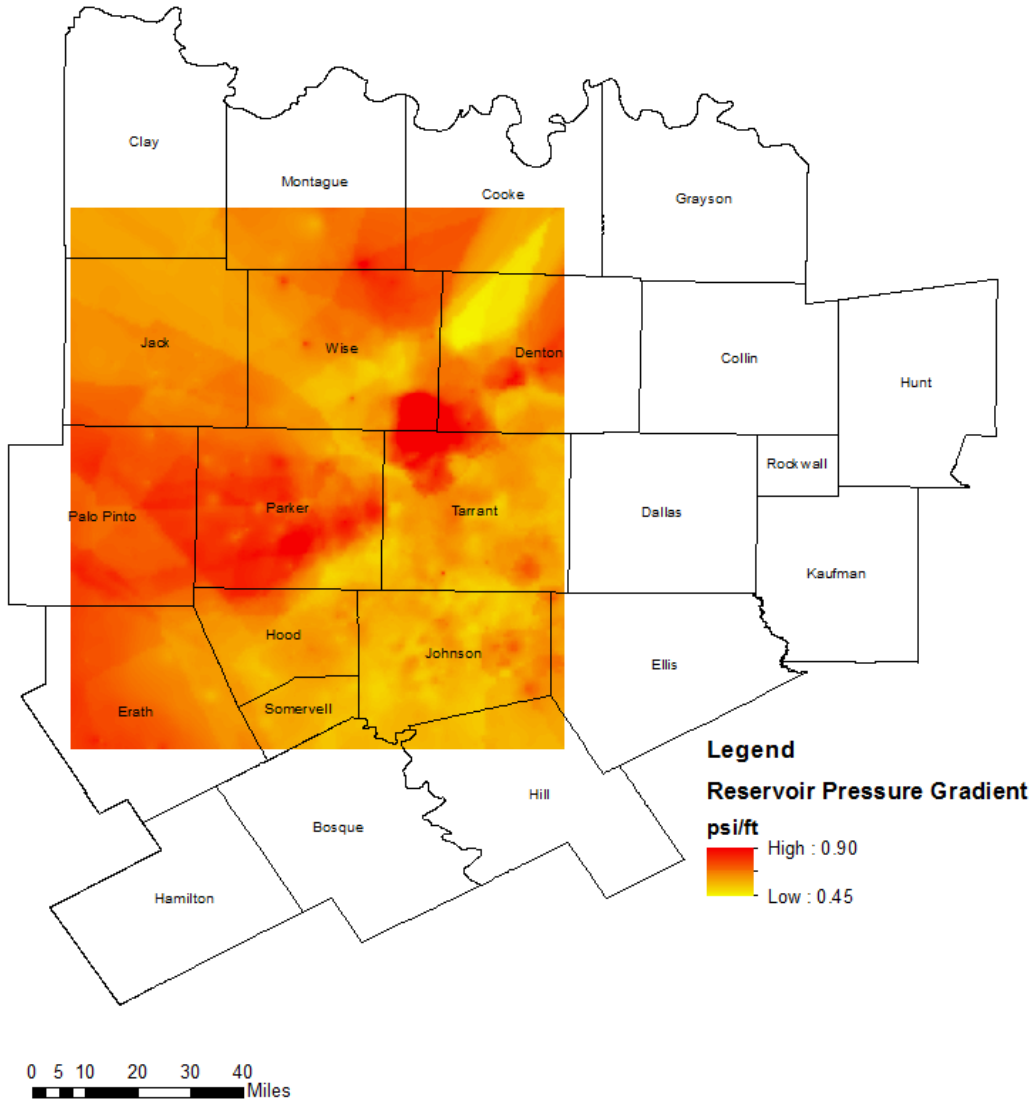


Fig. 3-22: Map of Barnett Shale Reservoir Pressure Gradient over Study Region

The range of the reservoir pressure gradients in this model layer are between 0.45 – 0.90 psi/ft as can be seen from Figure 3-22.

3.4.2 GROUNDWATER DATA

Water quality data was plotted both spatially (in ArcGIS) and temporally to examine trends in the raw data. For each county in the study area, all data available for the constituents listed in Table 3-7 was plotted in ArcGIS using relative size symbology to denote the relative concentration of the samples taken. This is shown in Figure 3-23 for Dissolved Alpha (pc/L) samples over the region, the remaining plots are located in Appendix A.

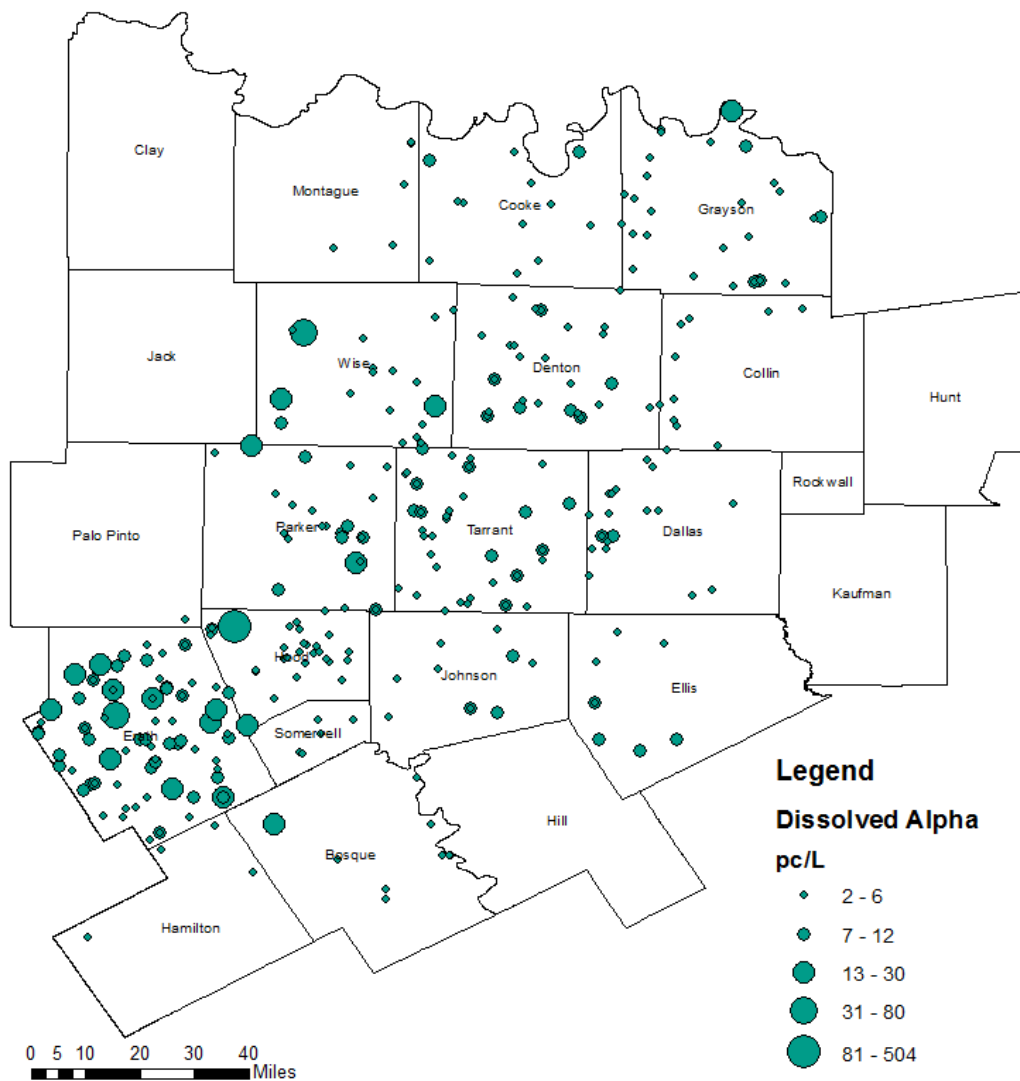


Fig. 3-23: Water samples locations denoted by relative measurements in Dissolved Alpha (pc/L)

From the plots in Appendix A (and the examples shown above for Dissolved Alpha in Figure 3-223) denoting relative constituent concentrations, it can be seen that there is some clustering of sample concentrations in the region, but it is not the same among all the constituents.

In order to determine trends in the data, if any, constituents with historical and current samples were plotted temporally using only samples taken in Denton, Hood, Johnson, Somervell, Parker, Tarrant and Wise counties, the counties with highest number of gas wells. Water sample measurements for the constituent concentrations for the 7 counties were plotted versus time in order to see if a significant trend in water quality changes could be gleaned for the time frame between 2001 and in 2011 (see Figures 3-24 to 3-41).

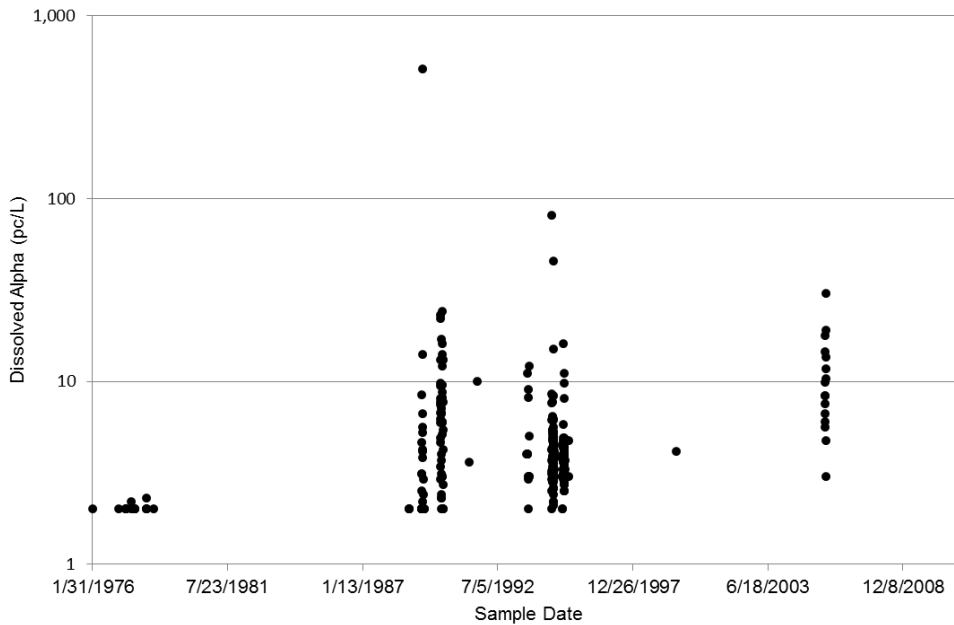


Fig. 3-24: Sample of Dissolved Alpha from 1988-2011 in Denton, Johnson, Somervell, Parker, Tarrant, and Wise counties

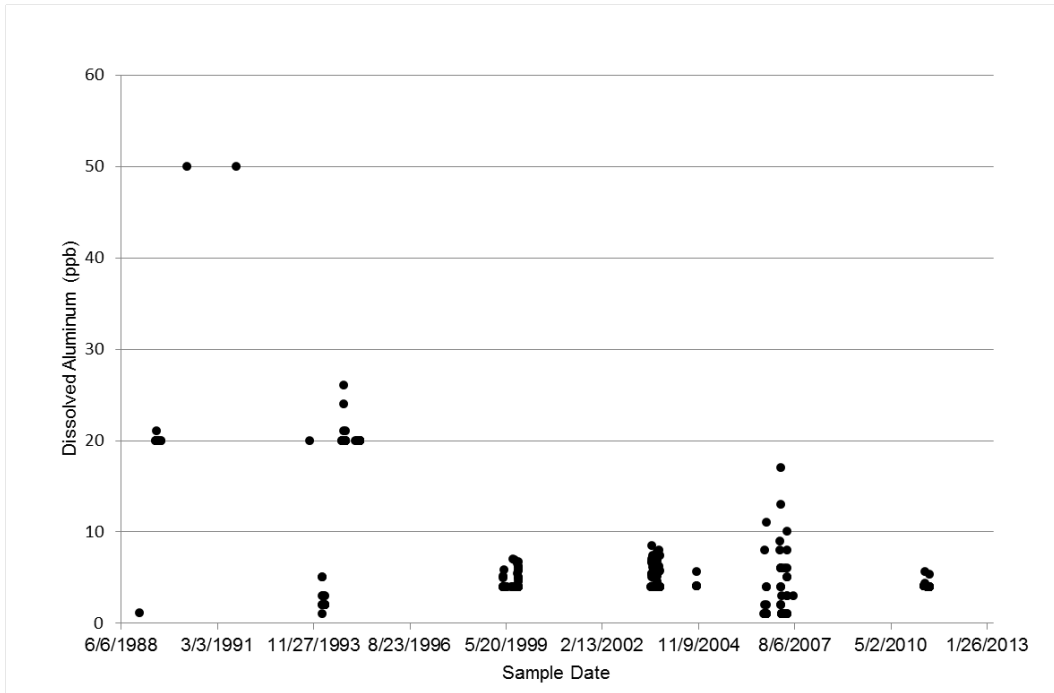


Fig. 3-25: Sample of Dissolved Aluminum from 1988-2011 in Denton, Johnson, Somervell, Parker, Tarrant, and Wise counties

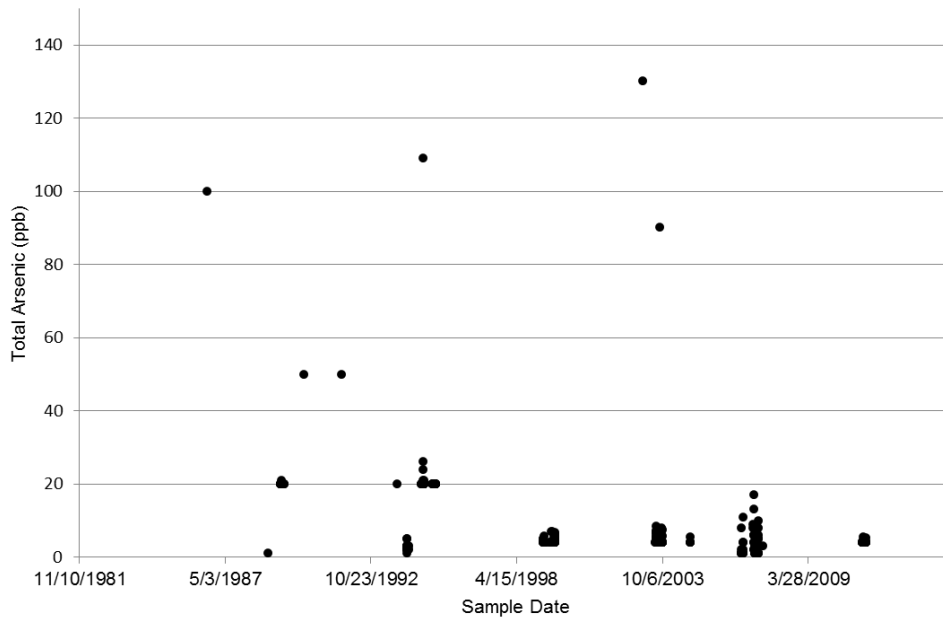


Fig. 3-26: Samples of Total Arsenic from 1985-2011 in Denton, Johnson, Somervell, Parker, Tarrant, and Wise counties

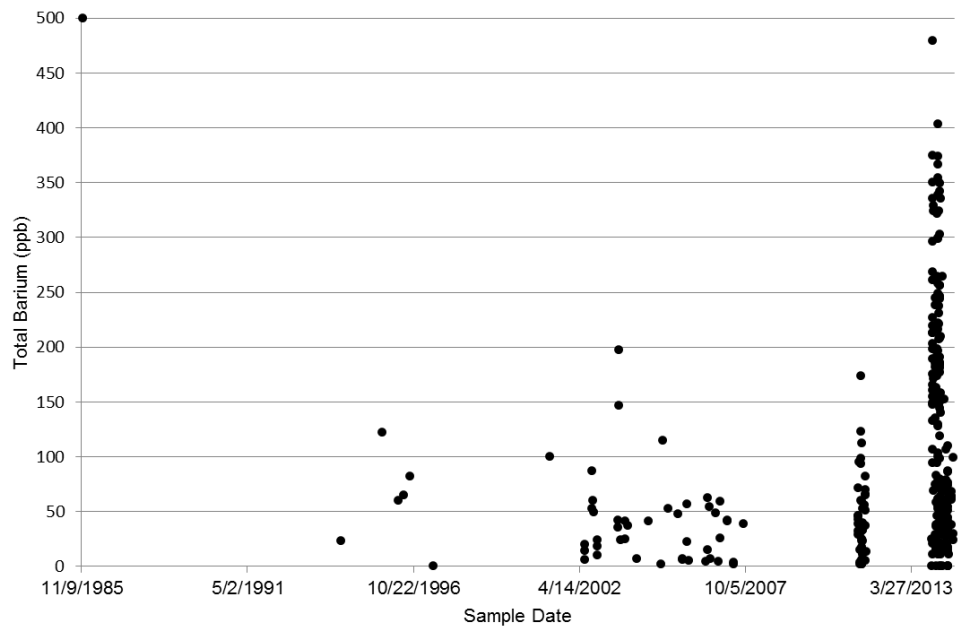


Fig. 3-27: Samples of Total Barium from 1985-2011 in Denton, Johnson, Somervell, Parker, Tarrant, and Wise counties

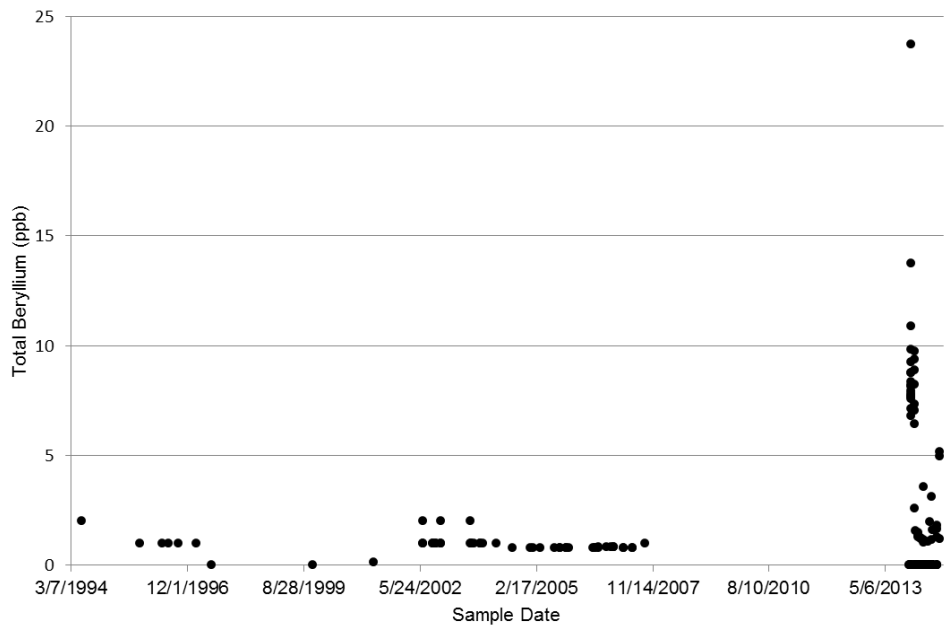


Fig. 3-28: Samples of Total Beryllium from 1985-2011 in Denton, Johnson, Somervell, Parker, Tarrant, and Wise counties

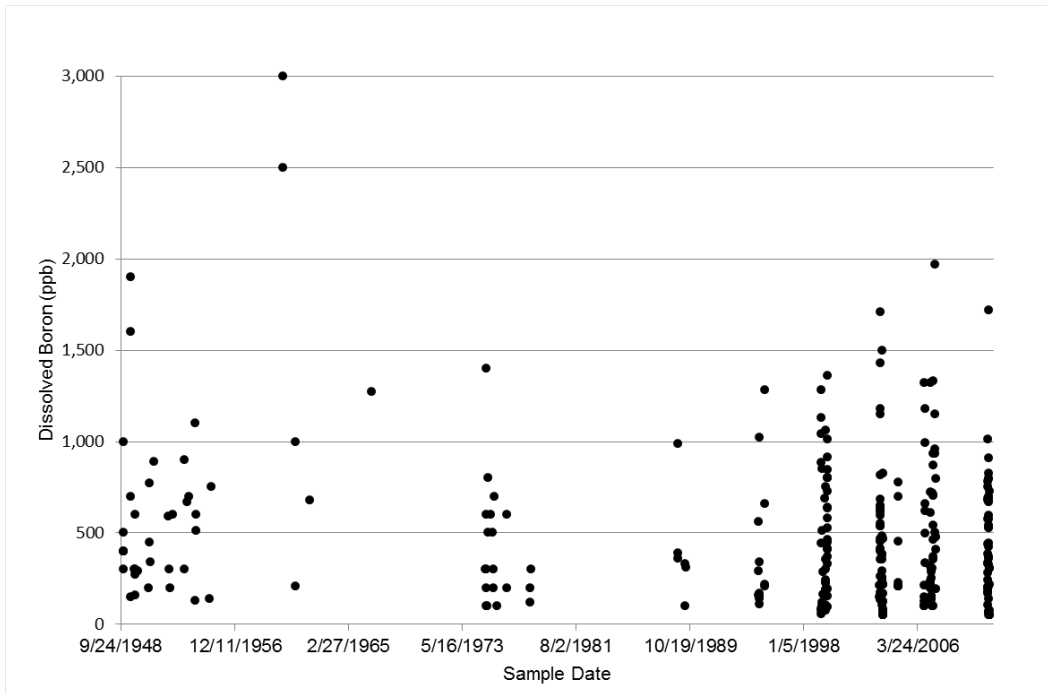


Fig. 3-29: Samples of Dissolved Boron from 1988-2011 in Denton, Johnson, Somervell, Parker, Tarrant, and Wise counties

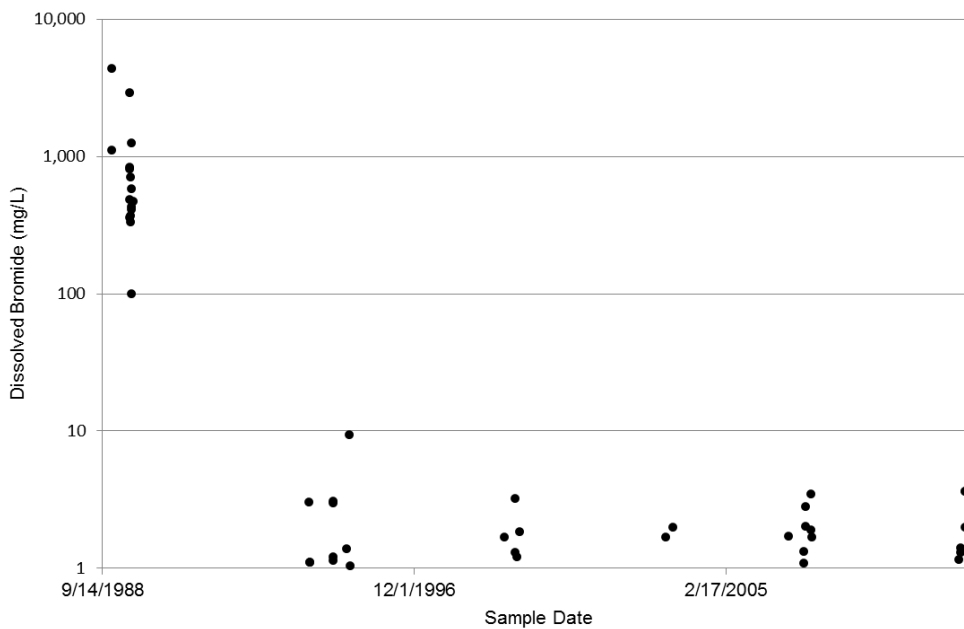


Fig. 3-30: Samples of Dissolved Bromide from 1988-2011 in Denton, Johnson, Somervell, Parker, Tarrant, and Wise counties

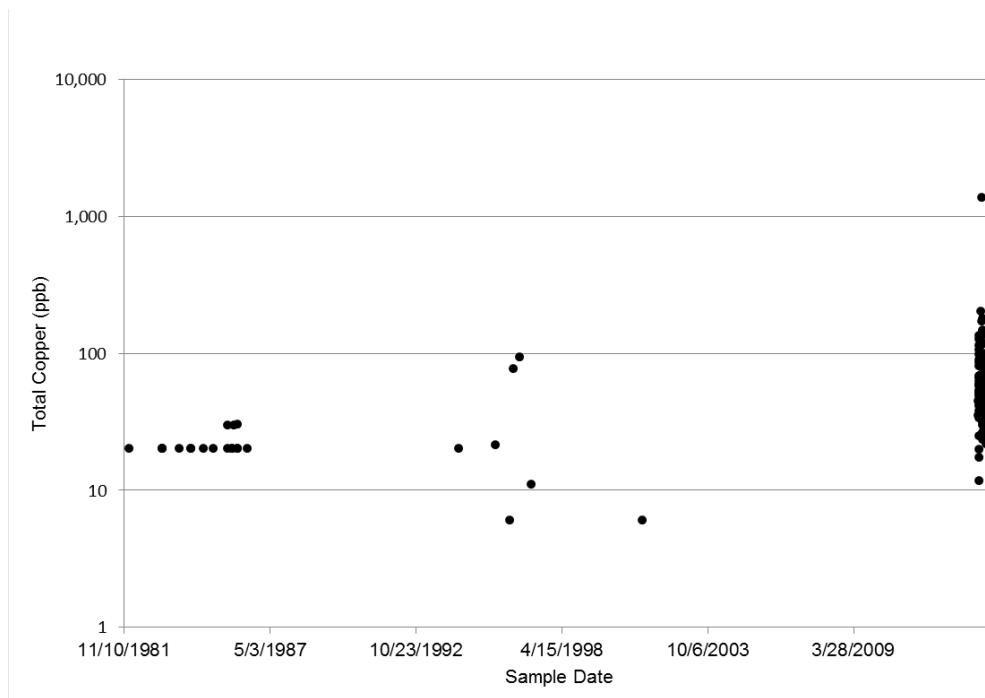


Fig. 3-31: Samples of Total Copper from 1988-2011 in Denton, Johnson, Somervell, Parker, Tarrant, and Wise counties

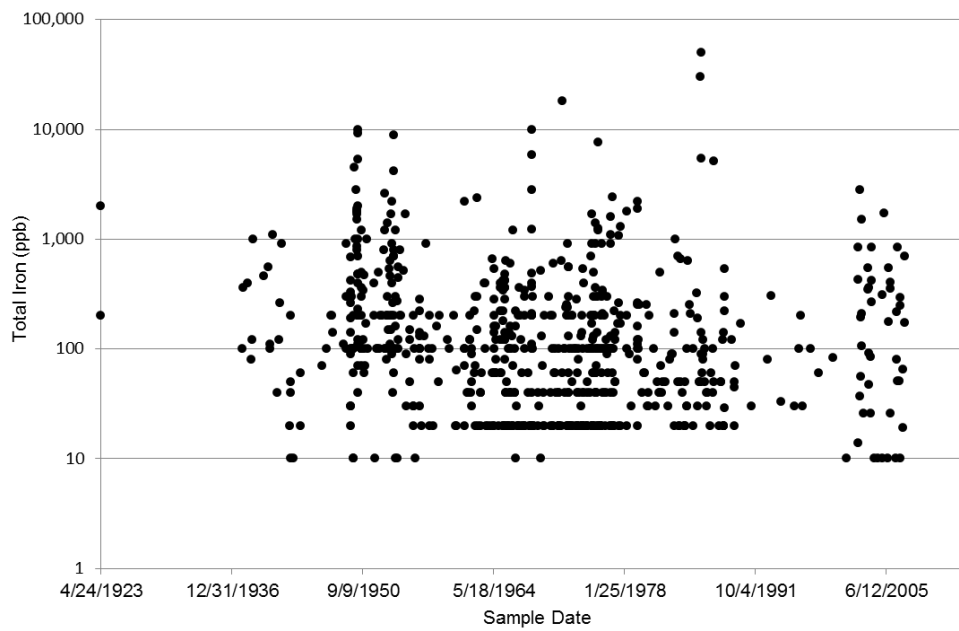


Fig. 3-32: Samples of Dissolved Iron from 1986-2011 in Denton, Johnson, Somervell, Parker, Tarrant, and Wise counties

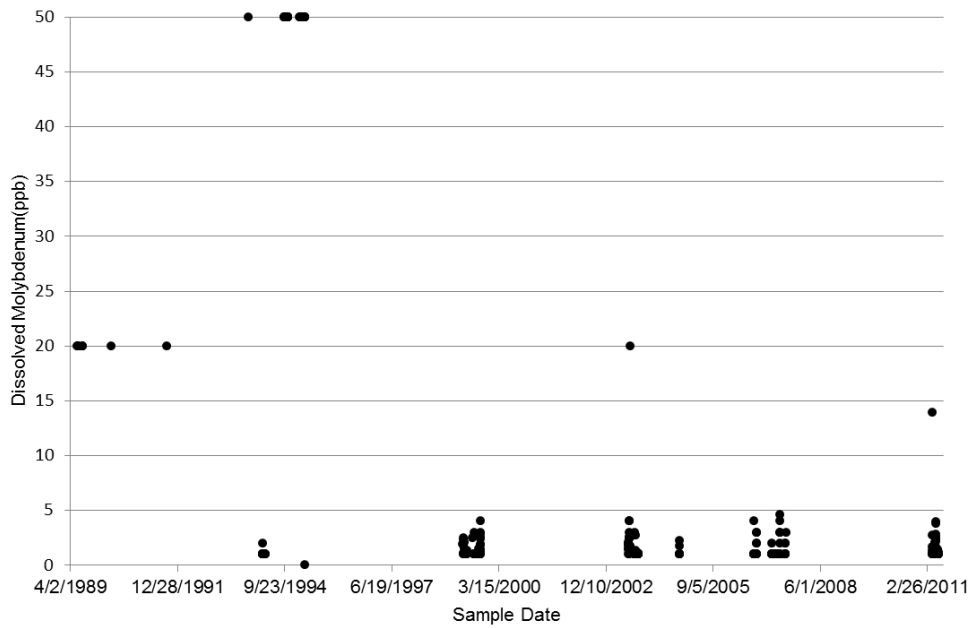


Fig. 3-33: Samples of Dissolved Molybdenum from 1986-2011 in Denton, Johnson, Somervell, Parker, Tarrant, and Wise counties

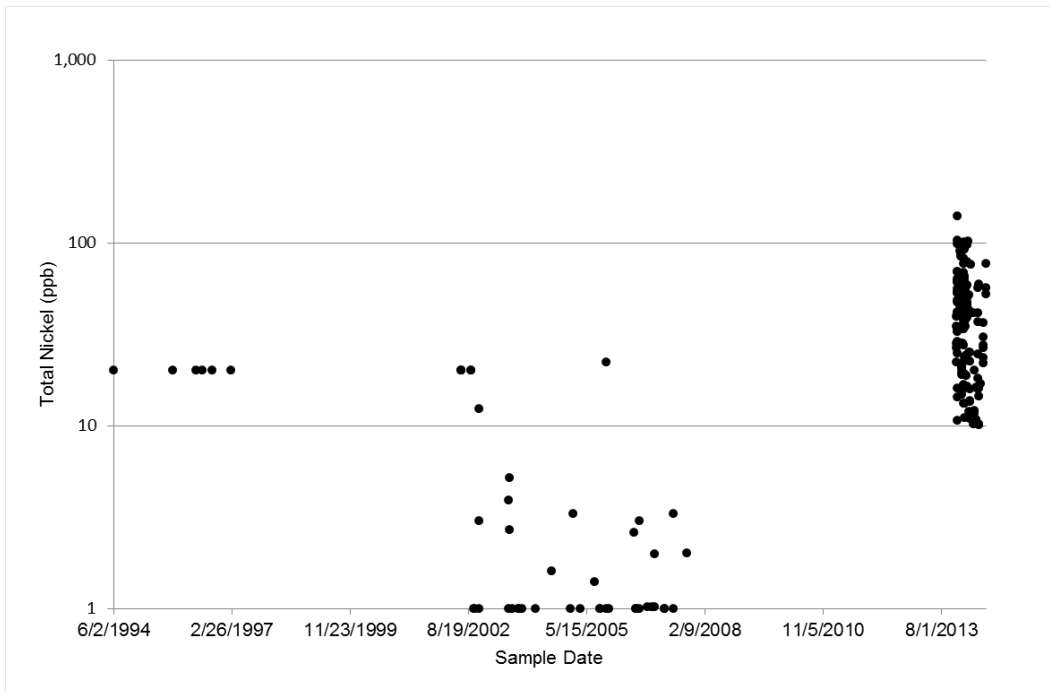


Fig. 3-34: Samples of Total Nickel from 1990-2011 in Denton, Johnson, Somervell, Parker, Tarrant, and Wise counties

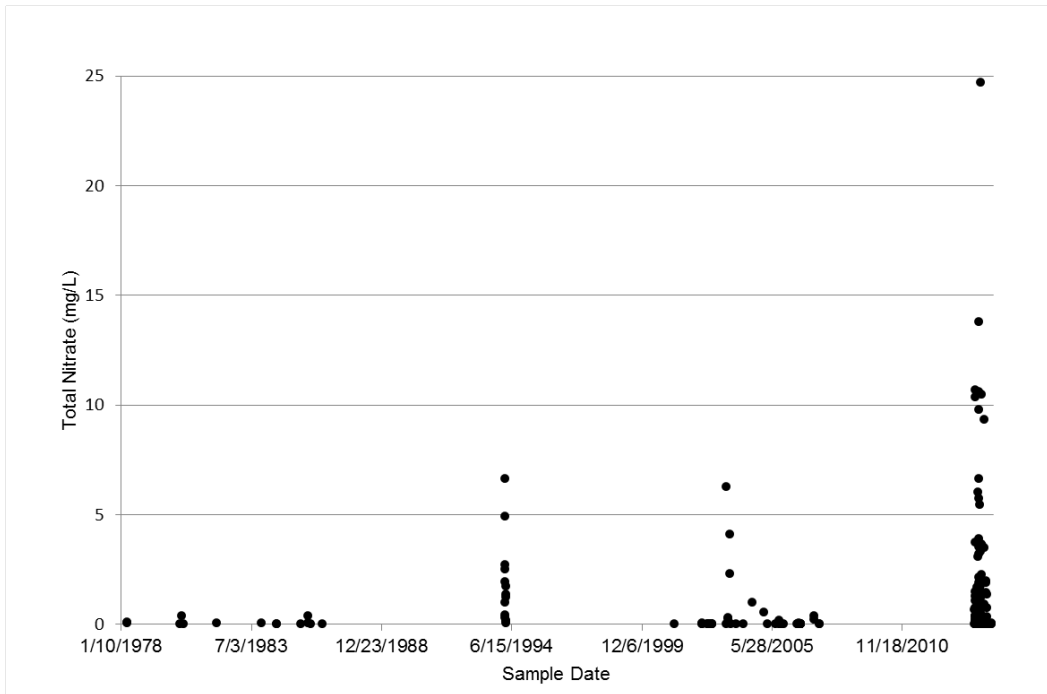


Fig. 3-35: Samples of Total Nitrate from 1990-2011 in Denton, Johnson, Somervell, Parker, Tarrant, and Wise counties

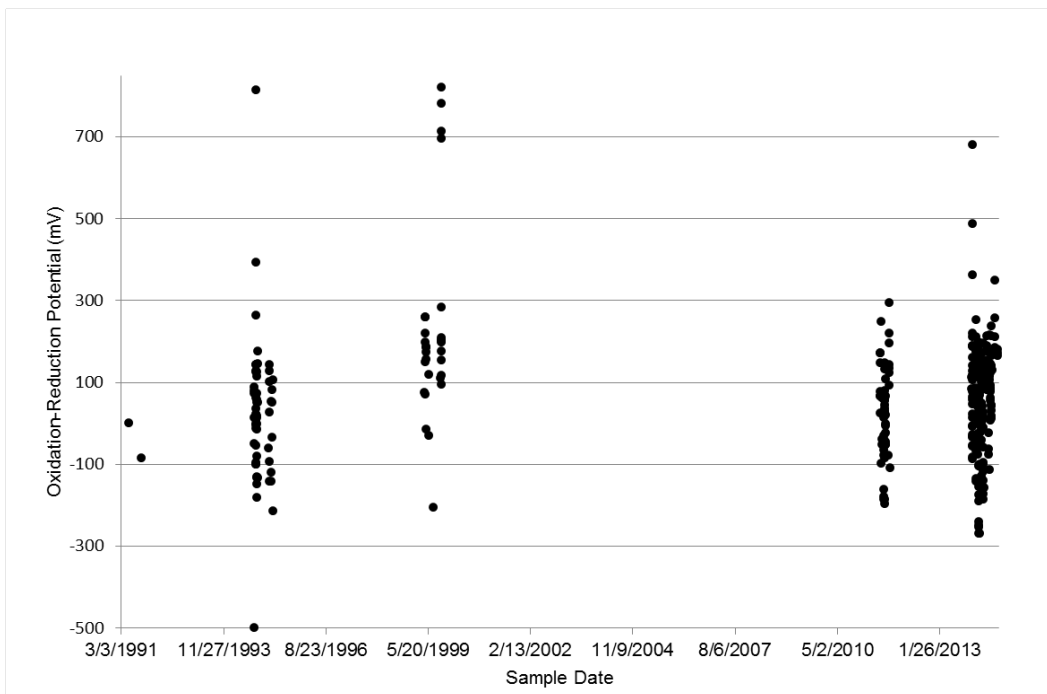


Fig. 3-36: Samples of Oxidation Reduction Potential from 1990-2011 in Denton, Johnson, Somervell, Parker, Tarrant, and Wise counties

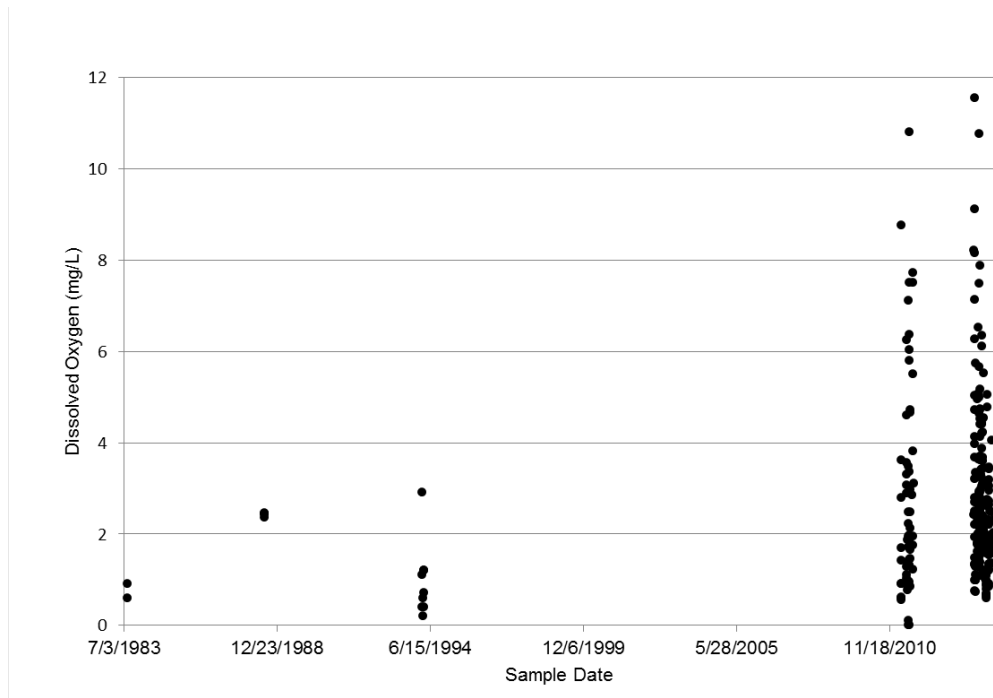


Fig. 3-37: Samples of Dissolved Oxygen from 1988-2011 in Denton, Johnson, Somervell, Parker, Tarrant, and Wise counties

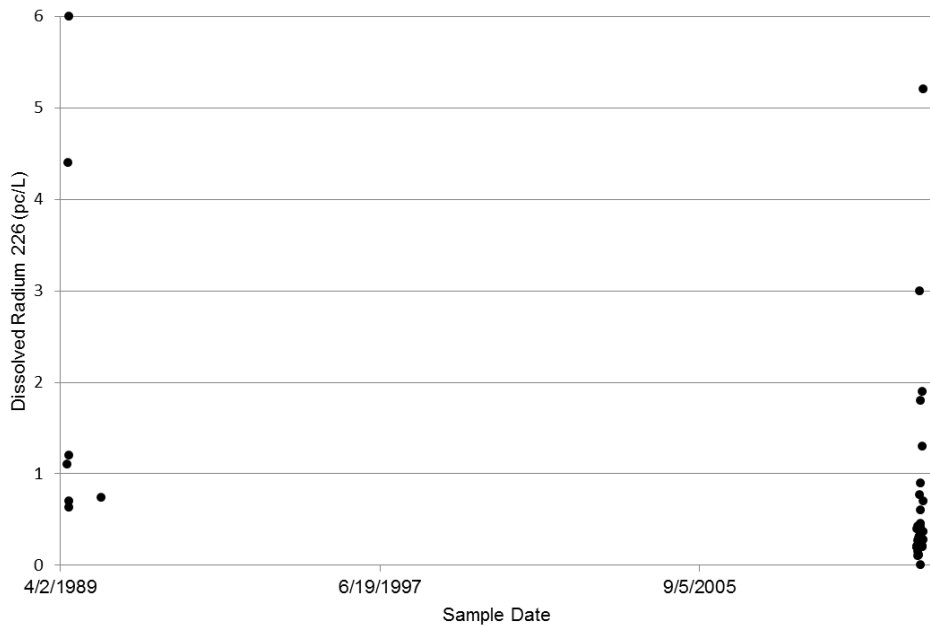


Fig. 3-38: Samples of Dissolved Radium 226 from 1988-2011 in Denton, Johnson, Somervell, Parker, Tarrant, and Wise counties

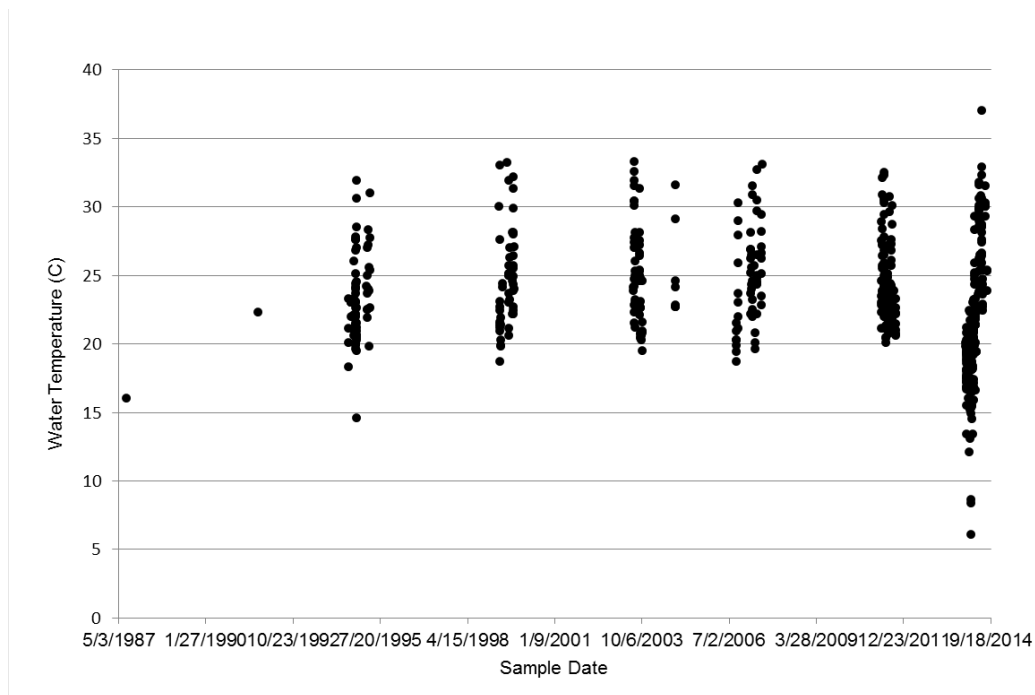


Fig. 3-41: Samples of Water Temperature from 1987-2011 in Denton, Johnson, Somervell, Parker, Tarrant, and Wise counties

The scatter plots of Total Barium, Total Beryllium, and Total Nitrate concentrations demonstrate a significantly increased range of measurements in the years after 2011, indicating a possible relationship between the increase in concentration of these constituents and gas well production in the region. In the remaining scatterplots, an apparent trend over time is not immediately evident as the data are generally variable with a broad range of measured concentrations. It may be erroneous, however, based solely on the observation, to conclude from these plots that there were no changes in groundwater quality over time, and thus no effects from hydraulic fracturing on groundwater quality. Finding correlations between groundwater quality and hydraulic fracturing activities must be considered in a spatial context that is regional rather than a local basis because of the combined effect of multiple fracturing wells on bottom hole pressures, and the potential for wellbore failures/pathways for interaction between the fractured zone and the groundwater aquifer. This will be discussed further in Chapter 4.

Contour plots of water quality samples taken before 2001 and from 2011-2014 are shown in Appendix B. Also discussed and presented in Chapter 5 and Appendix C will be results of the analysis comparing the groundwater data sets taken before 2001 and from 2011 to 2014.

4 METHODS

The methods used in the thesis emphasize spatial relationships between groundwater quality changes and the presence hydraulic fracturing activity. The analyses mainly use ArcGIS to extract the appropriate data necessary for analysis. The statistical analyses are performed in Minitab and some of the methods use Matlab.

4.1 VISUAL CORRELATIONS OF GROUNDWATER CHANGE

The purpose of visual correlations is to provide a spatial representation of groundwater constituent changes over the study region, comparing water quality before 2001 and from 2011-2014. Contour plots are created in ArcGIS denoting the relative changes in constituent concentrations over the study area. The map of gas wells is overlaid with contour plots in the same map in order to determine if a pattern in the constituent changes visually correlates to the location of gas wells. In a second plot, the changes in groundwater constituent concentrations relative to changing reservoir pressure gradient over the region are observed by overlaying a contour of the RPG (see Figure 4-1 and Appendix C) over the water quality changes. It is hypothesized that a higher reservoir pressure gradient will have a visual pattern that correlates to higher changes in groundwater constituent concentrations.

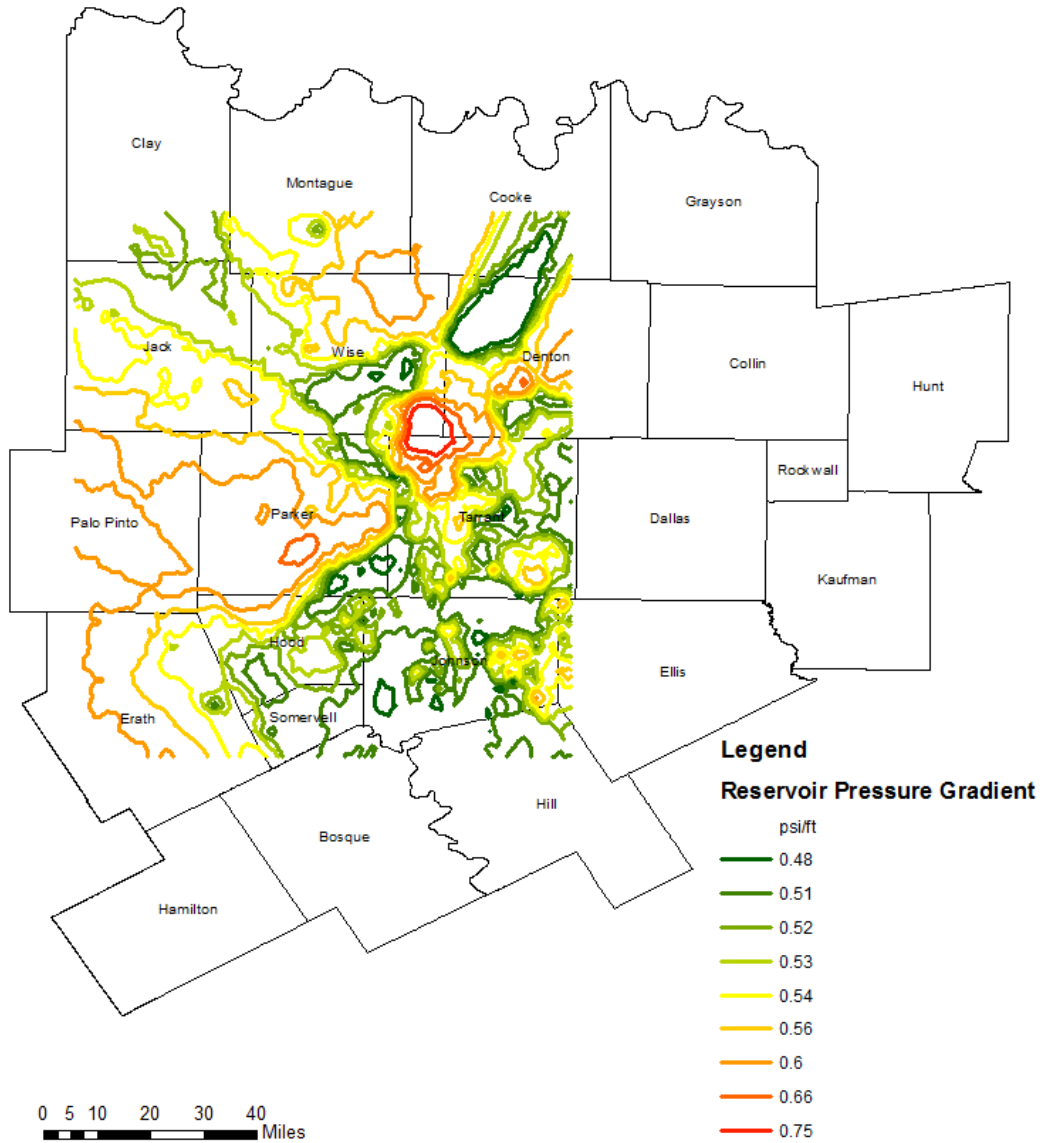


Fig. 4-1: Contours of the Reservoir Pressure Gradient in the Study Region

Conclusions may be visually deduced as the color scale of both the plot of groundwater change and the contour of the RPG is the same, a continuous color scale between green and red. The greater values in the color scale are represented by red, and the lesser values are represented by green. Ultimately, a strong visual correlation between constituent changes, well locations, and bottom hole pressure may point to a particular

constituent that may be a strong indicator variable for demonstrating that groundwater quality changes may be related to hydraulic fracturing activity.

4.1.1 CONTOURING CONSTITUENT CHANGES

Before creating contour plots of change in constituent concentrations, however, contour plots were created for each constituent, one using samples taken before 2001 where data was available, and one for samples taken in 2011-2014. Contour plots to represent the groundwater constituent concentration changes were created for 20 of 31 constituents where historical data was available. Some of the constituents measured by UTA do not have corresponding historical samples available from the Texas Water Development Board so they were excluded from this visual analysis. A summary of the data used in each contour plot is shown in Table 4-1.

In ArcGIS, the Radial Basis Function was used to contour the constituents. This method is generally used in groundwater modeling (Kresic, 2006, p. 78) where water data sets are generally small. In this model, some of the contours created a negative value in the plot. In this case, the Inverse Distance Weighting method was used instead. Contour plots that were created for water quality samples taken in before 2001 and from 2011-2014, these plots are shown in Appendix B. Table 4-1 summarizes the data utilized and the contour method used in each contour plot. Note that the numerical values denoted by the color scales, and the locations of water samples are not the same for every contour plot.

Table 4-1: Summary of Data Used in Contour Plots

Constituent		Time Frame	Years	Contour Type (IDW/RBF)	Number of Samples	Units	Max Sample Value	Min Sample Value	Max Contour Value	Min Contour Value
Alpha	Dissolved	Before 2001	1976-1999	RBF	271	pc/L	504	2	240	2.26
Alpha	Dissolved	After 2011	2011	RBF	93	pc/L	15	2.7	11	3.38
Aluminum	Dissolved	Before 2001	1986-2000	RBF	413	ppb	220	1	130	3.91
Aluminum	Dissolved	After 2011	2011	RBF	94	ppb	9	4	7	4
Arsenic	Total	Before 2001	1977-1999	RBF	43	ppb	20	0.01	18	1.92
Arsenic	Total	After 2011	2011-2014	RBF	454	ppb	161	0	79	0.14
Barium	Total	Before 2001	1985-2000	RBF	17	ppb	500	0.05	398	14.33
Barium	Total	After 2011	2011-2014	RBF	454	ppb	4,380	0	1,576	16.89
Benzene	Total	After 2011	2013-2014	RBF	379	mg/L	0.0846	0	0.0485	0
Beryllium	Total	Before 2001	1994-2000	RBF	16	ppb	1	0	4	0.23
Beryllium	Total	After 2011	2013-2014	RBF	379	ppb	24	0	14	0
Boron	Dissolved	Before 2001	1975-1999	RBF	282	ppb	2,570	0.36	1,697	74.97
Boron	Dissolved	After 2011	2011	RBF	94	ppb	1,720	50	1,720	50.05
Bromide	Total	After 2011	2013-2014	RBF	379	mg/L	3	0	2,600	0.06
Bromide	Dissolved	Before 2001	1988-1999	RBF	384	mg/L	4,380	0	2	0.05
Bromide	Dissolved	After 2011	2011	RBF	94	mg/L	4	0.02	2	0
Chloride	Total	After 2011	2013-2014	RBF	379	mg/L	816	0.96	521	6.53
Copper	Total	Before 2001	1980-1999	RBF	53	ppb	340	0.01	245	6.94
Copper	Total	After 2011	2013-2014	RBF	379	ppb	1,371	0	892	14.75
Dissolved Oxygen	Dissolved	Before 2001	1983-1994	IDW	23	mg/L	6	0.1	6	0.1
Dissolved Oxygen	Dissolved	After 2011	2011-2014	RBF	441	mg/L	29	0	10	0.86
Ethanol	Total	After 2011	2013-2014	RBF	454	mg/L	168	0	54	0
Ethyl Benzene	Total	After 2011	2013-2014	RBF	379	mg/L	0	0	0	0
Iron	Total	Before 2001	1975-2000	RBF	450	ppb	58,500	0	29,153	37.36
Iron	Total	After 2011	2013-2014	RBF	379	ppb	12,314	0	6,204	5.91
Methanol	Total	After 2011	2013-2014	RBF	454	mg/L	45	0	32	0
Molybdenum	Total	After 2011	2013-2014	RBF	379	ppb	109	0	91	1.5
Molybdenum	Dissolved	Before 2001	1989-1999	RBF	388	ppb	50	1	48	2.96
Molybdenum	Dissolved	After 2011	2011	RBF	94	ppb	5	1	4	1
Nickel	Total	Before 2001	1994-1998	RBF	12	ppb	20	0.01	20	1.56
Nickel	Total	After 2011	2013-2014	RBF	379	ppb	160	0	115	0.53
Nitrate	Total	Before 2001	1995-1998	IDW	85	mg/L	2	0.01	7	0.01
Nitrate	Total	After 2011	2013-2014	RBF	379	mg/L	25	0	12	0
pH		After 2011	2011-2014	RBF	452	pH	9	5.89	9	6.72

Table 4-1 Continued

Phosphorus	Dissolved	Before 2001	1989-1999	IDW	218	mg/L	5	0	5	0
Phosphorus	Dissolved	After 2011	2011	RBF	94	mg/L	0	0.02	0	0.02
Radium 226	Dissolved	Before 2001	1977-1990	RBF	57	pc/L	22	0.2	22	0.2
Radium 226	Dissolved	After 2011	2011	RBF	93	pc/L	6	0.1	4	0.18
Radium 228	Dissolved	Before 2001	1988-1990	RBF	57	pc/L	3	1	3	1
Radium 228	Dissolved	After 2011	2011	RBF	93	pc/L	4	0.9	3	1.06
Redox Potential		Before 2001	1990-1999	RBF	269	mV	820	-499.4	565	-209.88
Redox Potential		After 2011	2011-2014	RBF	452	mV	680	-269.4	365	-194.41
Selenium	Total	Before 2001	1977-1998	RBF	36	ppb	50	0.05	45	0.09
Selenium	Total	After 2011	2011-2014	RBF	453	ppb	109	0	61	0.01
Sulfate	Total	After 2011	2013-2014	RBF	379	mg/L	612	0	553	8.6
Temperature		Before 2001	1983-1999	IDW	344	°C	48	13.3	48	14.6
Temperature		After 2011	2011-2014	IDW	545	°C	47	6.1	47	6.37
Total Dissolved Solids	Dissolved	After 2011	2011-2014	RBF	452	mg/L	1,892	0	1,406	64.45
Vanadium	Dissolved	Before 2001	1989-1999	RBF	366	ppb	20	1	18	1.98
Vanadium	Dissolved	After 2011	2011	RBF	94	ppb	4	1	3	1.02
Zinc	Total	Before 2001	1980-1998	RBF	64	ppb	490	0.07	338	11.73
Zinc	Total	After 2011	2013-2014	RBF	379	ppb	12,048	0	3,805	0

*RBF: Radial Basis Function (Spline)

*IDW: Inverse Distance Weighting

The number of samples, sample locations, and extent of the contour plots vary per constituent, as can be seen in the figures of the contour plots located in Appendix B. For sample locations associated with a non-detected value, zero was used at that sample location in the contour plots. A grid of data points was created to overlay the contour plots. This grid is shown in Figure 4-2 and has 19,594 data points over 15,048 mi². Note that some of the data points are located outside the extent of some of the contour plots as not all constituent contour data are in the same locations and thus are not the same size (see Appendix B and Appendix C).

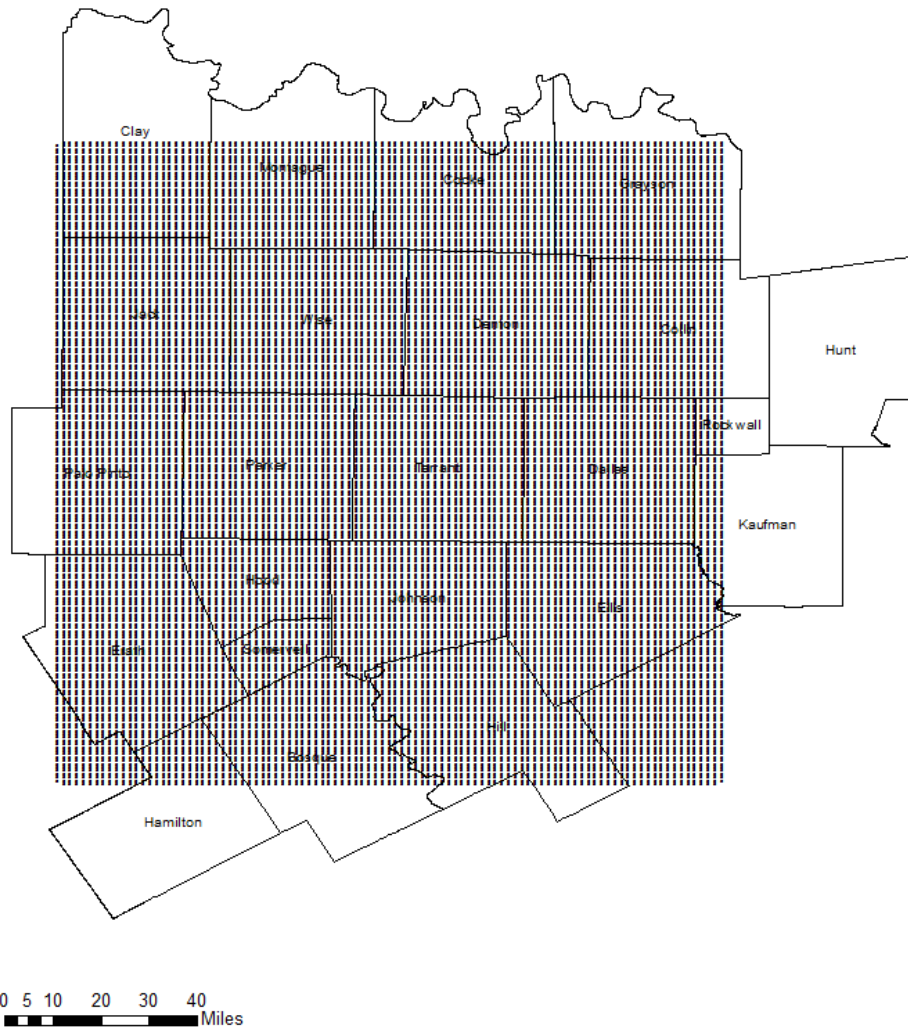


Fig. 4-2: Locations of Extraction Points

At these data point locations, the contour values were extracted from the plots (listed in Table 4-1) for Dissolved Alpha, Dissolved Aluminum, Total Arsenic, Total Barium, Total Beryllium, Dissolved Boron, Dissolved Bromide, Total Copper, Dissolved Oxygen, Total Iron, Dissolved Molybdenum, Total Nickel, Total Nitrate, Dissolved Phosphorus, Dissolved Radium 226, Dissolved Radium 228, Redox Potential, Total Selenium, Water Temperature, Dissolved Vanadium, and Total Zinc. This was accomplished using the Extract Multi-Values to Points function in ArcGIS. These values and the corresponding location points were exported into an Excel spreadsheet.

For the data points in the grid containing both a historical and current value, a difference between the values was taken. Note that the contour plots are not the same size and extent, therefore the difference between the current and historical values were calculated at data points located where the historical and current contour plots overlapped. The differences calculated in the spreadsheet were reimported into ArcGIS. The Inverse Distance Weighting contour function was applied to difference values of the data points, thus creating the contour plots of constituent change.

4.2 NONPARAMETRIC TEST FOR EVALUATING GROUNDWATER QUALITY

Normally distributed data sets use parametric statistical tests in order to analyze trends over time. In the case where the data does not follow a normal distribution, a nonparametric statistical test may be used. Nonparametric tests are based the median of the data set rather than the mean (Paulson, 2003, p. 519). Nonparametric statistical tests are often applied in the study of groundwater samples (Van Belle et al., 1984), where data sets are generally small due to budget constraints, and small sample sizes do not generally follow a normal distribution. Nonparametric tests are less powerful than parametric statistical tests, however, a rejection of the null hypothesis using a nonparametric test is more likely to be true (Paulson, 2003, pg. 520). In this thesis, nonparametric test are applied in order to determine if statistical significance of relative measurements in groundwater quality exist in the region between water samples taken near gas well and water samples not taken near gas wells. Different types of nonparametric tests may be applied depending upon the data set of interest. This study uses the Mann-Whitney U-Test.

The Mann Whitney U-Test is used to compare the distribution of two data sets that are randomly sampled, independent, and that could be ranked, where sample sets

are not necessarily equal in size (Paulson, 2003, p. 525). Minitab returns the results of this test as a W-Value from which the statistical P-Value is calculated. The formulas shown in Equation 4-1 through 4-3 (adapted from <http://support.minitab.com/en-us/minitab/17/topic-library/basic-statistics-and-graphs/hypothesis-tests/nonparametrics-tests/calculating-mann-whitney-statistics>, 1-23-15) are used to calculate the P-value,

$$\text{where Mean of } W = 0.5(n_1(n_1 + n_2 + 1)), \quad \mathbf{[4-1]}$$

$$\text{and Variance of } W = n_1 * n_2(n_1 + n_2 + 1)/12, \quad \mathbf{[4-2]}$$

where n_1 and n_2 are the number of observations in the first and second samples

$$\text{respectively, and } Z = (|W - \text{Mean of } W| - 0.5) / \text{sqrt}(\text{Variance of } W), \quad \mathbf{[4-3]}$$

and the P-Value is determined from the Normal Probability Distribution.

In this study, the P-value of significance was for a two-tailed test with a 0.95 confidence interval. Results yielding a P-value less than 0.5 are considered statistically significant.

The Mann Whitney U-Test was applied to compare and contrast constituent samples taken in proximity to gas extraction, and away from gas extraction for all constituent samples taken between 2011-2014. The water samples were divided to compare water samples taken at locations where there are no gas wells existing within 1 mile (Control Group) versus water wells that have at least one gas well within a 1 mile distance (Test Group). This was determined using a Matlab code, where the locations of the water wells were calculated versus the locations of the gas wells using the haversine function. For accuracy, the locations of the gas wells were converted from NAD27 to NAD 83 coordinate locations in ArcGIS in order to match the coordinate values of the gas wells to the water samples. Note that although the UTA samples were provided in WGS84 coordinate systems, there is virtually no difference between the NAD83 and WGS84 coordinate notations. The sample locations of the Control Group and Test Group are shown in Figure 4-3.

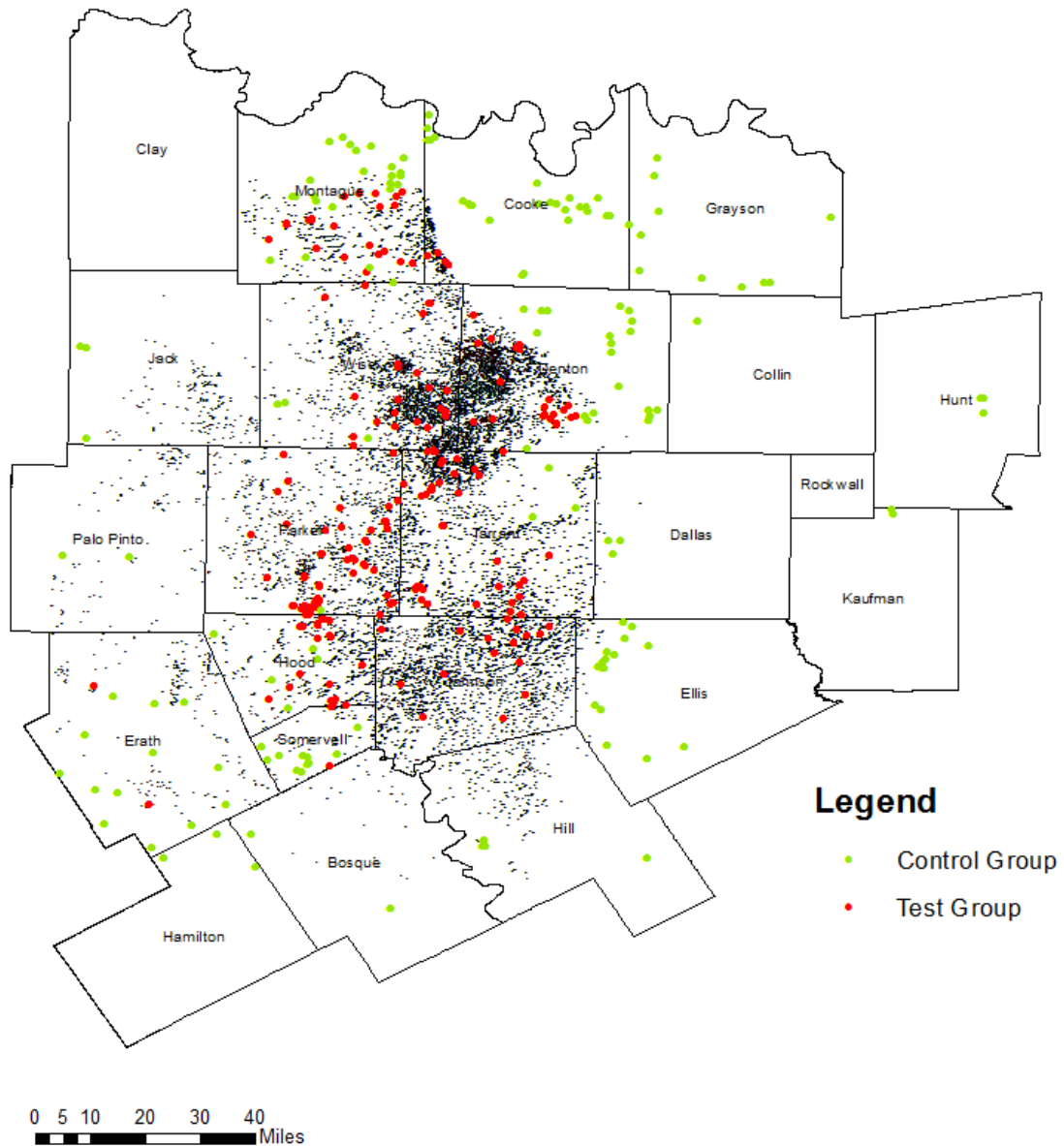


Fig. 4-3: Locations of Control Group Samples and Test Group Samples

Many of the samples taken in these ground water data sets were Non-Detected (ND) values. A non-parametric test was performed for each constituent three times, each test accounting for the non-detect values differently: (1) in the first test, the ND values were set to zero, (2) in the second test, the ND values were set to $\frac{1}{2}$ the detection limit (as defined by the measuring instrument, and (3) in the third test the ND values were

excluded. The ND values for the various constituents in the data set are shown in Table 4-2 below.

Table 4-2: Constituent Detection Limits

Constituent	Detection Limit (mg/L)	1/2 Detection Limit (mg/L)	1/2 Detection Limit (ppb)
Arsenic	0.00001	0.00001	0.01
Barium	0.01000	0.00500	5.00
Benzene	0.02000	0.01000	10.00
Beryllium	0.00100	0.00050	0.50
Bromide	0.00400	0.00200	2.00
Chloride	0.00698	0.00349	3.49
Copper	0.01000	0.00500	5.00
Dissolved Oxygen	0.10000	0.05000	50.00
Ethanol	0.20000	0.10000	100.00
Ethyl Benzene	0.01000	0.00500	5.00
Iron	0.01000	0.00500	5.00
Methanol	0.50000	0.25000	250.00
Molybdenum	0.00100	0.00050	0.50
Nickel	0.01000	0.00500	5.00
Nitrate	0.01300	0.00650	6.50
Selenium	0.00006	0.00003	0.03
Sulfate	0.01969	0.00985	9.85
Zinc	0.01000	0.00500	5.00

The non-detect values shown in Table 4-2 are based upon the measuring instruments used in the UTA sample set. Non-detect values were not differentiated within the TWDB samples. There were no zero samples found in the TWDB data sets meaning that the absolute minimum sample value recorded is the detection limit. Because of this results of Dissolved Alpha, Dissolved Aluminum, Dissolved Boron, Dissolved Molybdenum, Dissolved Radium 226, Dissolved Radium 228, and Dissolved Vanadium were the same for all three methods of dealing with non-detects that were described above since these samples were only taken from the Texas Water Development Board dataset.

4.3 MODEL ANALYSIS OF WATER CONSTITUENT PREDICTIONS, BOTTOM HOLE PRESSURE, AND GAS WELL DENSITY

The analyses in this section evaluate the relationship between water constituent concentration, bottom hole pressure, and gas well density. The analysis relies on groundwater samples for all constituents taken in 2011-2014. First, the shapefile of gas well locations was converted to a raster using the Point to Raster tool in the Arc Toolbox (see Figure 4-4).

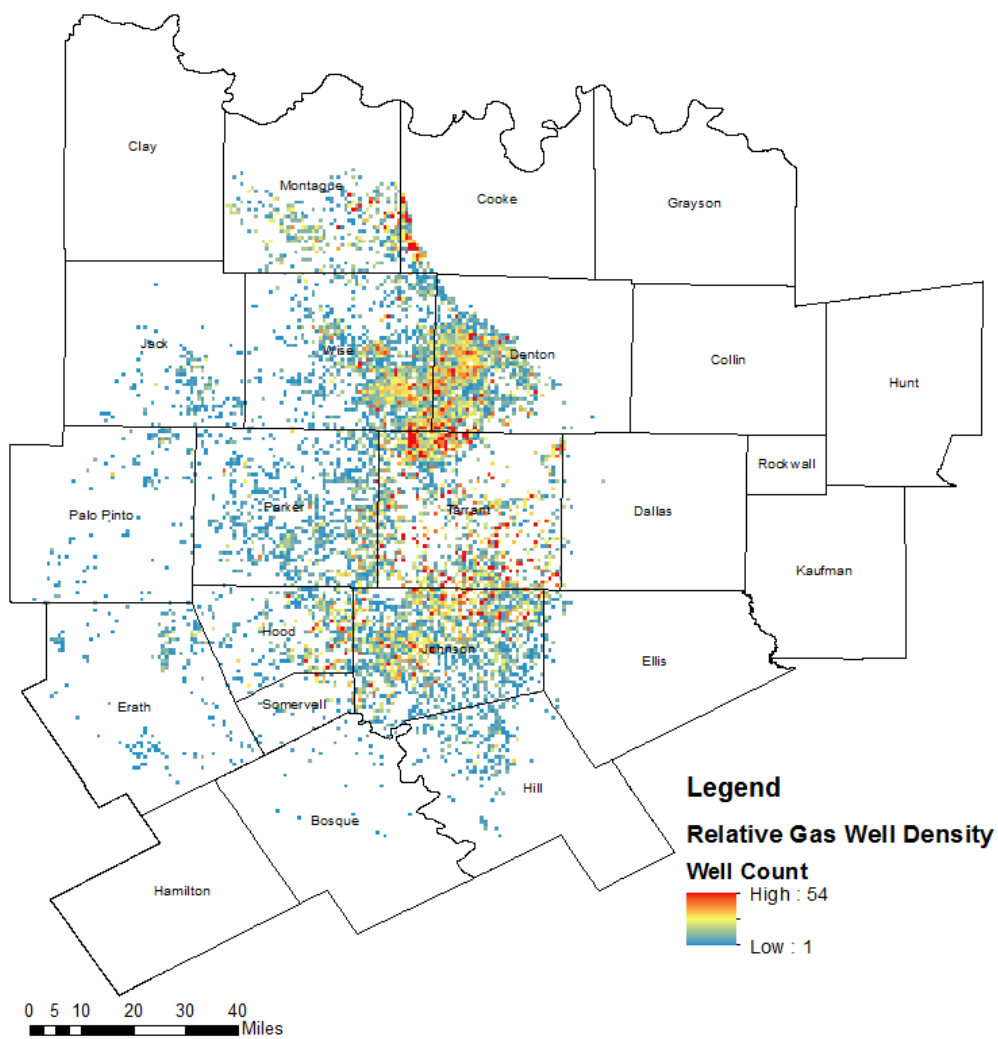


Fig. 4-4: Raster of Relative Gas Well Density per raster cell

The raster displays a grid of rectangular cells. Each raster cell is 0.01 squared degrees, which represents an area of 0.4 squared miles. Note that the cell boundaries are greater in length than the maximum distance of groundwater flow estimated in this thesis. The count of gas wells within each pixel is color coded in the raster shown in Figure 4-4, thus red indicates a higher count of gas wells within the pixel than the yellow does, for example. A grid of data points was created to overlay individual cells within a portion of this raster. The data points are used in the analysis, where the values of the local reservoir pressure gradient, well count, and the water constituent concentrations were extracted from contour plots of these data using the Extract Multi-Value Points function. This grid of data points is shown in Figure 4-5.

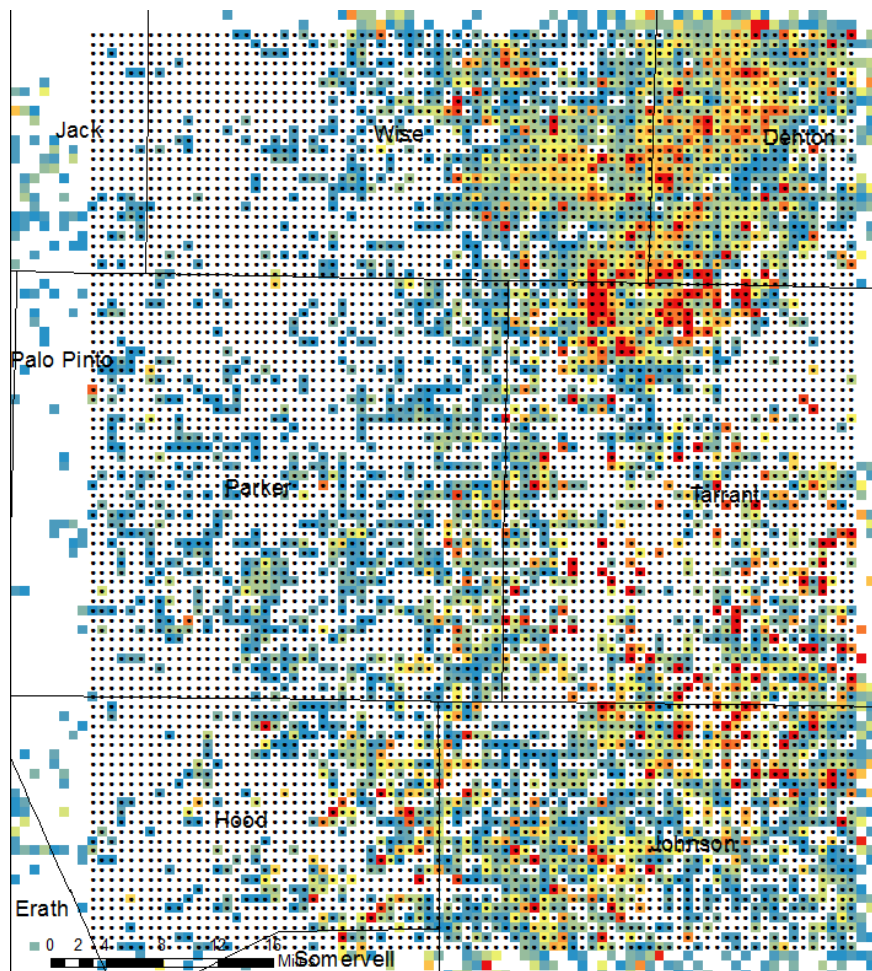


Fig. 4-5: Grid of Data Points overlaying raster cells

Water constituent values were extracted from the contour plots of water samples from 2011-2014 at each of these data points, as well as the RPG and well density.

The data points were separated by relative well density. The data was separated into a high well density category, semi-dense, and zero density. Cells considered to have a high density had a well count of 18-54, semi-dense had 1-17, and zero density had 0. The high well density category was further separated by pressure gradient. The reservoir pressure gradient was divided into several categories of 0.4-0.49 psi/ft, 0.5-0.59 psi/ft, 0.6-0.69 psi/ft, 0.7-0.79 psi/ft, and 0.8 and greater psi/ft. The Subgroups of data, based upon these divisions and used in this analysis are described in Table 4-3 below.

Table 4-3: Subgroup Descriptions

Subgroup Number	Wells Per 0.4 mi²	Reservoir Pressure Gradient (psi/ft)	Number of Data Points
1	0	-	4161
2	18-54	0.43 - 0.49	35
3	18-54	0.50 - 0.59	68
4	18-54	0.60 - 0.69	22
5	18-54	0.70 - 0.79	9
6	18-54	0.80 - 0.89	11

4.3.1 EVALUATION OF SUBGROUP 1 VERSUS SUBGROUP 6

The aim of the analysis is to determine if there is any difference in the data distributions between Subgroup 1, the Control Group, and Subgroup 6, the Test Group. Subgroup 6 is considered the group with the highest risk areas in the model due to a high density of gas wells and a high reservoir pressure gradient. The Mann-Whitney U-Test was performed in Minitab for each constituent. The results were returned as a W-

value as explained in Section 4.2.1. The data in Subgroup 1 and Subgroup 6 was also plotted in Boxplots in Minitab for distribution comparison (Appendix D). The abbreviations for the constituents used in the Results are shown in Table 4-4.

Table 4-4: Abbreviations Referenced in Analysis Results

ABBREVIATION	CONSTITUENT	UNITS
ALP	Alpha, Dissolved	pc/L
AL	Aluminum, Dissolved	ppb
AS	Arsenic, Total	ppb
BA	Barium, Total	ppb
BENZ	Benzene, Total	mg/L
BERY	Beryllium, Total	ppb
BO	Boron, Dissolved	ppb
BR.TOT	Bromide, Total	mg/L
BR.DIS	Bromide, Dissolved	mg/L
CL	Chloride, Total	mg/L
CU	Copper, Total	ppb
DO	Dissolved Oxygen	mg/L
ETH	Ethanol, Total	mg/L
ETHB	Ethyl Benzene, Total	mg/L
FE	Iron, Total	ppb
METH	Methanol, Total	mg/L
MOLY.TOT	Molybdenum, Total	ppb
MOLY.DIS	Molybdenum, Dissolved	ppb
NI	Nickel, Total	ppb
NIT	Nitrate, Total	mg/L
pH	pH	
PHOS	Phosphorous, Dissolved	mg/L
R226	Radium 226, Dissolved	pc/L
R228	Radium 228, Dissolved	pc/L
ORP	Redox Potential	mV
SE	Selenium, Total	ppb
SULF	Sulfate, Total	mg/L
T	Water Temperature	C
TDS	Total Dissolved Solids	mg/L
VAN	Vanadium, Dissolved	ppb
ZI	Zinc, Total	ppb

4.3.2 CONSTITUENT CORRELATIONS

The purpose of the analysis is to find correlations in constituent concentrations within the data points per Subgroup. The analysis determines if elevated constituent concentrations have some correlation in the Control Group, Subgroup 1, versus the data points in Subgroups 2-6. A strong correlation between the constituents, especially between those that are naturally occurring and those that are not, will indicate that the elevated constituent concentrations are related and may be attributed to hydraulic fracturing activity.

A Matlab code was written in order to find correlations between the constituents within Subgroups 1-6. The R-squared value was obtained from a linear regression model for each constituent pair. The Matlab code was run 6 times (per Subgroup). An output matrix of 31 x 31 was obtained for each subgroup, with a row and column for each constituent, the cell intersected by each row and column containing the R-squared value for the two constituent variables. The cells with an R-squared value indicating a strong correlation, that is a value greater than 0.5, are highlighted in red for clarity.

4.4 CLUSTER ANALYSIS FOR UNDERSTANDING CONTAMINANT PATHWAYS IN HYDRAULICALLY FRACTURED WELL

The analysis examines gas well design parameters as a means of identifying the origin of annular pathways in a gas well. Leaks in the wellbore may be the result of insufficient cementing, casing failures, or unset packers, but the study does not incorporate specific knowledge of these occurrences. Rather it focuses on wellbore completion design parameters that may be associated with the origin of these types ruptures in the wellbore system. A ruptured wellbore creates a micro-annulus in the

wellbore system where contact is made with the water table. The analysis hypothesizes that gas well failures may share certain wellbore completion parameters that could indicate the origin of the micro-annulus in the wellbore. The wellbore completion parameters of interest are explained as follows:

1. **Intermediate Casing/Bottom Hole Casing:** The size of the casing is important to the wellbore system, where pressure ratings vary with casing size. Smaller casing sizes result in higher hydraulic fracturing pressures, increasing the risk for failure.
2. **Wellbore Azimuth:** Subsurface stresses could weaken the integrity of a horizontal wellbore depending on the orientation of the wellbore azimuth in relation to the direction of greatest principle stress in the earth. Wells drilled in the direction of greatest principal stress will be less likely to experience a collapsed hole in the lateral section versus well drilled opposite the direction of principal stress that may collapse. If the subsurface stress direction is somewhat consistent throughout the region, then gas wells drilled perpendicular to this stress may be at an increased risk for failure, and thus water contamination.
3. **Fluid Volume:** Greater volume of fluid pumped could mean that the casing will be exposed to high pressures for a longer duration, weakening the integrity of the well. Additionally, greater fluid pumped means that the hydraulic fractures are longer, releasing a greater amount of gas into the wellbore system.
4. **Weight of Sand:** The more sand that is pumped downhole may cause erosion of the perforations and form a fracture in the cemented wellbore. More sand implies longer fractures or else, longer lateral lengths.

5. **Volume of Acid:** More acid pumped will cause break down of the formation, with the potential to create space between the cement and the rock.
6. **True Vertical Depth:** The deeper the gas well, the further away the producing zone would be from the water table so contaminants have further to travel and are less likely to contaminate the water.
7. **Depth of Shallowest Perforation:** Perforations closer to the surface aquifer decrease the distance from the water table to the wellbore system, increasing the chance of water contamination.
8. **Measured Depth:** A longer measured depth through the entire extent of a wellbore increases the probability of an insufficient cement job, either in the horizontal or vertical section of a wellbore.
9. **Volume of N₂:** Nitrogen gas is usually injected into shallower wells and may act as a mobilizer of contaminants as it flows freely back to the surface.
10. **Depth of Barnett Shale:** the greater the depth of the Barnett Shale, the greater pressure is required to treat the formation, a source of stress on the wellbore system. Additionally, if high temperatures are flowing through the wellbore system, it may have a significant affect on the water table, increasing the water temperature.
11. **Bottom Hole Pressure/Reservoir Pressure Gradient:** the bottom hole pressure will increase the flow of natural gas from the reservoir.
12. **Wells existing in 1 Mile:** the more gas wells existing in 1 mile radius from the water well increase the possibility of a contaminant pathway to groundwater from a gas well. Even if the specific contaminant pathway is not understood, a correlation between the number of gas wells and

groundwater quality change helps establish a relationship between hydraulic fracturing and groundwater quality changes.

These parameters were defined for 2,049 gas wells in the region (see Section 3.3.3); at each well location, the Depth of the Paluxy Aquifer and the Bottom Hole Pressure was extracted from the ArcGIS model. In the analysis, BHP was analyzed instead of RPG since there is not enough variability in the data values of RPG for a meaningful cluster analysis. After compiling the data, Acid Volume was omitted from the data set as it was determined that the records showed inconsistent reporting of this variable. Eleven (11) clusters were tested in the analysis, based upon the wellbore parameters described above. The clusters are listed in Table 4-5.

Table 4-5: Description of Clusters Analyzed

No.	Cluster	Description
1	Surface Casing Diameter (in)	-
2	Bottom Hole Casing Diameter (in)	-
3	Injected Fluid (bbl)	-
4	Injected Sand (lbs)	-
5	Total Vertical Depth (ft)	-
6	Injected Nitrogen (scf)	-
7	Length of Lateral (ft)	= Measured Depth - Total Vertical Depth (Vertical Wells = 0, Horizontal Wells > 0)
8	Aquifer-Perforation Thickness (ft)	= Depth of Shallowest Perforation - Depth of Paluxy Aquifer
9	Direction of Azimuth (deg)	<i>Clusters determined for Horizontal Wells only</i>
10	Number of Wells in 1 Mile distance	-
11	Bottom Hole Pressure (psi)	-

The purpose of the Cluster Analysis is to determine if the wellbore design parameters are strongly associated with a high concentration of tracer found in the groundwater at the cluster location. Based upon the results of the previous analyses in the thesis (See

Chapter 5), Beryllium is used as a tracer. A high cluster value that is associated with a high Beryllium concentration in the groundwater demonstrates a link between a specific wellbore parameter and groundwater quality change. Using ArcGIS, the Cluster function was applied to each of the aforementioned gas well completion parameters. The Outlier Analysis in ArcGIS uses Local Moran's I spatial autocorrelation function, where I is the spatial statistic of spatial association. The formulas for this function are shown in Equations 4-4 through 4-8 (adapted from <http://resources.arcgis.com/en/help/main/10.1/index.html#//005p00000012000000>, 4-7-15).

The Local Morans's I Statistic of spatial association is

$$I_i = \frac{x_i - \bar{X}}{S_i^2} \sum_{j=1, j \neq i}^n w_{i,j} (x_j - \bar{X}) \quad , \quad [4-4]$$

where x_i is an attribute for feature I, \bar{X} is the mean of the corresponding attribute, $w_{i,j}$ is the spatial weight between feature I and j, and

$$S_i^2 = \frac{\sum_{j=1, j \neq i}^n (x_j - \bar{X})^2}{n - 1} - \bar{X}^2 \quad , \quad [4-5]$$

with n equating to the total number of features.

The z_{I_i} - score for the statistics are computed as

$$z_{I_i} = \frac{I_i - E[I_i]}{\sqrt{V[I_i]}} \quad , \quad [4-6]$$

where

$$E[I_i] = \frac{\sum_{j=1, j \neq i}^n w_{ij}}{n - 1} \quad \text{and} \quad [4-7]$$

$$V[I_i] = E[I_i^2] - E[I_i]^2 \quad [4-8]$$

The program returns an output of clusters denoted by HH, HL, LH, LL, and Not Significant variables. These are described in Table 4-6.

Table 4-6: Cluster Descriptions of ArcGIS Cluster and Outlier Analysis (adapted from <http://resources.arcgis.com/en/help/main/10.1/index.html#//005p00000012000000>)

CLUSTER CATEGORY	DEFINITION
HH	A cluster of high value data points
HL	A cluster of low value data points surrounding a high value data point
LH	A cluster of high value data points surrounding a low value data point
LL	A cluster of low value data points surrounding a high value data point
Not Significant	A cluster of data points that do not share common attributes

Based upon the cluster descriptions in Table 4-6, the cluster categories of interest in this study were HH and LL. For each cluster analysis performed, the HH and LL clusters were compared using a Mann Whitney U-Test of the corresponding Beryllium concentrations at the cluster locations. In other words, if a statistically significant concentration in Beryllium (tracer) is detected between locations of the HH and LL clusters, then the cluster may indicate if the wellbore design parameter is associated with a contaminant pathway in the wellbore system.

5 RESULTS

5.1 VISUAL CORRELATIONS OF GROUNDWATER QUALITY CHANGE

The plots produced in the analysis demonstrate visual correlation for some constituent changes. In the plot of Dissolved Alpha, shown in Figure 5-1, the area on the map with the greatest increase in Dissolved Alpha concentration corresponds to the location with the greatest density of gas wells, and in areas of the map where there are fewer gas wells, the increase in Dissolved Alpha concentration is less.

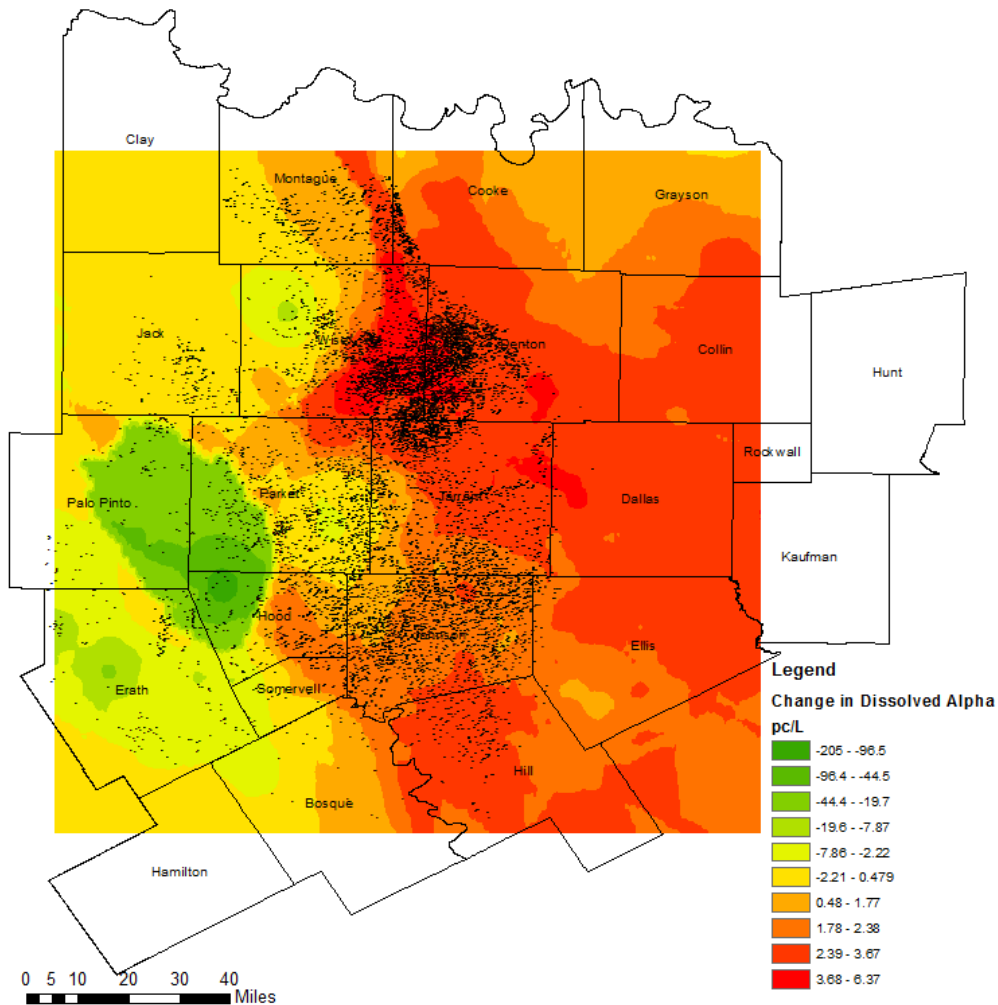


Fig. 5-1: Change in Dissolved Alpha (pc/L) in study region and gas well locations

Based upon the understanding that naturally occurring radioactive materials (NORM) are associated with natural gas production, existing in the reservoir rock and produced fluid, it might be expected that the concentration of Gross Alpha decay would increase in the groundwater if the NORM are entering the groundwater system. Figure 5-2 shows the plot of change in Dissolved Alpha concentration with the Reservoir Pressure Gradient contours.

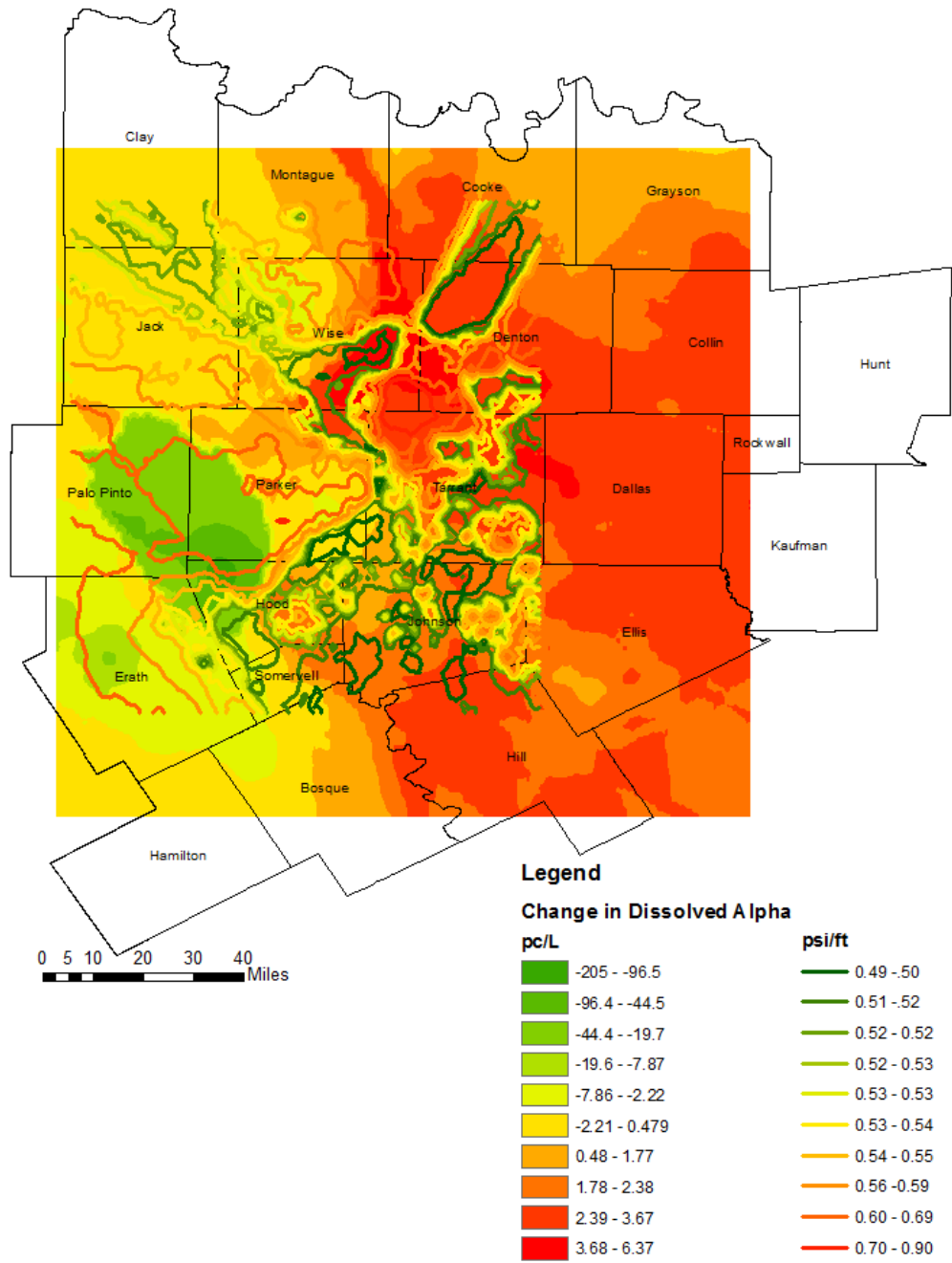


Fig. 5-2: Change in Dissolved Alpha (pc/L) in study region and contour of RPG (psi/ft)

This plot does not demonstrate a strong visual correlation between the Reservoir Pressure Gradient and relative change in concentration. The remaining plots are located in Appendix C. With the exception of the plots of Total Barium, and Total Beryllium

changes, most of the plots do not demonstrate an apparent correlation between the constituent changes, location of gas wells, and reservoir pressure gradient.

In Figure C-4, the location of gas wells appears strongly correlated to the greatest positive changes in Total Beryllium. In Figure C-24 the RPG has some correlation to the changes in Beryllium. In Figure C-23 there is a correlation between the positive changes in Total Barium and the RPG.

5.2 NONPARAMETRIC TEST FOR EVALUATING WATER QUALITY

The results of Mann-Whitney U-Tests do not strongly indicate that proximity to gas wells is associated with degraded water quality. The conclusions of the tests where the ND values were included may be misleading, however, as there are a large number of non-detect values for some of the constituents. The results of the Mann-Whitney U-Test are presented in Table 5-1 through 5-3, where the statistically significant differences in median concentrations are highlighted in blue.

Table 5-1: P-Value Determinations of Mann-Whitney U-Test for when Non-Detects are included as Zero Values

Constituent	Null Hypothesis	Number of Samples		Median		Minitab Output <i>W</i>	Calculation of P-Value for a 2 Tailed Test and 0.95 Confidence Interval				Result <i>Accept (1)/ Reject (0)</i>
		<i>n1</i>	<i>n2</i>	<i>n1</i>	<i>n2</i>		<i>Mean of W</i>	<i>Variance of W</i>	<i>Z-Value</i>	<i>P-Value</i>	
Alpha, Dissolved	n1 = n2	32	46	5.05	4.65	1,320	1,264	9,691	0.56	0.58	1
Aluminum, Dissolved	n1 = n2	33	46	4.00	4.00	1,263	1,320	10,120	0.56	0.58	1
Arsenic, Total	n1 = n2	218	119	0.67	0.93	35,056	36,842	730,700	2.09	0.04	0
Barium, Total	n1 = n2	217	119	68.84	74.10	36,370	36,565	725,196	0.23	0.82	1
Benzene, Total	n1 = n2	178	105	0.00	0.00	25,883	25,276	442,330	0.91	0.36	1
Beryllium, Total	n1 = n2	178	105	0.00	0.00	24,691	25,276	442,330	0.88	0.38	1
Boron, Dissolved	n1 = n2	33	46	324.00	257.50	1,354	1,320	10,120	0.33	0.74	1
Bromide, Dissolved	n1 = n2	33	46	0.11	0.12	1,239	1,320	10,120	0.81	0.42	1
Bromide, Total	n1 = n2	178	105	0.00	0.00	24,024	25,276	442,330	1.88	0.06	1
Chloride, Total	n1 = n2	178	105	23.08	34.26	23,626	25,276	442,330	2.48	0.01	0
Copper, Total	n1 = n2	178	105	52.86	57.29	24,392	25,276	442,330	1.33	0.18	1
Dissolved Oxygen	n1 = n2	215	111	2.31	1.89	36,897	35,153	650,321	2.16	0.03	0
Ethanol, Total	n1 = n2	49	119	0.32	0.00	4,677	4,141	82,120	1.87	0.06	1
Ethyl Benzene	n1 = n2	178	105	0.00	0.00	25,384	25,276	442,330	0.16	0.87	1
Iron	n1 = n2	178	105	44.50	42.60	24,703	25,276	442,330	0.86	0.39	1
Methanol	n1 = n2	49	119	0.00	0.00	4,222	4,141	82,120	0.28	0.78	1
Molybdenum, Dissolved	n1 = n2	33	46	1.20	1.10	1,336	1,320	10,120	0.15	0.88	1
Molybdenum, Total	n1 = n2	178	105	18.92	20.08	25,360	25,276	442,330	0.13	0.90	1
Nickel	n1 = n2	178	105	25.83	24.63	25,387	25,276	442,330	0.17	0.87	1
Nitrate	n1 = n2	178	105	0.00	0.00	24,944	25,276	442,330	0.50	0.62	1
pH	n1 = n2	217	119	7.94	8.33	36,187	36,565	725,196	0.44	0.66	1
Phosphorus	n1 = n2	33	46	0.02	0.02	1,407	1,320	10,120	0.86	0.39	1
Radium 226	n1 = n2	32	46	0.31	0.30	1,252	1,264	9,691	0.12	0.90	1
Radium 228	n1 = n2	32	46	1.20	1.30	1,214	1,264	9,691	0.50	0.62	1
Redox Potential	n1 = n2	217	119	62.92	66.90	35,299	36,565	725,196	1.49	0.14	1
Selenium	n1 = n2	217	119	0.16	0.09	39,161	36,565	725,196	3.05	0.00	0
Sulfate	n1 = n2	178	105	53.29	49.52	25,925	25,276	442,330	0.98	0.33	1
Temperature	n1 = n2	249	165	21.40	23.10	46,801	51,668	1,420,856	4.08	0.00	0
Total Dissolved Solids	n1 = n2	217	119	468.00	546.00	34,082	36,565	725,196	2.92	0.00	0
Vanadium	n1 = n2	33	46	1.50	1.70	1,261	1,320	10,120	0.58	0.56	1
Zinc	n1 = n2	178	105	0.00	0.00	25,351	25,276	442,330	0.11	0.91	1

*n1: Test Group

*n2: Control Group

Table 5-2: P-Value Determinations of Mann-Whitney U-Test for when Non-Detects are included as ½ the Detection Limit

Constituent	Null Hypothesis	Number of Samples		Median		Minitab Output	Calculation of P-Value for a 2 Tailed Test and 0.95 Confidence Interval				Result
		n1	n2	n1	n2		W	Mean of W	Variance of W	Z-Value	
Alpha, Dissolved	n1 = n2	32	46	5.05	4.65	1,320	1,264	9,691	0.56	0.58	1
Aluminum, Dissolved	n1 = n2	33	46	4.00	4.00	1,263	1,320	10,120	0.56	0.58	1
Arsenic, Total	n1 = n2	218	119	0.67	0.93	35,056	36,842	730,700	2.09	0.04	0
Barium, Total	n1 = n2	217	119	68.84	74.10	36,370	36,565	725,196	0.23	0.82	1
Benzene, Total	n1 = n2	178	105	0.01	0.01	25,883	25,276	442,330	0.91	0.36	1
Beryllium, Total	n1 = n2	178	105	0.00	0.00	24,691	25,276	442,330	0.88	0.38	1
Boron, Dissolved	n1 = n2	33	46	324.00	257.50	1,354	1,320	10,120	0.33	0.74	1
Bromide, Dissolved	n1 = n2	33	46	0.11	0.12	1,239	1,320	10,120	0.81	0.42	1
Bromide, Total	n1 = n2	178	105	0.00	0.00	24,024	25,276	442,330	1.88	0.06	1
Chloride, Total	n1 = n2	178	105	23.08	34.26	23,626	25,276	442,330	2.48	0.01	0
Copper, Total	n1 = n2	178	105	53.31	57.29	24,392	25,276	442,330	1.33	0.18	1
Dissolved Oxygen	n1 = n2	215	111	2.31	1.89	36,897	35,153	650,321	2.16	0.03	0
Ethanol, Total	n1 = n2	49	119	0.32	0.10	4,677	4,141	82,120	1.87	0.06	1
Ethyl Benzene	n1 = n2	178	105	0.01	0.01	25,384	25,276	442,330	0.16	0.87	1
Iron	n1 = n2	178	105	44.50	42.60	24,703	25,276	442,330	0.86	0.39	1
Methanol	n1 = n2	49	119	0.25	0.25	4,222	4,141	82,120	0.28	0.78	1
Molybdenum, Dissolved	n1 = n2	33	46	1.20	1.10	1,336	1,320	10,120	0.15	0.88	1
Molybdenum, Total	n1 = n2	178	105	18.92	20.08	25,360	25,276	442,330	0.13	0.90	1
Nickel	n1 = n2	178	105	25.83	24.63	25,387	25,276	442,330	0.17	0.87	1
Nitrate	n1 = n2	178	105	0.01	0.01	24,944	25,276	442,330	0.50	0.62	1
pH	n1 = n2	217	119	7.94	8.33	36,187	36,565	725,196	0.44	0.66	1
Phosphorus	n1 = n2	33	46	0.02	0.02	1,407	1,320	10,120	0.86	0.39	1
Radium 226	n1 = n2	32	46	0.31	0.30	1,252	1,264	9,691	0.12	0.90	1
Radium 228	n1 = n2	32	46	1.20	1.30	1,214	1,264	9,691	0.50	0.62	1
Redox Potential	n1 = n2	217	119	62.92	66.90	35,299	36,565	725,196	1.49	0.14	1
Selenium	n1 = n2	217	119	0.16	0.09	39,161	36,565	725,196	3.05	0.00	0
Sulfate	n1 = n2	178	105	53.29	49.52	25,925	25,276	442,330	0.98	0.33	1
Temperature	n1 = n2	249	165	21.40	23.10	46,801	51,668	1,420,856	4.08	0.00	0
Total Dissolved Solids	n1 = n2	217	119	468.00	546.00	34,082	36,565	725,196	2.92	0.00	0
Vanadium	n1 = n2	33	46	1.50	1.70	1,261	1,320	10,120	0.58	0.56	1
Zinc	n1 = n2	178	105	0.01	0.01	25,351	25,276	442,330	0.11	0.91	1

*n1: Test Group

*n2: Control Group

Table 5-3: P-Value Determinations of Mann-Whitney U-Test for when Non-Detects are Excluded from analysis

Constituent	Null Hypothesis	Number of Samples		Median		Minitab Output	Calculation of P-Value for a 2 Tailed Test and 0.95 Confidence Interval				Result
		n1	n2	n1	n2		W	Mean of W	Variance of W	Z-Value	
Alpha, Dissolved	n1 = n2	32	46	5.05	4.65	1,320	1,264	9,691	0.56	0.58	1
Aluminum, Dissolved	n1 = n2	33	46	4.00	4.00	1,263	1,320	10,120	0.56	0.58	1
Arsenic, Total	n1 = n2	213	117	0.70	0.95	33,545	35,252	687,404	2.06	0.04	0
Barium, Total	n1 = n2	212	118	69.73	76.46	35,080	35,086	690,025	0.01	0.99	1
Benzene, Total	n1 = n2	17	3	0.03	0.08	160	179	89	1.91	0.06	1
Beryllium, Total	n1 = n2	50	39	4.96	2.52	2,511	2,250	14,625	2.15	0.03	0
Boron, Dissolved	n1 = n2	51	42	0.29	0.37	2,205	2,397	16,779	1.48	0.14	1
Bromide, Dissolved	n1 = n2	33	46	0.11	0.12	1,239	1,320	10,120	0.81	0.42	1
Bromide, Total	n1 = n2	51	42	0.29	0.37	2,205	2,397	16,779	1.48	0.14	1
Chloride, Total	n1 = n2	178	105	23.08	34.26	23,626	25,276	442,330	2.48	0.01	0
Copper, Total	n1 = n2	175	105	53.31	57.29	23,861	24,588	430,281	1.11	0.27	1
Dissolved Oxygen	n1 = n2	213	111	2.33	1.89	36,468	34,613	640,331	2.32	0.02	0
Ethanol, Total	n1 = n2	28	50	1.44	1.06	1,202	1,106	9,217	0.99	0.32	1
Ethyl Benzene	n1 = n2	9	4	0.01	0.02	54	63	42	1.31	0.19	1
Iron	n1 = n2	141	88	74.30	65.80	16,072	16,215	237,820	0.29	0.77	1
Methanol	n1 = n2	6	11	6.74	6.39	48	54	99	0.55	0.58	1
Molybdenum, Dissolved	n1 = n2	33	46	1.20	1.10	1,336	1,320	10,120	0.15	0.88	1
Molybdenum, Total	n1 = n2	170	100	20.06	24.86	23,094	23,035	383,917	0.09	0.93	1
Nickel	n1 = n2	134	76	39.45	41.42	13,977	14,137	179,069	0.38	0.70	1
Nitrate	n1 = n2	72	47	0.77	0.68	4,391	4,320	33,840	0.38	0.70	1
pH	n1 = n2	217	119	7.94	8.33	36,187	36,565	725,196	0.44	0.64	1
Phosphorus	n1 = n2	33	46	0.02	0.02	1,407	1,320	10,120	0.86	0.40	1
Radium 226	n1 = n2	32	46	0.31	0.30	1,252	1,264	9,691	0.12	0.90	1
Radium 228	n1 = n2	32	46	1.20	1.30	1,214	1,264	9,691	0.50	0.62	1
Redox Potential	n1 = n2	217	119	62.92	66.90	35,299	36,565	725,196	1.49	0.14	1
Selenium	n1 = n2	211	103	0.17	0.11	34,450	33,233	570,491	1.61	0.11	1
Sulfate	n1 = n2	177	105	53.61	49.52	25,747	25,046	438,296	1.06	0.29	1
Temperature	n1 = n2	249	165	21.40	23.10	46,801	51,668	1,420,856	4.08	0.00	0
Total Dissolved Solids	n1 = n2	217	119	468.00	546.00	34,082	36,565	725,196	2.92	0.00	0
Vanadium	n1 = n2	33	46	1.50	1.70	1,261	1,320	10,120	0.58	0.56	1
Zinc	n1 = n2	86	49	36.32	44.66	5,769	5,848	47,759	0.36	0.72	1

*n1: Test Group

*n2: Control Group

The results of Test 1 and 2 determined a statistically significant difference between the control group and test group for Arsenic, Chloride, Dissolved Oxygen, Methanol, Selenium, Water Temperature, and Total Dissolved Solids. The median of the test group samples, however, was lower than the control group, with the exception of Dissolved Oxygen which was higher, and Methanol in which the median concentration was the same in both groups. These results do not support the contention that degraded water quality is associated with gas well production and hydraulic fracturing.

In Test 3, where the non-detect values were omitted, the results demonstrated a statistically significant difference in median concentration between Arsenic, Beryllium, Chloride, Dissolved Oxygen, Water Temperature, and Total Dissolved Solids. The median of the test group was less for all constituents except for Beryllium, where the median concentration was higher.

5.3 MODEL ANALYSIS OF WATER CONSTITUENT PREDICTIONS, BOTTOM HOLE PRESSURE, AND GAS WELL DENSITY

In Subgroups 1-6, the maximum, minimum, mean, and median concentrations of the constituents were found (Table 5-4). Included in this table are the Primary Drinking Water MCL values regulated by the EPA (note that there are not Primary drinking water standards for all the constituents studied in this thesis). Any of the values in the Table that exceed a designated MCL threshold are highlighted in yellow.

Table 5-4: Distribution Values of Constituent Concentrations Detected in Subgroups 1-6

Constituent	SUBGROUP 1				SUBGROUP 2				SUBGROUP 3				MCL	UNITS
	Maximum	Minimum	Mean	Median	Maximum	Minimum	Mean	Median	Maximum	Minimum	Mean	Median		
ALP	10.21	4.20	5.97	5.73	7.92	4.66	5.53	5.39	8.51	4.57	5.82	5.64	15	pc/L
AL	4.77	4.00	4.12	4.10	4.28	4.04	4.14	4.13	4.38	4.00	4.13	4.12		ppb
AS	13.72	0.00	1.39	0.00	6.96	0.53	1.71	1.36	10.83	0.00	2.46	1.49	10	ppb
BA	305.86	21.69	133.88	141.13	120.24	35.67	59.40	44.90	170.20	26.94	58.30	43.89	2000	ppb
BENZ	0.036	0.000	0.002	0.001	0.015	0.000	0.004	0.004	0.013	0.000	0.002	0.001	0.005	mg/L
BERY	9.04	0.00	1.71	1.61	4.35	0.00	0.79	0.20	5.45	0.00	1.33	1.01	4	ppb
BO	1607.26	51.18	314.03	246.29	651.34	195.87	474.89	506.61	855.14	217.73	457.75	516.78		ppb
BR.DIS	1.81	0.10	0.46	0.29	1.44	0.11	0.30	0.19	1.59	0.11	0.39	0.23		mg/L
BR.TOT	0.97	0.00	0.25	0.16	0.43	0.00	0.08	0.08	0.68	0.00	0.13	0.09		mg/L
CL	505.57	7.78	63.78	39.04	83.15	11.62	30.73	30.03	102.74	8.05	35.48	30.17		mg/L
CU	887.72	27.16	67.83	60.53	222.53	38.71	59.03	54.83	72.16	34.82	56.41	58.59	1300	ppb
DO	7.28	0.99	3.09	3.06	3.61	1.19	1.99	1.90	4.74	1.23	2.44	2.37		mg/L
ETH	24.33	0.00	1.58	0.72	7.42	0.00	1.23	0.01	10.53	0.00	1.50	0.18		mg/L
ETHB	0.01	0.00	0.00	0.00	0.00	0.00	0.00	0.00	0.00	0.00	0.00	0.00	0.7	ppb
FE	1277.93	7.35	187.26	141.92	545.63	29.79	126.18	105.89	585.51	23.72	129.82	74.41		ppb
METH	17.52	0.00	1.39	0.68	16.10	0.00	1.30	0.00	8.22	0.00	1.00	0.02		mg/L
NIT	8.33	0.00	1.50	1.27	2.00	0.11	0.86	0.57	4.41	0.10	0.96	0.57		mg/L
NI	84.56	2.53	37.54	42.68	47.60	4.52	15.03	8.53	47.88	3.41	17.97	15.09		ppb
MOLY.DIS	3.24	1.01	1.56	1.50	1.99	1.06	1.64	1.65	2.37	1.01	1.70	1.69		ppb
MOLY.TOT	63.86	3.40	29.21	33.30	36.01	5.35	13.02	8.47	37.08	5.43	15.24	12.12		mg/L
PH	9.14	7.03	7.85	7.65	8.86	7.42	8.46	8.68	9.03	7.31	8.43	8.47		
PHOS	0.04	0.02	0.02	0.02	0.03	0.02	0.03	0.02	0.04	0.02	0.02	0.02		mg/L
*R226	2.61	1.08	1.41	1.43	1.58	1.22	1.30	1.26	1.76	1.18	1.35	1.32	5	pc/L
*R228	2.05	0.19	0.69	0.70	0.80	0.36	0.56	0.55	1.55	0.23	0.60	0.57	5	pc/L
ORP	314.93	-191.21	71.93	72.04	142.45	26.31	85.52	90.72	143.71	-123.42	68.08	73.94		mV
SE	36.47	0.02	3.21	1.13	5.19	0.07	0.76	0.29	5.50	0.07	0.96	0.37	50	ppb
SULF	271.76	23.42	71.93	70.75	137.55	44.49	88.71	81.62	115.45	34.64	70.73	67.97		m/L
TDS	1406.46	64.45	492.48	505.85	761.03	122.80	558.86	574.11	751.66	67.41	479.54	511.70		mg/L
T	30.59	10.82	20.94	20.31	29.13	19.92	25.23	24.74	28.95	14.78	23.60	22.49		C
VAN	2.93	1.05	1.79	1.84	1.99	1.06	1.59	1.66	2.40	1.06	1.66	1.75		ppb
ZI	2116.03	0.00	87.64	41.02	179.98	0.71	46.07	21.03	1357.95	0.44	110.91	23.96		ppb

Constituent	SUBGROUP 4				SUBGROUP 5				SUBGROUP 6				MCL	UNITS
	Maximum	Minimum	Mean	Median	Maximum	Minimum	Mean	Median	Maximum	Minimum	Mean	Median		
ALP	8.08	6.55	6.98	6.98	6.97	6.43	6.65	6.63	7.23	6.44	6.58	6.53	15	pc/L
AL	4.20	4.04	4.12	4.13	4.12	4.09	4.11	4.11	4.10	4.07	4.08	4.08		ppb
AS	3.65	0.48	1.93	1.56	2.82	1.57	2.00	1.69	1.88	0.74	1.28	1.25	10	ppb
BA	133.48	24.16	48.96	41.65	86.75	41.69	61.91	61.43	118.74	80.25	97.45	95.24	2000	ppb
BENZ	0.004	0.000	0.001	0.000	0.004	0.000	0.001	0.001	0.003	0.000	0.002	0.002	0.005	mg/L
BERY	2.82	0.44	1.66	1.64	4.34	1.76	2.61	2.35	5.54	2.18	4.47	4.60	4	ppb
BO	543.66	266.43	408.01	414.78	432.81	249.67	315.77	311.68	273.02	141.31	200.40	198.63		ppb
BR.DIS	1.33	0.57	0.71	0.65	0.73	0.56	0.65	0.64	0.98	0.62	0.67	0.64		mg/L
BR.TOT	0.61	0.09	0.34	0.37	0.44	0.07	0.24	0.24	0.14	0.03	0.05	0.04		mg/L
CL	45.48	7.34	25.07	26.09	24.35	9.99	14.05	12.23	22.10	8.14	15.55	16.26		mg/L
CU	68.48	43.99	58.45	58.33	76.36	58.06	64.23	62.76	78.05	58.29	72.22	72.84	1300	ppb
DO	4.08	2.01	2.57	2.46	3.24	1.79	2.48	2.41	3.33	1.70	2.36	2.25		mg/L
ETH	7.39	0.00	0.84	0.30	2.18	0.29	0.65	0.47	3.30	0.75	1.54	1.16		mg/L
ETHB	0.00	0.00	0.00	0.00	0.00	0.00	0.00	0.00	0.00	0.00	0.00	0.00	0.7	ppb
FE	67.25	25.21	38.44	32.55	66.13	31.19	42.09	36.90	64.61	41.84	55.01	56.81		ppb
METH	4.66	0.00	0.99	1.08	1.59	0.97	1.19	1.17	3.81	1.18	2.34	2.23		mg/L
NIT	0.83	0.38	0.63	0.67	0.67	0.41	0.53	0.54	0.51	0.34	0.44	0.44		mg/L
NI	38.19	10.43	20.11	19.34	37.15	18.88	25.73	22.52	41.74	33.54	38.74	39.47		ppb
MOLY.DIS	1.97	1.28	1.69	1.70	1.80	1.52	1.65	1.65	1.70	1.36	1.55	1.55		ppb
MOLY.TOT	29.06	7.80	15.07	14.42	27.80	14.33	19.17	16.63	31.38	25.11	28.81	29.30		mg/L
PH	9.16	7.76	8.71	8.81	8.80	8.00	8.47	8.45	8.22	7.84	8.03	8.06		
PHOS	0.03	0.02	0.02	0.02	0.02	0.02	0.02	0.02	0.02	0.02	0.02	0.02		mg/L
*R226	1.61	1.34	1.44	1.44	1.56	1.42	1.47	1.44	1.78	1.58	1.67	1.67	5	pc/L
*R228	0.80	0.43	0.51	0.48	0.61	0.48	0.54	0.51	0.87	0.62	0.72	0.71	5	pc/L
ORP	101.00	1.71	58.36	67.27	89.46	26.25	65.36	70.58	96.26	24.22	57.97	58.66		mV
SE	1.07	0.15	0.60	0.52	0.91	0.53	0.65	0.58	0.54	0.23	0.41	0.44	50	ppb
SULF	69.28	35.10	47.39	43.52	61.62	41.16	46.42	42.41	57.75	39.06	47.57	48.59		m/L
TDS	598.55	221.84	387.17	390.50	393.47	228.17	312.72	321.64	315.50	208.99	274.60	278.02		mg/L
T	26.06	19.20	23.71	24.06	23.98	22.01	22.82	22.49	22.25	20.12	21.44	21.78		C
VAN	1.75	1.25	1.55	1.57	1.63	1.46	1.54	1.55	1.60	1.34	1.54	1.57		ppb
ZI	37.74	4.01	19.12	19.37	35.65	19.04	25.34	23.64	48.06	33.42	38.65	37.82		ppb

Primary MCL. Source: <http://water.epa.gov/drink/contaminants/index.cfm#one>
 *Radium 226 and Radium 228 have a combined MCL of 5 pc/L

As shown in the chart, the maximum concentration values detected exceed the enforceable standard for Arsenic, Benzene, and Beryllium. In Subgroup 6, however, the median and mean concentrations of Beryllium exceed the MCL threshold designated by

the EPA. Boxplots of the data distributions for each constituent in Subgroup 1 and Subgroup 6 are located in Appendix D.

5.3.1 MANN-WHITNEY U-TEST FOR SUBGROUP 1 AND SUBGROUP 6

The Mann-Whitney U-Test was applied to compare the distribution of concentrations in Subgroup 1 and Subgroup 6 for all the constituents. The results demonstrate a statistically significant difference between the median concentrations for most of the constituents. Total Arsenic, Total Beryllium, Dissolved Bromide, Total Copper, Total Ethanol, Total Methanol, Dissolved Radium 228, and Water Temperature have a greater median concentration in Subgroup 6 than in Subgroup 1. Dissolved Aluminum, Total Bromide, Total Chloride, Dissolved Oxygen, Total Iron, Total Selenium, Total Sulfate, Total Dissolved Solids, and Dissolved Vanadium have a lower median concentration in Subgroup 1. The median concentration of Nitrate in both groups was 0. The results are shown in Table 5-5.

Table 5-5: Results of Mann-Whitney U-Test for Subgroups 1 and 6

Constituent	Null Hypothesis	Number of Samples		Median		Minitab Output <i>W</i>	Calculation of P-Value for a 2 Tailed Test and 0.95 Confidence Interval				Result <i>Accept (1)/ Reject (0)</i>
		<i>n1</i>	<i>n2</i>	<i>n1</i>	<i>n2</i>		<i>Mean of W</i>	<i>Variance of W</i>	<i>Z-Value</i>	<i>P-Value</i>	
Alpha, Dissolved	n1 = n2	11	4161	6.53	5.73	30,710	22,952	15,916,865	1.94	0.05	1
Aluminum, Dissolved	n1 = n2	11	4161	4.08	4.10	14,661	22,952	15,916,865	2.08	0.04	0
Arsenic, Total	n1 = n2	11	4161	1.25	0.00	31,148	22,952	15,916,865	2.05	0.04	0
Barium, Total	n1 = n2	11	4161	95.24	141.13	16,487	22,952	15,916,865	1.62	0.11	1
Benzene, Total	n1 = n2	11	4161	0.0024	0.0013	26,864	22,952	15,916,865	0.98	0.33	1
Beryllium, Total	n1 = n2	11	4161	4.60	1.62	43,121	22,952	15,916,865	5.06	0.00	0
Boron, Dissolved	n1 = n2	11	4161	198.63	246.29	15,508	22,952	15,916,865	1.87	0.06	1
Bromide, Dissolved	n1 = n2	11	4161	0.64	0.29	32,268	22,952	15,916,865	2.34	0.02	0
Bromide, Total	n1 = n2	11	4161	0.04	0.16	12,271	22,952	15,916,865	2.68	0.01	0
Chloride, Total	n1 = n2	11	4161	16.26	39.04	3,167	22,952	15,916,865	4.96	0.00	0
Copper, Total	n1 = n2	11	4161	72.84	60.53	35,829	22,952	15,916,865	3.23	0.00	0
Dissolved Oxygen	n1 = n2	11	4161	2.25	3.06	10,732	22,952	15,916,865	3.06	0.00	0
Ethanol, Total	n1 = n2	11	4161	1.16	0.72	31,332	22,952	15,916,865	2.10	0.04	0
Ethyl Benzene	n1 = n2	11	4161	0.0005	0.0000	25,551	22,952	15,916,865	0.65	0.52	1
Iron	n1 = n2	11	4161	56.81	141.92	7,599	22,952	15,916,865	3.85	0.00	0
Methanol	n1 = n2	11	4161	2.23	0.68	36,230	22,952	15,916,865	3.33	0.00	0
Molybdenum, Dissolved	n1 = n2	11	4161	1.55	1.50	26,901	22,952	15,916,865	0.99	0.32	1
Molybdenum, Total	n1 = n2	11	4161	29.30	33.30	19,631	22,952	15,916,865	0.83	0.41	1
Nickel	n1 = n2	11	4161	0.44	1.27	5,192	22,952	15,916,865	4.45	0.00	0
Nitrate	n1 = n2	11	4161	0.00	0.00	18,570	22,952	15,916,865	1.10	0.03	0
pH	n1 = n2	11	4161	8.06	7.65	29,879	22,952	15,916,865	1.74	0.08	1
Phosphorus	n1 = n2	11	4161	0.02	0.02	29,500	22,952	15,916,865	1.64	0.10	1
Radium 226	n1 = n2	11	4161	0.71	0.70	25,212	22,952	15,916,865	0.57	0.57	1
Radium 228	n1 = n2	11	4161	1.67	1.42	45,437	22,952	15,916,865	5.64	0.00	0
Redox Potential	n1 = n2	11	4161	58.66	72.04	19,394	22,952	15,916,865	0.89	0.37	1
Selenium	n1 = n2	11	4161	0.44	1.13	12,520	22,952	15,916,865	2.61	0.01	0
Sulfate	n1 = n2	11	4161	48.59	70.75	10,036	22,952	15,916,865	3.24	0.00	0
Temperature	n1 = n2	11	4161	21.78	20.32	30,492	22,952	15,916,865	1.89	0.00	0
Total Dissolved Solids	n1 = n2	11	4161	278.02	505.85	5,091	22,952	15,916,865	4.48	0.00	0
Vanadium	n1 = n2	11	4161	1.57	1.84	11,039	22,952	15,916,865	2.99	0.00	0
Zinc	n1 = n2	11	4161	37.82	41.02	21,707	22,952	15,916,865	0.31	0.76	1

*n1 = Subgroup 6 (Test Group)

*n2 = Subgroup 1 (Control Group)

Based upon the results in Table 5-6, nine (9) of the constituents tested have a relationship to degraded water quality, where the mean of Subgroup 6 is greater than Subgroup 1, except for Dissolved Oxygen which showed a lower concentration. Boxplots of these Subgroup 1 and 6 distributions are in Appendix D.

Table 5-6: Statistically Significant Distribution Differences Between Subgroups 1 and 6
Statistically Significant Distribution Differences

Constituent	Conclusion
Arsenic, Total	Median Concentration of Subgroup 6 is GREATER THAN that of Subgroup 1
Beryllium, Total	Median Concentration of Subgroup 6 is GREATER THAN that of Subgroup 1
Bromide, Dissolved	Median Concentration of Subgroup 6 is GREATER THAN that of Subgroup 1
Copper, Total	Median Concentration of Subgroup 6 is GREATER THAN that of Subgroup 1
Dissolved Oxygen	Median Concentration of Subgroup 6 is LESS THAN that of Subgroup 1
Ethanol, Total	Median Concentration of Subgroup 6 is GREATER THAN that of Subgroup 1
Methanol, Total	Median Concentration of Subgroup 6 is GREATER THAN that of Subgroup 1
Radium 228	Median Concentration of Subgroup 6 is GREATER THAN that of Subgroup 1
Temperature	Median Concentration of Subgroup 6 is GREATER THAN that of Subgroup 1

The greater temperature in the Subgroup 6 data corresponds to the lower Dissolved Oxygen levels. The increased Arsenic in the data points may be expected since Arsenic is present in natural gas as trimethylarsine and processing plants are equipped to remove it (Kidnay & Parrish, 2006, p. 211). Bromide, from the shale reservoir may be dissolved in water particles produced with the natural gas, where as it travels through the micro-annulus is contacting the water table and explains an increase the presence of Dissolved Bromide, although, interestingly there is not statistically significant difference in Total Bromide concentrations between the Subgroups. The increased Copper may be associated with the hydraulic fracturing chemicals or shale rock properties. Ethanol is likely related to the hydraulic fracturing chemicals. The increase in Radium 228, and the increased Beryllium (a radionuclide) may be attributed to the produced gas as shale formations have naturally occurring radioactive materials.

5.3.2 R-SQUARED VALUES BETWEEN CONSTITUENTS

The results of the analysis demonstrate a strong correlation between constituent concentrations in the data subgroups associated with a high reservoir pressure gradient and high density of gas wells. The output from the Matlab code for Subgroups 1-6 is shown in Table 5-7 through 5-12, where R-squared values greater than 0.5 are highlighted in red.

Table 5-7: R-Squared Values for Data Extracted in Subgroup 1

	ALP	AL	AS	BA	BENZ	BERY	BO	BR.DISS	BR.TOT	CL	CU	DO	ETH	ETHB	FE	METH	NIT	NI	MOLY.DISS	MOLY.TOT	PH	PHOS	R226	R228	ORP	SE	SULF	TDS	TEMP	VAN	ZI
ALP		0.02	0.00	0.03	0.04	0.07	0.02	0.86	0.66	0.09	0.00	0.04	0.07	0.15	0.04	0.00	0.02	0.12	0.08	0.10	0.05	0.00	0.05	0.00	0.40	0.45	0.07	0.01	0.01	0.40	0.10
AL	0.02		0.00	0.01	0.00	0.00	0.06	0.00	0.01	0.00	0.13	0.02	0.02	0.10	0.00	0.02	0.01	0.01	0.00	0.01	0.02	0.05	0.01	0.04	0.10	0.01	0.00	0.04	0.07	0.01	0.13
AS	0.00	0.00		0.36	0.01	0.05	0.36	0.00	0.02	0.04	0.02	0.08	0.04	0.02	0.00	0.01	0.11	0.13	0.28	0.14	0.09	0.02	0.00	0.05	0.07	0.01	0.00	0.28	0.13	0.00	0.01
BA	0.03	0.01	0.36		0.00	0.07	0.64	0.10	0.13	0.15	0.05	0.26	0.06	0.01	0.09	0.03	0.33	0.77	0.42	0.78	0.74	0.32	0.29	0.24	0.12	0.11	0.00	0.05	0.64	0.10	0.00
BENZ	0.04	0.00	0.01	0.00		0.04	0.01	0.02	0.03	0.26	0.00	0.02	0.32	0.00	0.01	0.07	0.02	0.00	0.01	0.00	0.01	0.00	0.00	0.00	0.06	0.05	0.24	0.12	0.00	0.06	0.03
BERY	0.07	0.00	0.05	0.07	0.04		0.01	0.09	0.04	0.01	0.02	0.08	0.02	0.15	0.21	0.00	0.09	0.31	0.05	0.32	0.33	0.08	0.17	0.00	0.11	0.05	0.00	0.22	0.17	0.23	0.04
BO	0.02	0.06	0.36	0.64	0.01	0.01		0.14	0.10	0.14	0.03	0.31	0.08	0.02	0.04	0.13	0.20	0.56	0.63	0.56	0.50	0.16	0.27	0.23	0.04	0.11	0.01	0.03	0.54	0.02	0.01
BR.DISS	0.86	0.00	0.00	0.10	0.02	0.09	0.14		0.59	0.14	0.00	0.09	0.02	0.08	0.02	0.09	0.03	0.25	0.24	0.22	0.14	0.02	0.15	0.01	0.37	0.36	0.05	0.01	0.07	0.24	0.07
BR.TOT	0.66	0.01	0.02	0.13	0.03	0.04	0.10	0.59		0.25	0.00	0.06	0.02	0.09	0.03	0.00	0.07	0.18	0.13	0.16	0.07	0.04	0.10	0.01	0.29	0.38	0.12	0.10	0.04	0.32	0.10
CL	0.09	0.00	0.04	0.15	0.26	0.01	0.14	0.14	0.25		0.01	0.03	0.27	0.03	0.00	0.06	0.01	0.14	0.12	0.11	0.05	0.06	0.09	0.03	0.00	0.07	0.33	0.43	0.07	0.03	0.05
CU	0.00	0.13	0.02	0.05	0.00	0.02	0.03	0.00	0.00	0.01		0.03	0.01	0.03	0.21	0.00	0.01	0.07	0.01	0.07	0.06	0.05	0.06	0.01	0.01	0.00	0.00	0.05	0.04	0.00	
DO	0.04	0.02	0.08	0.26	0.02	0.08	0.31	0.09	0.06	0.03	0.03		0.02	0.00	0.10	0.04	0.19	0.40	0.23	0.40	0.38	0.13	0.16	0.04	0.03	0.27	0.01	0.02	0.46	0.08	0.00
ETH	0.07	0.02	0.04	0.06	0.32	0.02	0.08	0.02	0.02	0.27	0.01	0.02		0.00	0.02	0.17	0.00	0.04	0.06	0.04	0.02	0.00	0.02	0.02	0.12	0.02	0.03	0.10	0.09	0.07	0.00
ETHB	0.15	0.10	0.02	0.01	0.00	0.15	0.02	0.08	0.09	0.03	0.03	0.00	0.00		0.01	0.01	0.02	0.00	0.00	0.00	0.00	0.01	0.01	0.17	0.12	0.04	0.07	0.01	0.00	0.22	0.14
FE	0.04	0.00	0.00	0.09	0.01	0.21	0.04	0.02	0.03	0.00	0.21	0.10	0.02	0.01		0.00	0.02	0.19	0.02	0.20	0.23	0.10	0.04	0.04	0.00	0.00	0.09	0.13	0.00	0.05	
METH	0.00	0.02	0.01	0.03	0.07	0.00	0.13	0.09	0.00	0.06	0.00	0.04	0.17	0.01	0.00		0.00	0.08	0.11	0.08	0.05	0.00	0.09	0.04	0.02	0.00	0.00	0.00	0.05	0.06	0.00
NIT	0.02	0.01	0.11	0.33	0.02	0.09	0.20	0.03	0.07	0.01	0.01	0.19	0.00	0.02	0.02	0.00		0.29	0.14	0.30	0.31	0.16	0.09	0.01	0.16	0.10	0.00	0.00	0.33	0.11	0.00
NI	0.12	0.01	0.13	0.77	0.00	0.31	0.56	0.25	0.18	0.14	0.07	0.40	0.04	0.00	0.19	0.08	0.29		0.44	0.99	0.91	0.33	0.43	0.18	0.15	0.23	0.01	0.00	0.67	0.22	0.02
MOLY.DISS	0.08	0.00	0.28	0.42	0.01	0.05	0.63	0.24	0.13	0.12	0.01	0.23	0.06	0.00	0.02	0.11	0.14	0.44		0.42	0.33	0.00	0.10	0.03	0.14	0.12	0.00	0.03	0.37	0.00	0.00
MOLY.TOT	0.10	0.01	0.14	0.78	0.00	0.32	0.56	0.22	0.16	0.11	0.07	0.40	0.04	0.00	0.20	0.08	0.30	0.99	0.42		0.92	0.34	0.42	0.20	0.15	0.22	0.01	0.00	0.67	0.23	0.02
PH	0.05	0.02	0.09	0.74	0.01	0.33	0.50	0.14	0.07	0.05	0.06	0.38	0.02	0.00	0.23	0.05	0.31	0.91	0.33	0.92		0.38	0.40	0.24	0.12	0.17	0.00	0.03	0.68	0.19	0.01
PHOS	0.00	0.05	0.02	0.32	0.00	0.08	0.16	0.02	0.04	0.06	0.05	0.13	0.00	0.01	0.10	0.00	0.16	0.33	0.00	0.34	0.38		0.33	0.31	0.01	0.07	0.02	0.00	0.28	0.26	0.00
R226	0.05	0.01	0.00	0.29	0.00	0.17	0.27	0.15	0.10	0.09	0.06	0.16	0.02	0.01	0.04	0.09	0.09	0.43	0.10	0.42	0.40	0.33		0.38	0.05	0.04	0.01	0.00	0.35	0.13	0.06
R228	0.00	0.04	0.05	0.24	0.00	0.00	0.23	0.01	0.01	0.03	0.01	0.04	0.02	0.17	0.04	0.04	0.01	0.18	0.03	0.20	0.24	0.31	0.38		0.00	0.01	0.01	0.00	0.12	0.03	0.00
ORP	0.40	0.10	0.07	0.12	0.06	0.11	0.04	0.37	0.29	0.00	0.01	0.03	0.12	0.12	0.00	0.02	0.16	0.15	0.14	0.15	0.12	0.01	0.05	0.00		0.20	0.03	0.03	0.04	0.31	0.04
SE	0.45	0.01	0.01	0.11	0.05	0.05	0.11	0.36	0.38	0.07	0.00	0.27	0.02	0.04	0.00	0.00	0.10	0.23	0.12	0.22	0.17	0.07	0.04	0.01	0.20		0.08	0.00	0.07	0.38	0.01
SULF	0.07	0.00	0.00	0.00	0.24	0.00	0.01	0.05	0.12	0.33	0.00	0.01	0.03	0.07	0.00	0.00	0.00	0.01	0.00	0.01	0.00	0.02	0.01	0.01	0.03	0.08		0.29	0.01	0.08	0.05
TDS	0.01	0.04	0.28	0.05	0.12	0.22	0.03	0.01	0.10	0.43	0.00	0.02	0.10	0.01	0.09	0.00	0.00	0.00	0.03	0.00	0.03	0.00	0.00	0.00	0.03	0.00	0.29		0.01	0.00	0.01
TEMP	0.01	0.07	0.13	0.64	0.00	0.17	0.54	0.07	0.04	0.07	0.05	0.46	0.09	0.00	0.13	0.05	0.33	0.67	0.37	0.67	0.68	0.28	0.35	0.12	0.04	0.07	0.01	0.01	0.07	0.00	
VAN	0.40	0.01	0.00	0.10	0.06	0.23	0.02	0.24	0.32	0.03	0.04	0.08	0.07	0.22	0.00	0.06	0.11	0.22	0.00	0.23	0.19	0.26	0.13	0.03	0.31	0.38	0.08	0.00	0.07		0.12
ZI	0.10	0.13	0.01	0.00	0.03	0.04	0.01	0.07	0.10	0.05	0.00	0.00	0.00	0.14	0.05	0.00	0.00	0.02	0.00	0.02	0.01	0.00	0.06	0.00	0.04	0.01	0.05	0.01	0.00	0.12	

Table 5-8: R-Squared Values for Data Extracted in Subgroup 2

	ALP	AL	AS	BA	BENZ	BERY	BO	BR.DISS	BR.TOT	CL	CU	DO	ETH	ETHB	FE	METH	NIT	NI	MOLY.DISS	MOLY.TOT	PH	PHOS	R226	R228	ORP	SE	SULF	TDS	TEMP	VAN	ZI
ALP		0.01	0.25	0.09	0.00	0.17	0.07	0.89	0.30	0.47	0.00	0.02	0.37	0.00	0.01	0.75	0.31	0.38	0.12	0.36	0.19	0.00	0.48	0.13	0.09	0.00	0.00	0.06	0.01	0.00	0.14
AL	0.01		0.00	0.24	0.09	0.11	0.45	0.02	0.06	0.11	0.02	0.46	0.24	0.02	0.03	0.06	0.16	0.16	0.33	0.19	0.20	0.01	0.17	0.10	0.13	0.06	0.55	0.43	0.55	0.08	0.21
AS	0.25	0.00		0.03	0.00	0.56	0.00	0.17	0.02	0.03	0.00	0.05	0.02	0.05	0.24	0.20	0.02	0.26	0.01	0.28	0.33	0.22	0.51	0.28	0.27	0.13	0.00	0.29	0.04	0.15	0.01
BA	0.09	0.24	0.03		0.02	0.16	0.66	0.23	0.06	0.00	0.05	0.71	0.66	0.14	0.06	0.35	0.10	0.65	0.39	0.64	0.73	0.00	0.41	0.41	0.65	0.30	0.51	0.59	0.56	0.15	0.04
BENZ	0.00	0.09	0.00	0.02		0.16	0.00	0.00	0.04	0.02	0.09	0.01	0.03	0.55	0.07	0.00	0.03	0.02	0.03	0.02	0.00	0.00	0.04	0.09	0.00	0.11	0.02	0.02	0.04	0.10	0.15
BERY	0.17	0.11	0.56	0.16	0.16		0.17	0.24	0.04	0.01	0.00	0.31	0.12	0.11	0.14	0.24	0.00	0.58	0.15	0.63	0.50	0.02	0.68	0.13	0.37	0.28	0.22	0.59	0.37	0.02	0.20
BO	0.07	0.45	0.00	0.66	0.00	0.17		0.28	0.00	0.02	0.01	0.60	0.71	0.13	0.00	0.28	0.09	0.54	0.80	0.53	0.38	0.17	0.28	0.15	0.24	0.06	0.74	0.46	0.64	0.40	0.06
BR.DISS	0.89	0.02	0.17	0.23	0.00	0.24	0.28		0.24	0.42	0.00	0.12	0.61	0.00	0.01	0.88	0.16	0.56	0.35	0.54	0.30	0.02	0.59	0.14	0.15	0.01	0.08	0.16	0.11	0.05	0.05
BR.TOT	0.30	0.06	0.02	0.06	0.04	0.04	0.00	0.24		0.78	0.00	0.08	0.00	0.11	0.04	0.03	0.40	0.02	0.05	0.01	0.03	0.12	0.01	0.05	0.10	0.05	0.02	0.06	0.00	0.00	0.16
CL	0.47	0.11	0.03	0.00	0.02	0.01	0.02	0.42	0.78		0.01	0.05	0.07	0.00	0.01	0.15	0.34	0.06	0.06	0.04	0.00	0.10	0.03	0.00	0.05	0.07	0.03	0.05	0.06	0.03	0.29
CU	0.00	0.02	0.00	0.05	0.09	0.00	0.01	0.00	0.00	0.01		0.00	0.02	0.11	0.02	0.01	0.04	0.01	0.00	0.00	0.00	0.02	0.00	0.02	0.10	0.00	0.01	0.01	0.04	0.09	0.13
DO	0.02	0.46	0.05	0.71	0.01	0.31	0.60	0.12	0.08	0.05	0.00		0.44	0.04	0.02	0.21	0.24	0.58	0.44	0.59	0.64	0.00	0.41	0.25	0.56	0.40	0.75	0.80	0.89	0.08	0.27
ETH	0.37	0.24	0.02	0.66	0.03	0.12	0.71	0.61	0.00	0.07	0.02	0.44		0.17	0.00	0.69	0.00	0.59	0.60	0.57	0.44	0.07	0.47	0.31	0.31	0.02	0.43	0.38	0.38	0.32	0.00
ETHB	0.00	0.02	0.05	0.14	0.55	0.11	0.13	0.00	0.11	0.00	0.11	0.04	0.17		0.02	0.02	0.14	0.00	0.05	0.00	0.00	0.12	0.02	0.07	0.01	0.08	0.08	0.01	0.01	0.49	0.05
FE	0.01	0.03	0.24	0.06	0.07	0.14	0.00	0.01	0.04	0.01	0.02	0.02	0.00	0.02		0.00	0.07	0.06	0.02	0.05	0.14	0.02	0.03	0.09	0.14	0.04	0.00	0.10	0.01	0.00	0.02
METH	0.75	0.06	0.20	0.35	0.00	0.24	0.28	0.88	0.03	0.15	0.01	0.21	0.69	0.02	0.00		0.07	0.58	0.29	0.59	0.45	0.00	0.70	0.27	0.31	0.02	0.10	0.27	0.17	0.03	0.02
NIT	0.31	0.16	0.02	0.10	0.03	0.00	0.09	0.16	0.40	0.34	0.04	0.24	0.00	0.14	0.07	0.07		0.01	0.02	0.01	0.06	0.00	0.01	0.03	0.05	0.07	0.24	0.17	0.28	0.05	0.55
NI	0.38	0.16	0.26	0.65	0.02	0.58	0.54	0.56	0.02	0.06	0.01	0.58	0.59	0.00	0.06	0.58	0.01		0.43	0.99	0.85	0.00	0.78	0.31	0.52	0.35	0.39	0.70	0.60	0.02	0.07
MOLY.DISS	0.12	0.33	0.01	0.39	0.03	0.15	0.80	0.35	0.05	0.06	0.00	0.44	0.60	0.05	0.02	0.29	0.02	0.43		0.41	0.20	0.35	0.21	0.01	0.10	0.02	0.64	0.29	0.46	0.49	0.04
MOLY.TOT	0.36	0.19	0.28	0.64	0.02	0.63	0.53	0.54	0.01	0.04	0.00	0.59	0.57	0.00	0.05	0.59	0.01	0.99	0.41		0.87	0.00	0.82	0.32	0.57	0.37	0.39	0.73	0.61	0.01	0.09
PH	0.19	0.20	0.33	0.73	0.00	0.50	0.38	0.30	0.03	0.00	0.00	0.64	0.44	0.00	0.14	0.45	0.06	0.85	0.20	0.87		0.06	0.73	0.48	0.75	0.50	0.33	0.81	0.60	0.00	0.11
PHOS	0.00	0.01	0.22	0.00	0.00	0.02	0.17	0.02	0.12	0.10	0.02	0.00	0.07	0.12	0.02	0.00	0.00	0.00	0.35	0.00	0.06		0.05	0.16	0.08	0.14	0.12	0.02	0.00	0.61	0.02
R226	0.48	0.17	0.51	0.41	0.04	0.68	0.28	0.59	0.01	0.03	0.00	0.41	0.47	0.02	0.03	0.70	0.01	0.78	0.21	0.82	0.73	0.05	0.41	0.55	0.24	0.22	0.64	0.40	0.01	0.05	
R228	0.13	0.10	0.28	0.41	0.09	0.13	0.15	0.14	0.05	0.00	0.02	0.25	0.31	0.07	0.09	0.27	0.03	0.31	0.01	0.32	0.48	0.16	0.41		0.47	0.13	0.10	0.37	0.18	0.00	0.00
ORP	0.09	0.13	0.27	0.65	0.00	0.37	0.24	0.15	0.10	0.05	0.10	0.56	0.31	0.01	0.14	0.31	0.05	0.52	0.10	0.57	0.75	0.08	0.55	0.47		0.48	0.30	0.67	0.42	0.00	0.09
SE	0.00	0.06	0.13	0.30	0.11	0.28	0.06	0.01	0.05	0.07	0.00	0.40	0.02	0.08	0.04	0.02	0.07	0.35	0.02	0.37	0.50	0.14	0.24	0.13	0.48		0.18	0.44	0.38	0.12	0.22
SULF	0.00	0.55	0.00	0.51	0.02	0.22	0.74	0.08	0.02	0.03	0.01	0.75	0.43	0.08	0.00	0.10	0.24	0.39	0.64	0.39	0.33	0.12	0.22	0.10	0.30	0.18		0.63	0.77	0.31	0.23
TDS	0.06	0.43	0.29	0.59	0.02	0.59	0.46	0.16	0.06	0.05	0.01	0.80	0.38	0.01	0.10	0.27	0.17	0.70	0.29	0.73	0.81	0.02	0.64	0.37	0.67	0.44	0.63		0.81	0.02	0.29
TEMP	0.01	0.55	0.04	0.56	0.04	0.37	0.64	0.11	0.06	0.05	0.04	0.89	0.38	0.01	0.01	0.17	0.28	0.60	0.46	0.61	0.60	0.00	0.40	0.18	0.42	0.38	0.77	0.81		0.06	0.38
VAN	0.00	0.08	0.15	0.15	0.10	0.02	0.40	0.05	0.00	0.03	0.09	0.08	0.32	0.49	0.00	0.03	0.05	0.02	0.49	0.01	0.00	0.61	0.01	0.00	0.00	0.12	0.31	0.02	0.06		0.02
ZI	0.14	0.21	0.01	0.04	0.15	0.20	0.06	0.05	0.16	0.29	0.13	0.27	0.00	0.05	0.02	0.02	0.55	0.07	0.04	0.09	0.11	0.02	0.05	0.00	0.09	0.22	0.23	0.29	0.38	0.02	

Table 5-9: R-Squared Values for Data Extracted in Subgroup 3

	ALP	AL	AS	BA	BENZ	BERY	BO	BR.DISS	BR.TOT	CL	CU	DO	ETH	ETHB	FE	METH	NIT	NI	MOLY.DISS	MOLY.TOT	PH	PHOS	R226	R228	ORP	SE	SULF	TDS	TEMP	VAN	ZI
ALP		0.17	0.02	0.00	0.01	0.00	0.02	0.86	0.39	0.11	0.00	0.00	0.16	0.16	0.10	0.32	0.25	0.06	0.08	0.04	0.00	0.11	0.18	0.02	0.06	0.00	0.04	0.00	0.04	0.03	0.18
AL	0.17		0.01	0.21	0.12	0.13	0.07	0.05	0.27	0.24	0.08	0.22	0.05	0.08	0.18	0.02	0.21	0.21	0.03	0.23	0.29	0.06	0.01	0.01	0.31	0.06	0.18	0.30	0.56	0.04	0.27
AS	0.02	0.01		0.05	0.01	0.49	0.23	0.00	0.00	0.00	0.12	0.00	0.11	0.04	0.12	0.02	0.00	0.15	0.14	0.16	0.22	0.13	0.15	0.02	0.14	0.92	0.02	0.40	0.01	0.17	0.02
BA	0.00	0.21	0.05		0.01	0.00	0.41	0.09	0.04	0.03	0.38	0.49	0.61	0.15	0.16	0.39	0.13	0.39	0.20	0.38	0.36	0.00	0.17	0.00	0.09	0.00	0.22	0.06	0.49	0.29	0.08
BENZ	0.01	0.12	0.01	0.01		0.09	0.11	0.04	0.05	0.01	0.02	0.11	0.03	0.08	0.01	0.04	0.01	0.10	0.22	0.10	0.01	0.04	0.00	0.11	0.02	0.00	0.33	0.09	0.13	0.06	0.05
BERY	0.00	0.13	0.49	0.00	0.09		0.06	0.00	0.04	0.09	0.14	0.07	0.02	0.15	0.16	0.00	0.00	0.42	0.00	0.45	0.39	0.04	0.04	0.05	0.20	0.50	0.07	0.62	0.20	0.04	0.00
BO	0.02	0.07	0.23	0.41	0.11	0.06		0.17	0.11	0.04	0.24	0.24	0.35	0.07	0.00	0.29	0.02	0.10	0.76	0.06	0.00	0.26	0.00	0.05	0.00	0.11	0.49	0.00	0.18	0.77	0.07
BR.DISS	0.86	0.05	0.00	0.09	0.04	0.00	0.17		0.31	0.09	0.01	0.05	0.35	0.06	0.05	0.58	0.16	0.19	0.27	0.15	0.03	0.16	0.24	0.00	0.04	0.00	0.14	0.01	0.00	0.18	0.09
BR.TOT	0.39	0.27	0.00	0.04	0.05	0.04	0.11	0.31		0.48	0.01	0.01	0.00	0.08	0.12	0.01	0.18	0.01	0.18	0.03	0.18	0.40	0.00	0.03	0.09	0.01	0.04	0.06	0.10	0.13	0.12
CL	0.11	0.24	0.00	0.03	0.01	0.09	0.04	0.09	0.48		0.09	0.09	0.03	0.00	0.07	0.00	0.12	0.04	0.02	0.08	0.21	0.12	0.01	0.04	0.05	0.00	0.02	0.25	0.15	0.02	0.08
CU	0.00	0.08	0.12	0.38	0.02	0.14	0.24	0.01	0.01	0.09		0.14	0.31	0.14	0.07	0.07	0.09	0.01	0.11	0.01	0.04	0.03	0.00	0.00	0.02	0.06	0.12	0.01	0.15	0.31	0.09
DO	0.00	0.22	0.00	0.49	0.11	0.07	0.24	0.05	0.01	0.09	0.14		0.29	0.03	0.11	0.24	0.32	0.52	0.24	0.47	0.37	0.00	0.07	0.06	0.16	0.02	0.42	0.31	0.65	0.21	0.02
ETH	0.16	0.05	0.11	0.61	0.03	0.02	0.35	0.35	0.00	0.03	0.31	0.29		0.00	0.01	0.61	0.01	0.28	0.31	0.26	0.18	0.05	0.12	0.00	0.00	0.06	0.30	0.04	0.23	0.30	0.00
ETHB	0.16	0.08	0.04	0.15	0.08	0.15	0.07	0.06	0.08	0.00	0.14	0.03	0.00		0.20	0.01	0.20	0.00	0.01	0.01	0.00	0.07	0.00	0.04	0.02	0.01	0.02	0.02	0.02	0.06	0.37
FE	0.10	0.18	0.12	0.16	0.01	0.16	0.00	0.05	0.12	0.07	0.07	0.11	0.01	0.20		0.00	0.20	0.23	0.00	0.24	0.36	0.11	0.02	0.00	0.18	0.18	0.00	0.24	0.22	0.01	0.21
METH	0.32	0.02	0.02	0.39	0.04	0.00	0.29	0.58	0.01	0.00	0.07	0.24	0.61	0.01	0.00		0.01	0.29	0.24	0.26	0.16	0.02	0.30	0.01	0.00	0.00	0.17	0.03	0.10	0.25	0.00
NIT	0.25	0.21	0.00	0.13	0.01	0.00	0.02	0.16	0.18	0.12	0.09	0.32	0.01	0.20	0.20	0.01		0.05	0.00	0.04	0.08	0.09	0.01	0.02	0.16	0.02	0.04	0.09	0.26	0.01	0.12
NI	0.06	0.21	0.15	0.39	0.10	0.42	0.10	0.19	0.01	0.04	0.01	0.52	0.28	0.00	0.23	0.29	0.05		0.17	0.98	0.72	0.00	0.28	0.01	0.14	0.27	0.35	0.55	0.56	0.08	0.00
MOLY.DISS	0.08	0.03	0.14	0.20	0.22	0.00	0.76	0.27	0.18	0.02	0.11	0.24	0.31	0.01	0.00	0.24	0.00	0.17		0.11	0.00	0.50	0.01	0.21	0.01	0.07	0.63	0.01	0.17	0.76	0.01
MOLY.TOT	0.04	0.23	0.16	0.38	0.10	0.45	0.06	0.15	0.03	0.08	0.01	0.47	0.26	0.01	0.24	0.26	0.04	0.98	0.11		0.79	0.02	0.31	0.00	0.13	0.29	0.28	0.56	0.55	0.04	0.01
PH	0.00	0.29	0.22	0.36	0.01	0.39	0.00	0.03	0.18	0.21	0.04	0.37	0.18	0.00	0.36	0.16	0.08	0.72	0.00	0.79		0.13	0.33	0.02	0.20	0.33	0.11	0.64	0.51	0.00	0.02
PHOS	0.11	0.06	0.13	0.00	0.04	0.04	0.26	0.16	0.40	0.12	0.03	0.00	0.05	0.07	0.11	0.02	0.09	0.00	0.50	0.02	0.13		0.13	0.18	0.19	0.16	0.15	0.05	0.01	0.41	0.05
R226	0.18	0.01	0.15	0.17	0.00	0.04	0.00	0.24	0.00	0.01	0.00	0.07	0.12	0.00	0.02	0.30	0.01	0.28	0.01	0.31	0.33	0.13		0.33	0.01	0.21	0.00	0.07	0.06	0.03	0.03
R228	0.02	0.01	0.02	0.00	0.11	0.05	0.05	0.00	0.03	0.04	0.00	0.06	0.00	0.04	0.00	0.01	0.02	0.01	0.21	0.00	0.02	0.18	0.33		0.00	0.02	0.15	0.02	0.06	0.20	0.00
ORP	0.06	0.31	0.14	0.09	0.02	0.20	0.00	0.04	0.09	0.05	0.02	0.16	0.00	0.02	0.18	0.00	0.16	0.14	0.01	0.13	0.20	0.19	0.01	0.00		0.18	0.11	0.36	0.41	0.00	0.10
SE	0.00	0.06	0.92	0.00	0.00	0.50	0.11	0.00	0.01	0.00	0.06	0.02	0.06	0.01	0.18	0.00	0.02	0.27	0.07	0.29	0.33	0.16	0.21	0.02	0.18		0.00	0.47	0.09	0.10	0.00
SULF	0.04	0.18	0.02	0.22	0.33	0.07	0.49	0.14	0.04	0.02	0.12	0.42	0.30	0.02	0.00	0.17	0.04	0.35	0.63	0.28	0.11	0.15	0.00	0.15	0.11	0.00		0.27	0.46	0.44	0.07
TDS	0.00	0.30	0.40	0.06	0.09	0.62	0.00	0.01	0.06	0.25	0.01	0.31	0.04	0.02	0.24	0.03	0.09	0.55	0.01	0.56	0.64	0.05	0.07	0.02	0.36	0.47	0.27		0.49	0.00	0.04
TEMP	0.04	0.56	0.01	0.49	0.13	0.20	0.18	0.00	0.10	0.15	0.15	0.65	0.23	0.02	0.22	0.10	0.26	0.56	0.17	0.55	0.51	0.01	0.06	0.06	0.41	0.09	0.46	0.49	0.14	0.11	
VAN	0.03	0.04	0.17	0.29	0.06	0.04	0.77	0.18	0.13	0.02	0.31	0.21	0.30	0.06	0.01	0.25	0.01	0.08	0.76	0.04	0.00	0.41	0.03	0.20	0.00	0.10	0.44	0.00	0.14		0.07
ZI	0.18	0.27	0.02	0.08	0.05	0.00	0.07	0.09	0.12	0.08	0.09	0.02	0.00	0.37	0.21	0.00	0.12	0.00	0.01	0.01	0.02	0.05	0.03	0.00	0.10	0.00	0.07	0.04	0.11	0.07	

Table 5-10: R-Squared Values for Data Extracted in Subgroup 4

	ALP	AL	AS	BA	BENZ	BERY	BO	BR.DISS	BR.TOT	CL	CU	DO	ETH	ETHB	FE	METH	NIT	NI	MOLY.DISS	MOLY.TOT	PH	PHOS	R226	R228	ORP	SE	SULF	TDS	TEMP	VAN	ZI
ALP		0.19	0.73	0.39	0.38	0.45	0.47	0.78	0.05	0.00	0.83	0.74	0.56	0.20	0.00	0.08	0.07	0.08	0.78	0.08	0.01	0.71	0.09	0.31	0.33	0.76	0.48	0.25	0.11	0.78	0.02
AL	0.19		0.56	0.11	0.57	0.69	0.09	0.01	0.78	0.33	0.26	0.04	0.03	0.37	0.58	0.27	0.71	0.43	0.31	0.44	0.55	0.41	0.43	0.19	0.20	0.54	0.44	0.89	0.13	0.24	0.55
AS	0.73	0.56		0.06	0.74	0.63	0.42	0.47	0.34	0.01	0.75	0.56	0.19	0.50	0.17	0.00	0.33	0.01	0.85	0.01	0.11	0.85	0.01	0.03	0.58	0.95	0.83	0.60	0.00	0.79	0.04
BA	0.39	0.11	0.06		0.00	0.00	0.34	0.64	0.28	0.25	0.20	0.52	0.91	0.01	0.41	0.48	0.24	0.65	0.22	0.65	0.64	0.08	0.66	0.84	0.02	0.10	0.01	0.09	0.57	0.28	0.56
BENZ	0.38	0.57	0.74	0.00		0.66	0.08	0.17	0.55	0.01	0.56	0.30	0.02	0.90	0.50	0.05	0.61	0.13	0.53	0.14	0.36	0.67	0.09	0.02	0.65	0.55	0.88	0.60	0.13	0.39	0.13
BERY	0.45	0.69	0.63	0.00	0.66		0.07	0.13	0.59	0.17	0.64	0.23	0.02	0.53	0.39	0.13	0.63	0.25	0.44	0.25	0.30	0.58	0.21	0.03	0.37	0.55	0.51	0.76	0.09	0.34	0.33
BO	0.47	0.09	0.42	0.34	0.08	0.07		0.60	0.00	0.05	0.25	0.43	0.37	0.01	0.05	0.09	0.01	0.17	0.68	0.16	0.09	0.39	0.10	0.37	0.15	0.58	0.21	0.06	0.37	0.78	0.06
BR.DISS	0.78	0.01	0.47	0.64	0.17	0.13	0.60		0.00	0.15	0.64	0.89	0.78	0.08	0.07	0.32	0.01	0.33	0.73	0.33	0.16	0.42	0.31	0.64	0.34	0.51	0.34	0.02	0.29	0.79	0.22
BR.TOT	0.05	0.78	0.34	0.28	0.55	0.59	0.00	0.00		0.33	0.20	0.01	0.15	0.43	0.01	0.37	0.88	0.63	0.13	0.63	0.75	0.20	0.61	0.38	0.18	0.25	0.38	0.80	0.43	0.08	0.68
CL	0.00	0.33	0.01	0.25	0.01	0.17	0.05	0.15	0.33		0.00	0.16	0.23	0.00	0.18	0.34	0.30	0.41	0.01	0.40	0.27	0.00	0.43	0.36	0.14	0.02	0.01	0.38	0.12	0.02	0.53
CU	0.83	0.26	0.75	0.20	0.56	0.64	0.25	0.64	0.20	0.00		0.73	0.36	0.43	0.05	0.03	0.23	0.00	0.74	0.00	0.01	0.64	0.01	0.12	0.53	0.67	0.64	0.36	0.00	0.68	0.00
DO	0.74	0.04	0.56	0.52	0.30	0.23	0.43	0.89	0.01	0.16	0.73		0.72	0.24	0.00	0.20	0.00	0.16	0.71	0.16	0.05	0.51	0.20	0.42	0.52	0.53	0.50	0.05	0.08	0.71	0.11
ETH	0.56	0.03	0.19	0.91	0.02	0.02	0.37	0.78	0.15	0.23	0.36	0.72		0.01	0.25	0.44	0.12	0.50	0.37	0.50	0.39	0.22	0.54	0.77	0.13	0.23	0.09	0.02	0.41	0.42	0.41
ETHB	0.20	0.37	0.50	0.01	0.90	0.53	0.01	0.08	0.43	0.00	0.43	0.24	0.01		0.53	0.04	0.53	0.15	0.34	0.16	0.35	0.47	0.09	0.05	0.66	0.31	0.75	0.39	0.22	0.21	0.11
FE	0.00	0.58	0.17	0.41	0.50	0.39	0.05	0.07	0.81	0.18	0.05	0.00	0.25	0.53		0.49	0.74	0.76	0.03	0.77	0.86	0.09	0.65	0.58	0.16	0.08	0.31	0.51	0.61	0.00	0.64
METH	0.08	0.27	0.00	0.48	0.05	0.13	0.09	0.32	0.37	0.34	0.03	0.20	0.44	0.04	0.49		0.30	0.75	0.04	0.76	0.52	0.00	0.67	0.59	0.01	0.00	0.00	0.24	0.36	0.07	0.69
NIT	0.07	0.71	0.33	0.24	0.61	0.63	0.01	0.01	0.88	0.30	0.23	0.00	0.12	0.53	0.74	0.30		0.57	0.11	0.57	0.71	0.22	0.51	0.36	0.19	0.21	0.35	0.77	0.43	0.05	0.58
NI	0.08	0.43	0.01	0.65	0.13	0.25	0.17	0.33	0.63	0.41	0.00	0.16	0.50	0.15	0.76	0.75	0.57		0.03	1.00	0.80	0.00	0.92	0.85	0.00	0.00	0.02	0.38	0.64	0.07	0.92
MOLY.DISS	0.78	0.31	0.85	0.22	0.53	0.44	0.68	0.73	0.13	0.01	0.74	0.71	0.37	0.34	0.03	0.04	0.11	0.03		0.02	0.00	0.76	0.01	0.19	0.55	0.86	0.70	0.31	0.07	0.97	0.00
MOLY.TOT	0.08	0.44	0.01	0.65	0.14	0.25	0.16	0.33	0.63	0.40	0.00	0.16	0.50	0.16	0.77	0.76	0.57	1.00	0.02		0.82	0.00	0.92	0.85	0.01	0.00	0.03	0.39	0.64	0.06	0.92
PH	0.01	0.55	0.11	0.64	0.36	0.30	0.09	0.16	0.75	0.27	0.01	0.05	0.39	0.35	0.86	0.52	0.71	0.80	0.00	0.82		0.07	0.73	0.69	0.11	0.05	0.19	0.52	0.69	0.00	0.75
PHOS	0.71	0.41	0.85	0.08	0.67	0.58	0.39	0.42	0.20	0.00	0.64	0.51	0.22	0.47	0.09	0.00	0.22	0.00	0.76	0.00	0.07	0.00	0.06	0.55	0.80	0.72	0.49	0.00	0.69	0.02	
R226	0.09	0.43	0.01	0.66	0.09	0.21	0.10	0.31	0.61	0.43	0.01	0.20	0.54	0.09	0.65	0.67	0.51	0.92	0.01	0.92	0.73	0.00		0.81	0.00	0.00	0.01	0.38	0.51	0.04	0.92
R228	0.31	0.19	0.03	0.84	0.02	0.03	0.37	0.64	0.38	0.36	0.12	0.42	0.77	0.05	0.58	0.59	0.36	0.85	0.19	0.85	0.69	0.06	0.81		0.02	0.06	0.01	0.16	0.68	0.27	0.71
ORP	0.33	0.20	0.58	0.02	0.65	0.37	0.15	0.34	0.18	0.14	0.53	0.52	0.13	0.66	0.16	0.01	0.19	0.00	0.55	0.01	0.11	0.55	0.00	0.02		0.43	0.74	0.21	0.04	0.46	0.00
SE	0.76	0.54	0.95	0.10	0.55	0.55	0.58	0.51	0.25	0.02	0.67	0.53	0.23	0.31	0.08	0.00	0.21	0.00	0.86	0.00	0.05	0.80	0.00	0.06	0.43		0.67	0.54	0.02	0.84	0.02
SULF	0.48	0.44	0.83	0.01	0.88	0.51	0.21	0.34	0.38	0.01	0.64	0.50	0.09	0.75	0.31	0.00	0.35	0.02	0.70	0.03	0.19	0.72	0.01	0.01	0.74	0.67		0.45	0.04	0.58	0.03
TDS	0.25	0.89	0.60	0.09	0.60	0.76	0.06	0.02	0.80	0.38	0.36	0.05	0.02	0.39	0.51	0.24	0.77	0.38	0.31	0.39	0.52	0.49	0.38	0.16	0.21	0.54	0.45		0.18	0.24	0.52
TEMP	0.11	0.13	0.00	0.57	0.13	0.09	0.37	0.29	0.43	0.12	0.00	0.08	0.41	0.22	0.61	0.36	0.43	0.64	0.07	0.64	0.69	0.00	0.51	0.68	0.04	0.02	0.04	0.18		0.12	0.50
VAN	0.78	0.24	0.79	0.28	0.39	0.34	0.78	0.79	0.08	0.02	0.68	0.71	0.42	0.21	0.00	0.07	0.05	0.07	0.97	0.06	0.00	0.69	0.04	0.27	0.46	0.84	0.58	0.24	0.12		0.01
ZI	0.02	0.55	0.04	0.56	0.13	0.33	0.06	0.22	0.68	0.53	0.00	0.11	0.41	0.11	0.64	0.69	0.58	0.92	0.00	0.92	0.75	0.02	0.92	0.71	0.00	0.02	0.03	0.52	0.50	0.01	

Table 5-11: R-Squared Values for Data Extracted in Subgroup 5

	ALP	AL	AS	BA	BENZ	BERY	BO	BR.DISS	BR.TOT	CL	CU	DO	ETH	ETHB	FE	METH	NIT	NI	MOLY.DISS	MOLY.TOT	PH	PHOS	R226	R228	ORP	SE	SULF	TDS	TEMP	VAN	ZI
ALP		0.78	0.39	0.24	0.18	0.20	0.64	0.55	0.45	0.20	0.26	0.17	0.33	0.01	0.09	0.01	0.35	0.12	0.01	0.11	0.25	0.19	0.01	0.00	0.43	0.28	0.19	0.68	0.39	0.04	0.18
AL	0.78		0.11	0.44	0.58	0.63	0.34	0.48	0.80	0.64	0.65	0.44	0.52	0.01	0.46	0.04	0.66	0.49	0.25	0.48	0.62	0.51	0.26	0.15	0.83	0.05	0.60	0.80	0.46	0.30	0.55
AS	0.39	0.11		0.02	0.00	0.02	0.17	0.62	0.00	0.01	0.01	0.10	0.02	0.09	0.18	0.11	0.00	0.13	0.01	0.13	0.04	0.01	0.33	0.42	0.04	0.96	0.01	0.33	0.00	0.00	0.07
BA	0.24	0.44	0.02		0.22	0.65	0.40	0.00	0.74	0.32	0.74	0.04	0.74	0.39	0.59	0.03	0.61	0.75	0.05	0.73	0.82	0.30	0.59	0.63	0.33	0.09	0.30	0.37	0.81	0.04	0.80
BENZ	0.18	0.58	0.00	0.22		0.72	0.00	0.24	0.59	0.94	0.54	0.68	0.29	0.02	0.66	0.16	0.61	0.58	0.70	0.59	0.51	0.72	0.50	0.27	0.75	0.01	0.79	0.38	0.13	0.73	0.54
BERY	0.20	0.63	0.02	0.65	0.72		0.07	0.08	0.85	0.80	0.95	0.43	0.62	0.02	0.84	0.03	0.78	0.92	0.52	0.92	0.89	0.63	0.75	0.58	0.72	0.08	0.70	0.50	0.42	0.49	0.94
BO	0.64	0.34	0.17	0.40	0.00	0.07		0.07	0.30	0.01	0.14	0.02	0.37	0.24	0.04	0.01	0.20	0.09	0.13	0.08	0.22	0.00	0.01	0.05	0.08	0.08	0.01	0.34	0.64	0.10	0.14
BR.DISS	0.55	0.48	0.62	0.00	0.24	0.08	0.07		0.09	0.23	0.08	0.58	0.00	0.12	0.01	0.00	0.06	0.00	0.19	0.00	0.03	0.31	0.02	0.12	0.49	0.59	0.25	0.55	0.03	0.30	0.01
BR.TOT	0.45	0.80	0.00	0.74	0.59	0.85	0.30	0.09		0.67	0.84	0.23	0.83	0.09	0.79	0.10	0.88	0.86	0.22	0.84	0.90	0.45	0.65	0.57	0.65	0.04	0.58	0.53	0.62	0.22	0.89
CL	0.20	0.64	0.01	0.32	0.94	0.80	0.01	0.23	0.67		0.68	0.63	0.30	0.00	0.78	0.17	0.57	0.67	0.70	0.68	0.66	0.70	0.59	0.33	0.87	0.02	0.94	0.40	0.24	0.71	0.63
CU	0.26	0.65	0.01	0.74	0.54	0.95	0.14	0.08	0.84	0.68		0.35	0.63	0.04	0.75	0.01	0.69	0.87	0.41	0.87	0.92	0.51	0.65	0.52	0.71	0.06	0.64	0.55	0.52	0.37	0.93
DO	0.17	0.44	0.10	0.04	0.68	0.43	0.02	0.58	0.23	0.63	0.35		0.05	0.17	0.20	0.00	0.22	0.19	0.81	0.19	0.19	0.70	0.09	0.00	0.71	0.08	0.57	0.47	0.01	0.90	0.20
ETH	0.01	0.01	0.09	0.39	0.02	0.02	0.24	0.12	0.09	0.00	0.04	0.17		0.00	0.07	0.11	0.05	0.10	0.18	0.09	0.10	0.02	0.13	0.25	0.01	0.13	0.00	0.00	0.28	0.16	0.10
ETHB	0.05	0.41	0.12	0.38	0.84	0.82	0.00	0.04	0.62	0.90	0.66	0.41	0.33	0.00	0.90	0.23	0.58	0.80	0.62	0.82	0.70	0.58	0.82	0.57	0.64	0.16	0.82	0.23	0.24	0.58	0.71
FE	0.09	0.46	0.18	0.59	0.66	0.84	0.04	0.01	0.79	0.78	0.75	0.20	0.54	0.07		0.25	0.67	0.93	0.36	0.94	0.87	0.42	0.93	0.79	0.55	0.25	0.72	0.22	0.44	0.32	0.86
METH	0.01	0.04	0.11	0.03	0.16	0.03	0.01	0.00	0.10	0.17	0.01	0.00	0.11	0.23	0.25		0.08	0.10	0.00	0.10	0.09	0.03	0.21	0.18	0.05	0.07	0.18	0.00	0.10	0.00	0.04
NIT	0.35	0.66	0.00	0.61	0.61	0.78	0.20	0.06	0.88	0.57	0.69	0.22	0.84	0.05	0.67	0.08		0.79	0.20	0.77	0.74	0.45	0.61	0.55	0.49	0.02	0.40	0.52	0.43	0.21	0.82
NI	0.12	0.49	0.13	0.75	0.58	0.92	0.09	0.00	0.86	0.67	0.87	0.19	0.72	0.10	0.93	0.10	0.79		0.32	1.00	0.93	0.43	0.91	0.83	0.52	0.22	0.58	0.31	0.50	0.27	0.98
MOLY.DISS	0.01	0.25	0.01	0.05	0.70	0.52	0.13	0.19	0.22	0.70	0.41	0.81	0.05	0.18	0.36	0.00	0.20	0.32		0.34	0.26	0.57	0.28	0.09	0.59	0.01	0.63	0.21	0.00	0.97	0.30
MOLY.TOT	0.11	0.48	0.13	0.73	0.59	0.92	0.08	0.00	0.84	0.68	0.87	0.19	0.69	0.09	0.94	0.10	0.77	1.00	0.34		0.93	0.44	0.92	0.82	0.52	0.23	0.60	0.30	0.49	0.29	0.98
PH	0.25	0.62	0.04	0.82	0.51	0.89	0.22	0.03	0.90	0.66	0.92	0.19	0.69	0.10	0.87	0.09	0.74	0.93	0.26	0.93		0.40	0.77	0.69	0.62	0.11	0.63	0.45	0.70	0.22	0.95
PHOS	0.19	0.51	0.01	0.30	0.72	0.63	0.00	0.31	0.45	0.70	0.51	0.70	0.23	0.02	0.42	0.03	0.45	0.43	0.57	0.44	0.40	0.40	0.33	0.15	0.68	0.00	0.61	0.44	0.13	0.67	0.45
R226	0.01	0.26	0.33	0.59	0.50	0.75	0.01	0.02	0.65	0.59	0.65	0.09	0.52	0.13	0.93	0.21	0.61	0.91	0.28	0.92	0.77	0.33		0.92	0.34	0.43	0.51	0.10	0.35	0.22	0.83
R228	0.00	0.15	0.42	0.63	0.27	0.58	0.05	0.12	0.57	0.33	0.52	0.00	0.60	0.25	0.79	0.18	0.55	0.83	0.09	0.82	0.69	0.15	0.92		0.15	0.54	0.27	0.04	0.39	0.05	0.75
ORP	0.43	0.83	0.04	0.33	0.75	0.72	0.08	0.49	0.65	0.87	0.71	0.71	0.28	0.01	0.55	0.05	0.49	0.52	0.59	0.52	0.62	0.68	0.34	0.15		0.01	0.88	0.66	0.30	0.64	0.55
SE	0.28	0.05	0.96	0.09	0.01	0.08	0.08	0.59	0.04	0.02	0.06	0.08	0.08	0.13	0.25	0.07	0.02	0.22	0.01	0.23	0.11	0.00	0.43	0.54	0.01		0.02	0.20	0.01	0.00	0.16
SULF	0.19	0.60	0.01	0.30	0.79	0.70	0.01	0.25	0.58	0.94	0.64	0.57	0.20	0.00	0.72	0.18	0.40	0.58	0.63	0.60	0.63	0.61	0.51	0.27	0.88	0.02		0.36	0.28	0.64	0.54
TDS	0.68	0.80	0.33	0.37	0.38	0.50	0.34	0.55	0.53	0.40	0.55	0.47	0.35	0.00	0.22	0.00	0.52	0.31	0.21	0.30	0.45	0.44	0.10	0.04	0.66	0.20	0.36		0.39	0.27	0.40
TEMP	0.39	0.46	0.00	0.81	0.13	0.42	0.64	0.03	0.62	0.24	0.52	0.01	0.53	0.28	0.44	0.10	0.43	0.50	0.00	0.49	0.70	0.13	0.35	0.39	0.30	0.01	0.28	0.39	0.00	0.50	0.54
VAN	0.04	0.30	0.00	0.04	0.73	0.49	0.10	0.30	0.22	0.71	0.37	0.90	0.04	0.16	0.32	0.00	0.21	0.27	0.97	0.29	0.22	0.67	0.22	0.05	0.64	0.00	0.64	0.27	0.00		0.26
ZI	0.18	0.55	0.07	0.80	0.54	0.94	0.14	0.01	0.89	0.63	0.93	0.20	0.78	0.10	0.86	0.04	0.82	0.98	0.30	0.98	0.95	0.45	0.83	0.75	0.55	0.16	0.54	0.40	0.54	0.26	

Table 5-12: R-Squared Values for Data Extracted in Subgroup 6

	ALP	AL	AS	BA	BENZ	BERY	BO	BR.DISS	BR.TOT	CL	CU	DO	ETH	ETHB	FE	METH	NIT	NI	MOLY.DISS	MOLY.TOT	PH	PHOS	R226	R228	ORP	SE	SULF	TDS	TEMP	VAN	ZI
ALP		0.29	0.14	0.33	0.44	0.84	0.11	0.95	0.86	0.34	0.79	0.44	0.59	0.32	0.03	0.07	0.11	0.54	0.34	0.47	0.00	0.70	0.00	0.39	0.08	0.29	0.24	0.05	0.11	0.77	0.21
AL	0.29		0.25	0.00	0.01	0.37	0.85	0.16	0.44	0.02	0.07	0.01	0.01	0.03	0.02	0.61	0.01	0.33	0.09	0.29	0.08	0.03	0.58	0.08	0.30	0.13	0.02	0.24	0.16	0.09	0.56
AS	0.14	0.25		0.23	0.28	0.09	0.44	0.24	0.02	0.51	0.46	0.76	0.45	0.14	0.09	0.36	0.13	0.04	0.70	0.03	0.14	0.27	0.80	0.81	0.89	0.88	0.36	0.82	0.69	0.25	0.12
BA	0.33	0.00	0.23		0.50	0.32	0.00	0.45	0.12	0.58	0.44	0.49	0.66	0.44	0.20	0.08	0.01	0.15	0.49	0.13	0.16	0.49	0.13	0.51	0.34	0.44	0.63	0.01	0.37	0.56	0.00
BENZ	0.44	0.01	0.28	0.50		0.36	0.01	0.58	0.14	0.92	0.52	0.63	0.71	0.93	0.68	0.00	0.01	0.51	0.62	0.52	0.05	0.75	0.08	0.42	0.33	0.37	0.91	0.07	0.18	0.79	0.02
BERY	0.84	0.37	0.09	0.32	0.36		0.16	0.83	0.73	0.24	0.80	0.44	0.67	0.33	0.02	0.16	0.00	0.74	0.23	0.66	0.00	0.55	0.00	0.27	0.04	0.17	0.19	0.04	0.03	0.73	0.43
BO	0.11	0.85	0.44	0.00	0.01	0.16		0.03	0.21	0.09	0.00	0.09	0.00	0.00	0.03	0.67	0.06	0.16	0.26	0.14	0.15	0.00	0.78	0.23	0.44	0.28	0.06	0.43	0.26	0.01	0.43
BR.DISS	0.95	0.16	0.24	0.45	0.58	0.83	0.03		0.74	0.49	0.86	0.58	0.73	0.42	0.07	0.03	0.09	0.55	0.53	0.49	0.01	0.83	0.04	0.54	0.16	0.41	0.38	0.09	0.16	0.90	0.17
BR.TOT	0.86	0.44	0.02	0.12	0.14	0.73	0.21	0.74		0.07	0.52	0.16	0.28	0.07	0.02	0.15	0.19	0.37	0.13	0.30	0.00	0.46	0.01	0.19	0.00	0.10	0.03	0.01	0.01	0.49	0.36
CL	0.34	0.02	0.51	0.58	0.92	0.24	0.09	0.49	0.07		0.52	0.76	0.72	0.78	0.61	0.05	0.00	0.29	0.78	0.30	0.04	0.66	0.28	0.62	0.60	0.60	0.96	0.19	0.41	0.68	0.01
CU	0.79	0.07	0.46	0.44	0.52	0.80	0.00	0.86	0.52	0.52		0.82	0.85	0.40	0.08	0.00	0.05	0.56	0.54	0.48	0.02	0.64	0.12	0.65	0.36	0.57	0.39	0.29	0.32	0.78	0.09
DO	0.44	0.01	0.76	0.49	0.63	0.44	0.09	0.58	0.16	0.76	0.82		0.88	0.50	0.26	0.06	0.01	0.36	0.75	0.33	0.05	0.55	0.38	0.79	0.72	0.77	0.64	0.49	0.52	0.65	0.00
ETH	0.59	0.01	0.45	0.66	0.71	0.67	0.00	0.73	0.28	0.72	0.85	0.88		0.63	0.27	0.00	0.00	0.55	0.66	0.51	0.00	0.68	0.16	0.65	0.43	0.55	0.66	0.22	0.29	0.83	0.06
ETHB	0.32	0.03	0.14	0.44	0.93	0.33	0.00	0.42	0.07	0.78	0.40	0.50	0.63		0.80	0.00	0.11	0.59	0.39	0.62	0.02	0.56	0.01	0.22	0.21	0.19	0.85	0.02	0.08	0.66	0.05
FE	0.03	0.02	0.09	0.20	0.68	0.02	0.03	0.07	0.02	0.61	0.08	0.26	0.27	0.80		0.03	0.21	0.25	0.23	0.30	0.06	0.23	0.03	0.07	0.20	0.08	0.73	0.01	0.05	0.25	0.00
METH	0.07	0.61	0.36	0.08	0.00	0.16	0.67	0.03	0.15	0.05	0.00	0.06	0.00	0.00	0.03		0.10	0.06	0.13	0.05	0.58	0.00	0.48	0.09	0.29	0.15	0.02	0.50	0.09	0.02	0.23
NIT	0.11	0.01	0.13	0.01	0.01	0.00	0.06	0.09	0.19	0.00	0.05	0.01	0.00	0.11	0.21	0.10		0.07	0.08	0.10	0.04	0.05	0.16	0.18	0.04	0.19	0.03	0.14	0.16	0.01	0.07
NI	0.54	0.33	0.04	0.15	0.51	0.74	0.16	0.55	0.37	0.29	0.56	0.36	0.55	0.59	0.25	0.06	0.07		0.14	0.99	0.06	0.45	0.04	0.09	0.02	0.05	0.27	0.02	0.00	0.62	0.51
MOLY.DISS	0.34	0.09	0.70	0.49	0.62	0.23	0.26	0.53	0.13	0.78	0.54	0.75	0.66	0.39	0.23	0.13	0.08	0.14		0.13	0.08	0.68	0.57	0.89	0.62	0.76	0.65	0.41	0.48	0.62	0.01
MOLY.TOT	0.47	0.29	0.03	0.13	0.52	0.66	0.14	0.49	0.30	0.30	0.48	0.33	0.51	0.62	0.30	0.05	0.10	0.99	0.13		0.08	0.44	0.05	0.07	0.01	0.03	0.29	0.02	0.01	0.60	0.52
PH	0.00	0.08	0.14	0.16	0.05	0.00	0.15	0.01	0.00	0.04	0.02	0.05	0.00	0.02	0.06	0.58	0.04	0.06	0.08	0.08		0.05	0.08	0.02	0.04	0.02	0.01	0.35	0.00	0.01	0.02
PHOS	0.70	0.03	0.27	0.49	0.75	0.55	0.00	0.83	0.46	0.66	0.64	0.55	0.68	0.56	0.23	0.00	0.05	0.45	0.68	0.44	0.05	0.09	0.54	0.21	0.40	0.57	0.10	0.14	0.91	0.10	
R226	0.00	0.58	0.80	0.13	0.08	0.00	0.78	0.04	0.01	0.28	0.12	0.38	0.16	0.01	0.03	0.48	0.16	0.04	0.57	0.05	0.08	0.09		0.64	0.72	0.67	0.19	0.66	0.62	0.05	0.35
R228	0.39	0.08	0.81	0.51	0.42	0.27	0.23	0.54	0.19	0.62	0.65	0.79	0.65	0.22	0.07	0.09	0.18	0.09	0.89	0.07	0.02	0.54	0.64		0.71	0.93	0.47	0.50	0.65	0.52	0.03
ORP	0.08	0.30	0.89	0.34	0.33	0.04	0.44	0.16	0.00	0.60	0.36	0.72	0.43	0.21	0.20	0.29	0.04	0.02	0.62	0.01	0.04	0.21	0.72	0.71		0.86	0.50	0.57	0.77	0.21	0.25
SE	0.29	0.13	0.88	0.44	0.37	0.17	0.28	0.41	0.10	0.60	0.57	0.77	0.55	0.19	0.08	0.15	0.19	0.05	0.76	0.03	0.02	0.40	0.67	0.93	0.86		0.45	0.53	0.77	0.37	0.12
SULF	0.24	0.02	0.36	0.63	0.91	0.19	0.06	0.38	0.03	0.96	0.39	0.64	0.66	0.85	0.73	0.02	0.03	0.27	0.65	0.29	0.01	0.57	0.19	0.47	0.50	0.45		0.09	0.32	0.61	0.01
TDS	0.05	0.24	0.82	0.01	0.07	0.04	0.43	0.09	0.01	0.19	0.29	0.49	0.22	0.02	0.01	0.50	0.14	0.02	0.41	0.02	0.35	0.10	0.66	0.50	0.57	0.53	0.09		0.40	0.09	0.05
TEMP	0.11	0.16	0.69	0.37	0.18	0.03	0.26	0.16	0.01	0.41	0.32	0.52	0.29	0.08	0.05	0.09	0.16	0.00	0.48	0.01	0.00	0.14	0.62	0.65	0.77	0.77	0.32	0.40		0.15	0.36
VAN	0.77	0.09	0.25	0.56	0.79	0.73	0.01	0.90	0.49	0.68	0.78	0.65	0.83	0.66	0.25	0.02	0.01	0.62	0.62	0.60	0.01	0.91	0.05	0.52	0.21	0.37	0.61	0.09	0.15		0.15
ZI	0.21	0.56	0.12	0.00	0.02	0.43	0.43	0.17	0.36	0.01	0.09	0.00	0.06	0.05	0.00	0.23	0.07	0.51	0.01	0.52	0.02	0.10	0.35	0.03	0.25	0.12	0.01	0.05	0.36	0.15	1.00

A general trend can be seen in Table 5-7 through Table 5-12 that an increase in reservoir pressure is accompanied by an increase in the correlation between constituent variables. In Tables 5-11 and 5-12, Subgroup 5 and Subgroup 6 have the greatest correlation between constituents, whereas the control group, Subgroup 1, has almost no correlations. Despite the low number of data points in Subgroups 5-6 and the lack of clustering between the spatial locations of these data points, there are high correlations between various constituents, strongly indicating that a large number of gas wells and a high reservoir pressure are impacting the concentration of groundwater constituents in these areas. In Subgroups 5-6, the concentration of Beryllium is strongly correlated to the concentration of the other constituents. This could indicate that the concentrations of naturally occurring constituents are elevated in concentration with a relationship to hydraulic fracturing of nearby gas wells.

5.4 CLUSTER ANALYSIS FOR UNDERSTANDING

CONTAMINANT PATHWAYS IN HYDRAULICALLY FRACTURED WELLS

The ArcGIS, a cluster analysis was generated for each cluster described in Table 4-5. The map of the clusters plotted in ArcGIS show the LL clusters in red, and the HH clusters in light green (Figure 5-3 – Figure 5-12). As can be visually deduced, the results of each cluster analysis vary, and the clusters of injected Fluid and Nitrogen demonstrated no significant clustering.

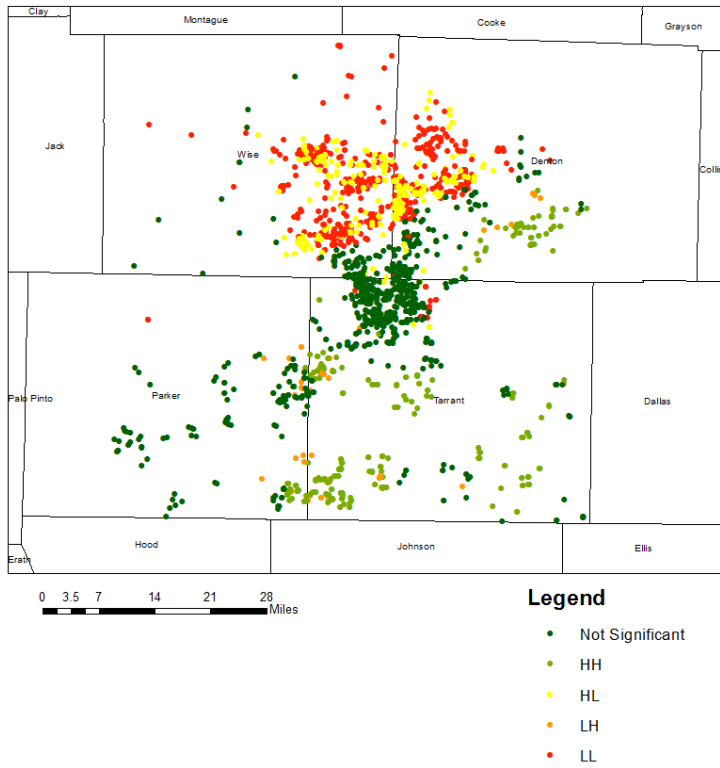


Fig. 5-3: ArcGIS Cluster Analysis of Surface Casing Values

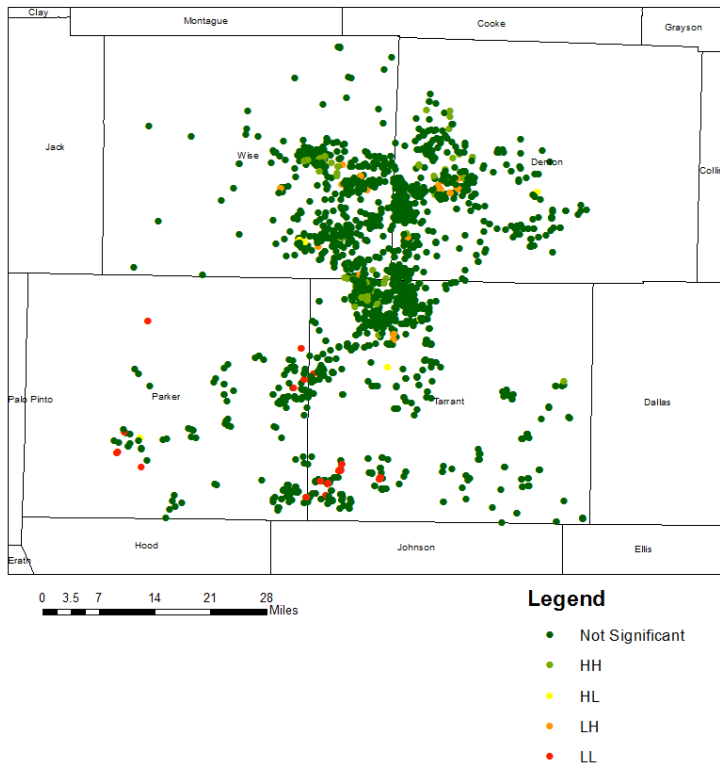


Fig. 5-4: ArcGIS Cluster Analysis of Bottom Hole Casing Values

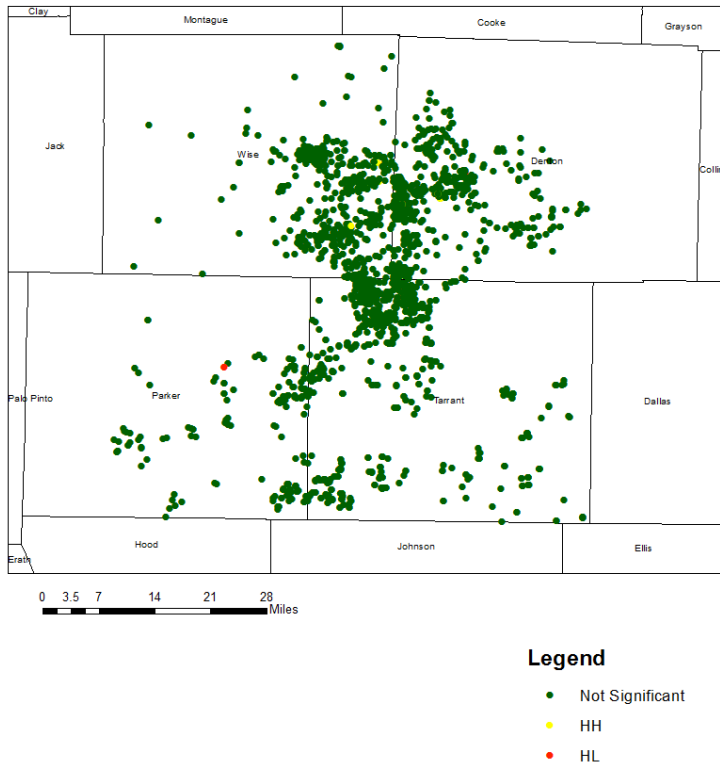


Fig. 5-5: ArcGIS Cluster Analysis of Injected Fluid Values

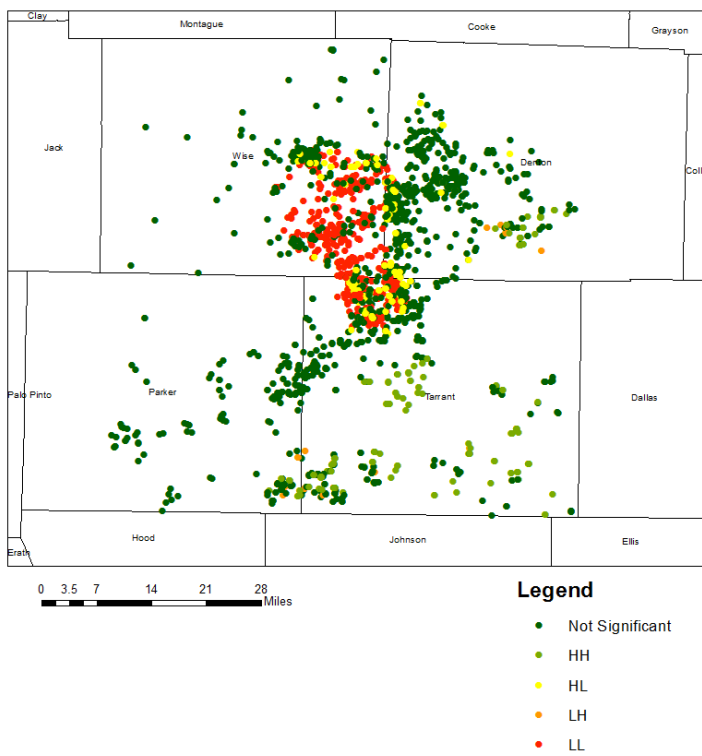
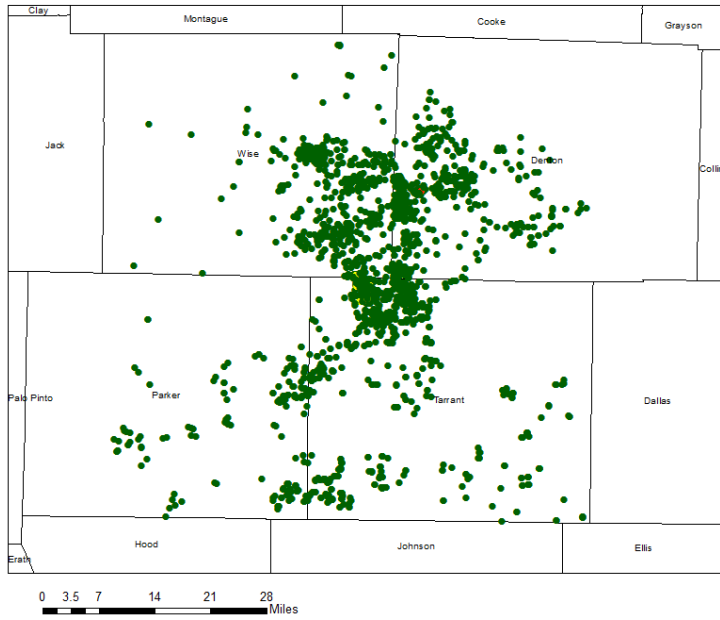


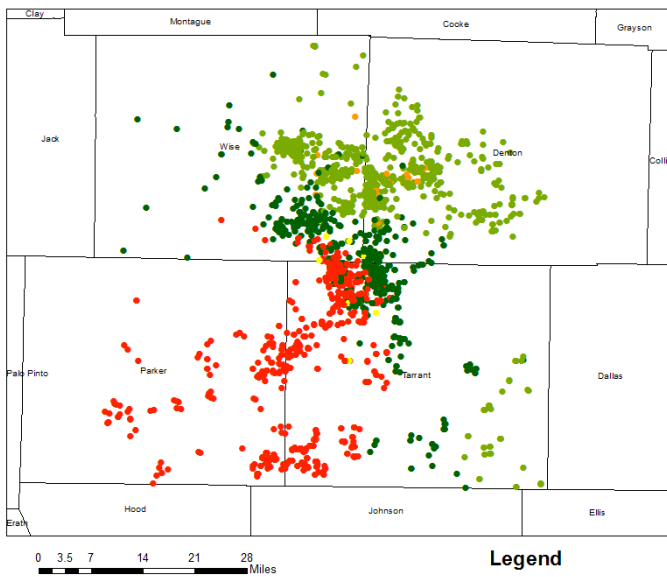
Fig. 5-6: ArcGIS Cluster Analysis of Injected Sand Values



Legend

- Not Significant
- HH
- HL

Fig. 5-7: ArcGIS Cluster Analysis of Injected Nitrogen Values



Legend

- Not Significant
- HH
- HL
- LH
- LL

Fig. 5-8: ArcGIS Cluster Analysis of Total Vertical Depth Values

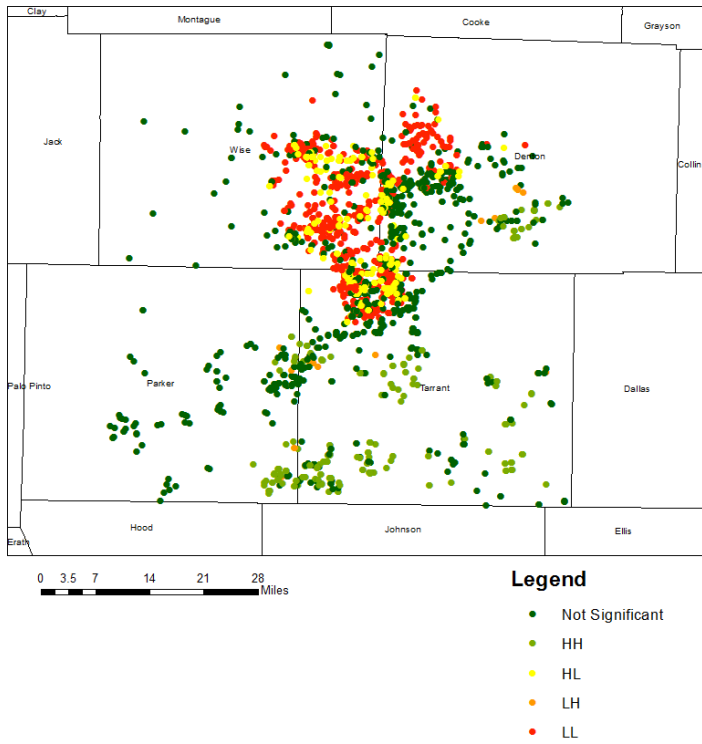


Fig. 5-9: ArcGIS Cluster Analysis of Lateral Length Values

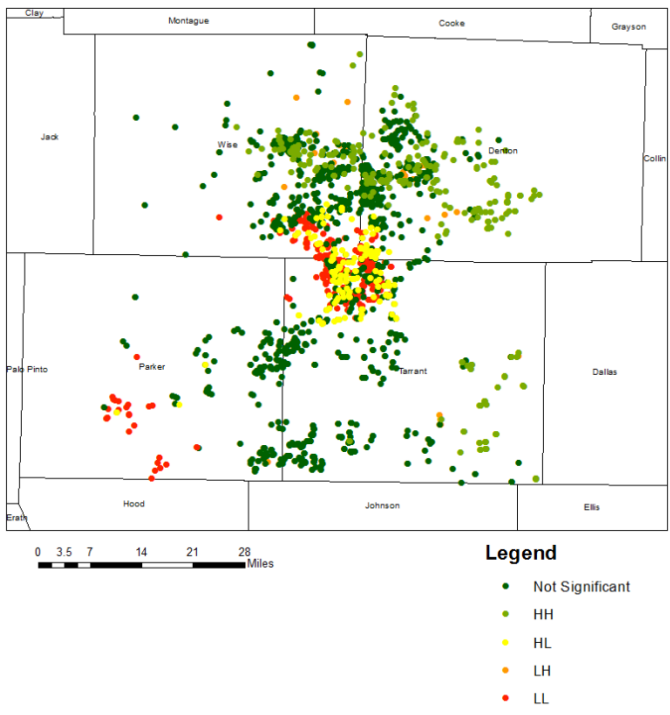


Fig. 5-10: ArcGIS Cluster Analysis of Aquifer to Perforation Thickness Values

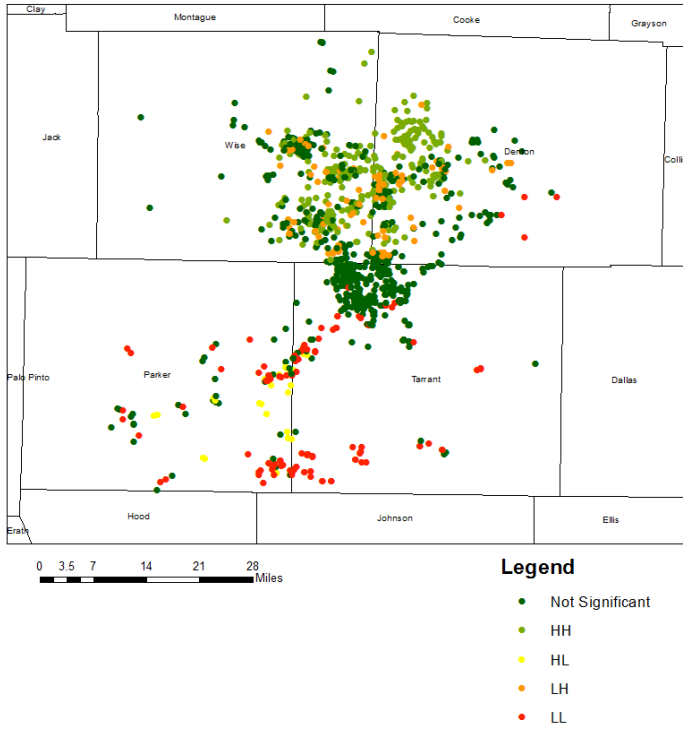


Fig. 5-11: ArcGIS Cluster Analysis of Azimuth Direction Values

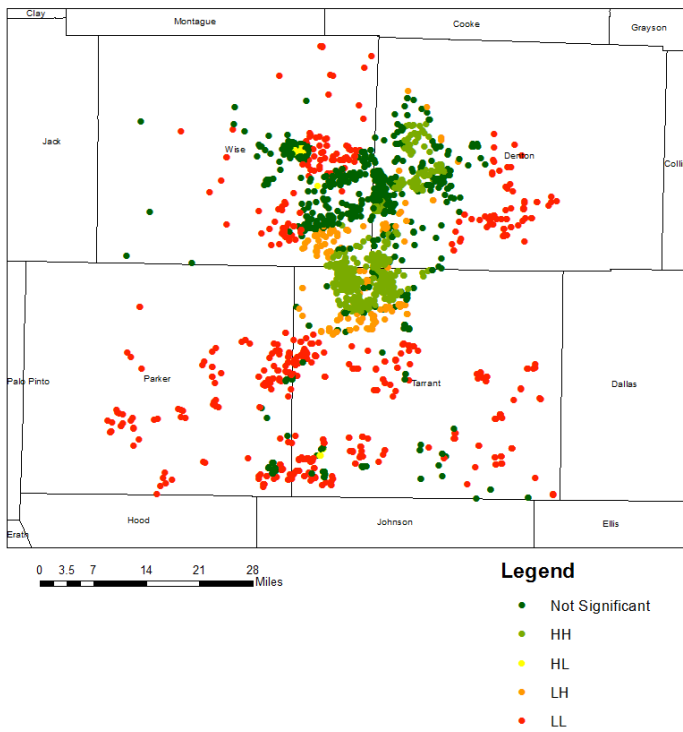


Fig. 5-12: ArcGIS Cluster Analysis Number of Surrounding Gas Wells (1 Mile) Values

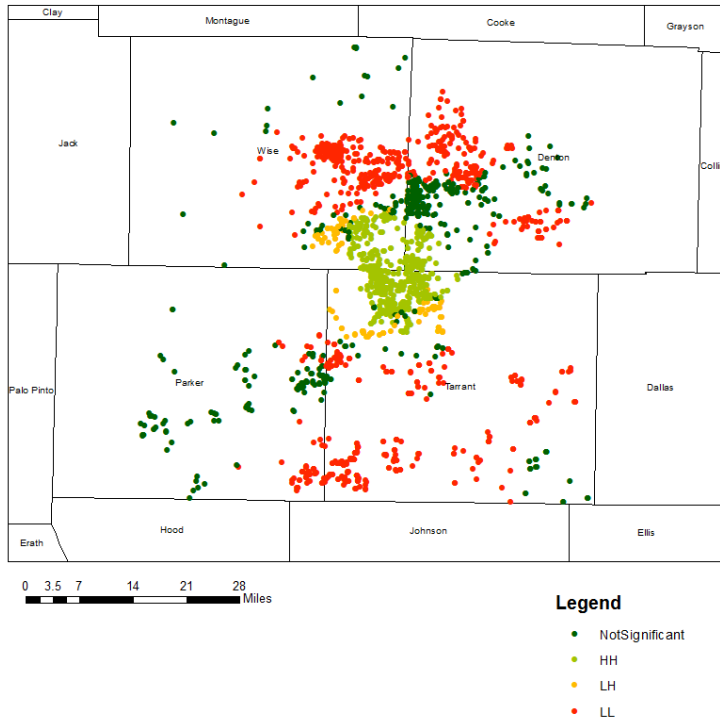


Fig. 5-13: ArcGIS Cluster Analysis of Bottom Hole Pressure

The plots of Injected Fluid (Cluster 3) and Nitrogen (Cluster 5) indicate that there was no significant clustering of these values so were omitted from evaluation. The remaining plots, which have significant HH and LL clustering, were evaluated. The corresponding values of Beryllium (ppb) were extracted at the cluster locations from the 2011-2014 Total Beryllium contour (Figure B-6). Beryllium was chosen as a tracer based upon the results in Sections 5.1-5.3 where this constituent was found to exhibit a relationship to hydraulic fracturing in all analyses. A comparison of the Beryllium concentrations extracted for the HH and LL clusters was made using the Mann-Whitney U-Test. The results of the Mann-Whitney U-Test are summarized in Table 5-13 (Clusters 3 and 5 are omitted).

Table 5-13: Mann-Whitney U-Test Evaluation of HH and LL Clusters of Wellbore Parameters using Beryllium Tracer Concentrations

CLUSTER NO.	CLUSTER DESCRIPTION	Null Hypothesis	Number of Samples		Median		Minitab Output <i>W</i>	Calculation of P-Value for a 2 Tailed Test and 0.95 Confidence Interval				Result	
			<i>n1</i>	<i>n2</i>	<i>n1</i>	<i>n2</i>		<i>Mean of W</i>	<i>Variance of W</i>	<i>Z-Value</i>	<i>P-Value</i>	Accept (1)/ Reject (0)	Conclusion
1	Surface Casing	n1 = n2	363	481	1.72	1.74	152,672	153,368	12,294,961	0.20	0.84	1	No statistically significant difference in median tracer concentration between large and small surface casing sizes
2	Bottom Hole Casing	n1 = n2	84	33	3.43	2.65	5,069	4,956	27,258	0.68	0.50	1	No statistically significant difference in median tracer concentration between large and small bottom hole casing sizes
4	Injected Proppant Weight	n1 = n2	204	508	1.33	2.24	47,235	72,726	6,157,468	10.27	0.00	0	Statistically significant greater mean tracer concentration in wells with a lower injected proppant weight
6	Total Vertical Depth	n1 = n2	721	706	1.30	2.89	338,540	514,794	60,574,094	22.65	0.00	0	Statistically significant lower mean tracer concentration in wells with a greater TVD
7	Length of Lateral	n1 = n2	294	684	1.74	2.16	116,508	143,913	16,406,082	6.77	0.00	0	Statistically significant lower mean tracer concentration in wells with a greater lateral length
8	Thickness Between Aquifer and Uppermost Gas Well Perforation	n1 = n2	307	380	1.30	2.45	63,048	105,608	6,688,507	16.46	0.00	0	A statistically significant greater median concentration of tracer in wells with a smaller thickness between the aquifer and uppermost perforation
9	Direction of Azimuth (Horizontal Wells only)	n1 = n2	274	110	1.68	2.30	46,784	52,745	966,992	6.06	0.00	0	A lower degree azimuth has a statistically significant greater mean concentration of tracer
10	Number of neighboring wells within 1 mile	n1 = n2	588	601	2.27	1.85	396,759	349,860	35,044,310	7.92	0.00	0	A higher concentration of wells within 1 mile results in a statistically significant higher mean concentration of tracer
11	Bottom Hole Pressure (psi)	n1 = n2	622	822	2.38	1.96	537,326	449,395	61,567,115	11.21	0.00	0	Higher bottom hole pressure clusters have a statistically significant higher concentration of tracer

*n1: HH Clusters
*n2: LL Clusters

The results presented in Table 5-13 demonstrate that the casing sizes in this data set do not have a significant impact on the mean level of tracer found in the gas wells. This is most likely because a majority of the wells were completed with nearly identical casing design, where Figures 5-3 and 5-4 show that almost all of the clusters are insignificant. The remaining wellbore parameters, however, have some demonstrable significance to the mean tracer detected in the cluster locations. The greater injected proppant weight was not associated with a higher median tracer concentration. This may indicate that the wellbore pathway is not necessarily associated with a horizontal wellbore since greater sand volumes are pumped in horizontal wells where there are multiple fracture zones. This also demonstrates that the fractures in the overburden geology cannot be a contaminant pathway as multiple fractures along a lateral would have to have a significantly higher tracer concentration if this were so. This also corresponds to results of the Lateral Length cluster, which essentially compares clusters of horizontal gas wells to vertical gas wells, where vertical gas wells had a lateral length of zero and the horizontal gas wells had a number greater than zero. The results demonstrate that the vertically drilled wells are associated with a greater median of tracer.

In clusters of a greater vertical depth, a lower mean concentration of tracer was detected indicating that a greater thickness lessens the potential for contamination. Likewise, a decreased thickness between the Aquifer and the uppermost perforation is associated with a higher mean concentration. This makes sense based upon an understanding of fracture extension, where fractures tend to extend upwards. In vertical wellbores this means that the fractures are parallel to the annulus, possibly creating a breach in the wellbore system. A higher density of wells is also associated with a higher median tracer. The direction of the horizontal azimuth cluster analysis was performed for the horizontal wellbores only. The results demonstrate that a lower directional degree,

that is drilled in the north-northeast direction, is associated with a higher median tracer concentration. The direction of greatest principal stress in the region is also in the north-northeast direction (worldstressmap.org). These results do not support the expected outcome where wells drilled opposite the direction of greatest principal stress will experience hole-collapse. However, these results may be somewhat skewed as the low cluster values are located in regions where there is not a high reservoir pressure gradient (see Figure 5-11).

6 DISCUSSION & CONCLUSIONS

The results from this research emphasize the need to study groundwater quality and hydraulic fracturing relationships in a spatial context, and with respect to the geophysical characteristics of the wellbore environment. This is particularly noted in comparing the results of Section 5.2 and 5.3 where an evaluation of the constituent concentrations based upon proximity to gas wells alone does not establish a strong relationship between groundwater quality changes and hydraulic fracturing activity. Using a model with more specific characterization of the wellbore environment, there are more statistically significant differences in median constituent concentrations detected and serve as an indication that degraded water quality has some relationship to hydraulic fracturing operations.

Additionally, the research in this thesis demonstrates that some groundwater constituents serve as better indicators of groundwater quality changes. In this study, the concentration of Beryllium was the strongest tracer for demonstrating a pathway between the gas wells and the groundwater. By identifying a tracer, the results of a cluster analysis of well design and hydraulic fracturing parameters was able to identify a possible origin of the contaminant pathway in the wellbore environment. This study concludes that hydraulic fractures in the vertical direction create a micro-annulus, where fractures in a lateral wellbore are less likely to create a rupture in the wellbore system. Ultimately, even though changes in groundwater quality are occurring due to hydraulic fracturing operations in gas wells, a majority of the detected concentrations do not exceed the EPA MCL limits for constituents tested. Of all the constituents tested, only one (Beryllium) appears to be both highly related to hydraulic fracturing and impacting the water at a level exceeding the legal threshold.

Improving hydraulic fracturing treatment and wellbore designs may reduce the impact of natural gas production on fresh water resources. The results of this thesis indicate that the hydraulic fracturing induced contaminant pathways are formed in the vertical section of a wellbore system. By limiting the fracture design to the lateral section of the wellbore, that is not fracking near the curve or vertical wellbore section, this may reduce the possibility of forming a micro-annulus.

This thesis demonstrates that the quality of groundwater is impacted by a high density of gas wells in an area. In the Barnett study area addressed in this research, the highest density of gas wells is located in the highest pressure gradient region. A high density of gas wells treated in a small area may cause an intersection of pressure cones in the subsurface, possibly increasing the reservoir pressure and/or fracture treatment pressure required for gas well treatment in the area. To what extent that may be occurring is unknown within the context of data available for this thesis. Future work on this subject matter, however, should further investigate this issue by incorporating more specific knowledge of the hydraulic fracturing treatment pressures, wellbore pressure limitations, and reservoir rock properties into the model.

REFERENCES

- Arthur, J. D., Bohm, B. K., & Cornue, D. (2009, January). "Environmental considerations of modern shale gas development". In *SPE Annual Technical Conference and Exhibition*. Society of Petroleum Engineers.
- Barker, C. (1990). "Calculated Volume and Pressure Changes During the Thermal Cracking of Oil to Gas in Reservoirs (1)". *AAPG Bulletin*, 74(8), 1254-1261.
- Bexte, D. C., Willis, M., De Bruijn, G. G., Eitzen, B., & Fouillard, E. (2008). Improved cementing practice prevents gas migration. *World Oil*, 229(6), 73-75.
- Bowker, K. A. (2007). "Barnett Shale gas production, Fort Worth Basin: Issues and discussion". *AAPG Bulletin*, 91(4), 523-533. doi: 10.1306/06190606018
- Bowman, S., Urbancic, T., & Baig, A. (2012). "Remote triggering of large events during hydraulic fracture stimulations".
- Brown, V. J. (2014). "Radionuclides in fracking wastewater: managing a toxic blend". *Environmental Health Perspectives*, 122(2), A50.
- Bruner, K. R., & Smosna, R. (2011). "A comparative study of the Mississippian Barnett Shale, Fort Worth Basin, and Devonian Marcellus Shale". *Appalachian Basin: Technical Report DOE/NETL-2011/1478*, National Energy Technology Laboratory (NETL) for The United States Department of Energy.
- Coughlin, B. J., & Arthur, J. D. (2011). "Cumulative impacts of shale-gas water management: considerations and challenges". In *SPE Americas E&P Health Safety Security and Environmental Conference*. Society of Petroleum Engineers.
- Barker, C. (1990). "Calculated Volume and Pressure Changes During the Thermal Cracking of Oil to Gas in Reservoirs (1)". *AAPG Bulletin*, 74(8), 1254-1261.
- Chermak, J. A., & Schreiber, M. E. (2014). "Mineralogy and trace element geochemistry of gas shales in the United States: Environmental Implications". *International Journal of Coal Geology*, 126, 32-44.

- Cohen, H. A., Parratt, T., & Andrews, C. B. (2013). "Potential Contaminant Pathways from Hydraulically Fractured Shale to Aquifers". *GroundWater*, 51(3), 317-319.
- Darrah, T. H., Vengosh, A., Jackson, R. B., Warner, N. R., & Poreda, R. J. (2014). "Noble gases identify the mechanisms of fugitive gas contamination in drinking-water wells overlying the Marcellus and Barnett Shales". *Proc Natl Acad Sci U S A*, 111(39), 14076-14081. doi: 10.1073/pnas.1322107111
- Davies, R., Foulger, G., Bindley, A., & Styles, P. (2013). "Induced seismicity and hydraulic fracturing for the recovery of hydrocarbons". *Marine and Petroleum Geology*, 45, 171-185. doi: 10.1016/j.marpetgeo.2013.03.016
- Deremble, L., Loizzo, M., Huet, B., Lecampion, B., & Quesada, D. (2010). "Assessment of leakage pathways along a cemented annulus". Paper presented at the Society of Petroleum Engineers - *SPE International Conference on CO2 Capture, Storage, and Utilization 2010*.
- Eaton, T. T. (2013). "Science-based decision-making on complex issues: Marcellus shale gas hydrofracking and New York City water supply". *Sci Total Environ*, 461-462, 158-169. doi: 10.1016/j.scitotenv.2013.04.093
- EIA, U. (2013). "Annual energy outlook 2013". *US Energy Information Administration, Washington, DC*.
- Finkel, M. L., & Hays, J. (2013). "The implications of unconventional drilling for natural gas: A global public health concern". *Public Health*, 127(10), 889-893.
- Flewelling, S. A., & Sharma, M. (2013). "Constraints on Upward Migration of Hydraulic Fracturing Fluid and Brine". *Ground Water*. doi: 10.1111/gwat.12095
- Fontenot, B. E., Hunt, L. R., Hildenbrand, Z. L., Carlton, D. D., Oka, H., Walton, J. L., . . . Schug, K. A. (2013). "An evaluation of water quality in private drinking water wells near natural gas extraction sites in the Barnett shale formation". *Environmental Science and Technology*, 47(17), 10032-10040.

- Freyman, M. (2014). "Hydraulic Fracturing & Water Stress: Water Demand by the Numbers". *Fracturación hidráulica y presión por el agua: Demanda de agua en números*, Ceres.
- Fry, M., Hoeinghaus, D. J., Ponette-Gonzalez, A. G., Thompson, R., & La Point, T. W. (2012). "Fracking vs. faucets: balancing energy needs and water sustainability at urban frontiers". *Environ Sci Technol*, 46(14), 7444-7445. doi: 10.1021/es302472y
- Garmezzy, A. (2013). "Balancing hydraulic fracturing's environmental and economic impacts: The need for a comprehensive federal baseline and the provision of local rights". *Duke Environmental Law and Policy Forum*, 23(2), 405-439.
- Gidley, J. L. (1989). Recent advances in hydraulic fracturing. (Vol 12). Society of Petroleum Engineers.
- Gordalla, B. C., Ewers, U., & Frimmel, F. H. (2013). "Hydraulic fracturing: A toxicological threat for groundwater and drinking-water?" *Environmental Earth Sciences*, 70(8), 3875-3893.
- Gross, S. A., Avens, H. J., Banducci, A. M., Sahmel, J., Panko, J. M., & Tvermoes, B. E. (2013). "Analysis of BTEX groundwater concentrations from surface spills associated with hydraulic fracturing operations". *Journal of the Air and Waste Management Association*, 63(4), 424-432.
- Harden, R. W. (2004). "Northern Trinity, Woodbine Aquifer Groundwater Availability Model". RW Harden & Assoc.
- Harkness, J. S., Dwyer, G. S., Warner, N. R., Parker, K. M., Mitch, W. A., & Vengosh, A. (2015). "Iodide, Bromide, and Ammonium in Hydraulic Fracturing and Oil and Gas Wastewaters: Environmental Implications". *Environmental Science & Technology*.
- Jackson, R. B., Vengosh, A., Darrah, T. H., Warner, N. R., Down, A., Poreda, R. J., . . . Karr, J. D. (2013). "Increased stray gas abundance in a subset of drinking water wells near Marcellus shale gas extraction". *Proc Natl Acad Sci U S A*, 110(28), 11250-11255. doi: 10.1073/pnas.1221635110

- Jackson, R. E., Gorody, A. W., Mayer, B., Roy, J. W., Ryan, M. C., & Van Stempvoort, D. R. (2013). "Groundwater protection and unconventional gas extraction: the critical need for field-based hydrogeological research". *GroundWater*, 51(4), 488-510. doi: 10.1111/gwat.12074
- Jarvie, Dan (2004). "Evaluation of Hydrocarbon Generation and Storage in the Barnett Shale, Fort Worth Basin, Texas". Humble Geochemical Services. Humble, TX.
- Kidnay, A. J., Parrish, W. R., & McCartney, D. G. (2011). Fundamentals of Natural Gas Processing (Vol. 218). CRC Press.
- Kissinger, A., Helmig, R., Ebigbo, A., Class, H., Lange, T., Sauter, M., . . . Jahnke, W. (2013). "Hydraulic fracturing in unconventional gas reservoirs: Risks in the geological system, part 2: Modelling the transport of fracturing fluids, brine and methane". *Environmental Earth Sciences*, 70(8), 3855-3873.
- Kresic, N. (2006). Hydrogeology and Groundwater Modeling. CRC press.
- Lancaster, D. E., McKetta, S. F., Hill, R. E., Guidry, F. K., & Jochen, J. E. (1992). "Reservoir evaluation, completion techniques, and recent results from Barnett Shale development in the Fort Worth Basin". Paper presented at the Proceedings - SPE Annual Technical Conference and Exhibition.
- Lange, T., Sauter, M., Heitfeld, M., Schetelig, K., Brosig, K., Jahnke, W., . . . Class, H. (2013). "Hydraulic fracturing in unconventional gas reservoirs: Risks in the geological system part 1". *Environmental Earth Sciences*, 70(8), 3839-3853.
- Lee, W. J., & Wattenbarger, R. A. (1996). Gas Reservoir Engineering (Vol. 5). Society of Petroleum Engineers.
- Lutz, B. D., Lewis, A. N., & Doyle, M. W. (2013). "Generation, transport, and disposal of wastewater associated with Marcellus Shale gas development". *Water Resources Research*, 49(2), 647-656.

- McBroom, M., Thomas, T., & Zhang, Y. (2012). "Soil erosion and surface water quality impacts of natural gas development in East Texas, USA". *Water (Switzerland)*, 4(4), 944-958.
- McKenzie, L. M., Witter, R. Z., Newman, L. S., & Adgate, J. L. (2012). "Human health risk assessment of air emissions from development of unconventional natural gas resources". *Science of the Total Environment*, 424, 79-87.
- Molofsky, L. J., Connor, J. A., Farhat, S. K., Wylie Jr, A. S., & Wagner, T. (2011). "Methane in Pennsylvania water wells unrelated to Marcellus shale fracturing". *Oil and Gas Journal*, 109(19), 54-67+93.
- Molofsky, L. J., Connor, J. A., Wylie, A. S., Wagner, T., & Farhat, S. K. (2013). "Evaluation of methane sources in groundwater in northeastern Pennsylvania". *Ground Water*, 51(3), 333-349. doi: 10.1111/gwat.12056
- Montgomery, S. L., Jarvie, D. M., Bowker, K. A., & Pollastro, R. M. (2006). "Mississippian Barnett Shale, Fort Worth basin, north-central Texas: Gas-shale play with multi-trillion cubic foot potential: Reply". *AAPG Bulletin*, 90(6), 967-969. doi: 10.1306/02090605186
- Murray, K. E. (2013). "State-scale perspective on water use and production associated with oil and gas operations, Oklahoma, U.S." *Environ Sci Technol*, 47(9), 4918-4925. doi: 10.1021/es4000593
- Myers, T. (2012). "Potential Contaminant Pathways from Hydraulically Fractured Shale to Aquifers". *GroundWater*, 50(6), 872-882.
- Osborn, S. G., Vengosh, A., Warner, N. R., & Jackson, R. B. (2011). "Methane contamination of drinking water accompanying gas-well drilling and hydraulic fracturing". *Proc Natl Acad Sci U S A*, 108(20), 8172-8176.
- Paulson, D. S. (2003). Applied Statistical Designs for the Researcher. CRC Press.
- Pratikno, H., Reese, D. E., & Maguire, M. M. (2013). "Production analysis in the Barnett Shale - Field example for reservoir characterization using public data". Paper presented at the Proceedings - SPE Annual Technical Conference and Exhibition.

- Rabinowitz, P. M., Slizovskiy, I. B., Lamers, V., Trufan, S. J., Holford, T. R., Dziura, J. D., . . . Stowe, M. H. (2015). "Proximity to natural gas wells and reported health status: Results of a household survey in Washington County, Pennsylvania". *Environmental Health Perspectives*, 123(1), 21-26. doi: 10.1289/ehp.1307732
- Rahm, B. G., Bates, J. T., Bertoia, L. R., Galford, A. E., Yoxtheimer, D. A., & Riha, S. J. (2013). "Wastewater management and Marcellus Shale gas development: Trends, drivers, and planning implications". *Journal of Environmental Management*, 120, 105-113.
- Rahm, D. (2011). "Regulating hydraulic fracturing in shale gas plays: The case of Texas". *Energy Policy*, 39(5), 2974-2981. doi: 10.1016/j.enpol.2011.03.009
- Révész, K. M., Breen, K. J., Baldassare, A. J., & Burruss, R. C. (2012). "Carbon and hydrogen isotopic evidence for the origin of combustible gases in water-supply wells in north-central Pennsylvania". *Applied Geochemistry*, 27(1), 361-375.
- Rich, A., Grover, J. P., & Sattler, M. L. (2014). "An exploratory study of air emissions associated with shale gas development and production in the Barnett Shale". *Journal of the Air and Waste Management Association*, 64(1), 61-72. doi: 10.1080/10962247.2013.832713.
- Rozell, D. J., & Reaven, S. J. (2012). "Water Pollution Risk Associated with Natural Gas Extraction from the Marcellus Shale". *Risk Analysis*, 32(8), 1382-1393.
- Rutqvist, J., Rinaldi, A. P., Cappa, F., & Moridis, G. J. (2013). "Modeling of fault reactivation and induced seismicity during hydraulic fracturing of shale-gas reservoirs". *Journal of Petroleum Science and Engineering*, 107, 31-44.
- Saiers, J. E., & Barth, E. (2012). "Potential Contaminant Pathways from Hydraulically Fractured Shale Aquifers". *Ground Water*, 50(6), 826-828.
- Smith, M. B., & Hannah, R. R. (1996). "High-permeability fracturing: the evolution of a technology". *Journal of Petroleum Technology*, 48, 628-633.
- Ternes, M. E. (2012). "Regulatory programs governing shale gas development". *Chemical Engineering Progress*, 108(8), 60-64.

- Tian, Y., & Ayers, W. B. (2010). "Barnett Shale (Mississippian), Fort Worth Basin, Texas: Regional variations in gas and oil production and reservoir properties". Paper presented at the Society of Petroleum Engineers - *Canadian Unconventional Resources and International Petroleum Conference 2010*.
- van Belle, G., & Hughes, J. P. (1984). "Nonparametric Tests for Trend in Water Quality". *Water Resources Research*, 20(1), 127-136. doi: 10.1029/WR020i001p00127
- Vidic, R. D., Brantley, S. L., Vandebossche, J. M., Yoxtheimer, D., & Abad, J. D. (2013). "Impact of shale gas development on regional water quality". *Science*, 340(6134).
- Walton, J., & Woocay, A. (2013). "Environmental issues related to enhanced production of natural gas by hydraulic fracturing". *Journal of Green Building*, 8(1), 62-71.
- Wang, Q., Chen, X., Jha, A. N., & Rogers, H. (2014). "Natural gas from shale formation - The evolution, evidences and challenges of shale gas revolution in United States". *Renewable and Sustainable Energy Reviews*, 30, 1-28.
- Warner, N. R., Jackson, R. B., Darrah, T. H., Osborn, S. G., Down, A., Zhao, K., . . . Vengosh, A. (2012). "Geochemical evidence for possible natural migration of Marcellus Formation brine to shallow aquifers in Pennsylvania". *Proc Natl Acad Sci U S A*, 109(30), 11961-11966.
- Waxman, H. A., Markey, E. J., & DeGette, D. (2011). "Chemicals used in hydraulic fracturing". *United States House of Representatives Committee on Energy and Commerce Minority Staff*.
- Ziemkiewicz, P. F., Quaranta, J. D., Darnell, A., & Wise, R. (2014). "Exposure pathways related to shale gas development and procedures for reducing environmental and public risk". *Journal of Natural Gas Science and Engineering*, 16, 77-84.
- Zoback, M. D., Kohli, A., Das, I., & McClure, M. W. (2012, January). "The importance of slow slip on faults during hydraulic fracturing stimulation of shale gas reservoirs". In *SPE Americas Unconventional Resources Conference*. Society of Petroleum Engineers.

APPENDIX A – GROUNDWATER QUALITY SAMPLES IN STUDY REGION

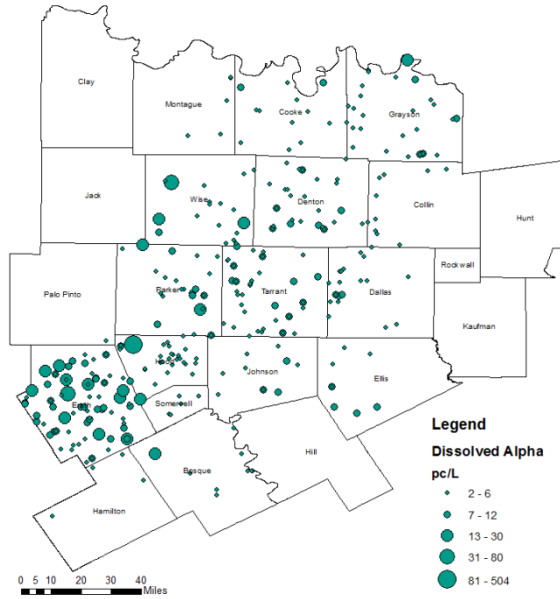


Fig. A- 1: Sample locations of Dissolved Alpha denoted by relative measurements in concentration (pc/L)

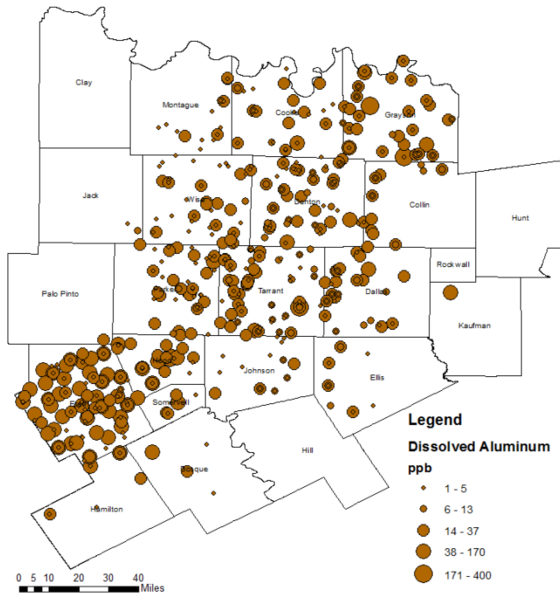


Fig. A- 2: Sample locations of Dissolved Aluminum denoted by relative measurements in concentration (ppb)

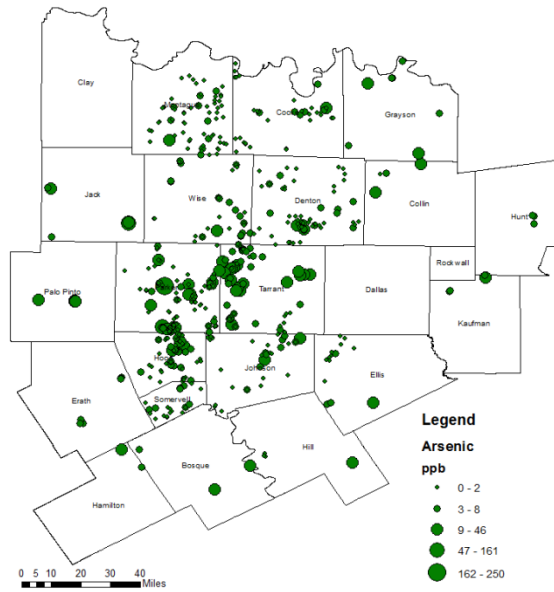


Fig. A- 3: Sample locations of Total Arsenic denoted by relative measurements in concentration (ppb)

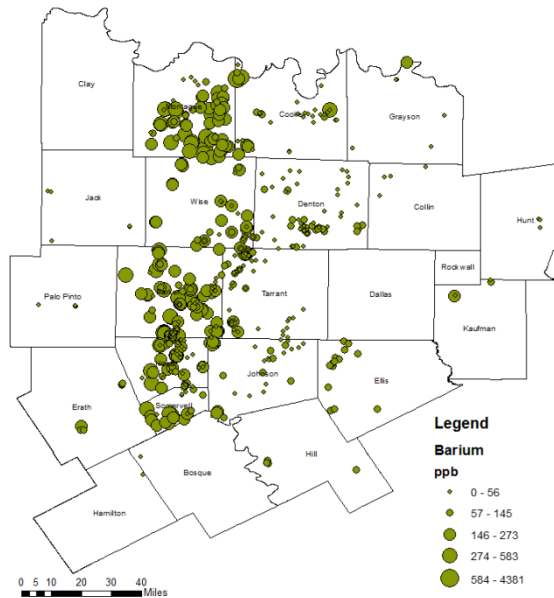


Fig. A- 4: Sample locations of Total Barium denoted by relative measurements in concentration (ppb)

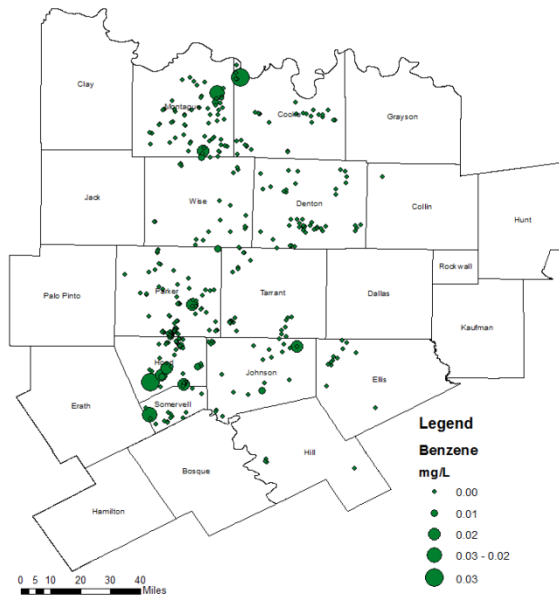


Fig. A- 5: Sample locations of Total Benzene denoted by relative measurements in concentration (mg/L)

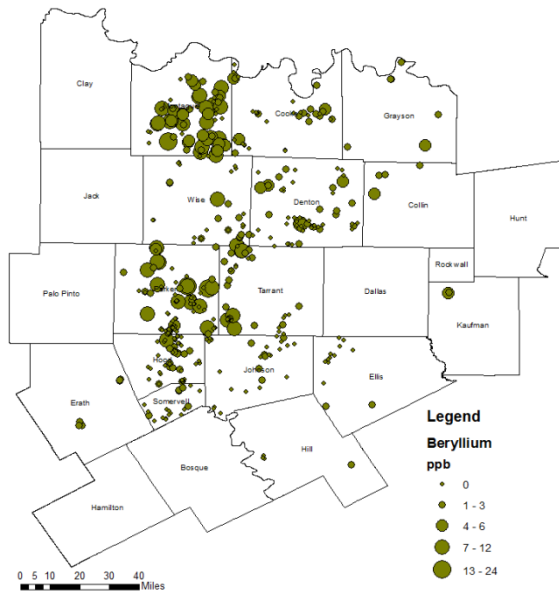


Fig. A- 6: Sample locations of Total Beryllium denoted by relative measurements in concentration (ppb)

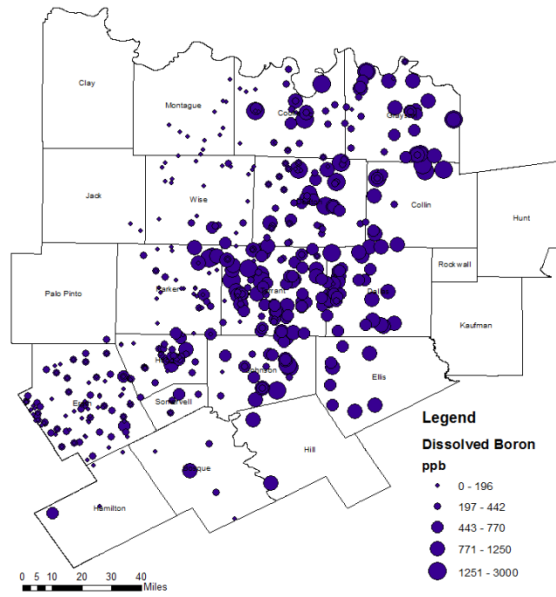


Fig. A- 7: Sample locations of Dissolved Boron denoted by relative measurements in concentration (ppb)

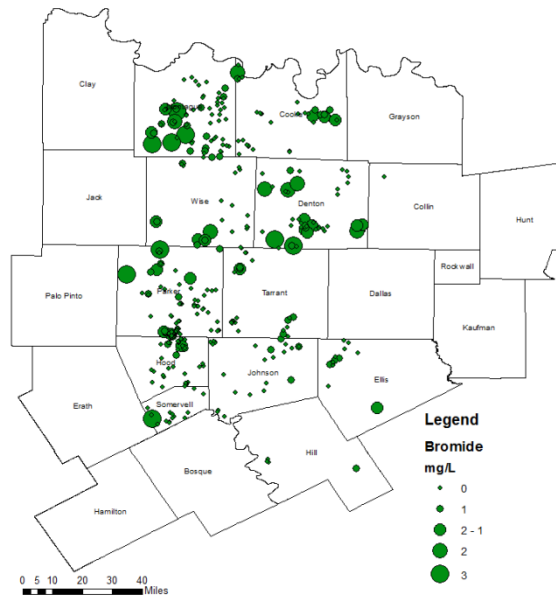


Fig. A- 8: Sample locations of Total Bromide denoted by relative measurements in concentration (mg/L)

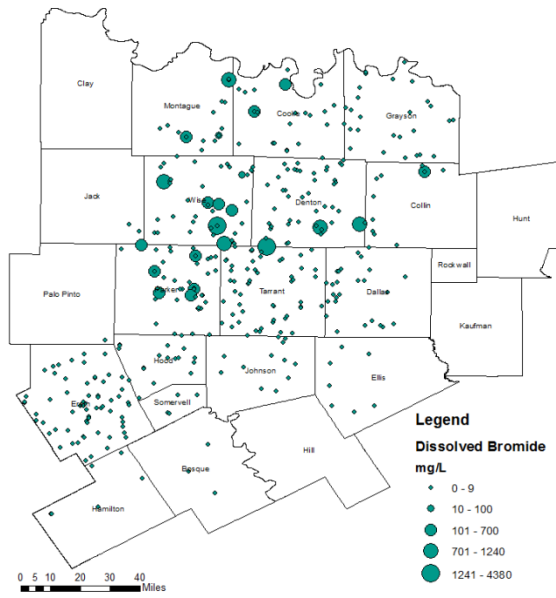


Fig. A- 9: Sample locations of Dissolved Bromide denoted by relative measurements in concentration (mg/L)

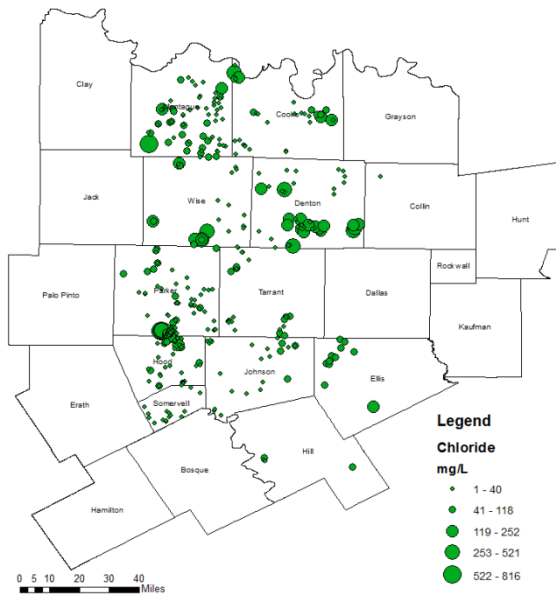


Fig. A- 10: Sample locations of Total Chloride denoted by relative measurements in concentration (mg/L)

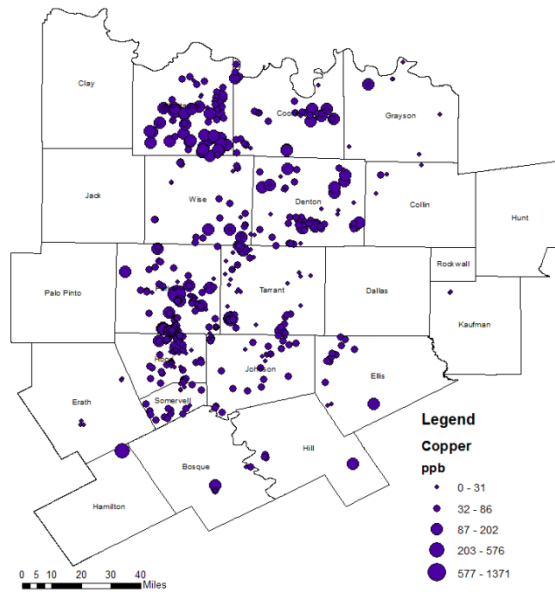


Fig. A- 11: Sample locations of Total Copper denoted by relative measurements in concentration (ppb)

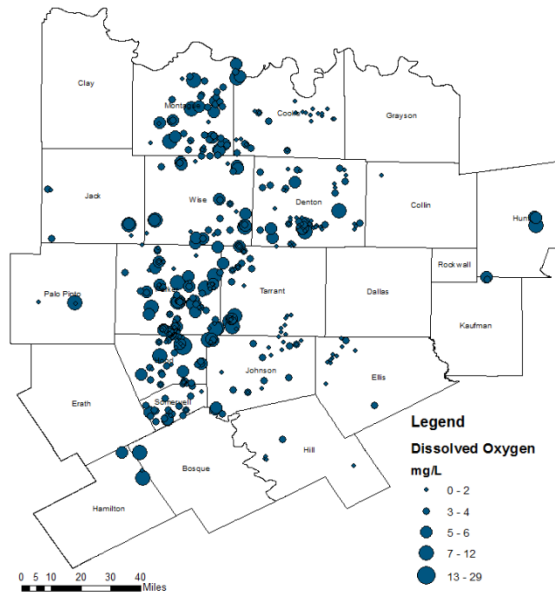


Fig. A- 12: Sample locations of Dissolved Oxygen denoted by relative measurements in concentration (mg/L)

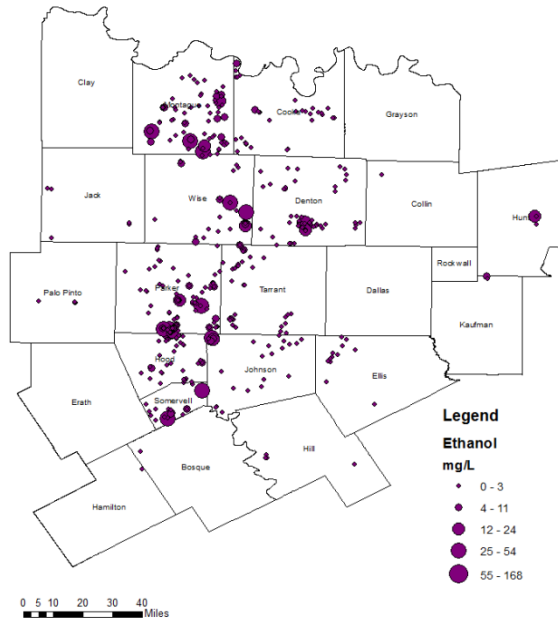


Fig. A- 13: Sample locations of Total Ethanol denoted by relative measurements in concentration (mg/L)

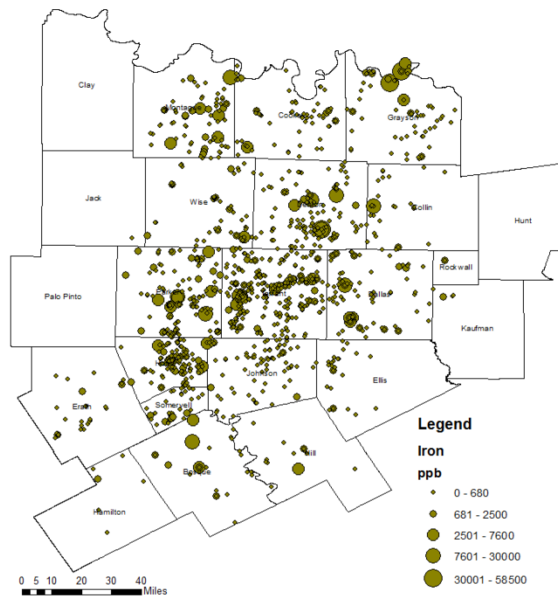


Fig. A- 14: Sample locations of Total Iron denoted by relative measurements in concentration (ppb)

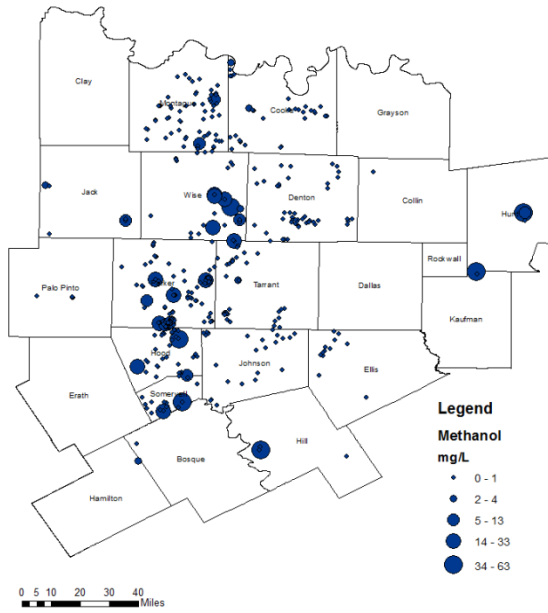


Fig. A- 15: Sample locations of Total Methanol denoted by relative measurements in concentration (mg/L)

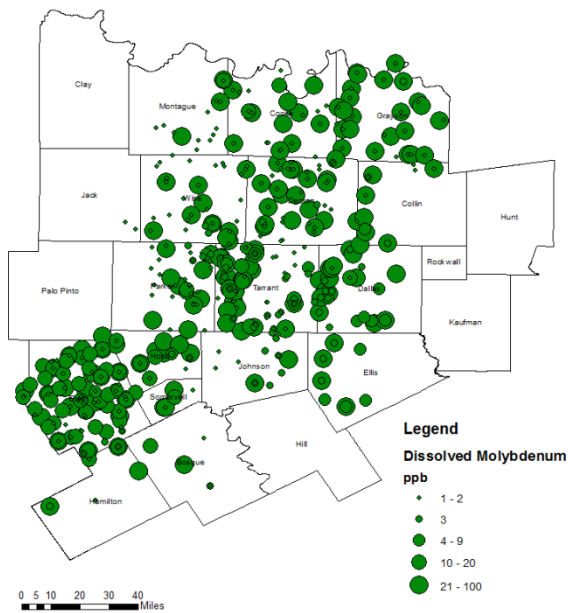


Fig. A- 16: Sample locations of Dissolved Molybdenum denoted by relative measurements in concentration (ppb)

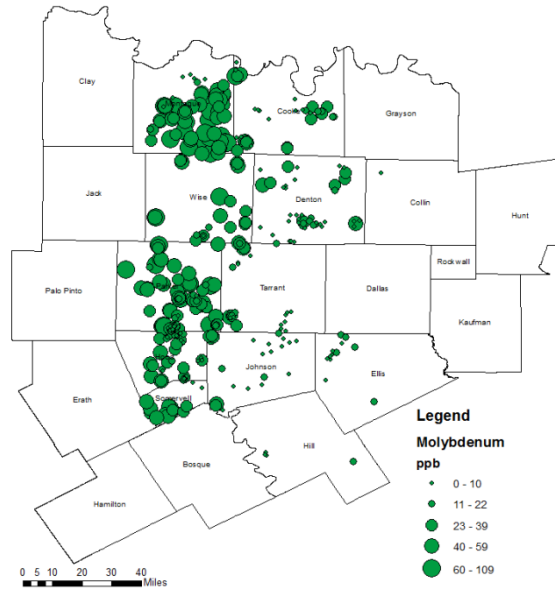


Fig. A- 17: Sample locations of Total Molybdenum denoted by relative measurements in concentration (ppb)

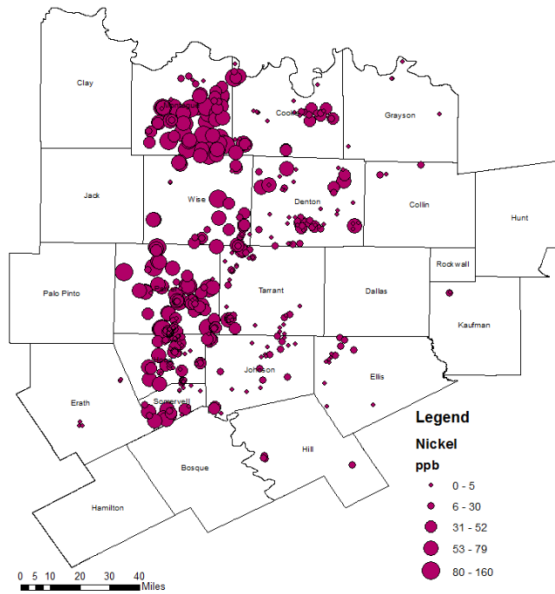


Fig. A- 18: Sample locations of Total Nickel denoted by relative measurements in concentration (ppb)

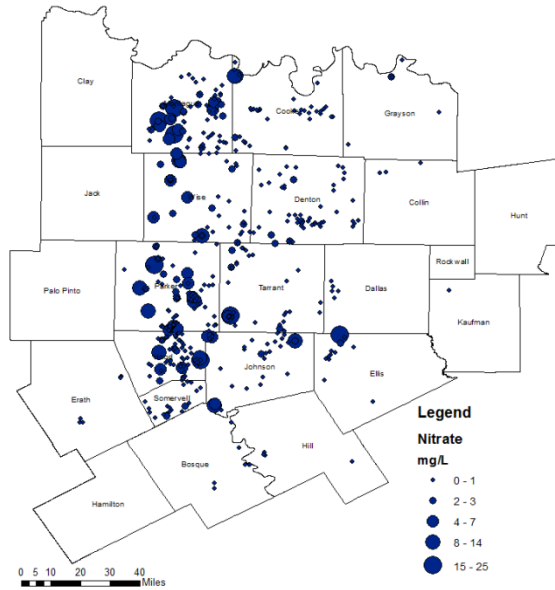


Fig. A- 19: Sample locations of Total Nitrate denoted by relative measurements in concentration (mg/L)

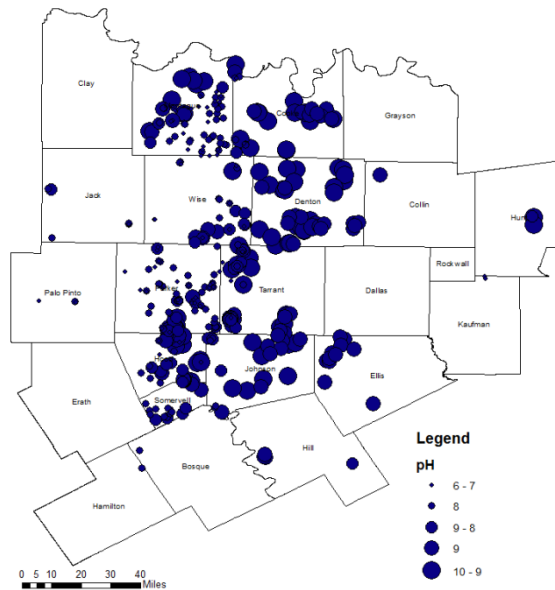


Fig. A- 20: Sample locations denoted by relative measurements of pH

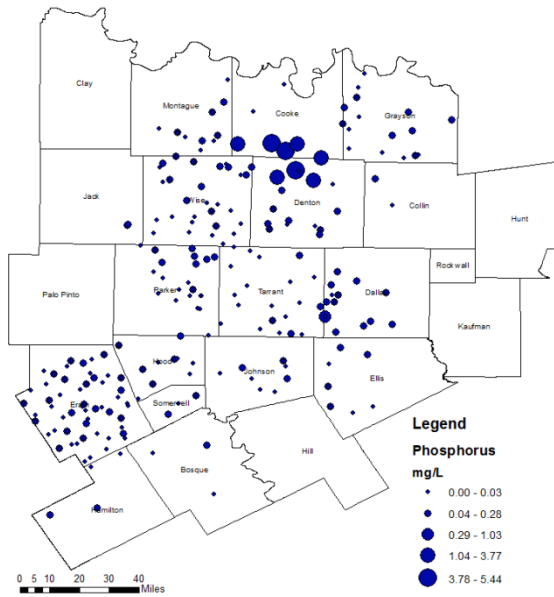


Fig. A- 21: Sample locations of Dissolved Phosphorus denoted by relative measurements in concentration (mg/L)

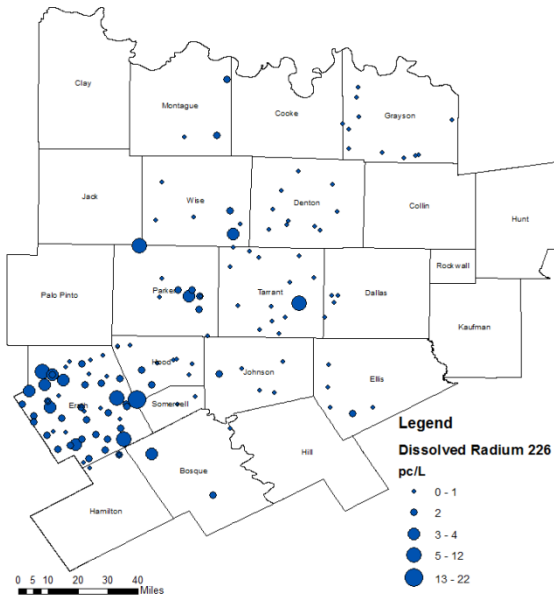


Fig. A- 22: Sample locations of Dissolved Radium 226 denoted by relative measurements in concentration (pc/L)

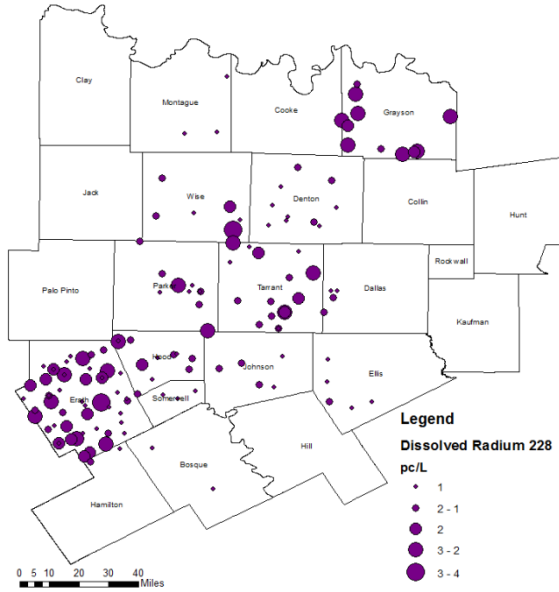


Fig. A- 23: Sample locations of Dissolved Radium 228 denoted by relative measurements in concentration (pc/L)

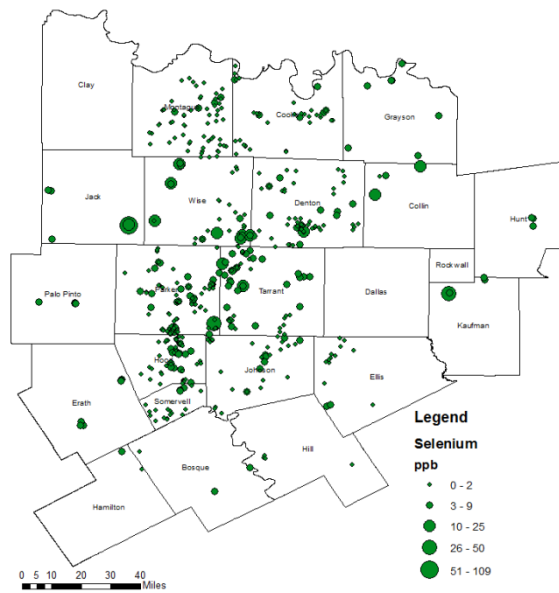


Fig. A- 24: Sample locations of Total Selenium denoted by relative measurements in concentration (ppb)

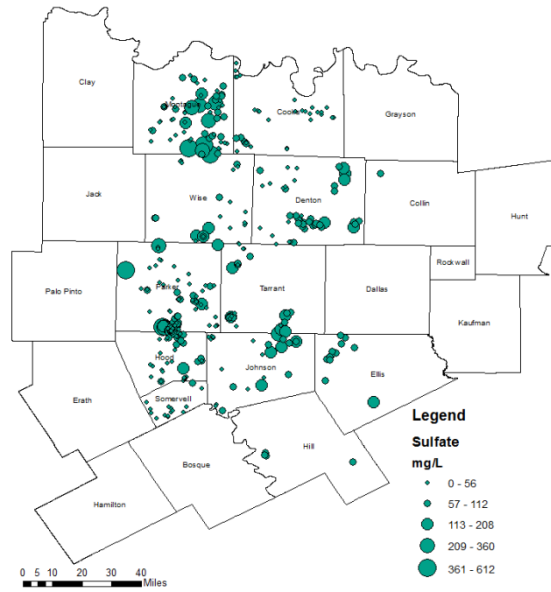


Fig. A- 25: Sample locations of Total Sulfate denoted by relative measurements in concentration (mg/L)

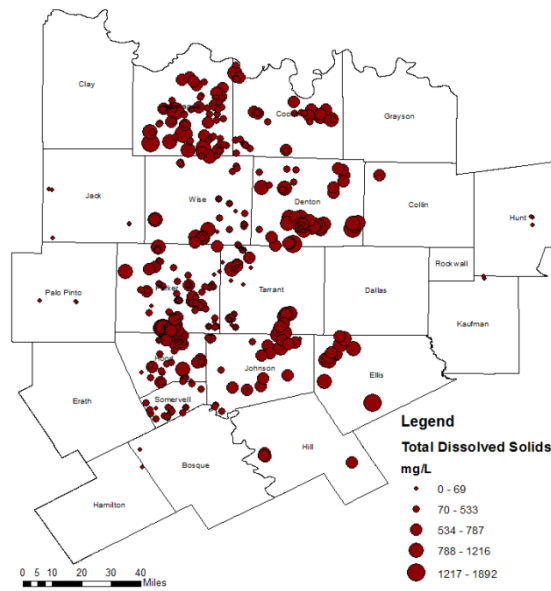


Fig. A- 26: Sample locations of Total Dissolved Solids denoted by relative measurements in concentration (mg/L)

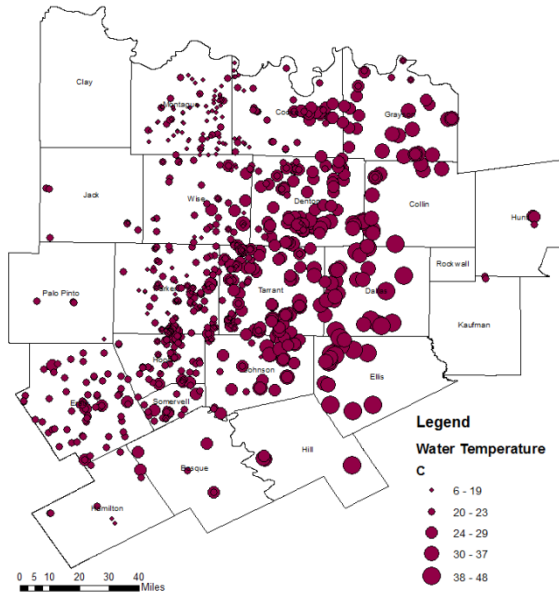


Fig. A- 27: Sample locations of Water Temperature denoted by relative measurements in concentration ($^{\circ}\text{C}$)

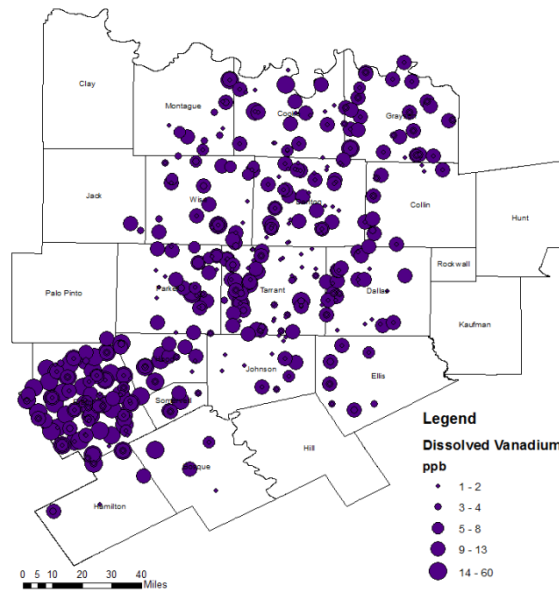


Fig. A- 28: Sample locations of Dissolved Vanadium denoted by relative measurements in concentration (ppb)

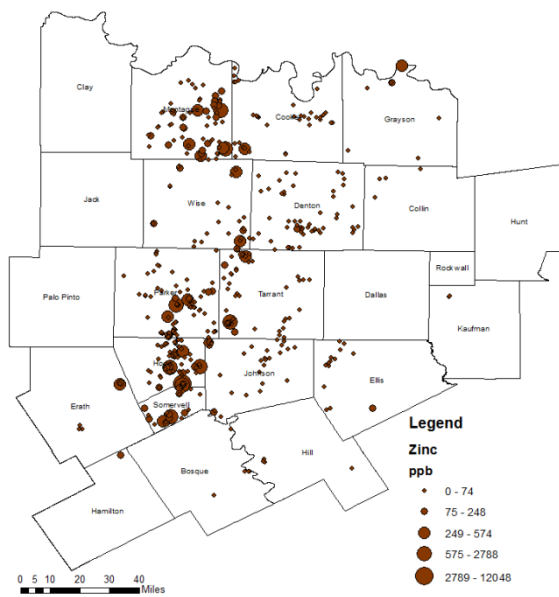


Fig. A- 29: Sample locations of Total Zinc denoted by relative measurements in concentration (ppb)

APPENDIX B – GROUNDWATER CONSTITUENT CONTOURS

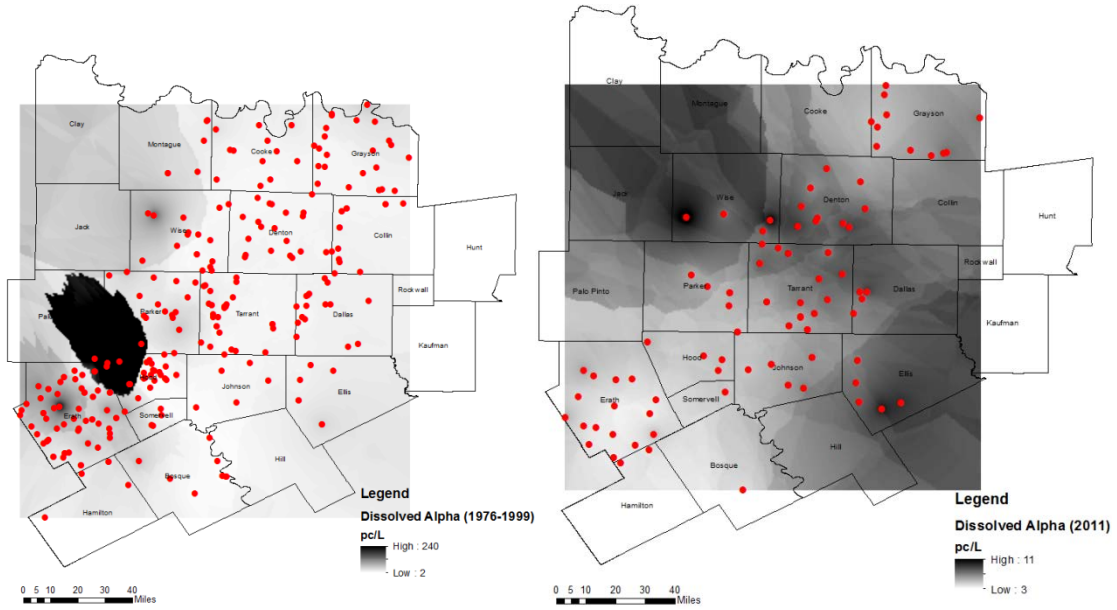


Fig. B- 1: Contour plots of Dissolved Alpha concentration in study region prior to 2001 (left) and after 2010 (right)
**Note that the numerical values of the color scale differ in each plot*

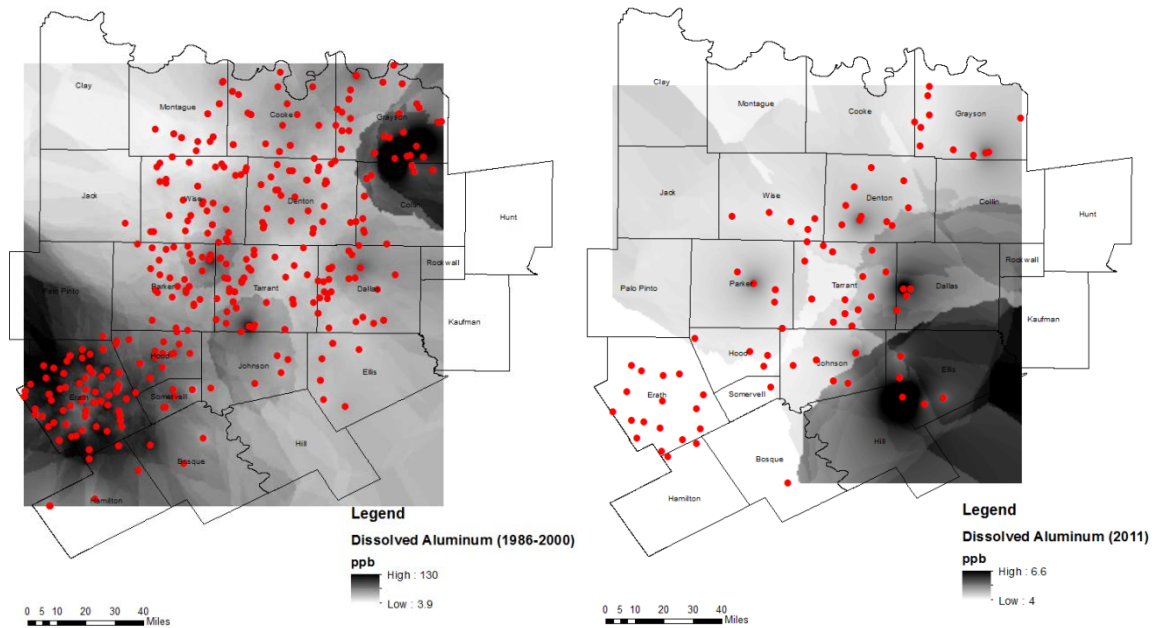


Fig. B- 2: Contour plots of Dissolved Aluminum concentration in study region prior to 2001 (left) and after 2010 (right)
**Note that the numerical values of the color scale differ in each plot*

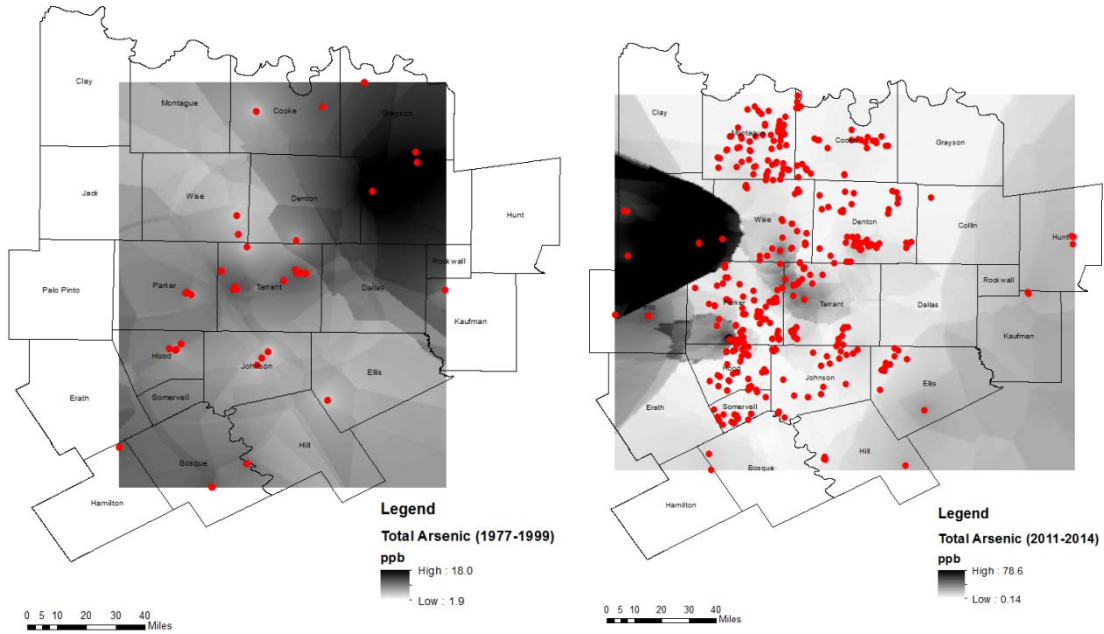


Fig. B- 3: Contour plots of Total Arsenic concentration in study region prior to 2001 (left) and after 2010 (right)
**Note that the numerical values of the color scale differ in each plot*

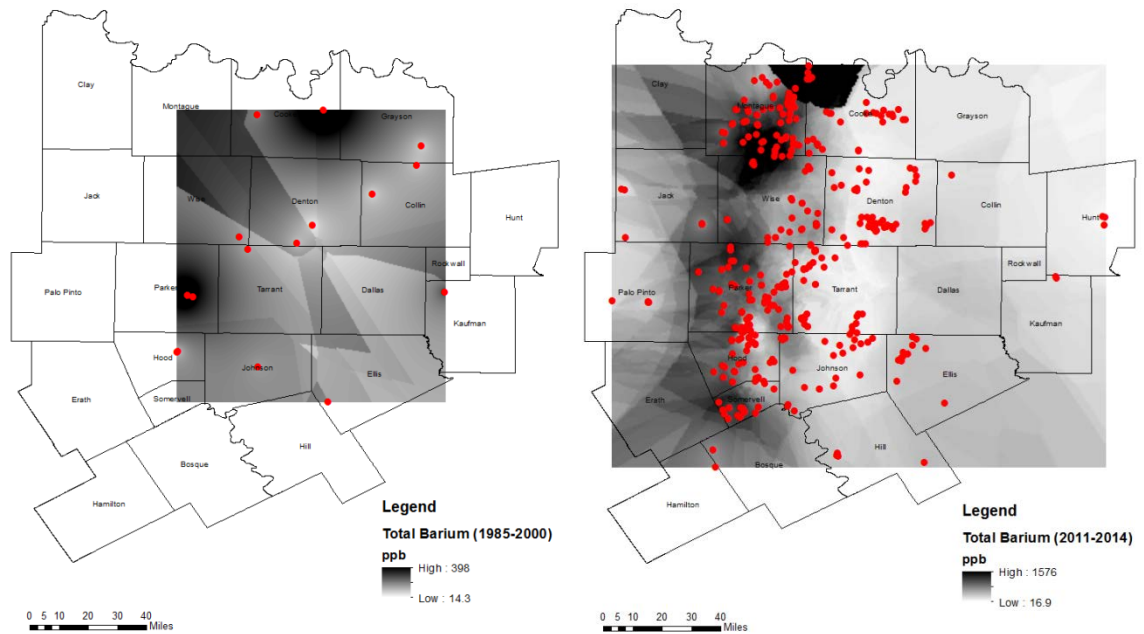


Fig. B- 4: Contour plots of Total Barium concentration in study region prior to 2001 (left) and after 2010 (right)
**Note that the numerical values of the color scale differ in each plot*

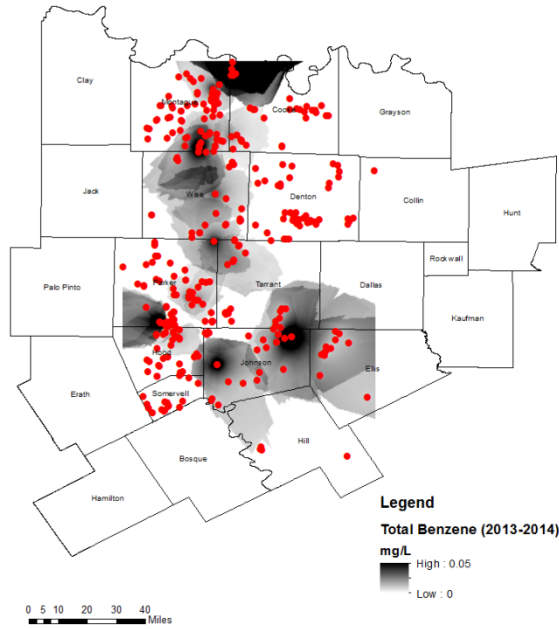


Fig. B- 5: Contour plot of Total Benzene concentration in the study region after 2010

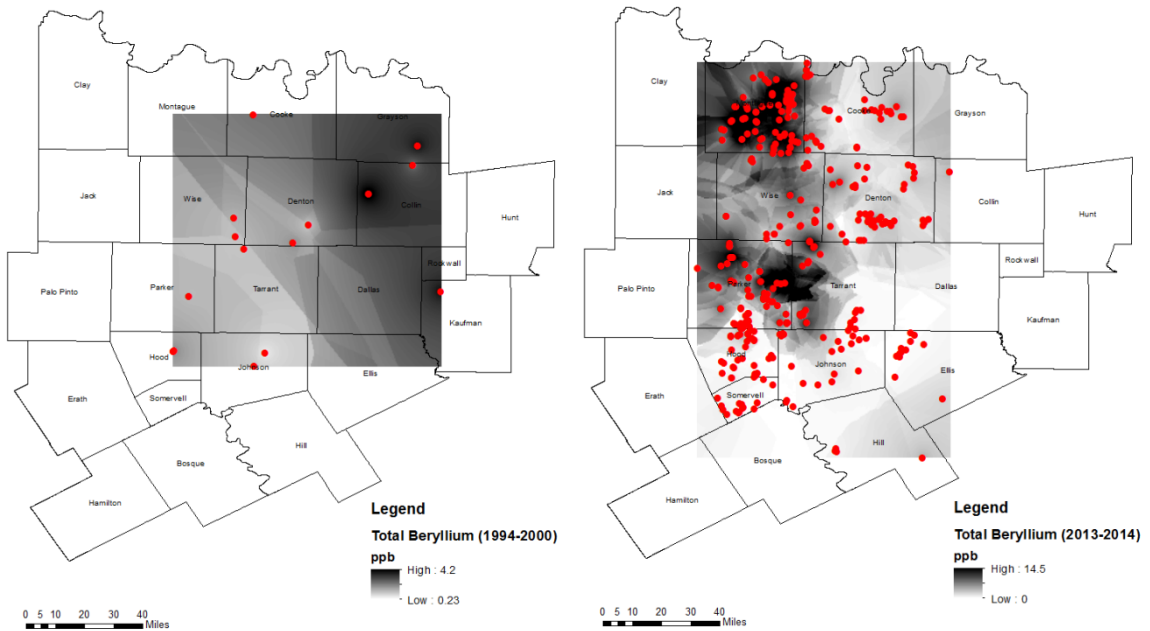


Fig. B- 6: Contour plots of Total Beryllium concentration in study region prior to 2001 (left) and after 2010 (right)

**Note that the numerical values of the color scale differ in each plot*

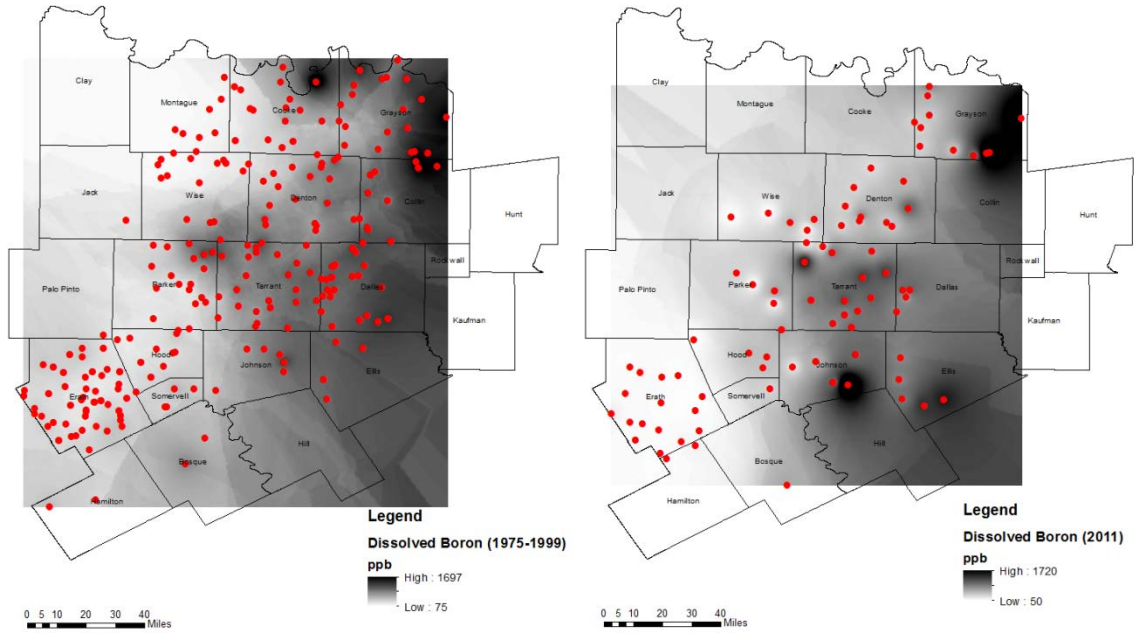


Fig. B- 7: Contour plots of Dissolved Boron concentration in study region prior to 2001 (left) and after 2010 (right)
**Note that the numerical values of the color scale differ in each plot*

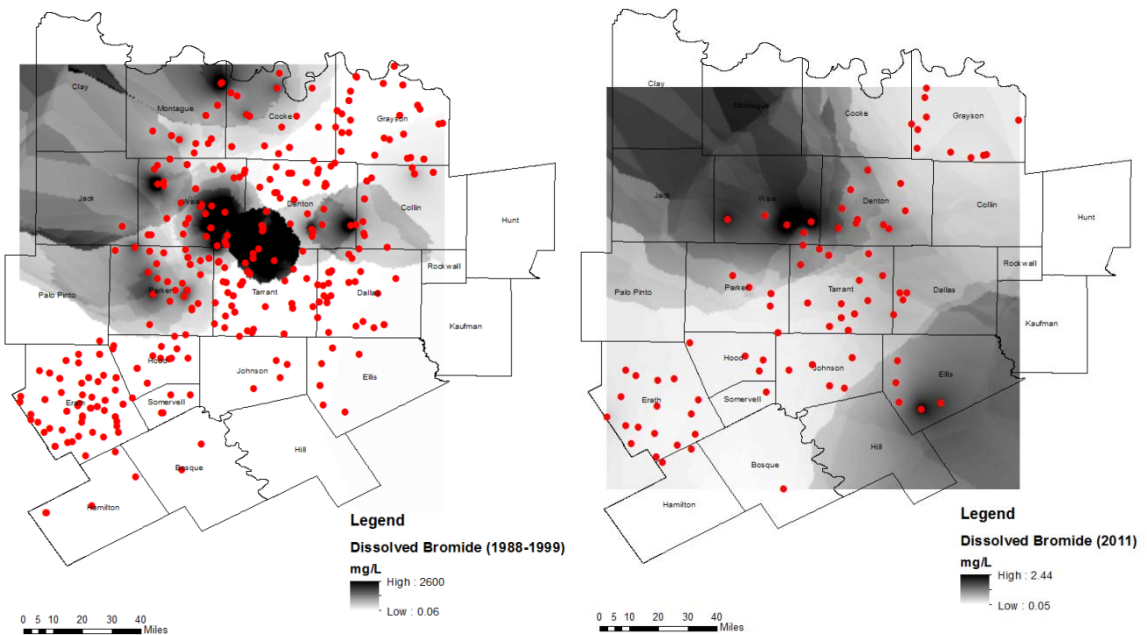


Fig. B- 8: Contour plots of Dissolved Bromide concentration in study region prior to 2001 (left) and after 2010 (right)
**Note that the numerical values of the color scale differ in each plot*

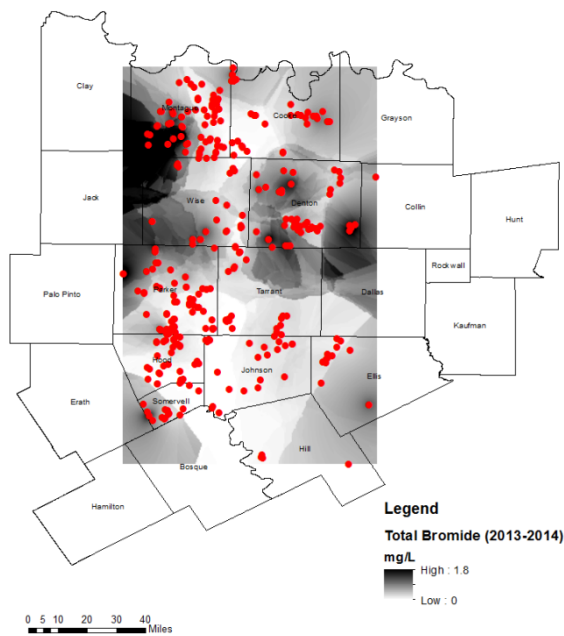


Fig. B- 9: Contour plot of Total Bromide concentration in the study region after 2010

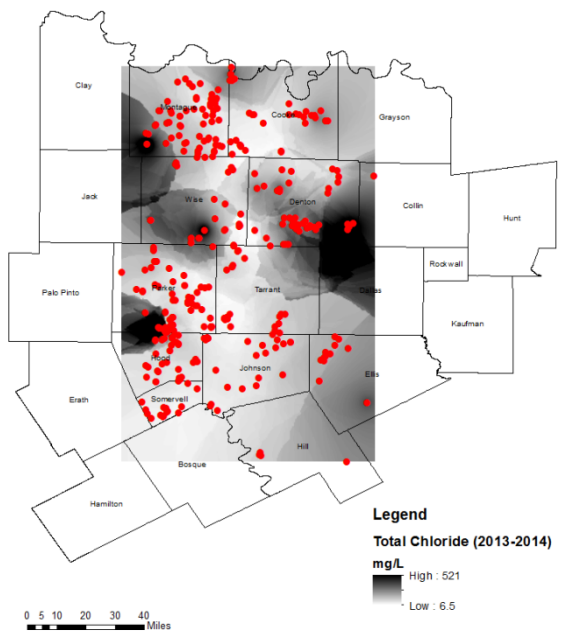


Fig. B- 10: Contour plot of Total Chloride concentration in the study region after 2010

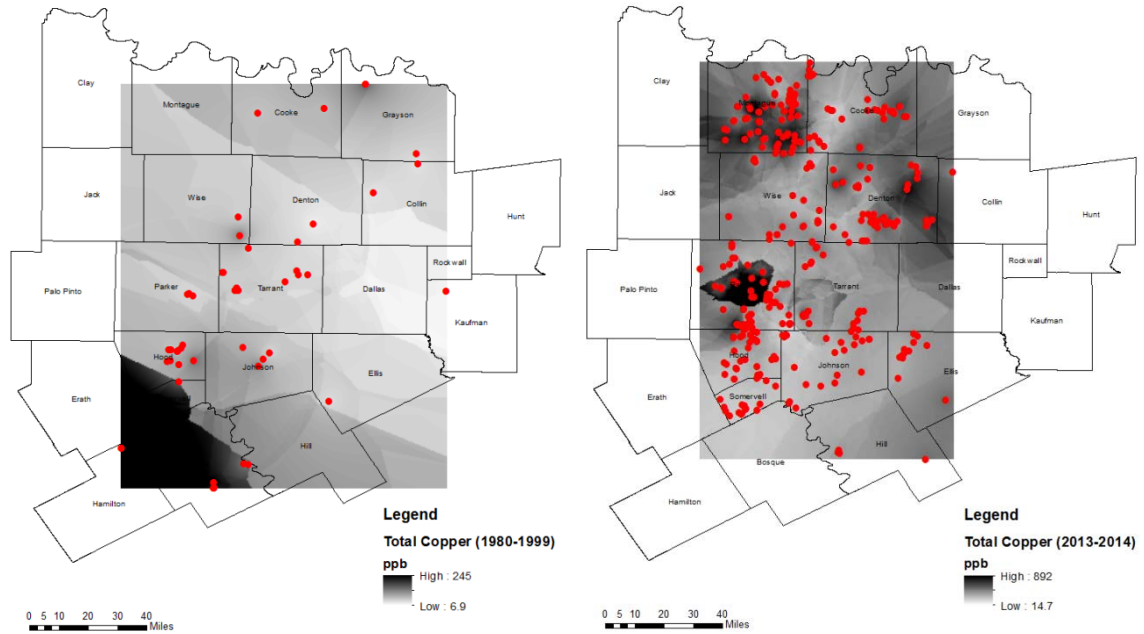


Fig. B- 11: Contour plots of Total Copper concentration in study region prior to 2001 (left) and after 2010 (right)
**Note that the numerical values of the color scale differ in each plot*

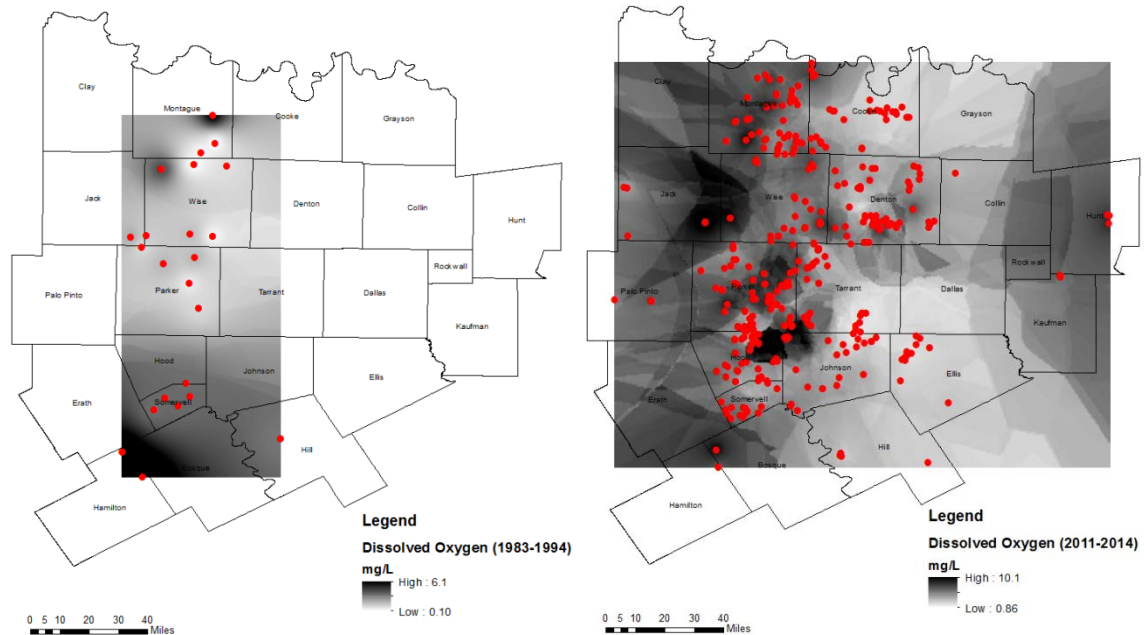


Fig. B- 12: Contour plots of Dissolved Oxygen concentration in study region prior to 2001 (left) and after 2010 (right)
**Note that the numerical values of the color scale differ in each plot*

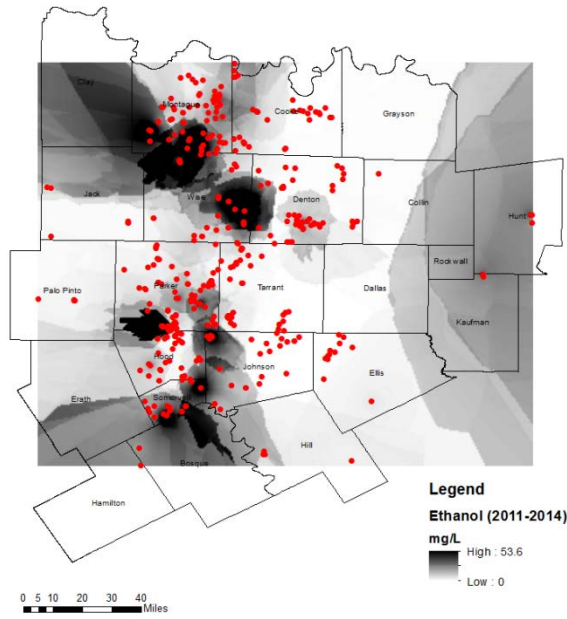


Fig. B- 13: Contour plot of Total Ethanol concentration in the study region after 2010

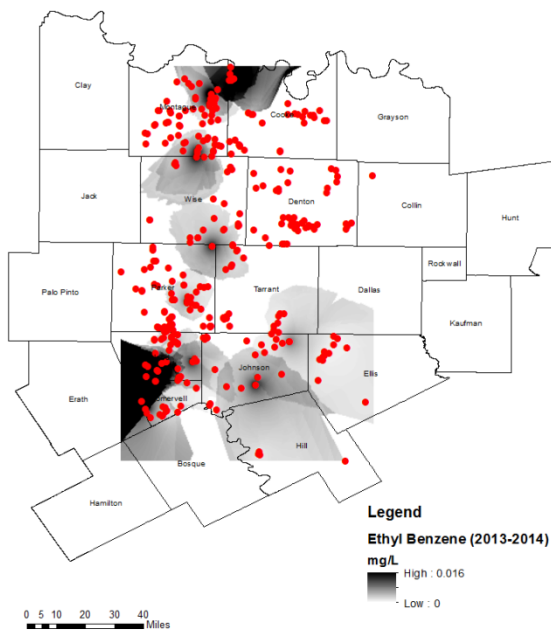


Fig. B- 14: Contour plot of Total Ethyl Benzene concentration in the study region after 2010

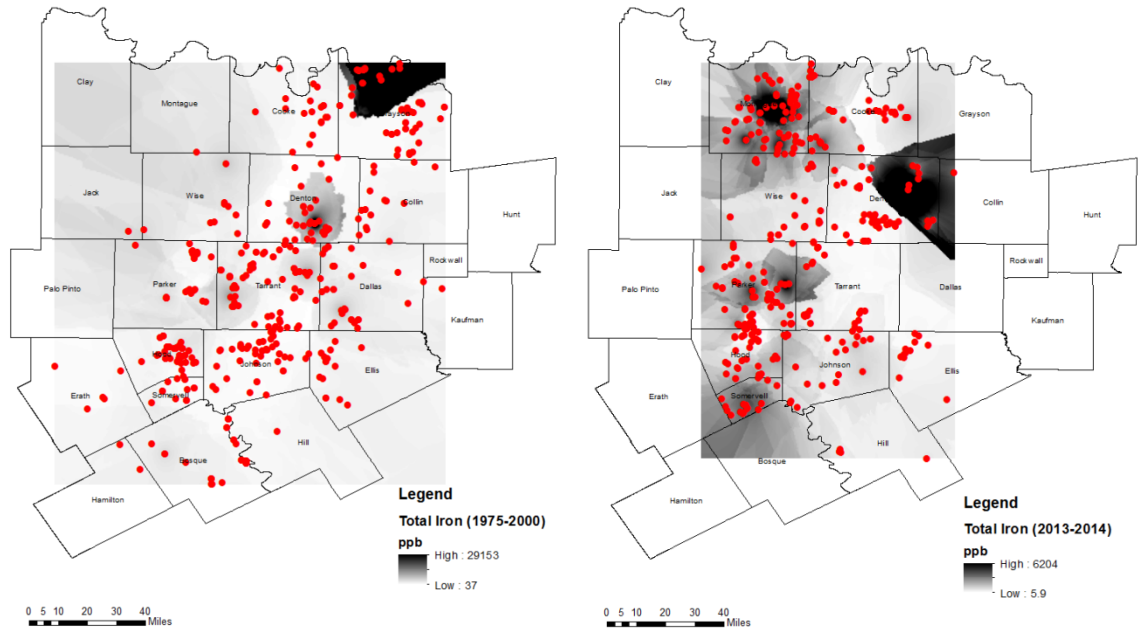


Fig. B- 15: Contour plots of Total Iron concentration in study region prior to 2001 (left) and after 2010 (right)
**Note that the numerical values of the color scale differ in each plot*

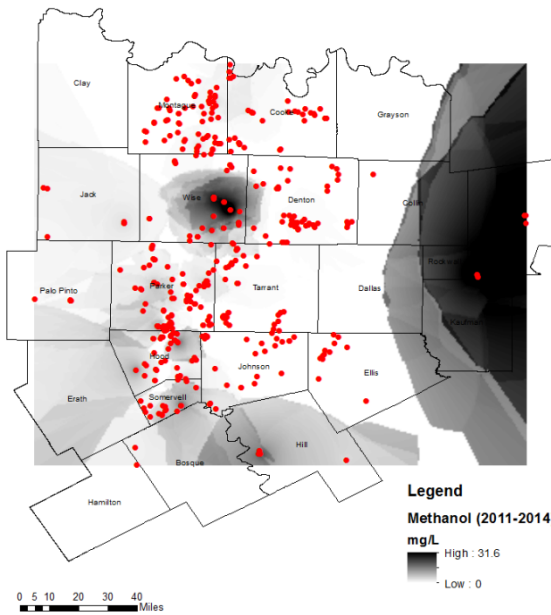


Fig. B- 16: Contour plot of Total Methanol concentration in the study region after 2010

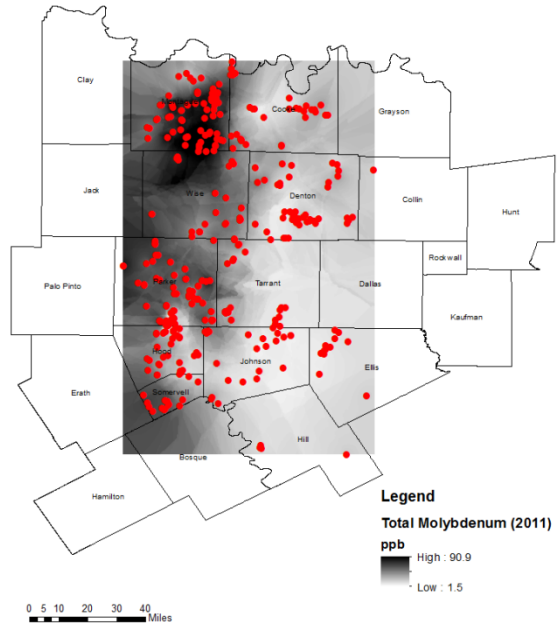


Fig. B- 17: Contour plot of Total Molybdenum concentration in the study region after 2010

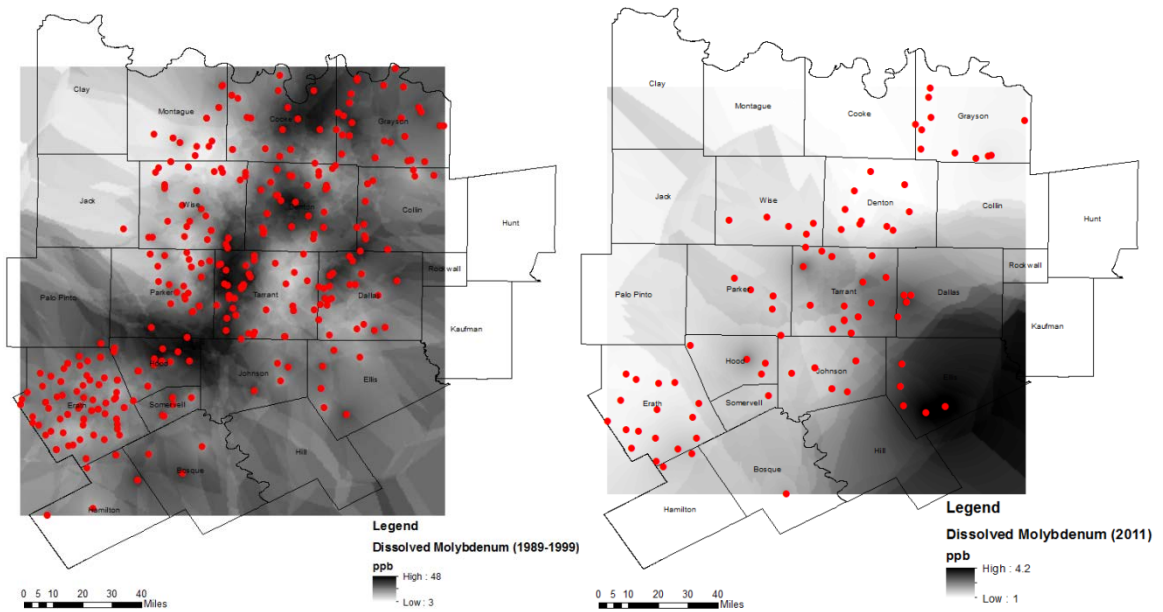


Fig. B- 18: Contour plots of Dissolved Molybdenum concentration in study region prior to 2001 (left) and after 2010 (right)

**Note that the numerical values of the color scale differ in each plot*

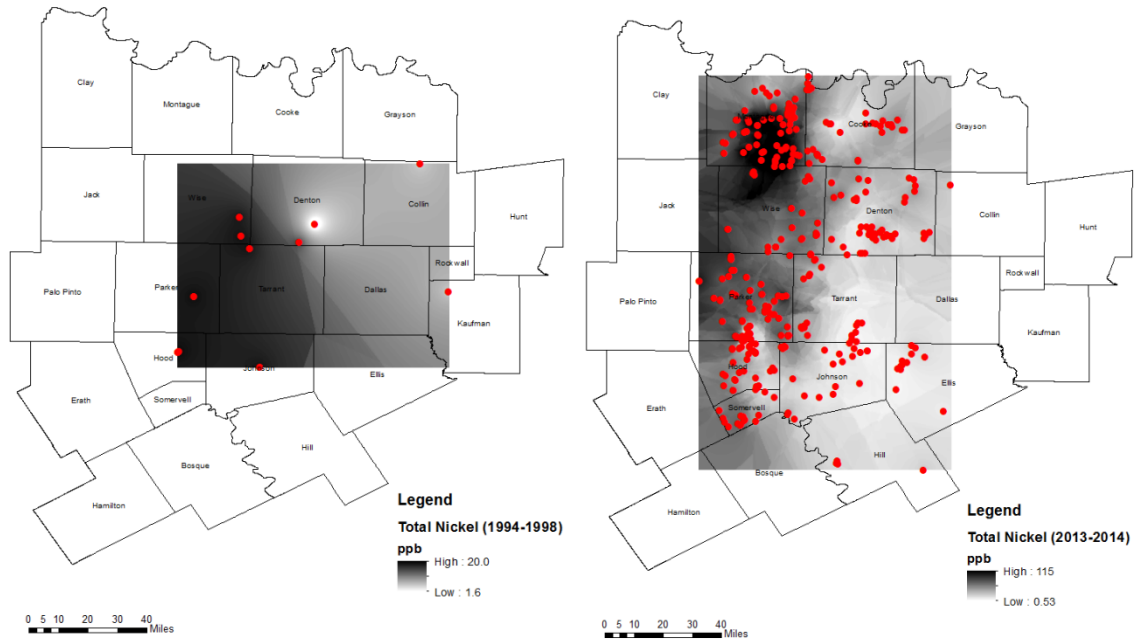


Fig. B- 19: Contour plots of Total Nickel concentration in study region prior to 2001 (left) and after 2010 (right)
**Note that the numerical values of the color scale differ in each plot*

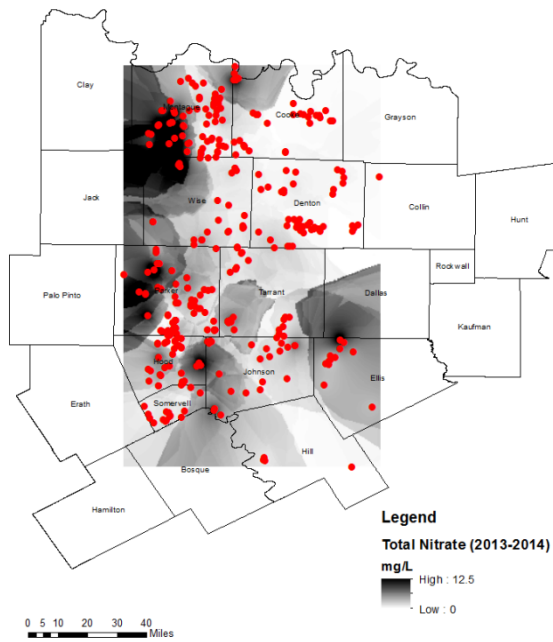


Fig. B- 20: Contour plot of Total Nitrate concentration in the study region after 2010

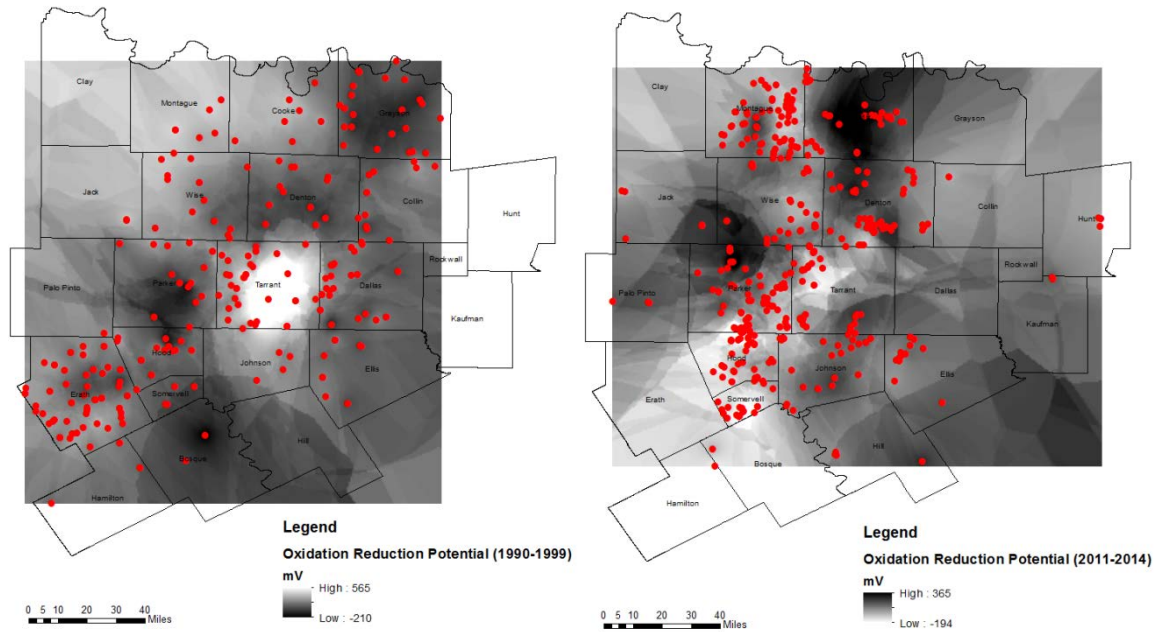


Fig. B- 21: Contour plots of Oxidation-Reduction Potential in study region prior to 2001 (left) and after 2010 (right)
**Note that the numerical values of the color scale differ in each plot*

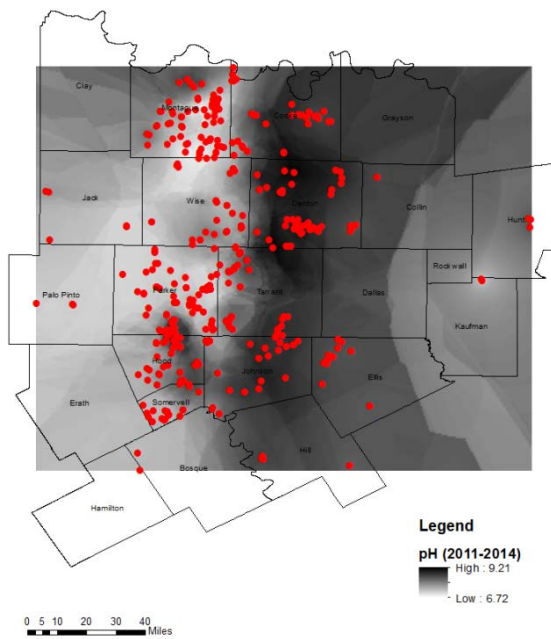


Fig. B- 22: Contour plot of pH in the study region after 2010

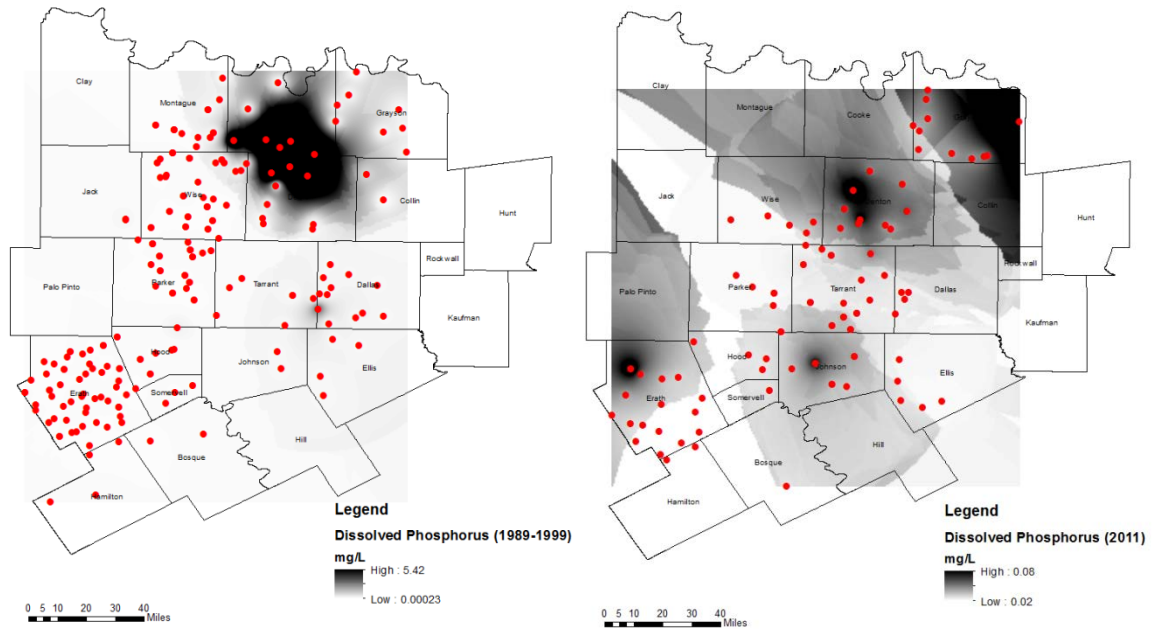


Fig. B- 23 Contour plots of Dissolved Phosphorus concentration in study region prior to 2001 (left) and after 2010 (right)
**Note that the numerical values of the color scale differ in each plot*

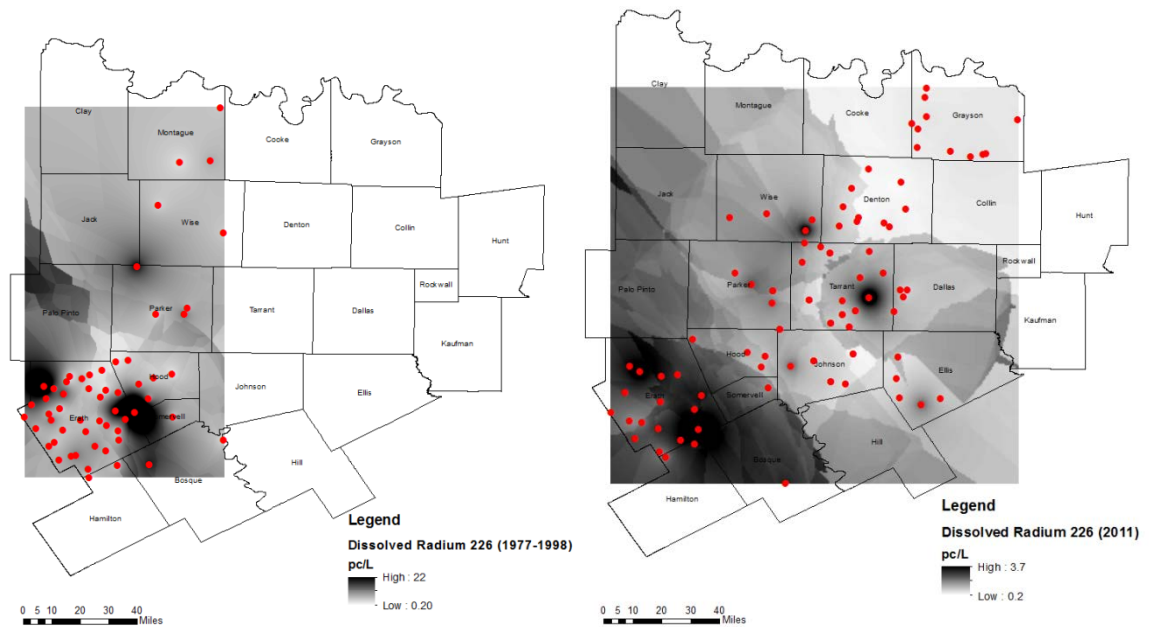


Fig. B- 24: Contour plots of Dissolved Radium 226 concentration in study region prior to 2001 (left) and after 2010 (right)
**Note that the numerical values of the color scale differ in each plot*

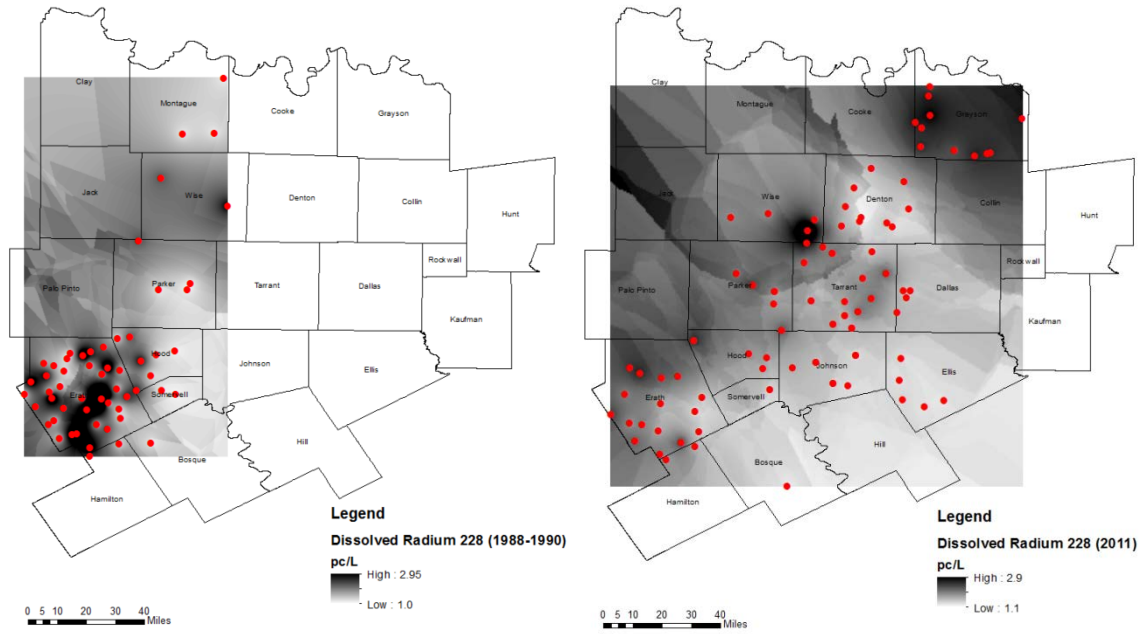


Fig. B- 25: Contour plots of Dissolved Radium 228 concentration in study region prior to 2001 (left) and after 2010 (right)
**Note that the numerical values of the color scale differ in each plot*

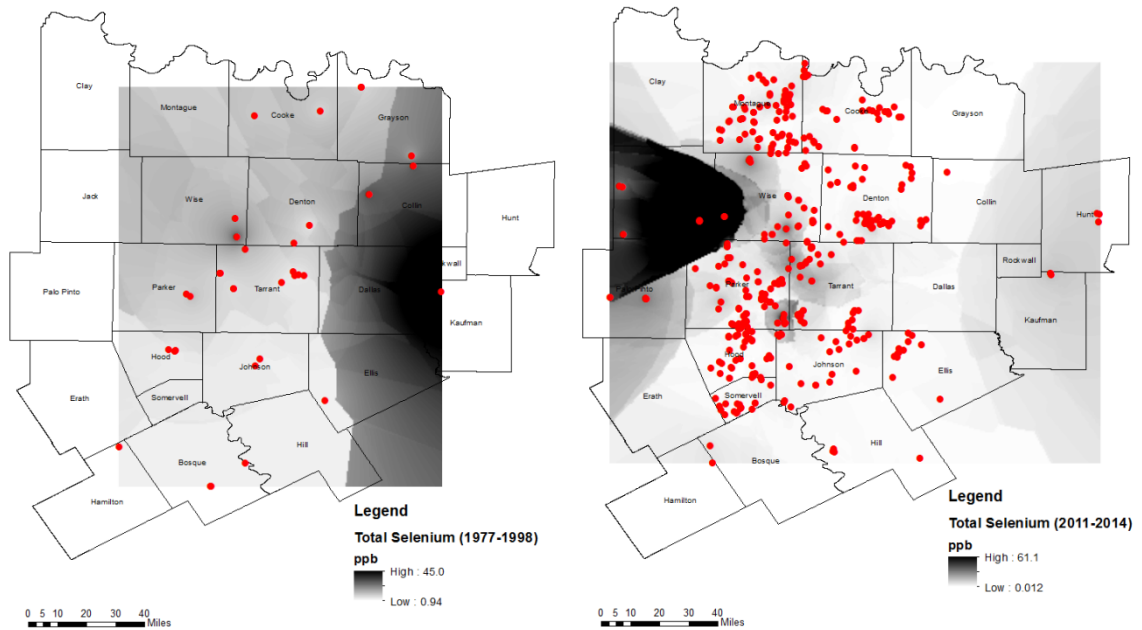


Fig. B- 26: Contour plots of Total Selenium concentration in study region prior to 2001 (left) and after 2010 (right)
**Note that the numerical values of the color scale differ in each plot*

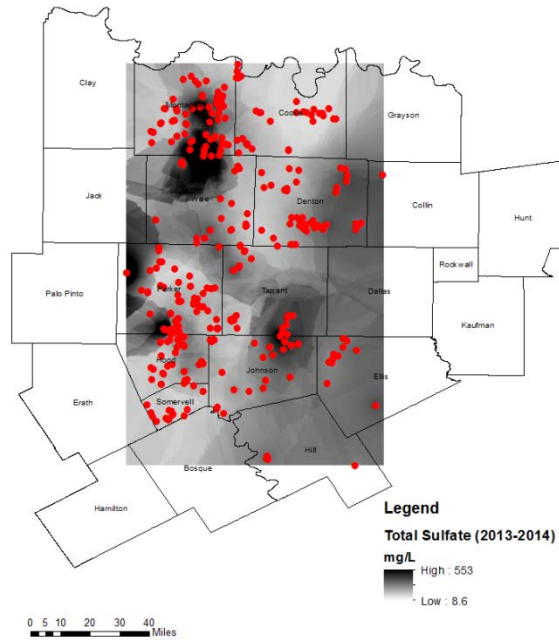


Fig. B- 27: Contour plots of Total Sulfate concentration in study region after 2010

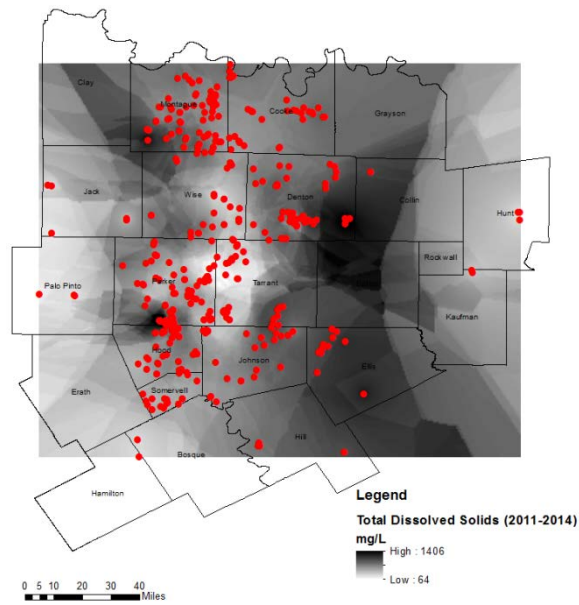


Fig. B- 28: Contour plots of Total Dissolved Solids concentration in study region after 2010

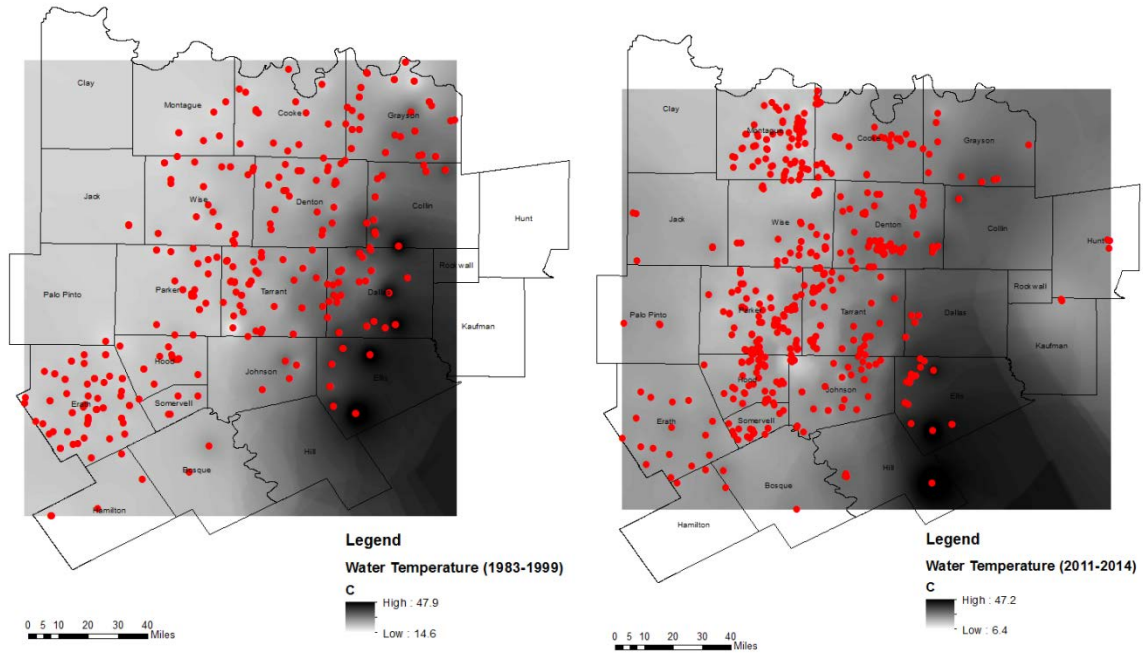


Fig. B- 29: Contour plots of Water Temperature in study region prior to 2001 (left) and after 2010 (right)

**Note that the numerical values of the color scale differ in each plot*

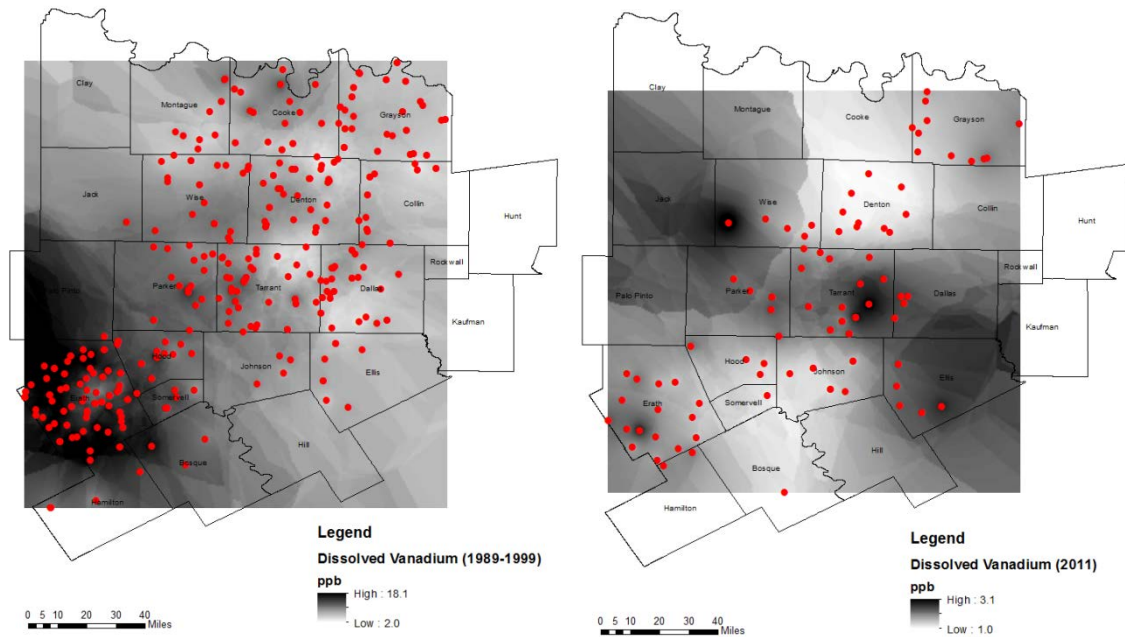


Fig. B- 30: Contour plots of Dissolved Vanadium concentration in study region prior to 2001 (left) and after 2010 (right)

**Note that the numerical values of the color scale differ in each plot*

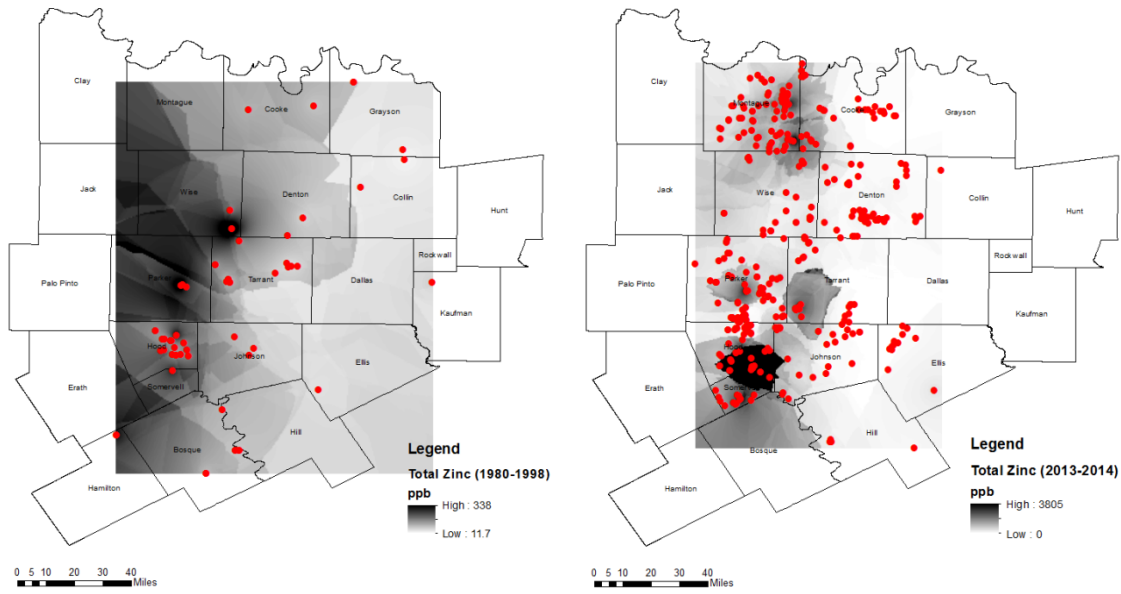


Fig. B- 31: Contour plots of Total Zinc concentration in study region prior to 2001 (left) and after 2010 (right)

**Note that the numerical values of the color scale differ in each plot*

APPENDIX C – GROUNDWATER CONSTITUENT CHANGE

PLOTS

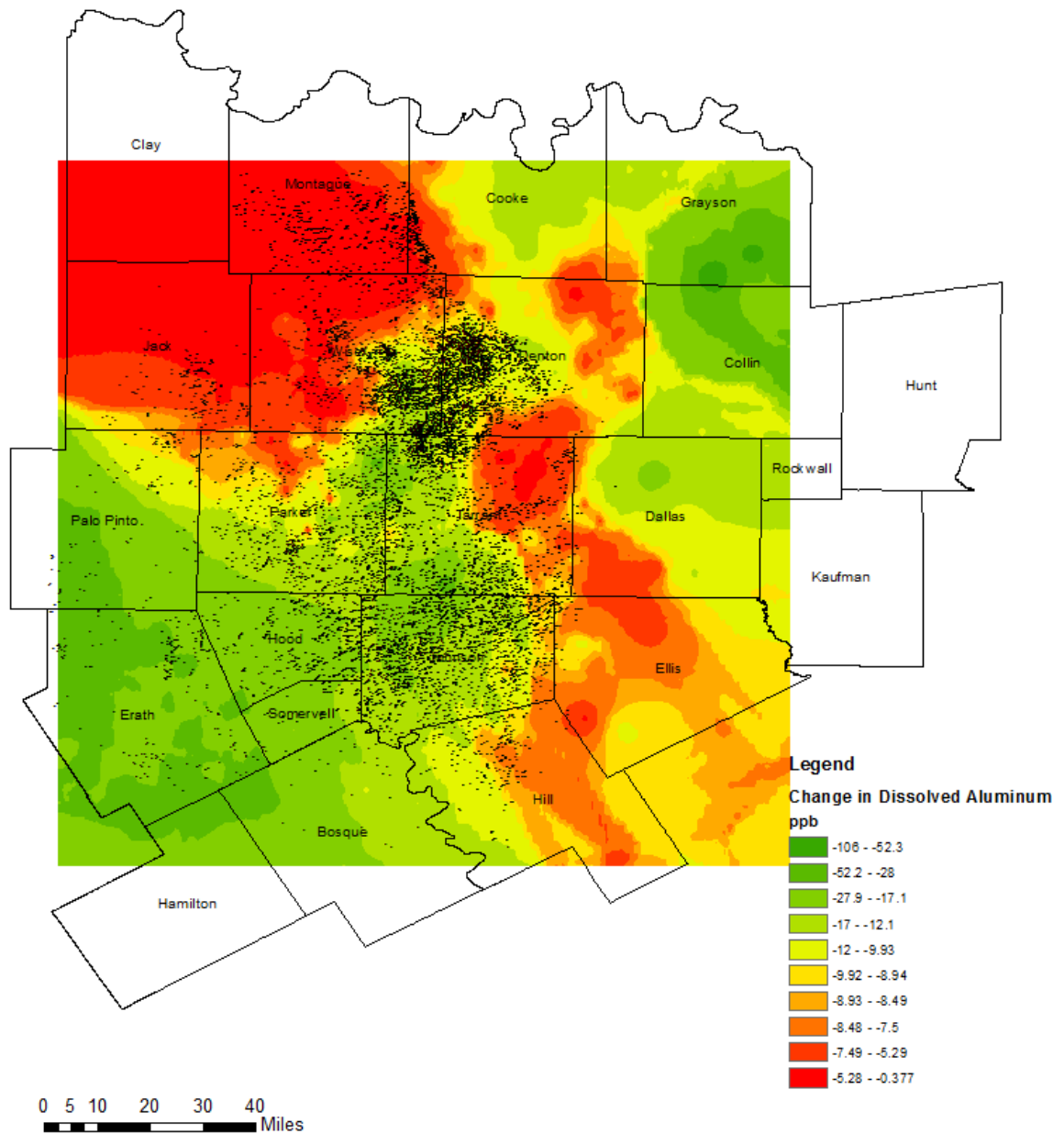


Fig. C- 1: Contour Plot of change in groundwater Dissolved Aluminum concentrations and gas well locations in the study region

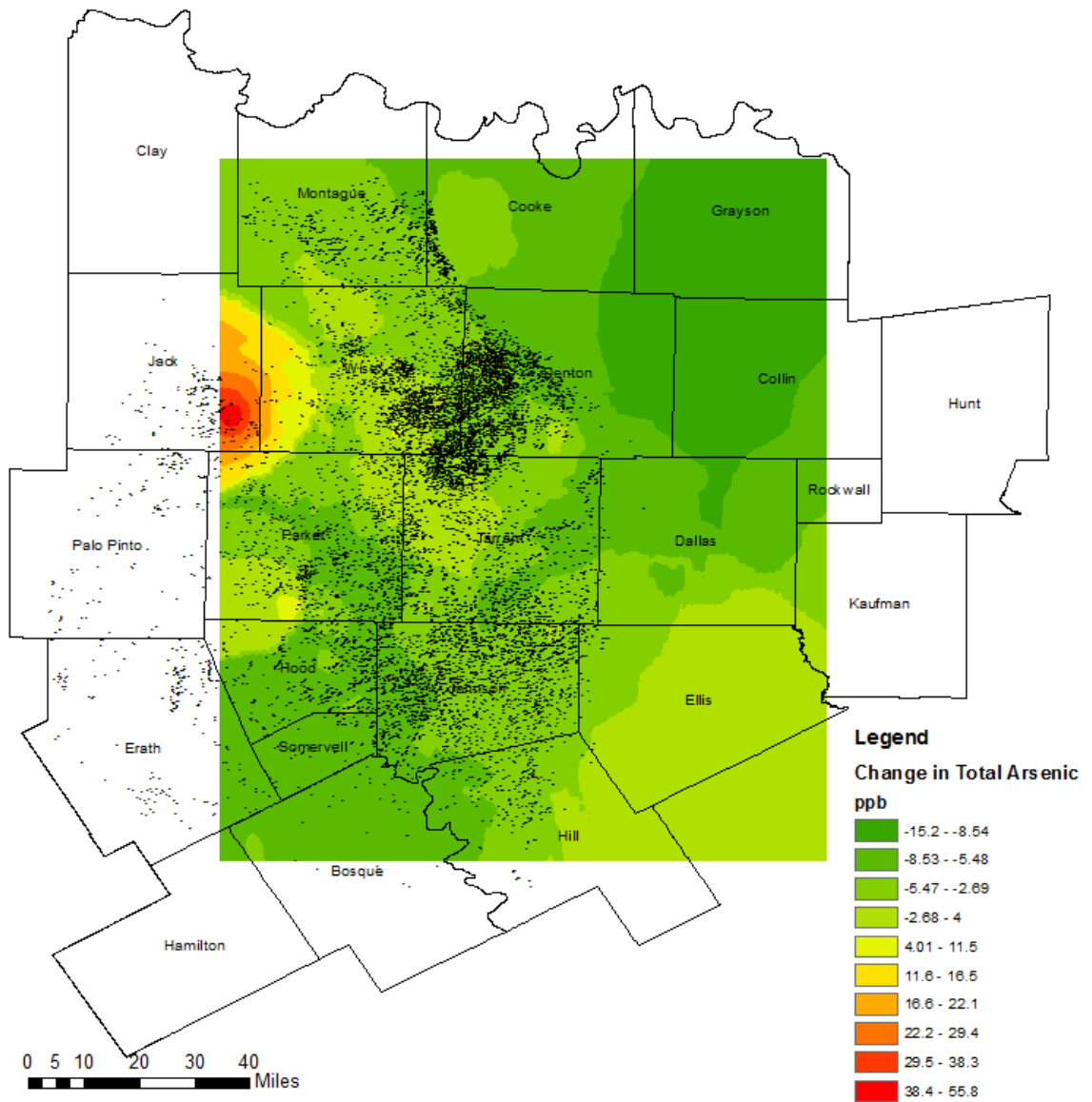


Fig. C- 2: Contour Plot of change in groundwater Total Arsenic concentrations and gas well locations in the study region

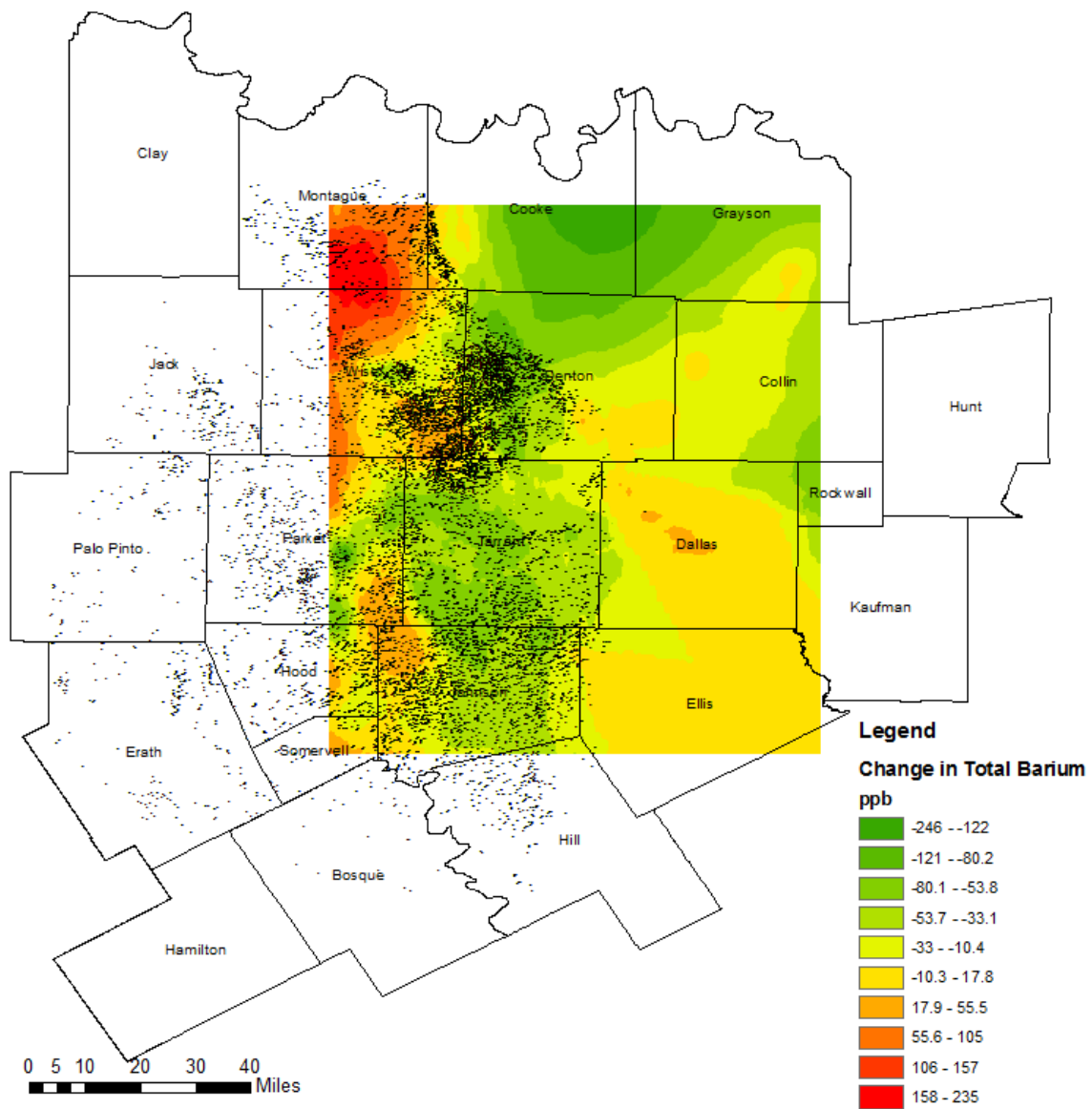


Fig. C- 3: Contour Plot of change in groundwater Total Barium concentrations and gas well locations in the study region

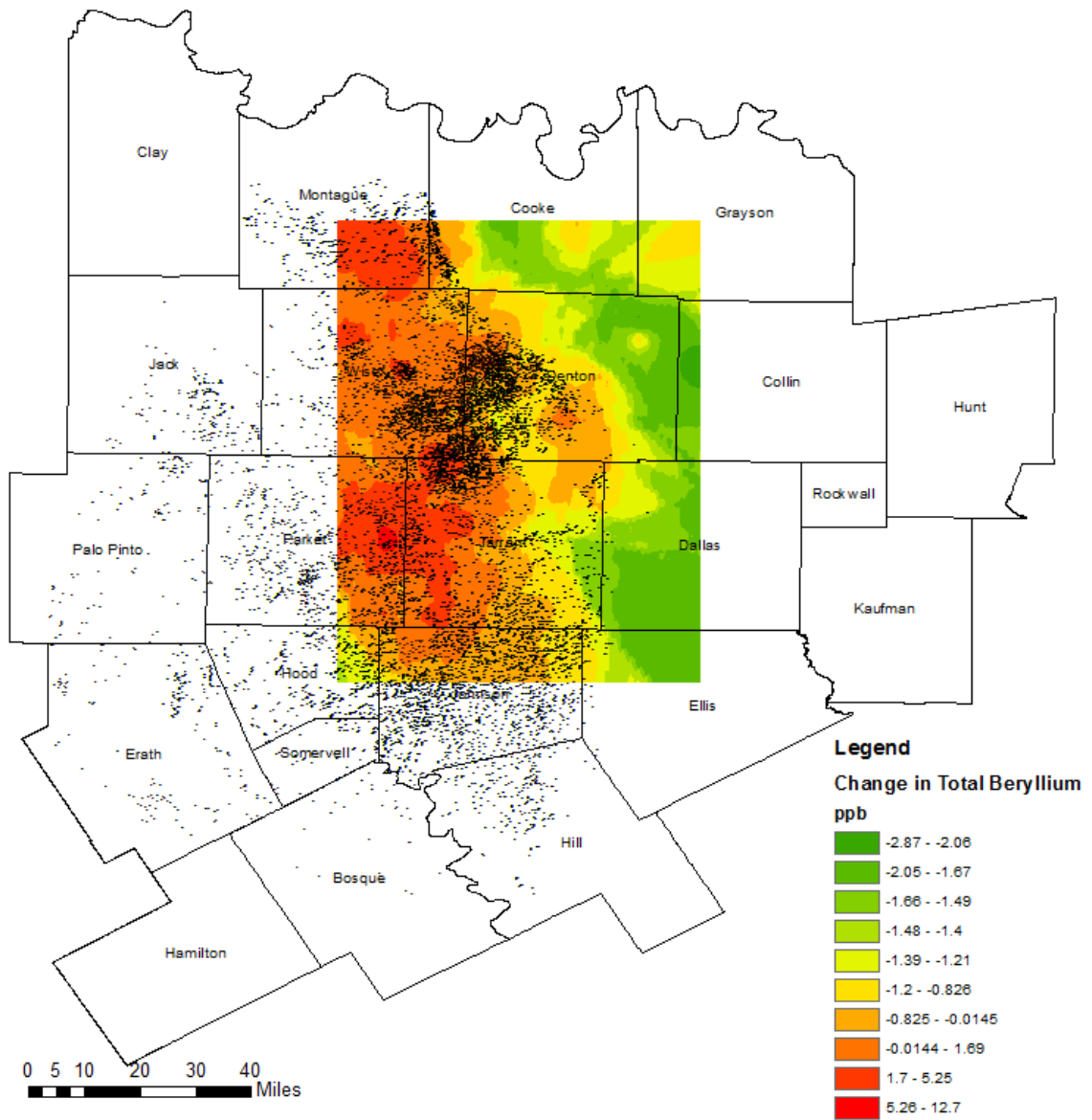


Fig. C- 4: Contour Plot of change in groundwater Total Beryllium concentrations and gas well locations in the study region

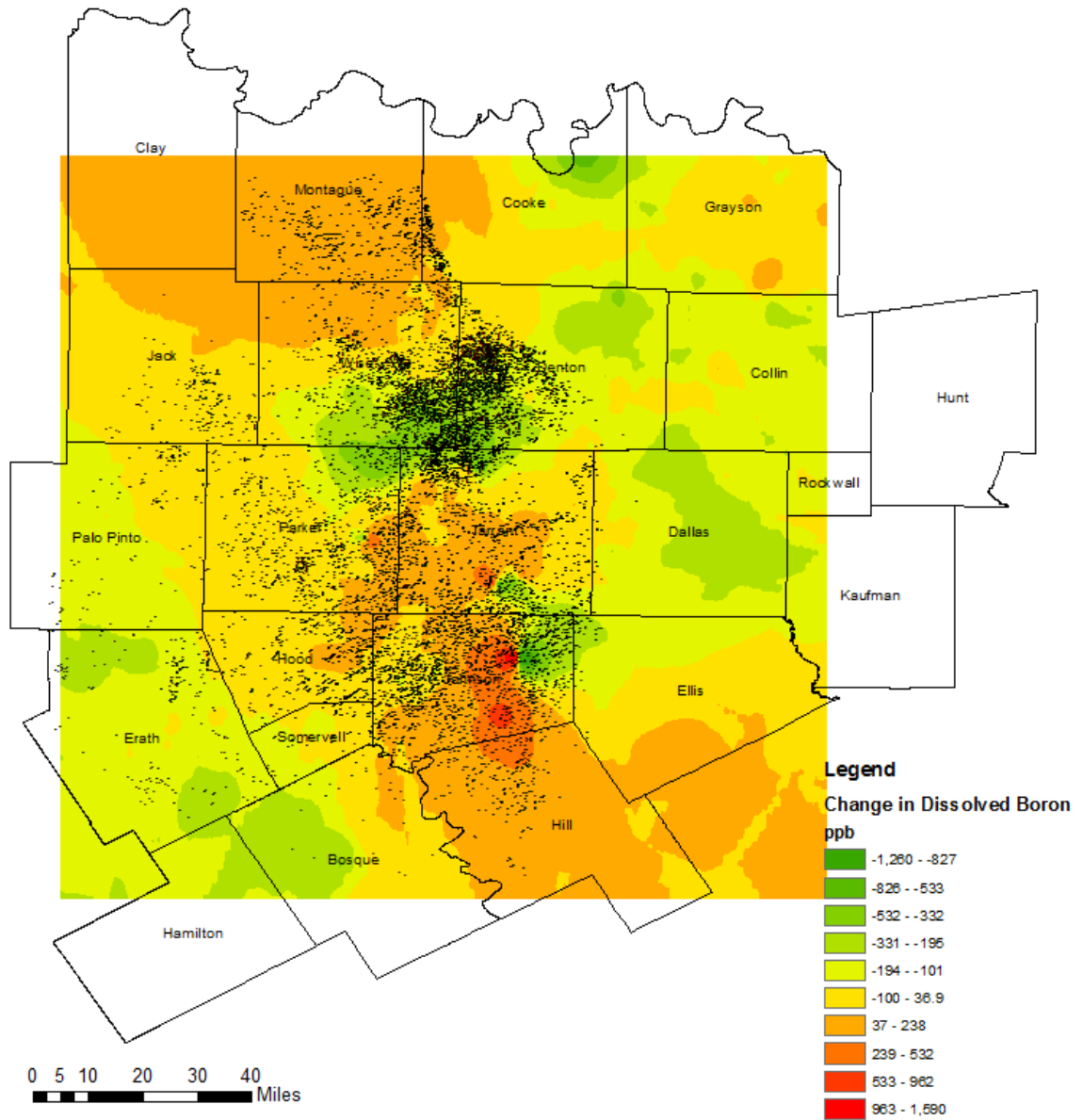


Fig. C- 5: Contour Plot of change in groundwater Dissolved Boron concentrations and gas well locations in the study region

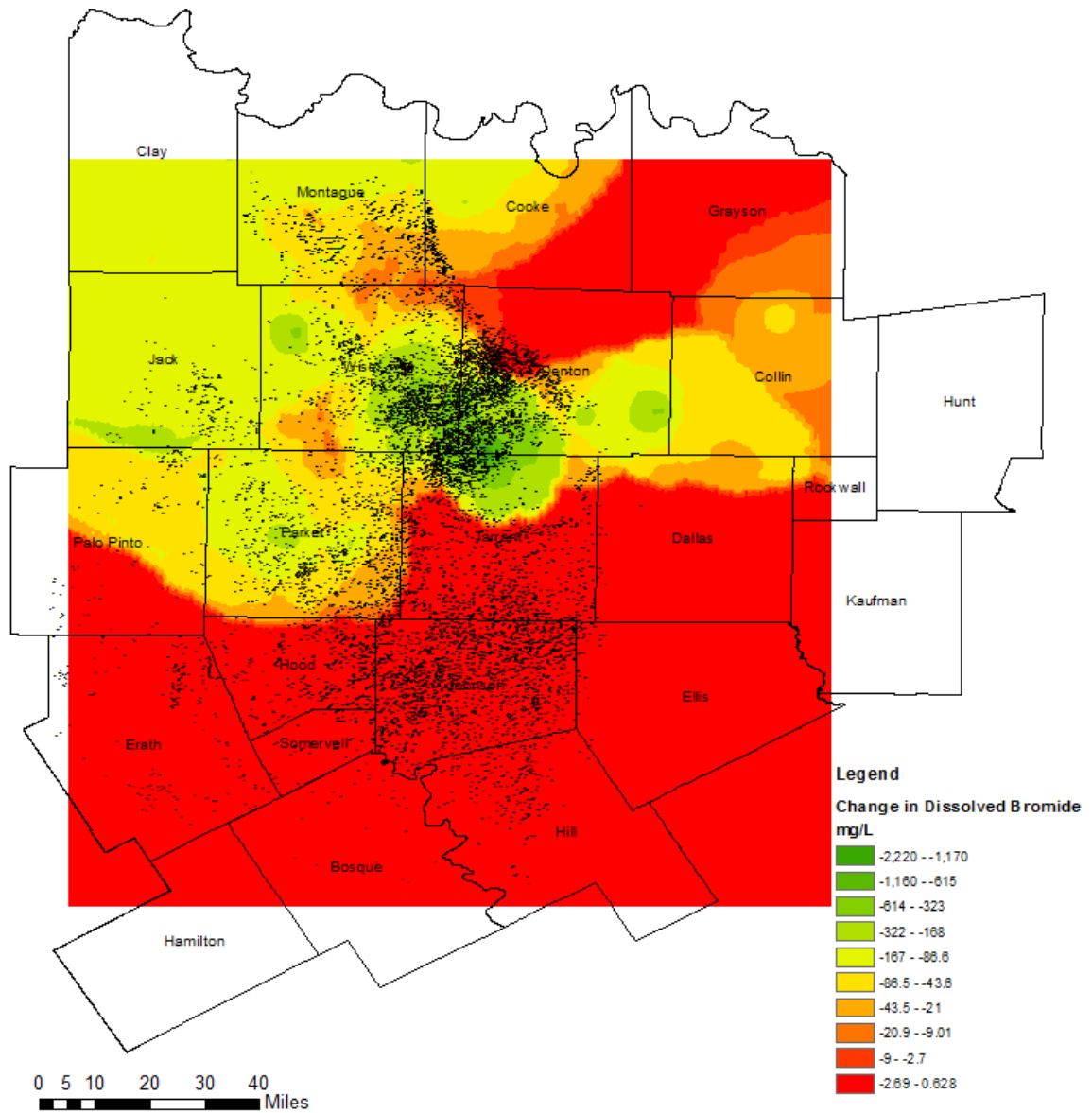


Fig. C- 6: Contour Plot of change in groundwater Dissolved Bromide concentrations and gas well locations in the study region

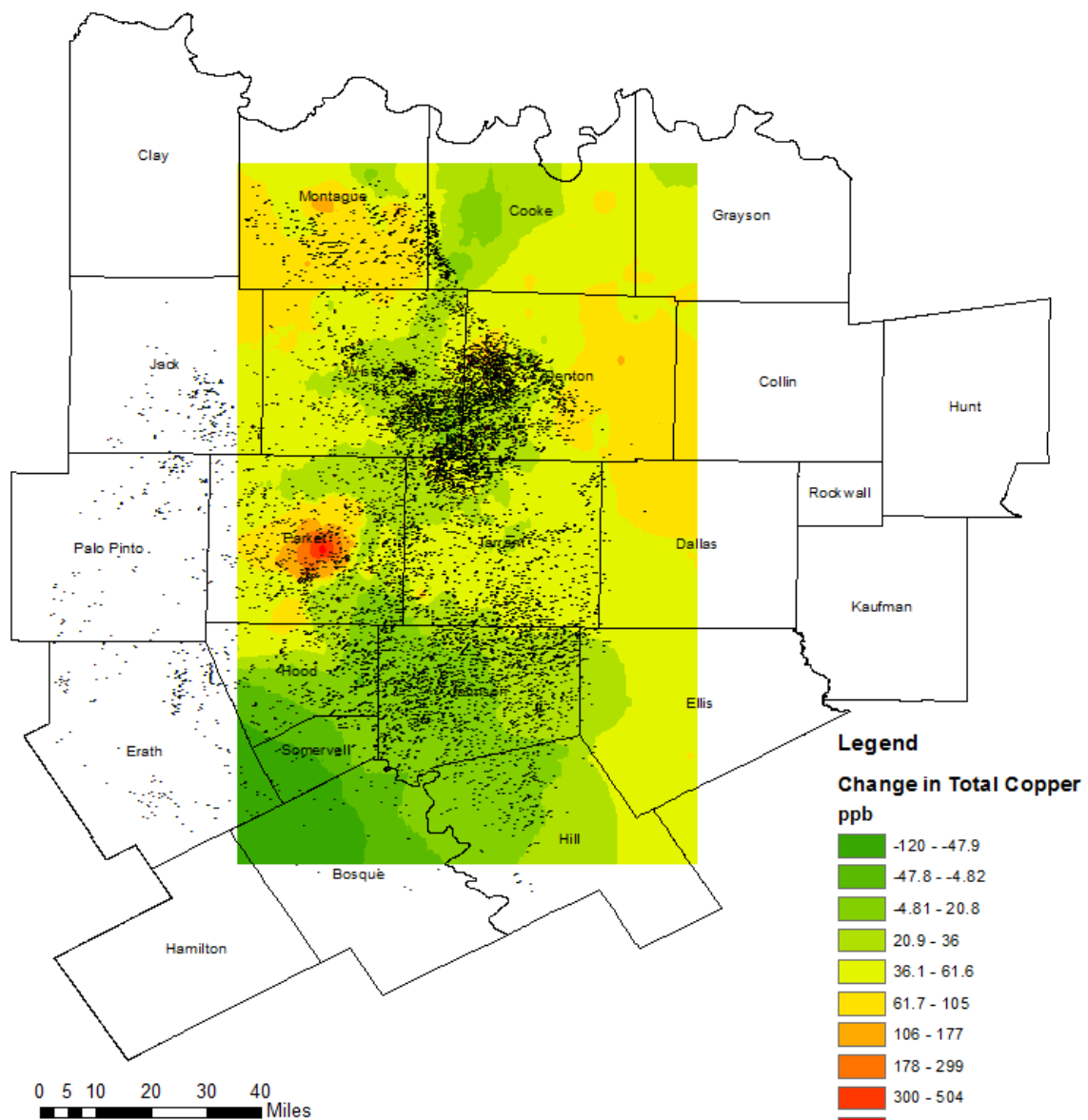


Fig. C- 7: Contour Plot of change in groundwater Total Copper concentrations and gas well locations in the study region

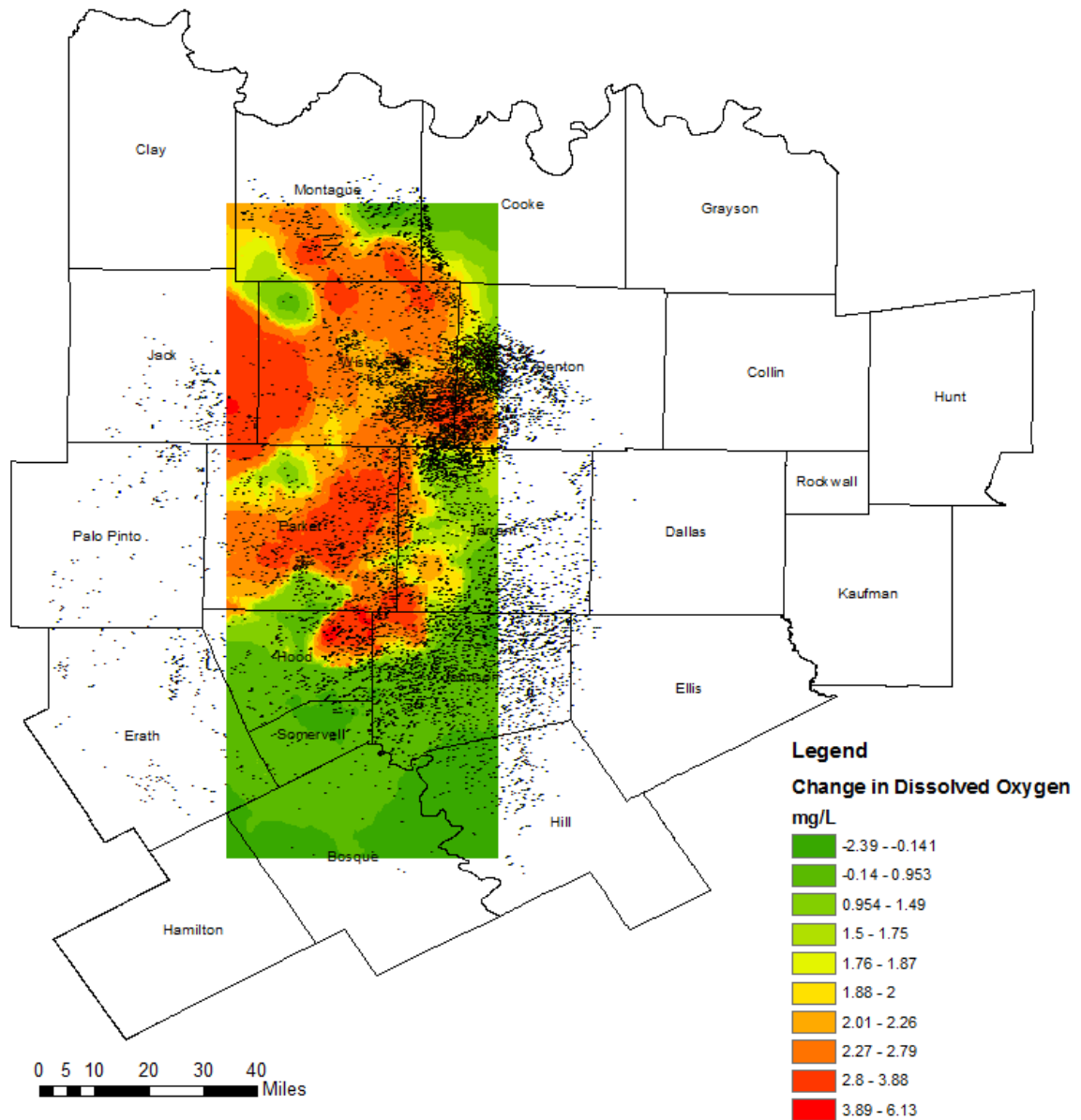


Fig. C- 8: Contour Plot of change in groundwater Dissolved Oxygen concentrations and gas well locations in the study region

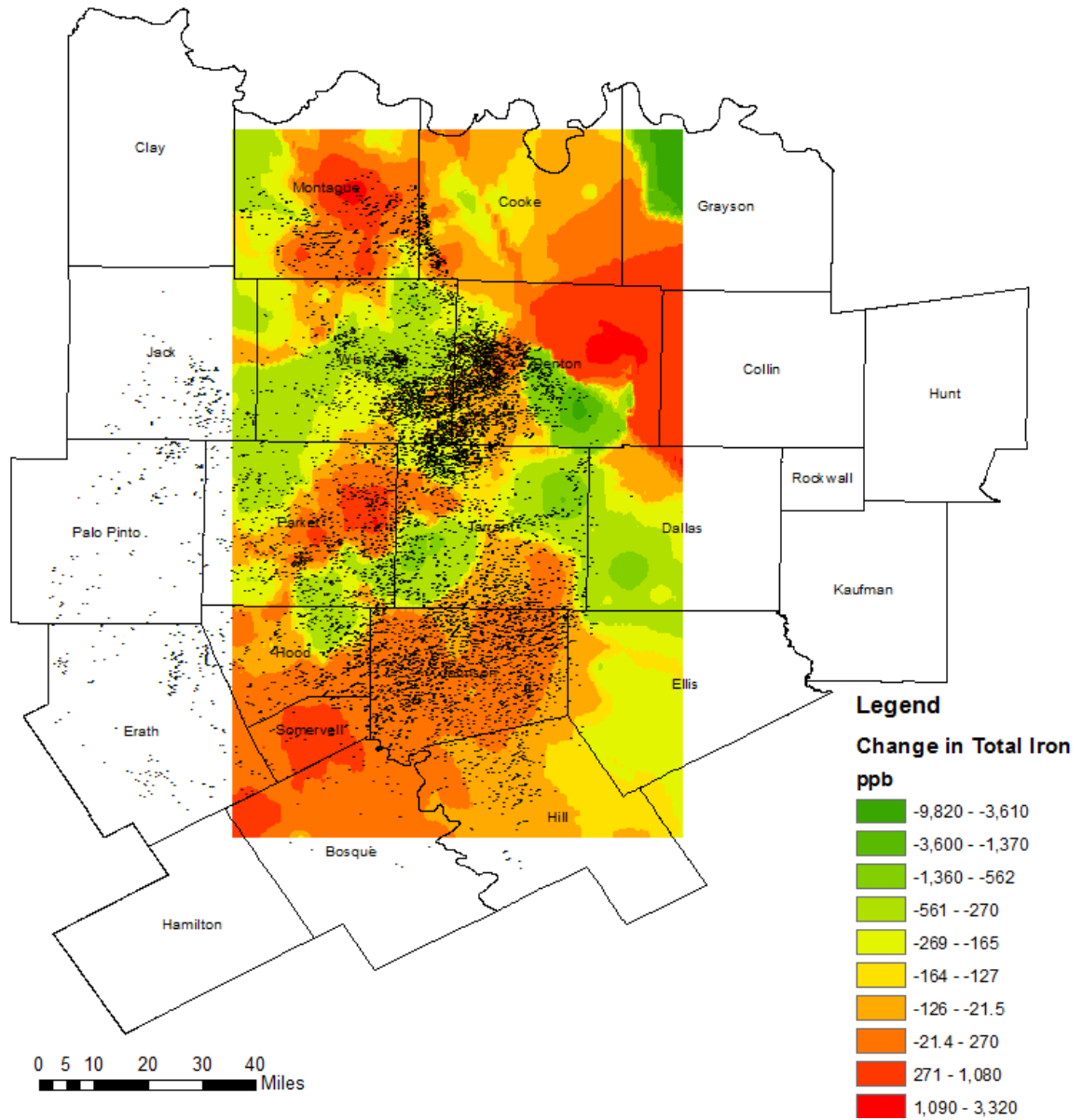


Fig. C- 9: Contour Plot of change in groundwater Total Iron concentrations and gas well locations in the study region

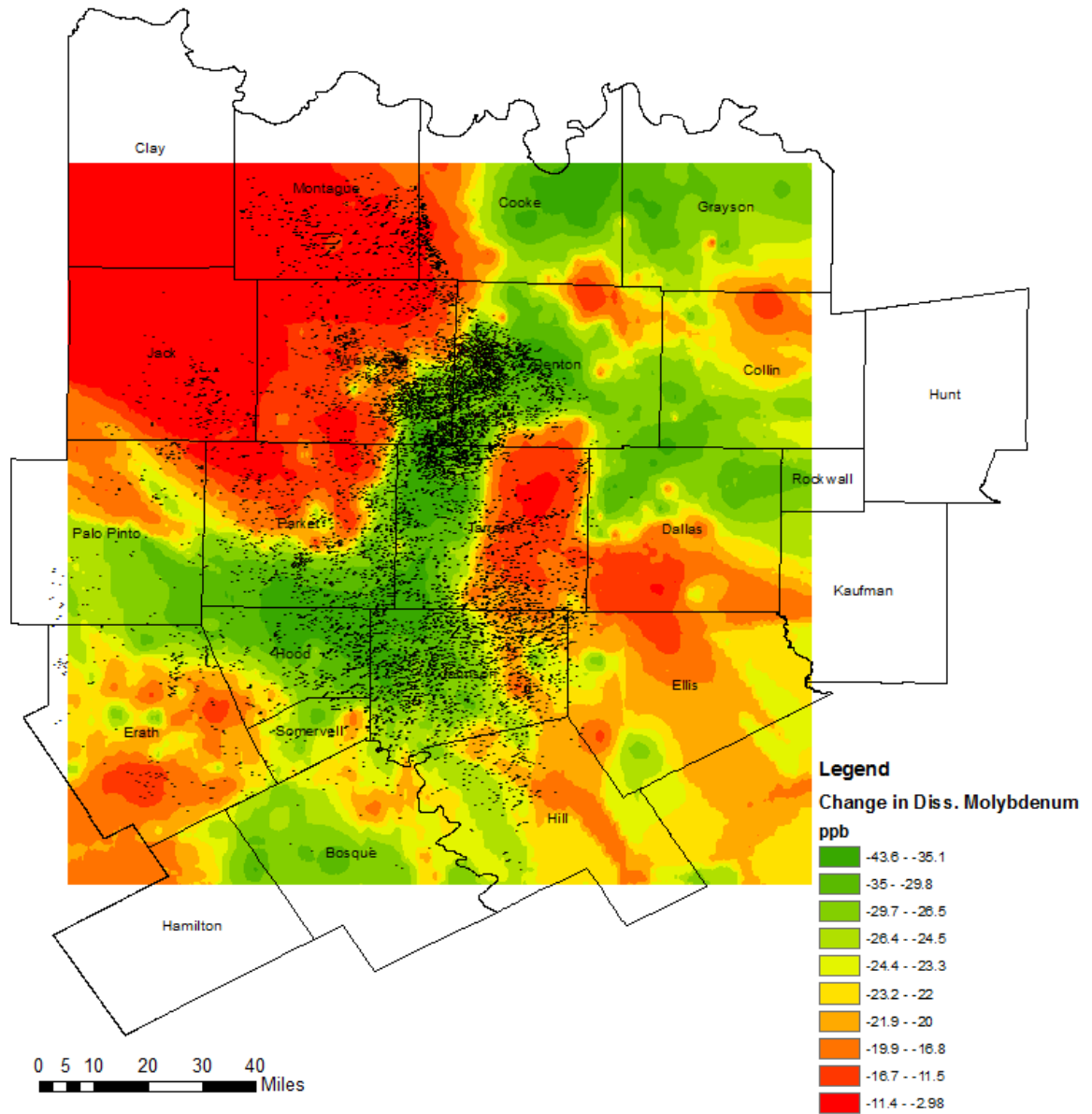


Fig. C- 10: Contour Plot of change in groundwater Dissolved Molybdenum concentrations and gas well locations in the study region

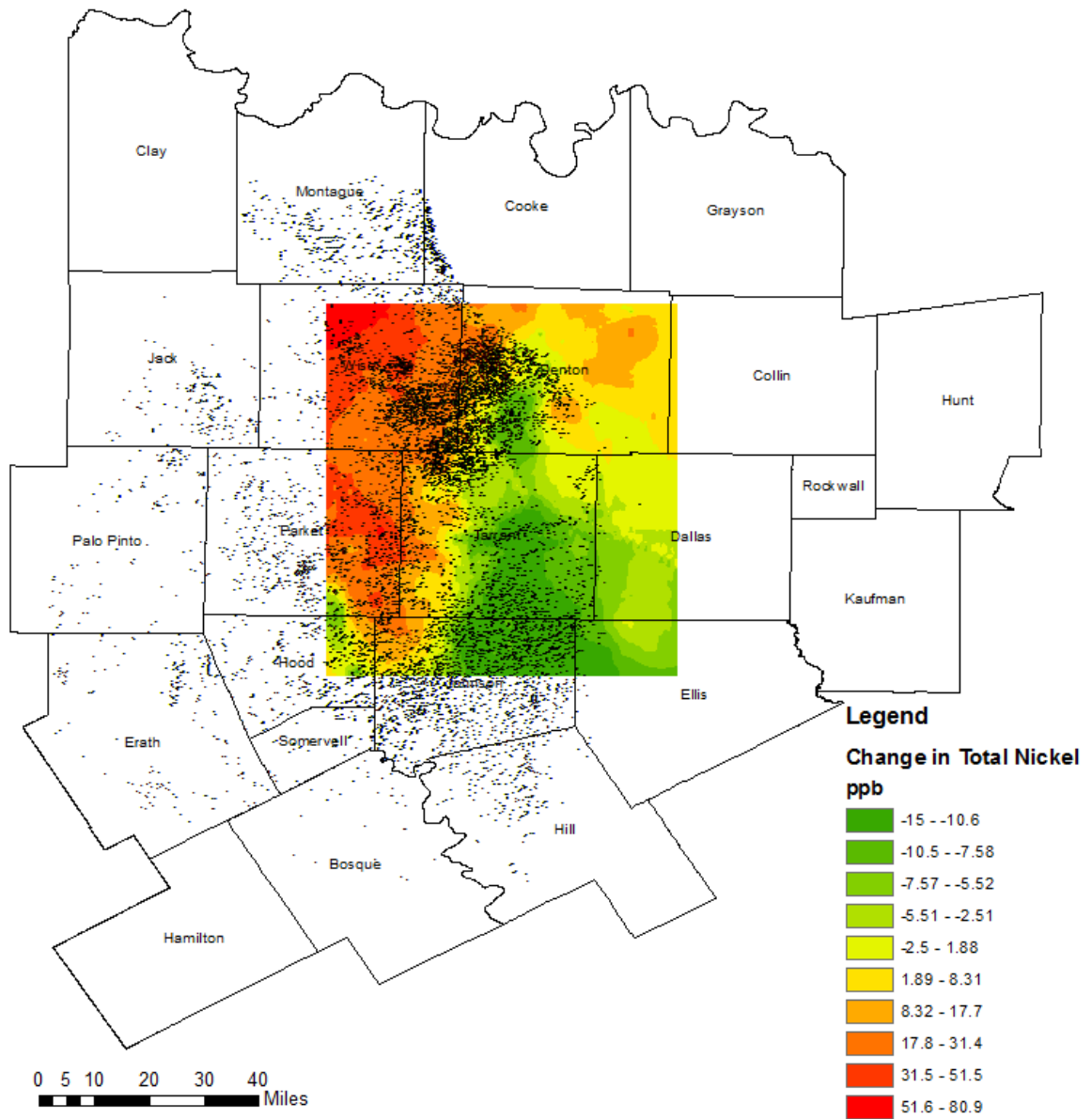


Fig. C- 11: Contour Plot of change in groundwater Total Nickel concentrations and gas well locations in the study region

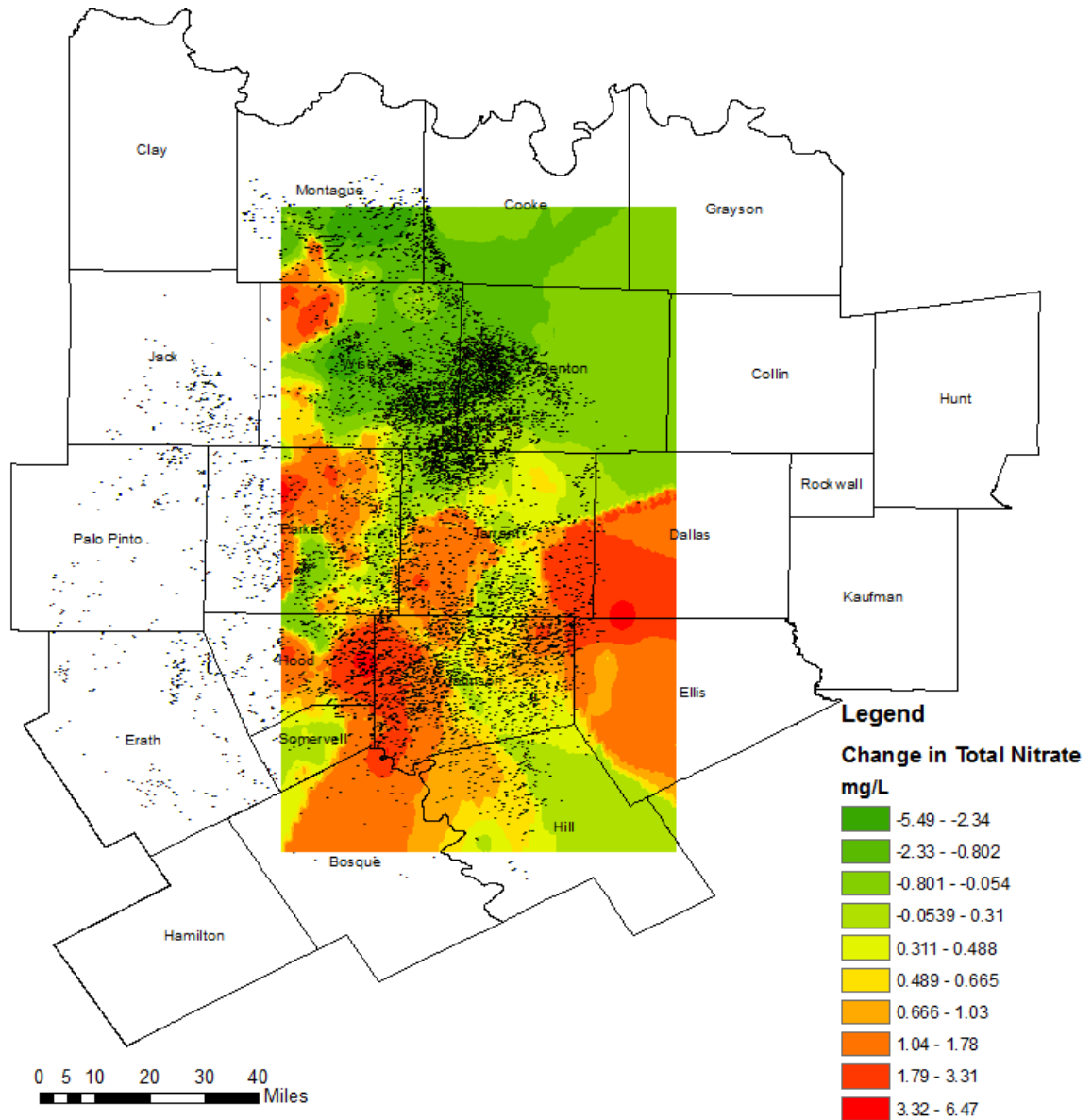


Fig. C- 12: Contour Plot of change in groundwater Total Nitrate concentrations and gas well locations in the study region

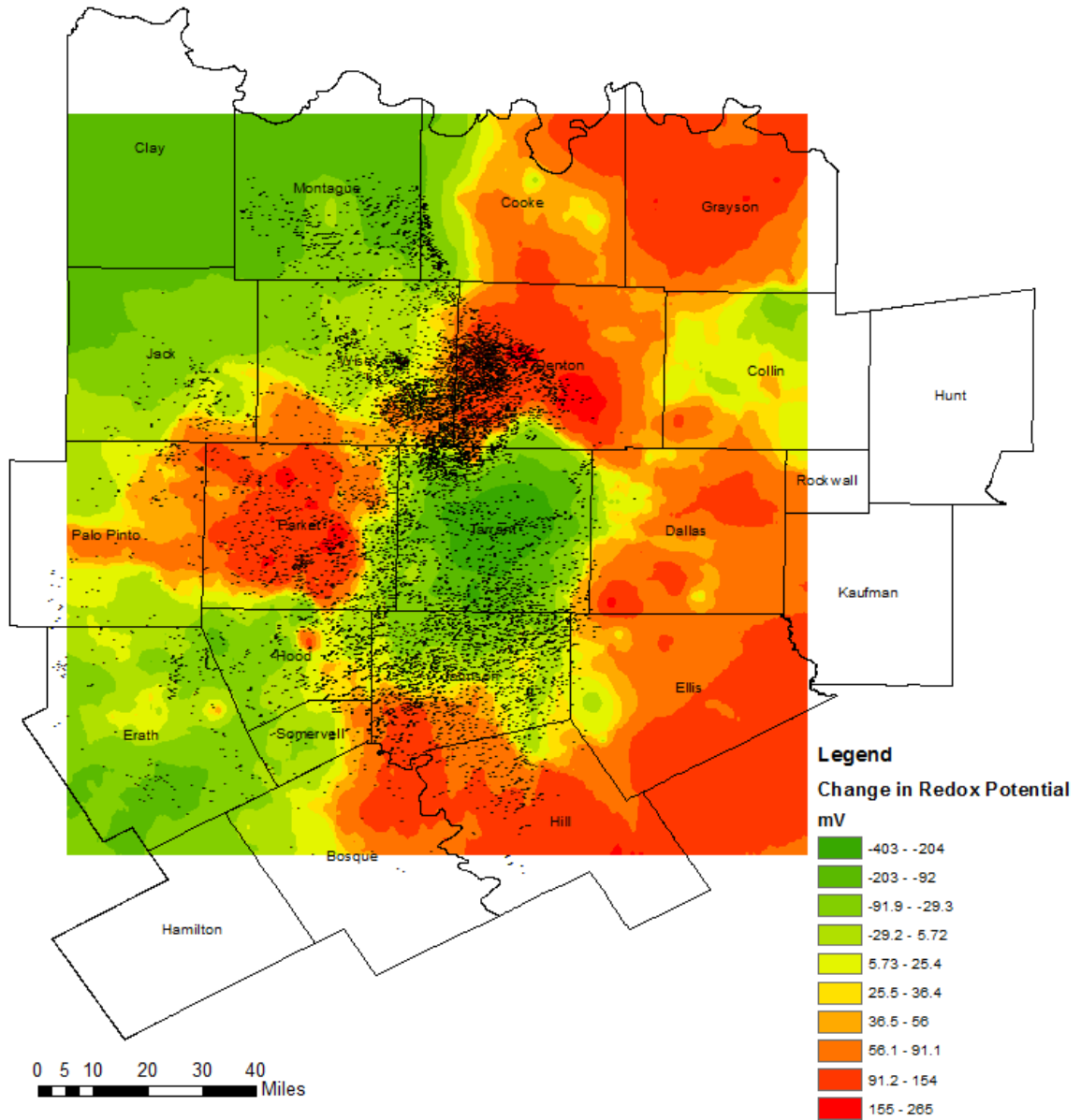


Fig. C- 13: Contour Plot of change in groundwater Oxidation-Reduction Potential and gas well locations in the study region

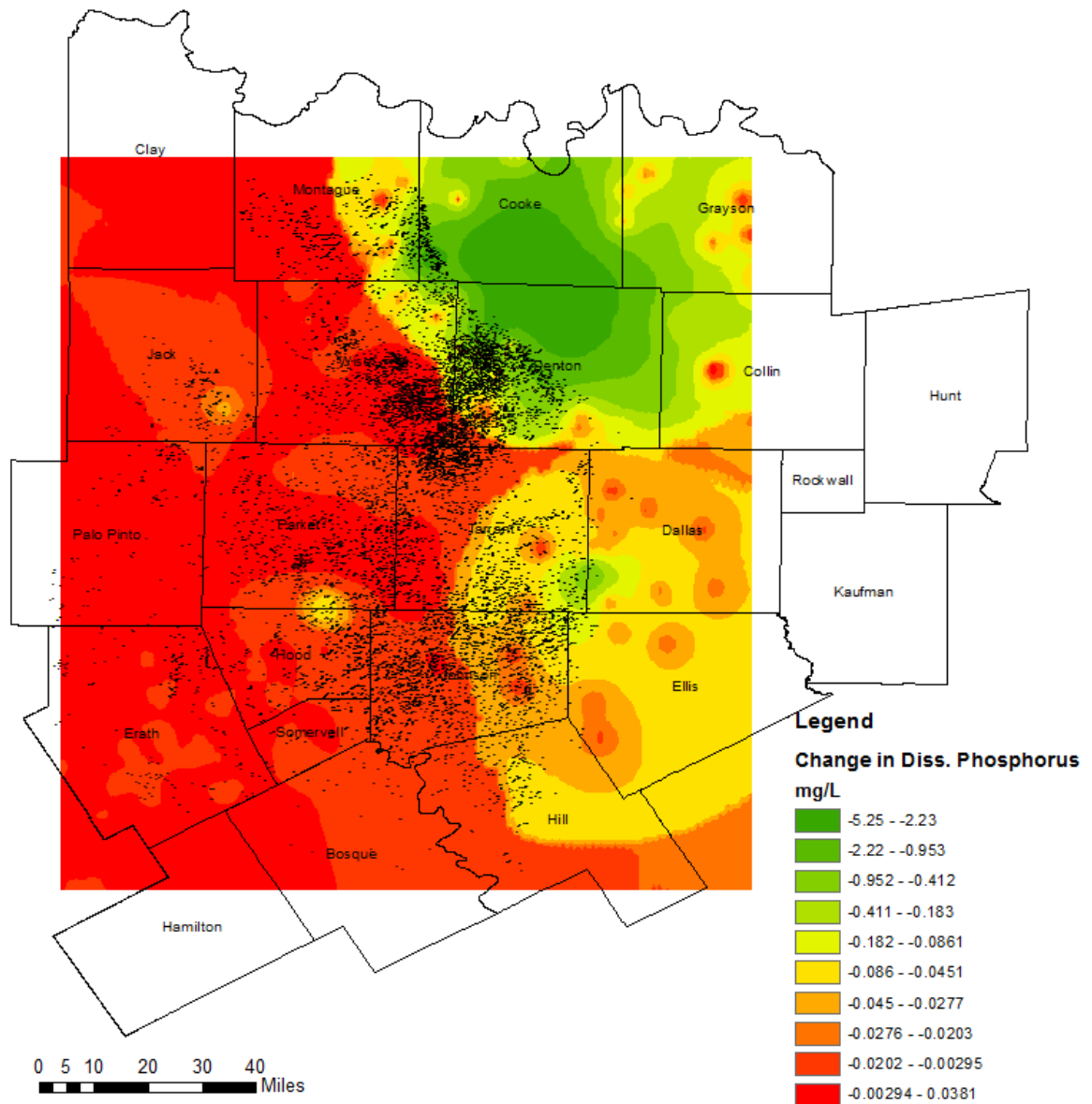


Fig. C- 14: Contour Plot of change in groundwater Dissolved Phosphorus concentrations and gas well locations in the study region

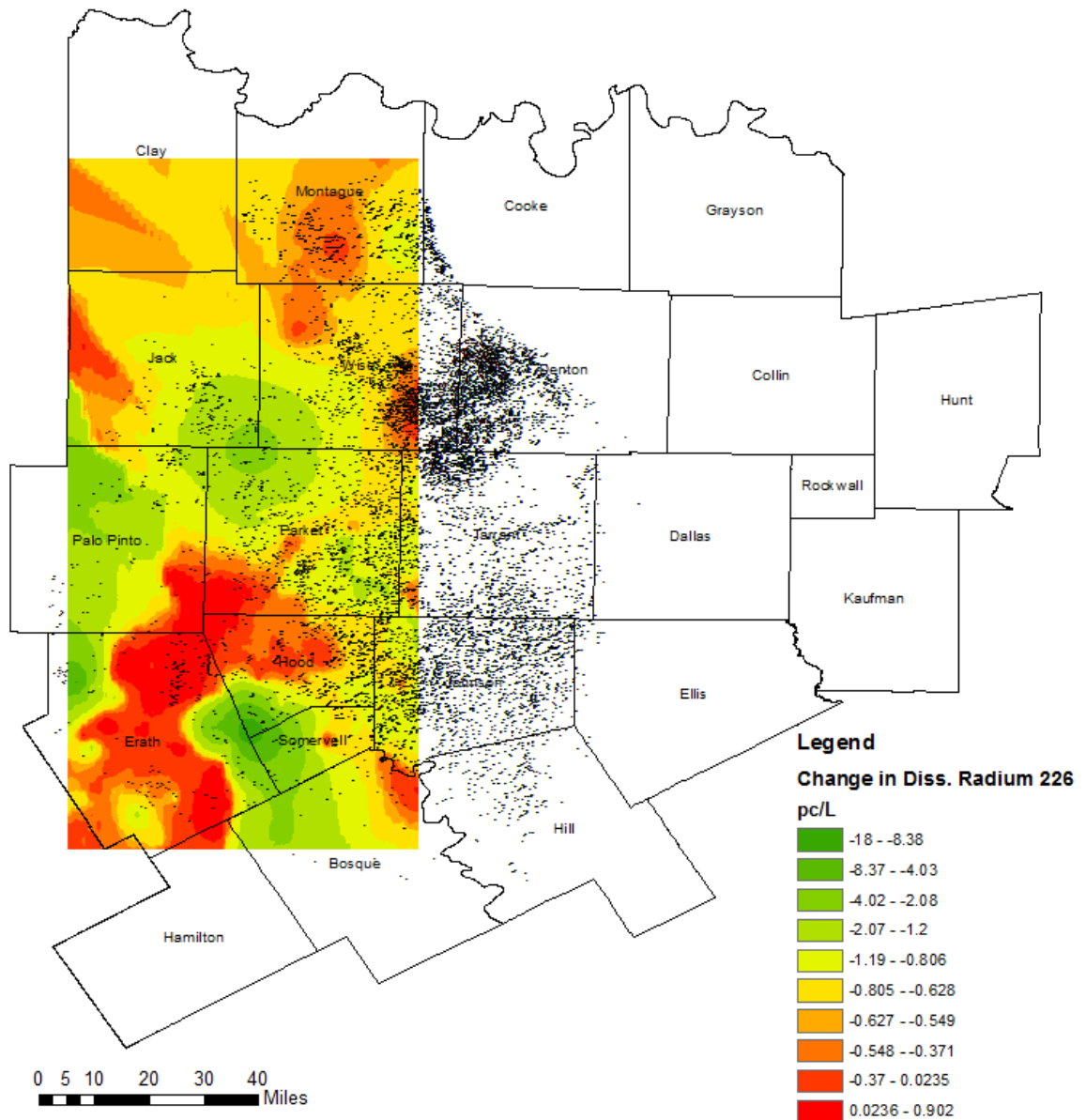


Fig. C- 15: Contour Plot of change in groundwater Dissolved Radium 226 concentrations and gas well locations in the study region

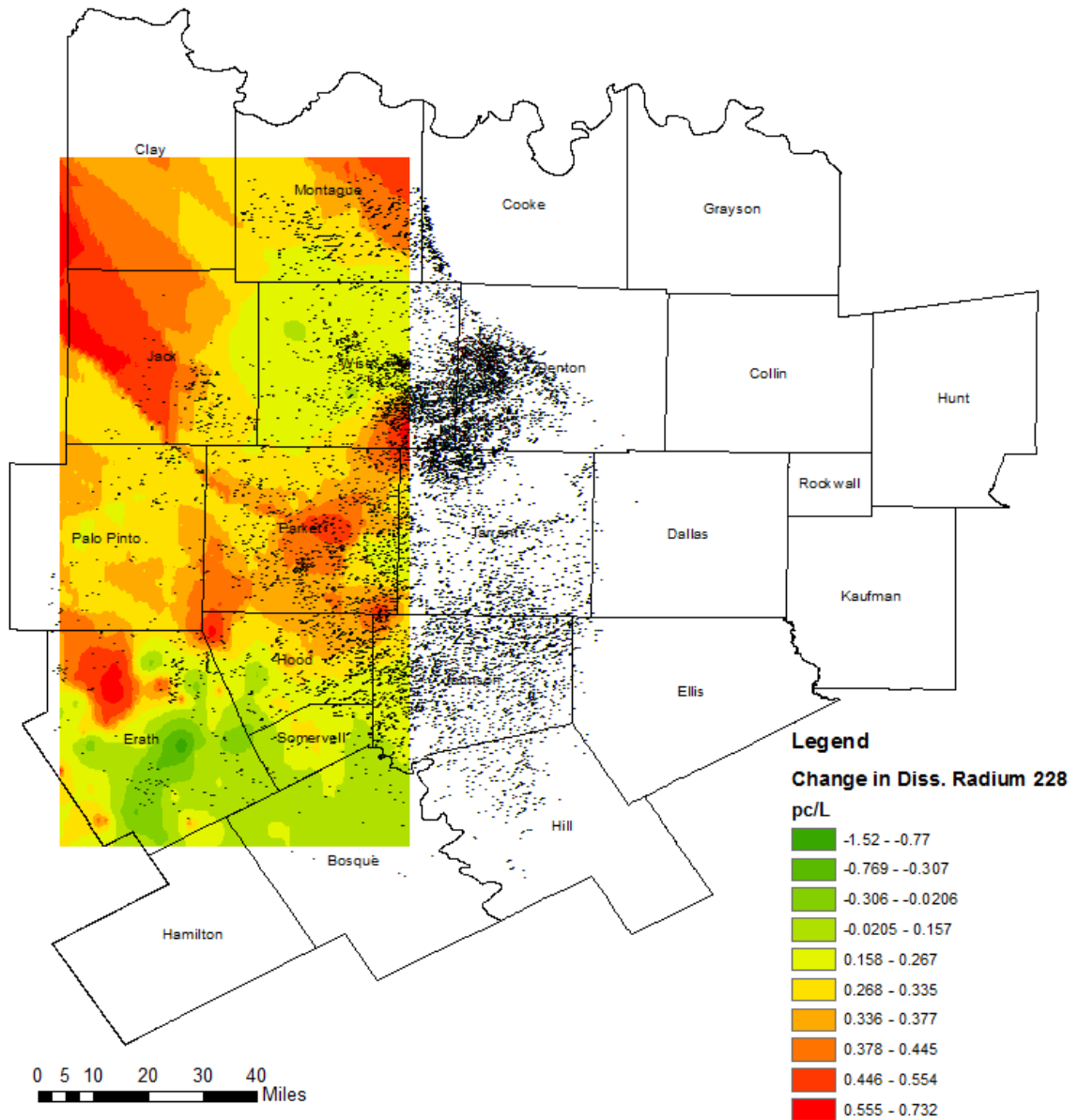


Fig. C- 16: Contour Plot of change in groundwater Dissolved Radium 228 concentrations and gas well locations in the study region

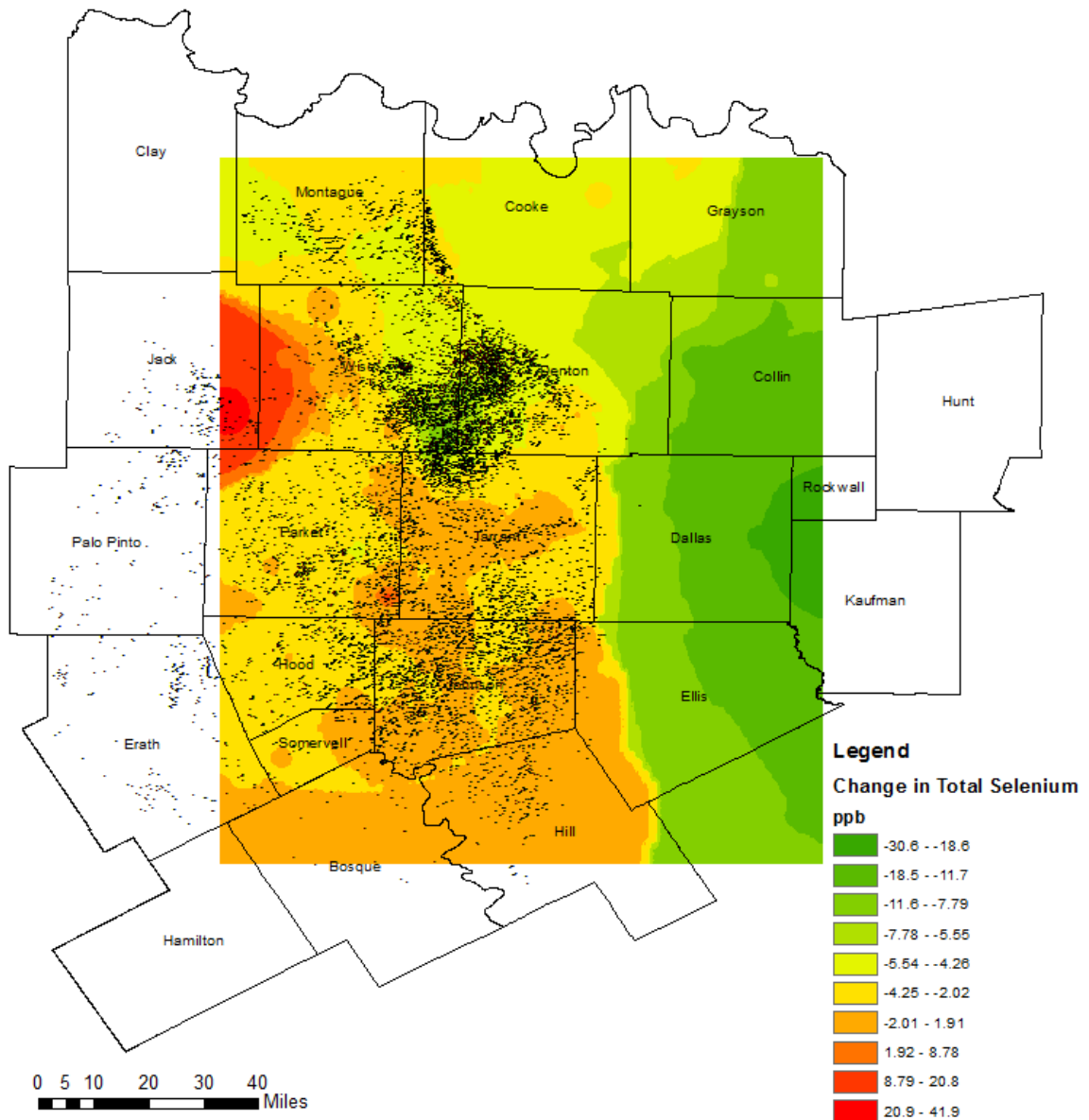


Fig. C- 17: Contour Plot of change in groundwater Total Selenium concentrations and gas well locations in the study region

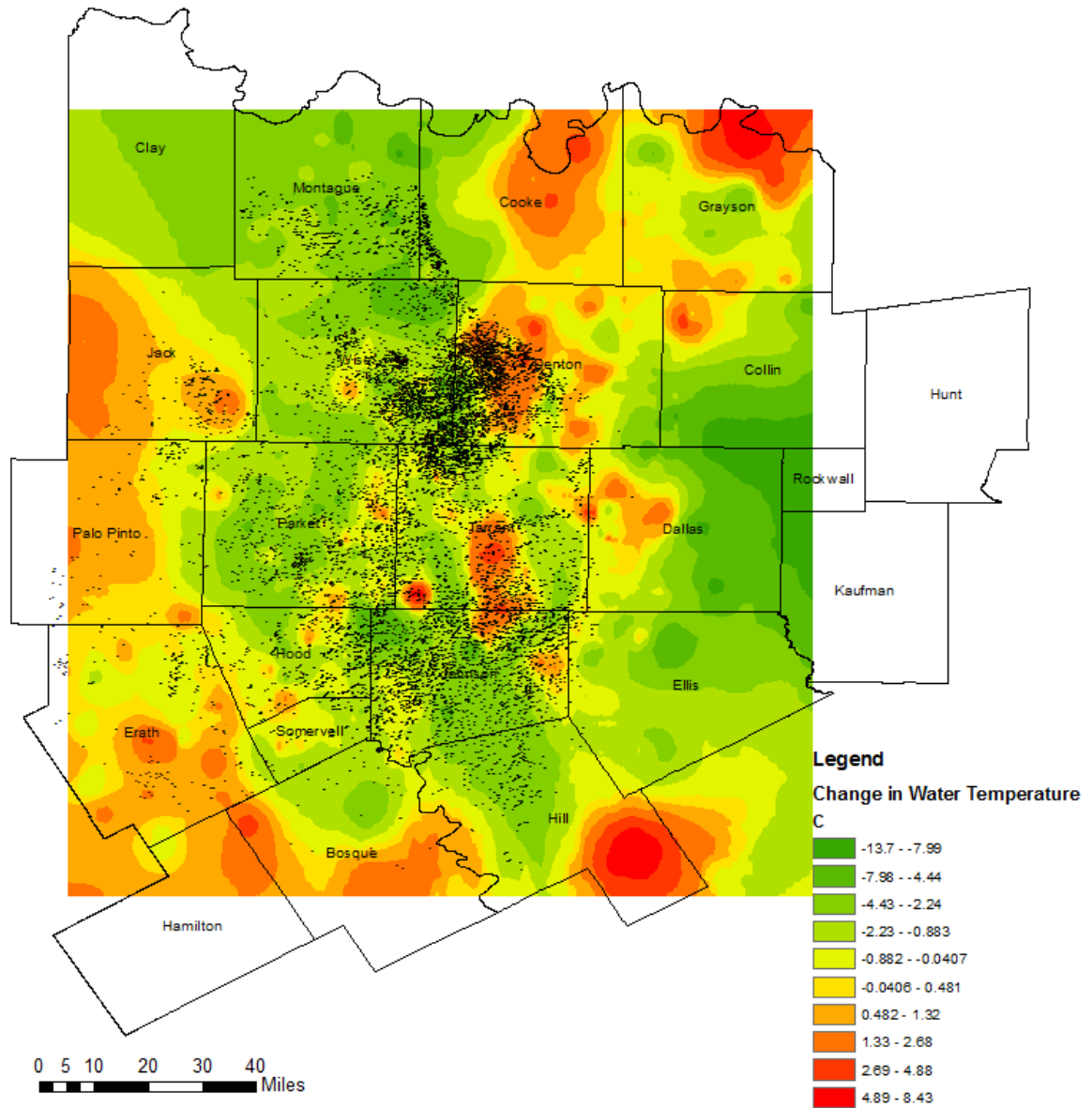


Fig. C- 18: Contour Plot of change in groundwater Temperature and gas well locations in the study region

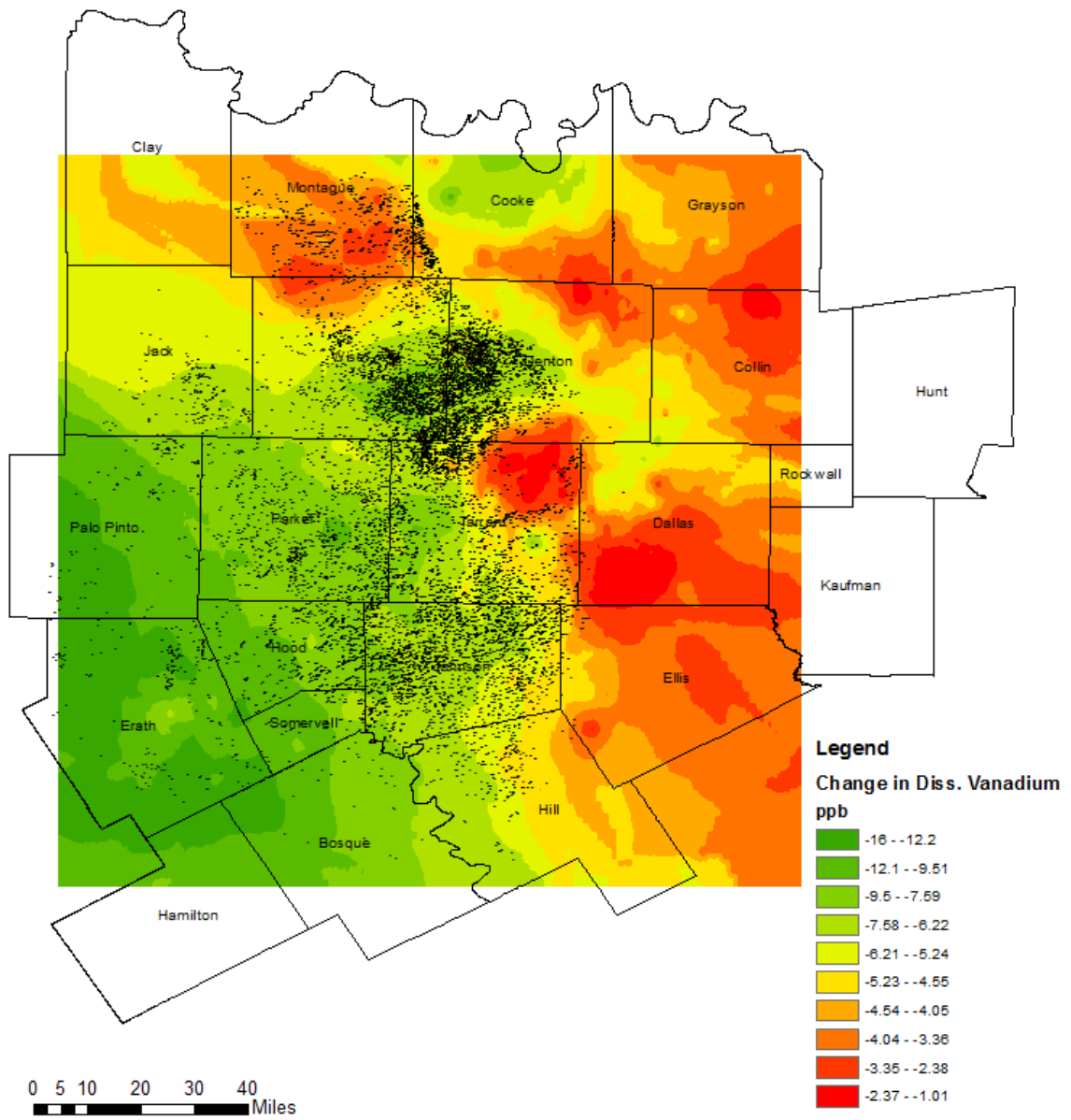


Fig. C- 19: Contour Plot of change in groundwater Dissolved Vanadium concentrations and gas well locations in the study region

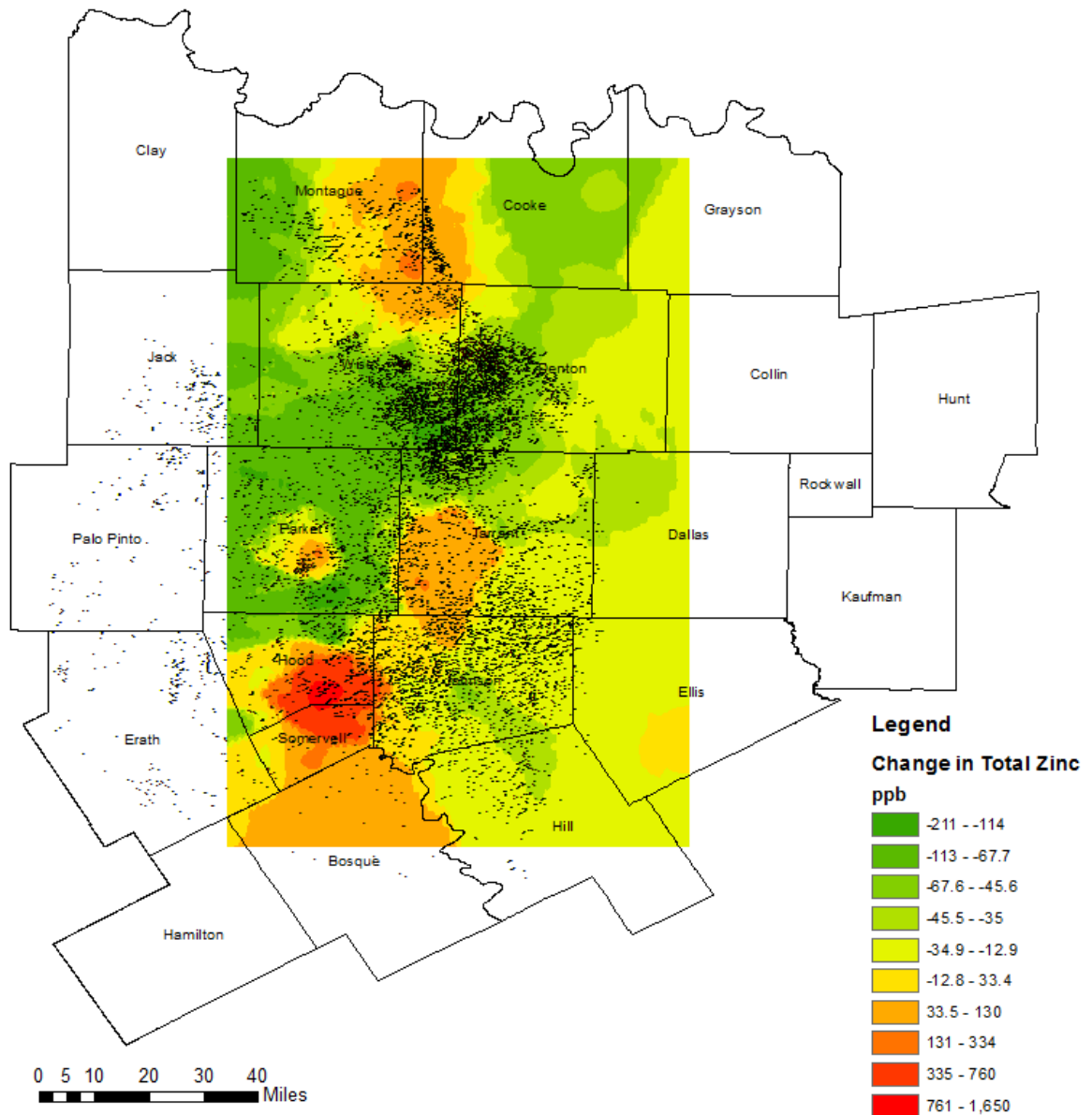


Fig. C- 20: Contour Plot of change in groundwater Total Zinc concentrations and gas well locations in the study region

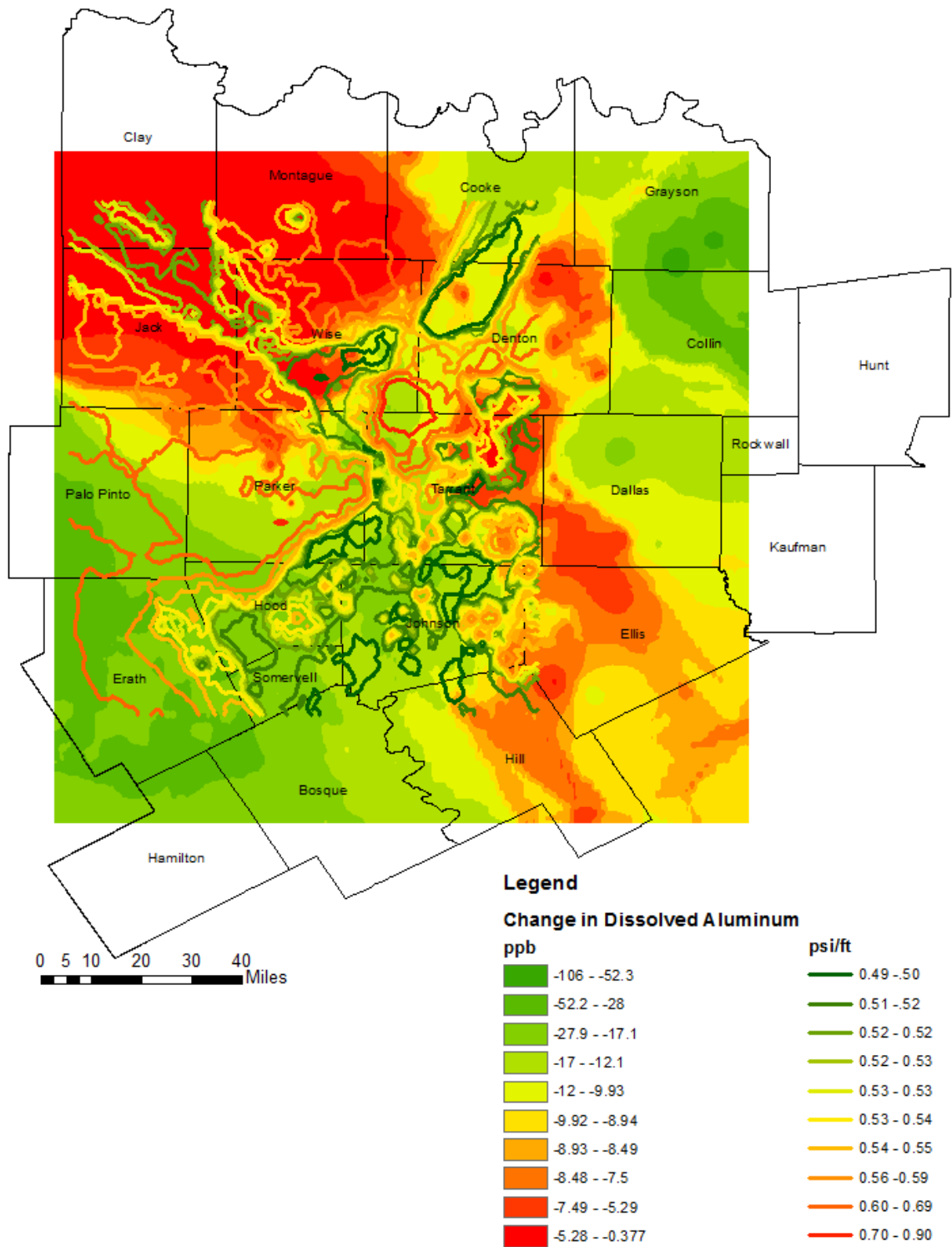


Fig. C- 21: Contour Plot of change in groundwater Total Zinc concentrations and Barnett Reservoir Pressure Gradient in the study region

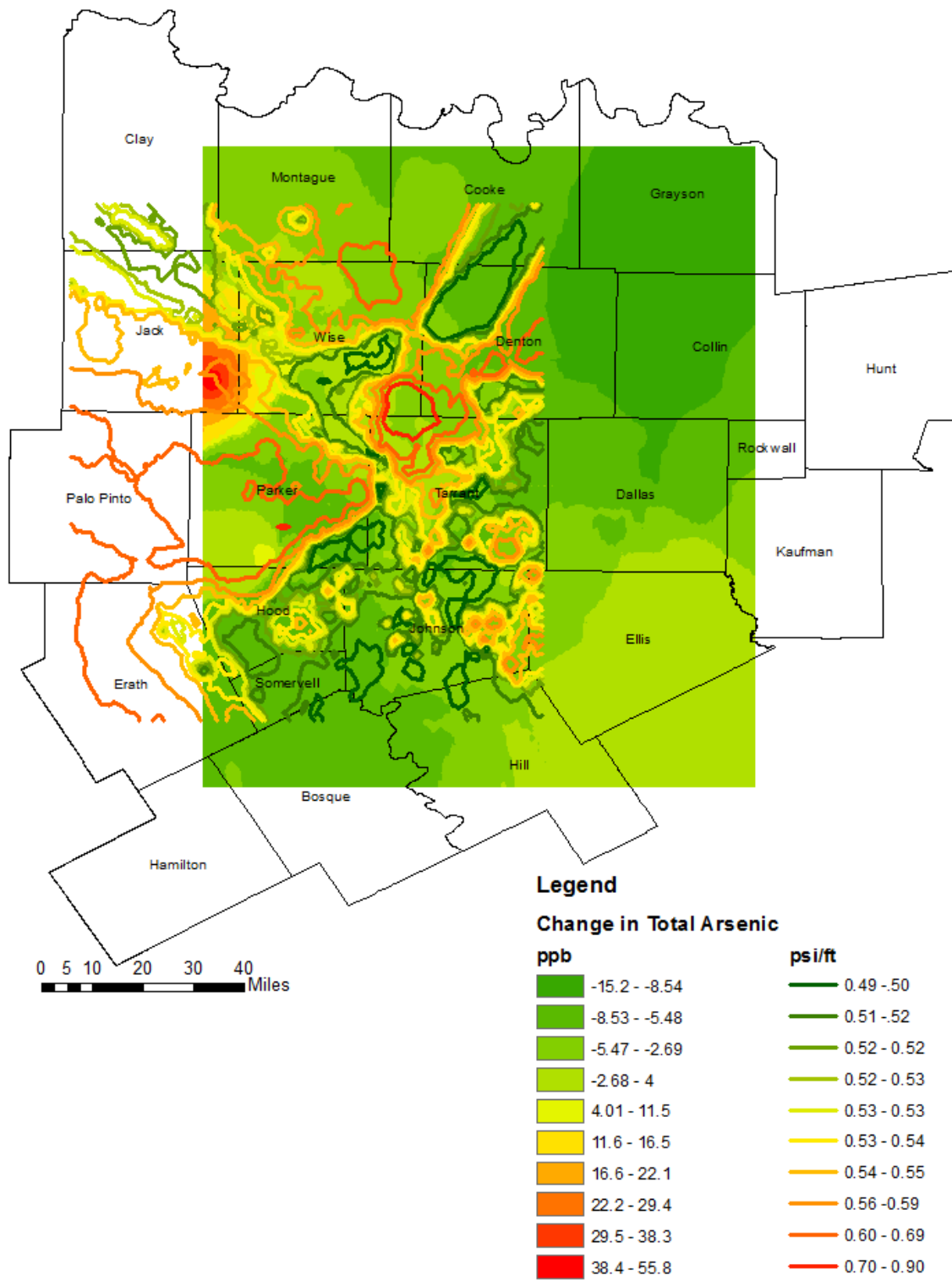


Fig. C- 22: Contour Plot of change in groundwater Total Arsenic concentrations and Barnett Reservoir Pressure Gradient in the study region

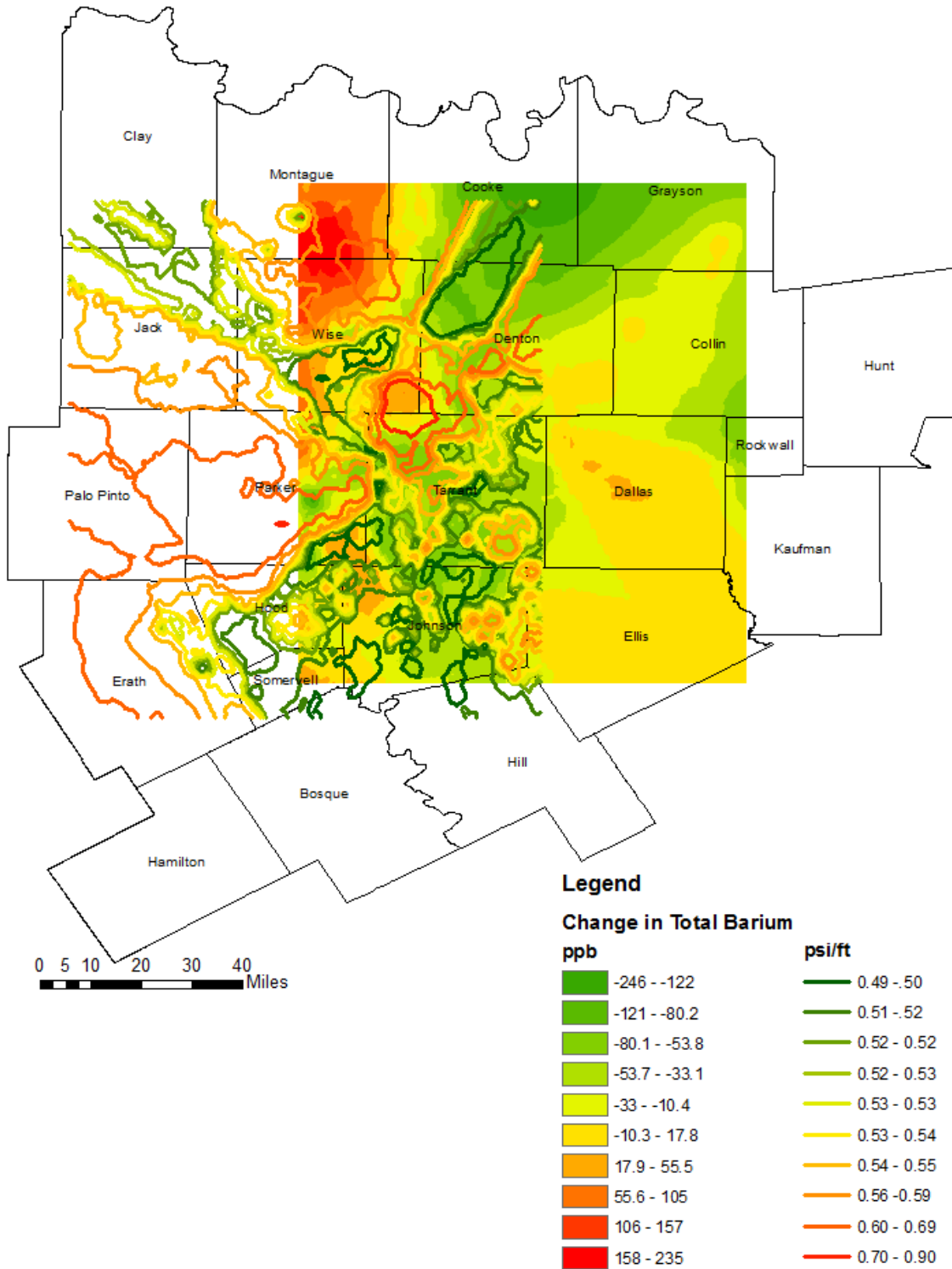


Fig. C- 23: Contour Plot of change in groundwater Total Barium concentrations and Barnett Reservoir Pressure Gradient in the study region

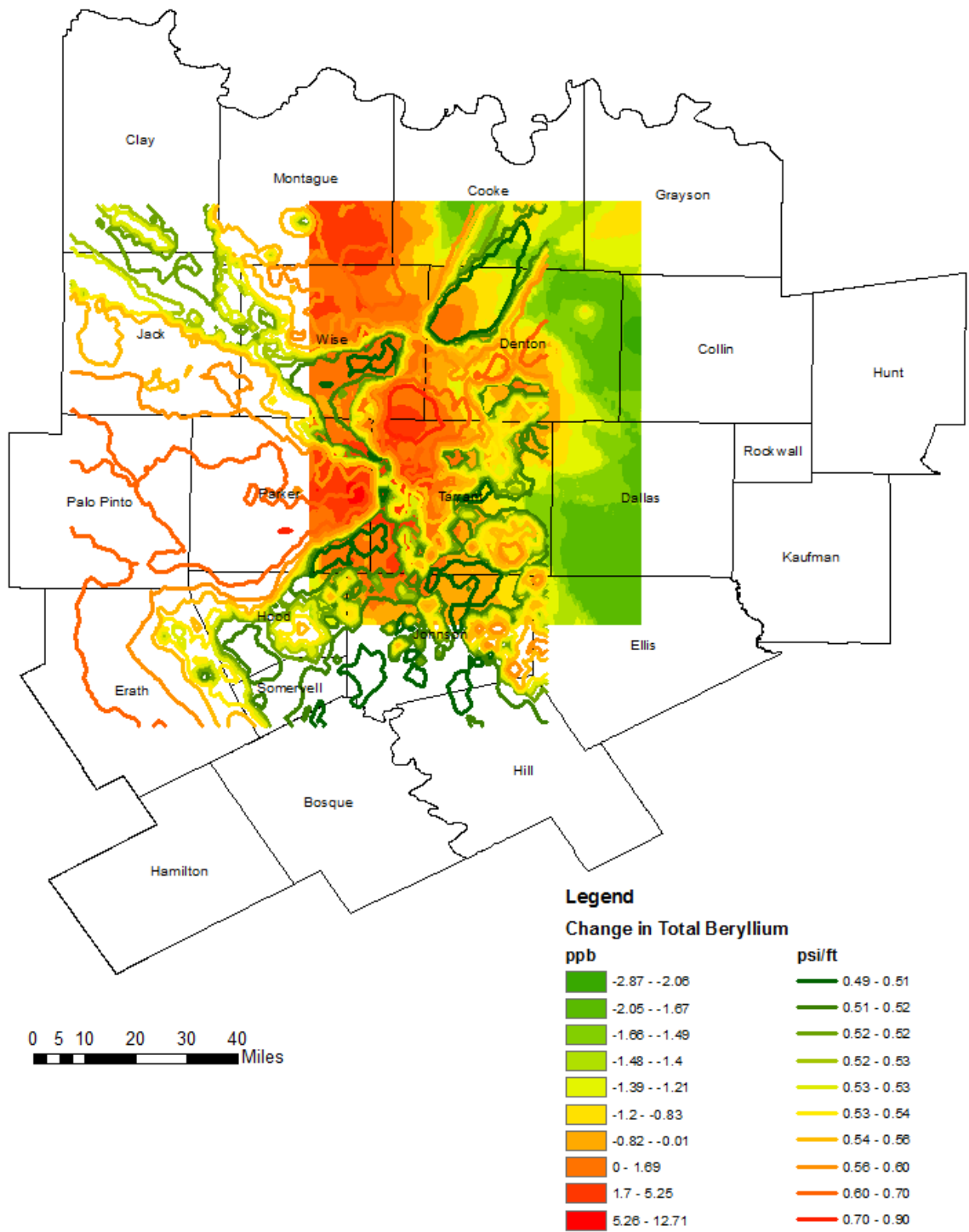


Fig. C- 24: Contour Plot of change in groundwater Total Beryllium concentrations and Barnett Reservoir Pressure Gradient in the study region

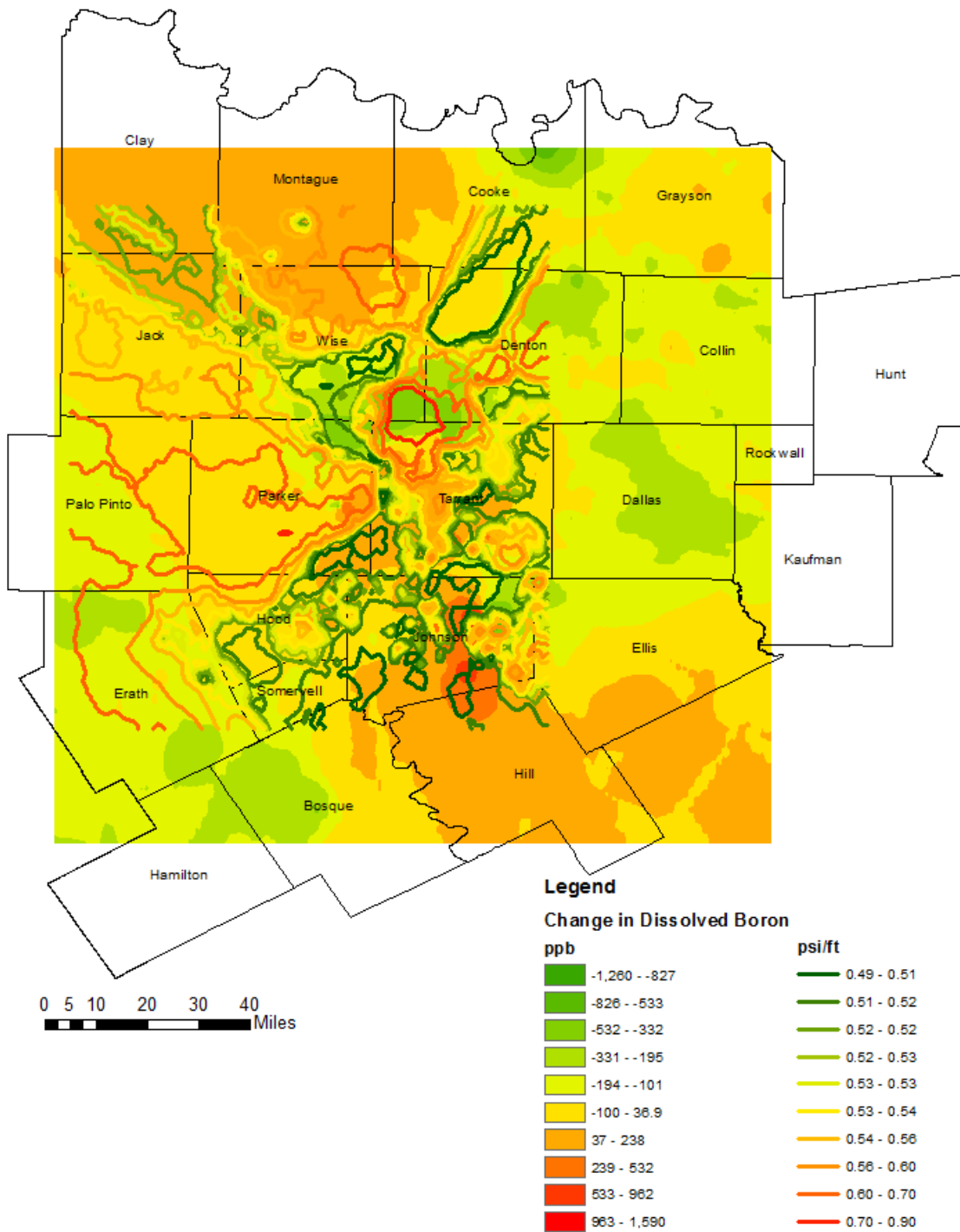


Fig. C- 25: Contour Plot of change in groundwater Total Boron concentrations and Barnett Reservoir Pressure Gradient in the study region

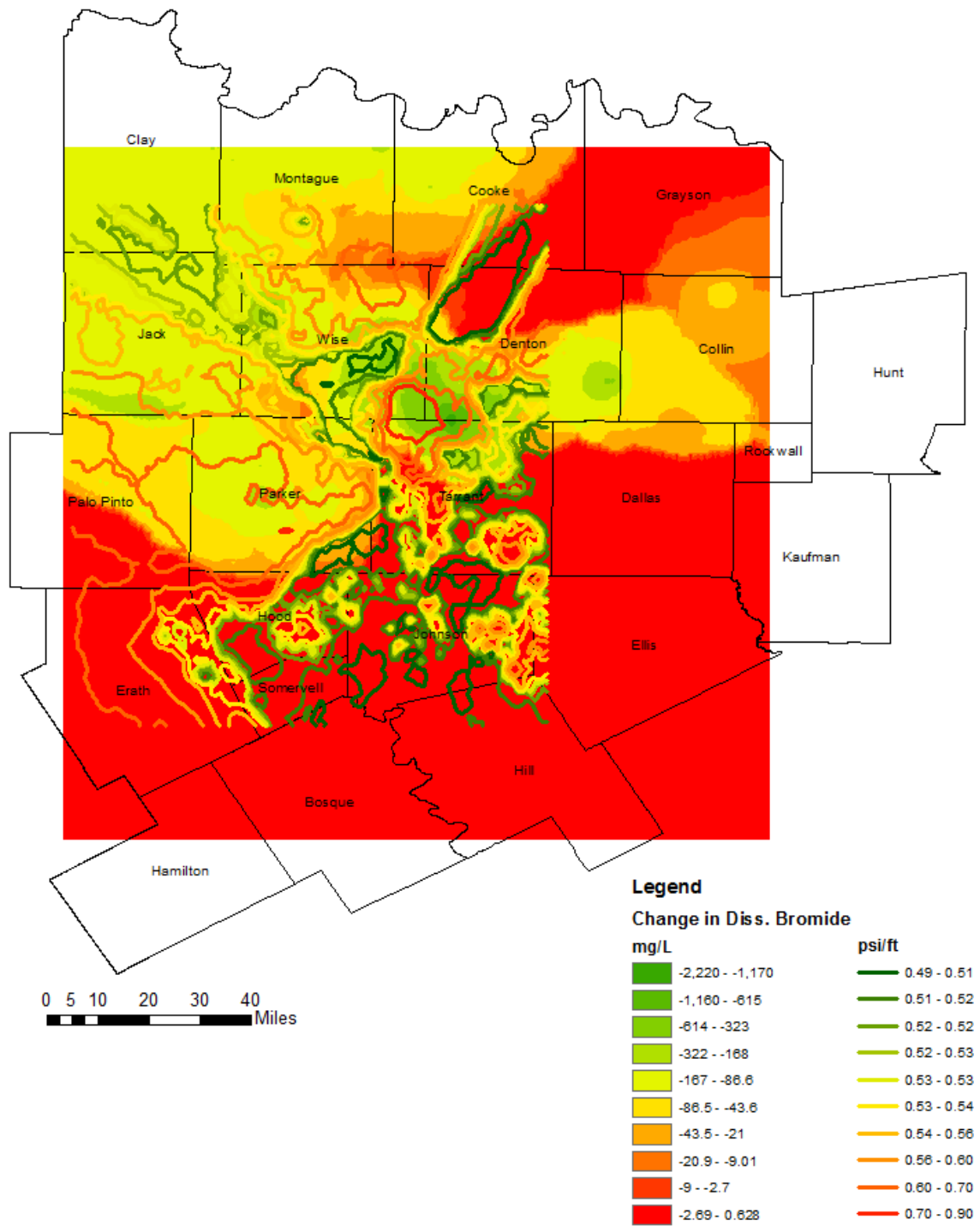


Fig. C- 26: Contour Plot of change in groundwater Dissolved Bromide concentrations and Barnett Reservoir Pressure Gradient in the study region

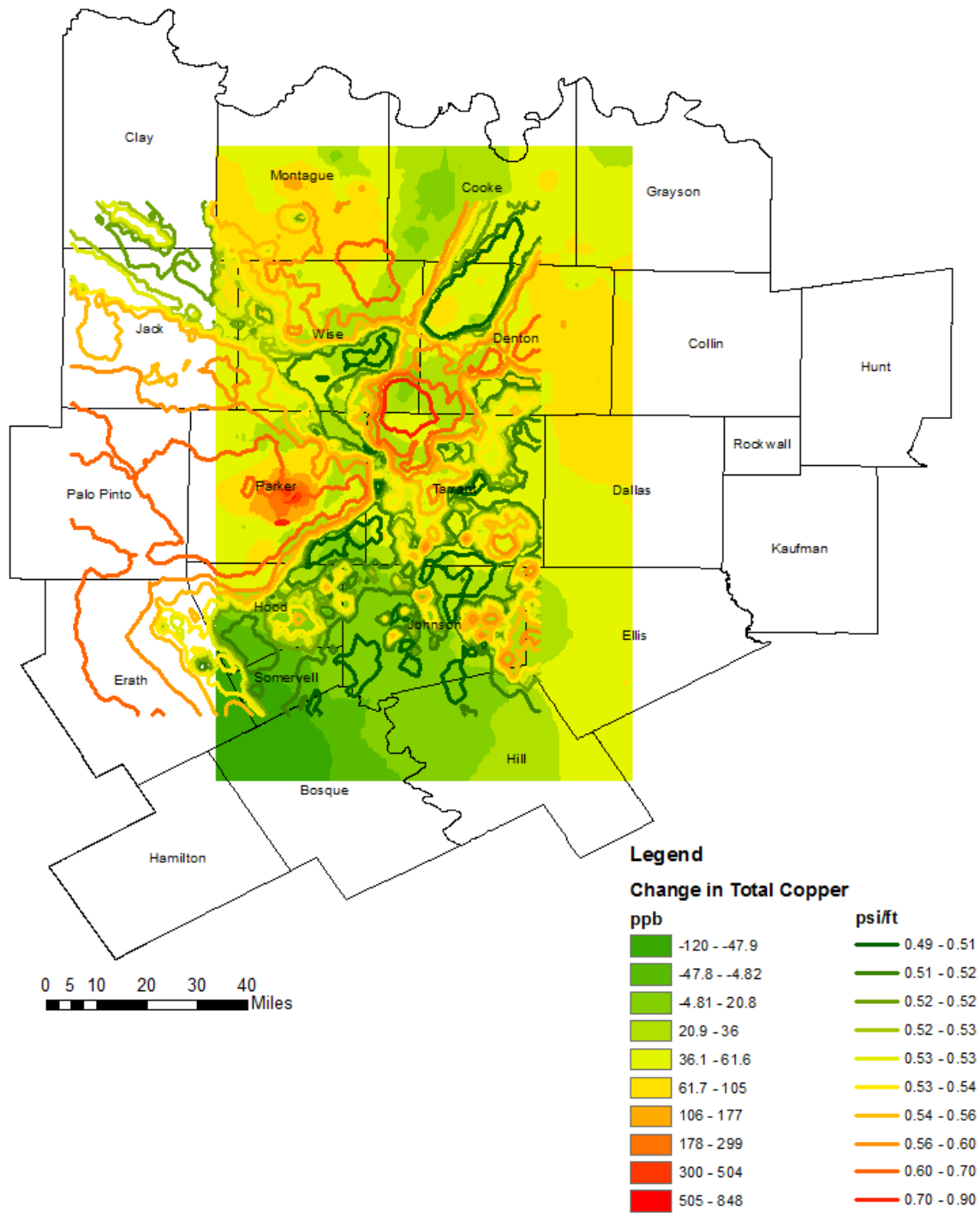


Fig. C- 27: Contour Plot of change in groundwater Total Copper concentrations and Barnett Reservoir Pressure Gradient in the study region

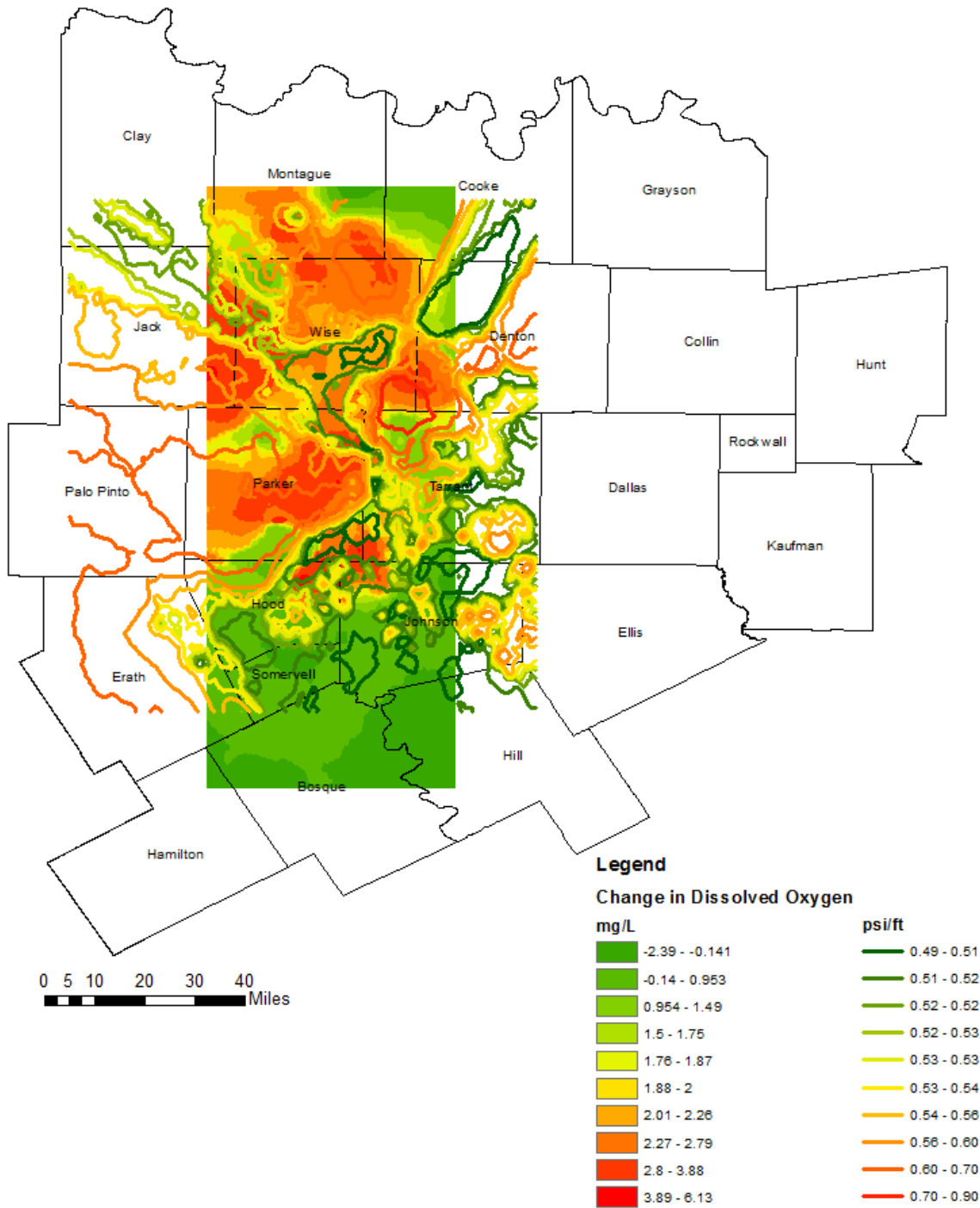


Fig. C- 28: Contour Plot of change in groundwater Dissolved Oxygen concentrations and Barnett Reservoir Pressure Gradient in the study region

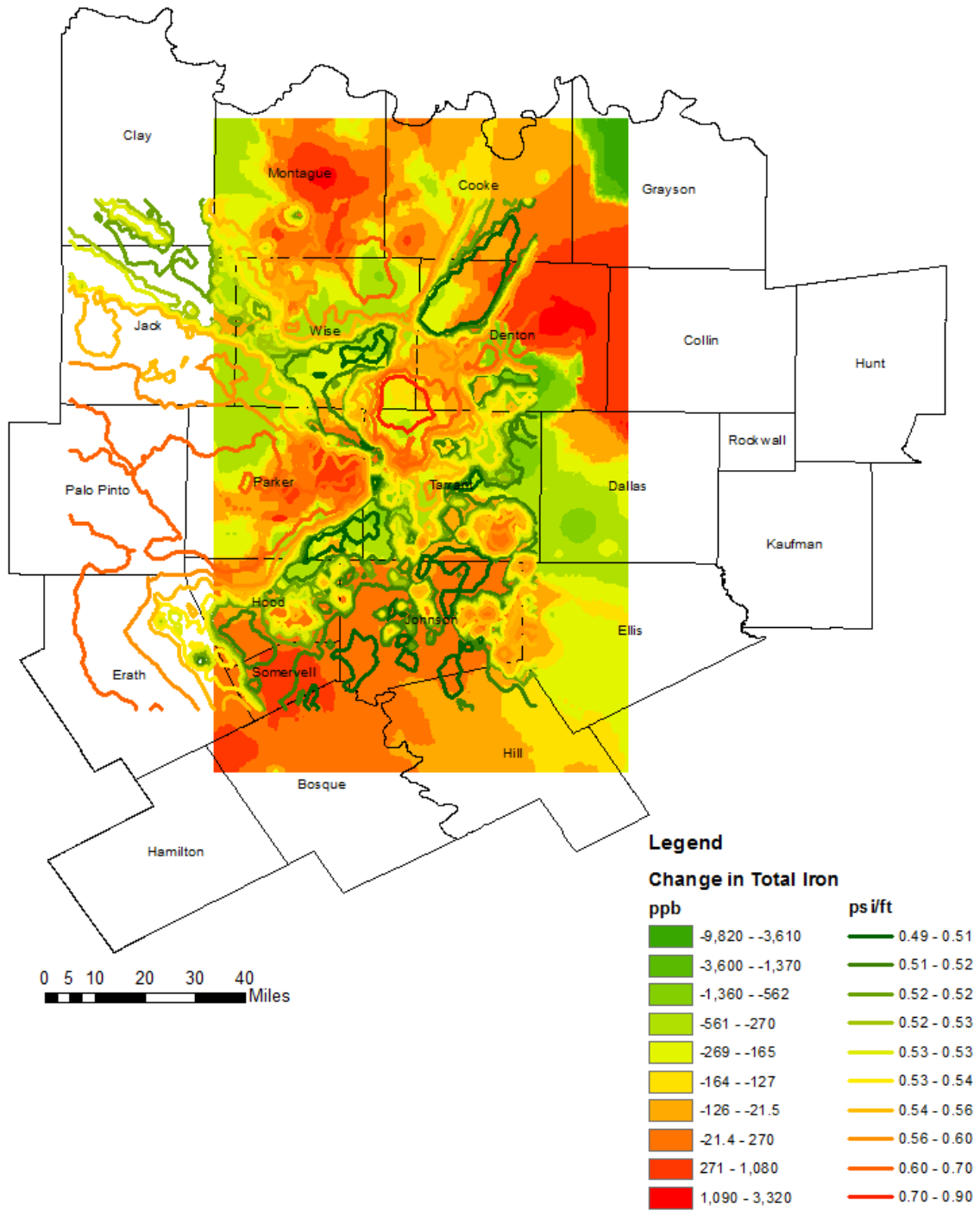


Fig. C- 29: Contour Plot of change in groundwater Total Iron concentrations and Barnett Reservoir Pressure Gradient in the study region

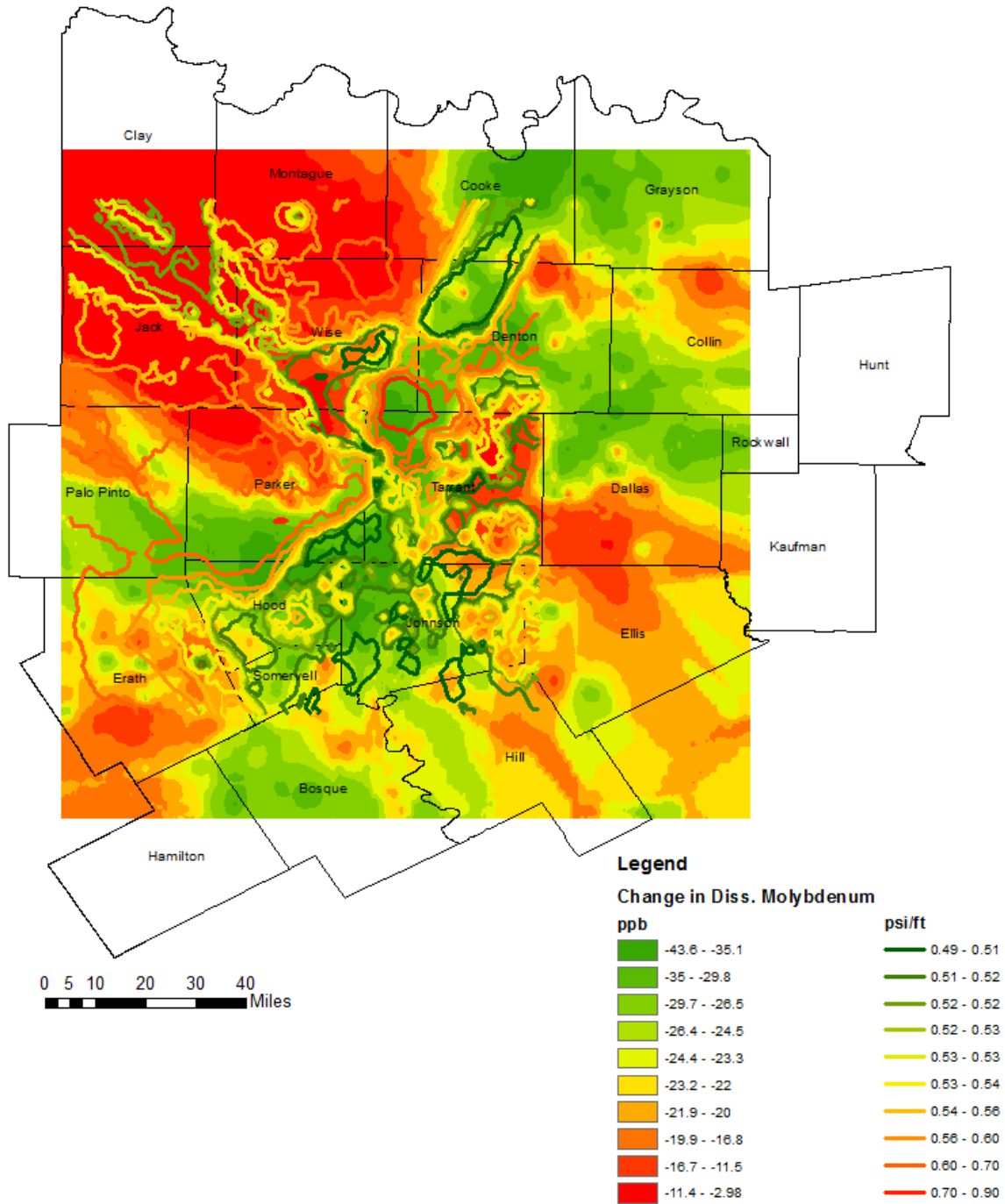


Fig. C- 30: Contour Plot of change in groundwater Dissolved Molybdenum concentrations and Barnett Reservoir Pressure Gradient in the study region

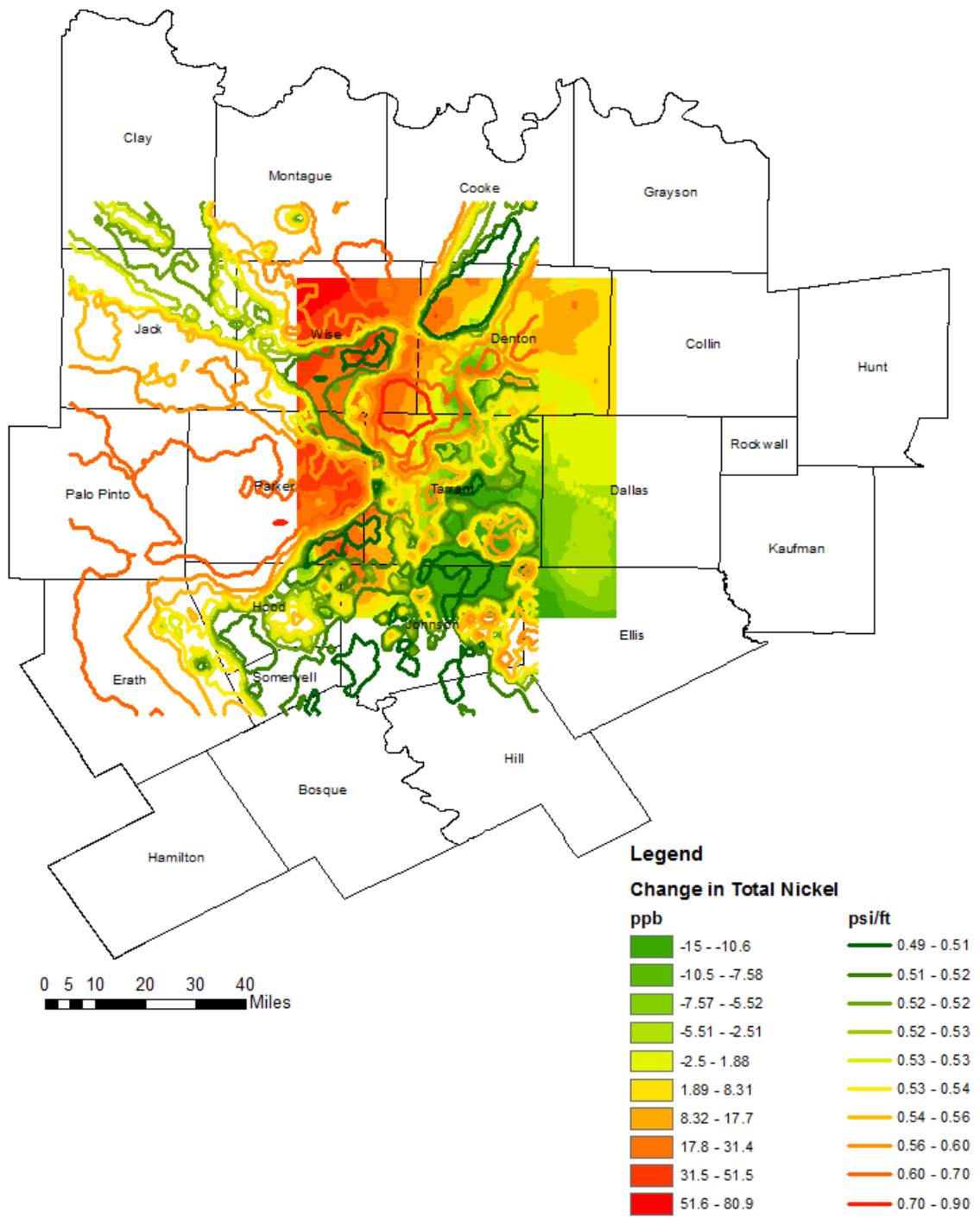


Fig. C- 31: Contour Plot of change in groundwater Total Nickel concentrations and Barnett Reservoir Pressure Gradient in the study region

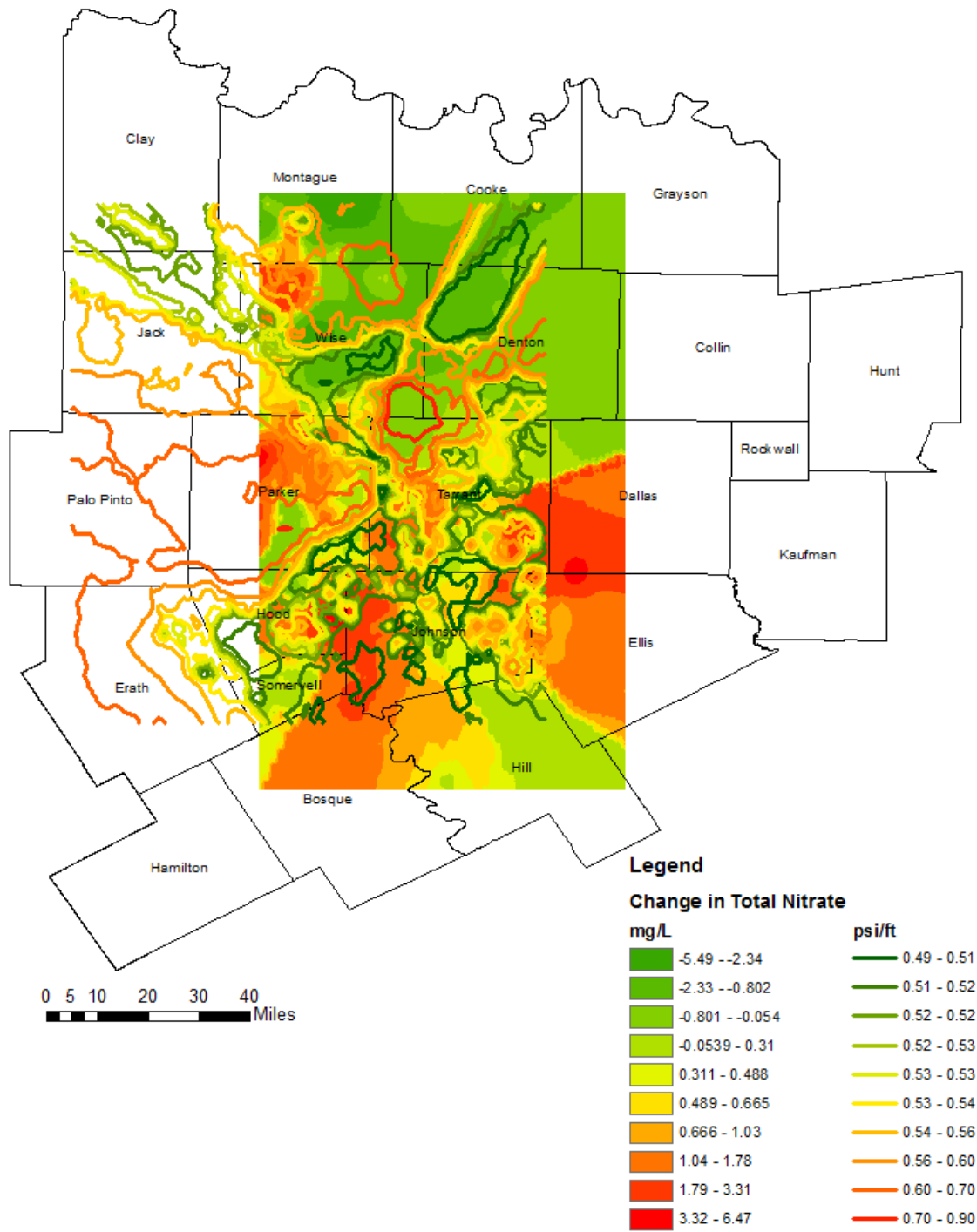


Fig. C- 32: Contour Plot of change in groundwater Total Nitrate concentrations and Barnett Reservoir Pressure Gradient in the study region

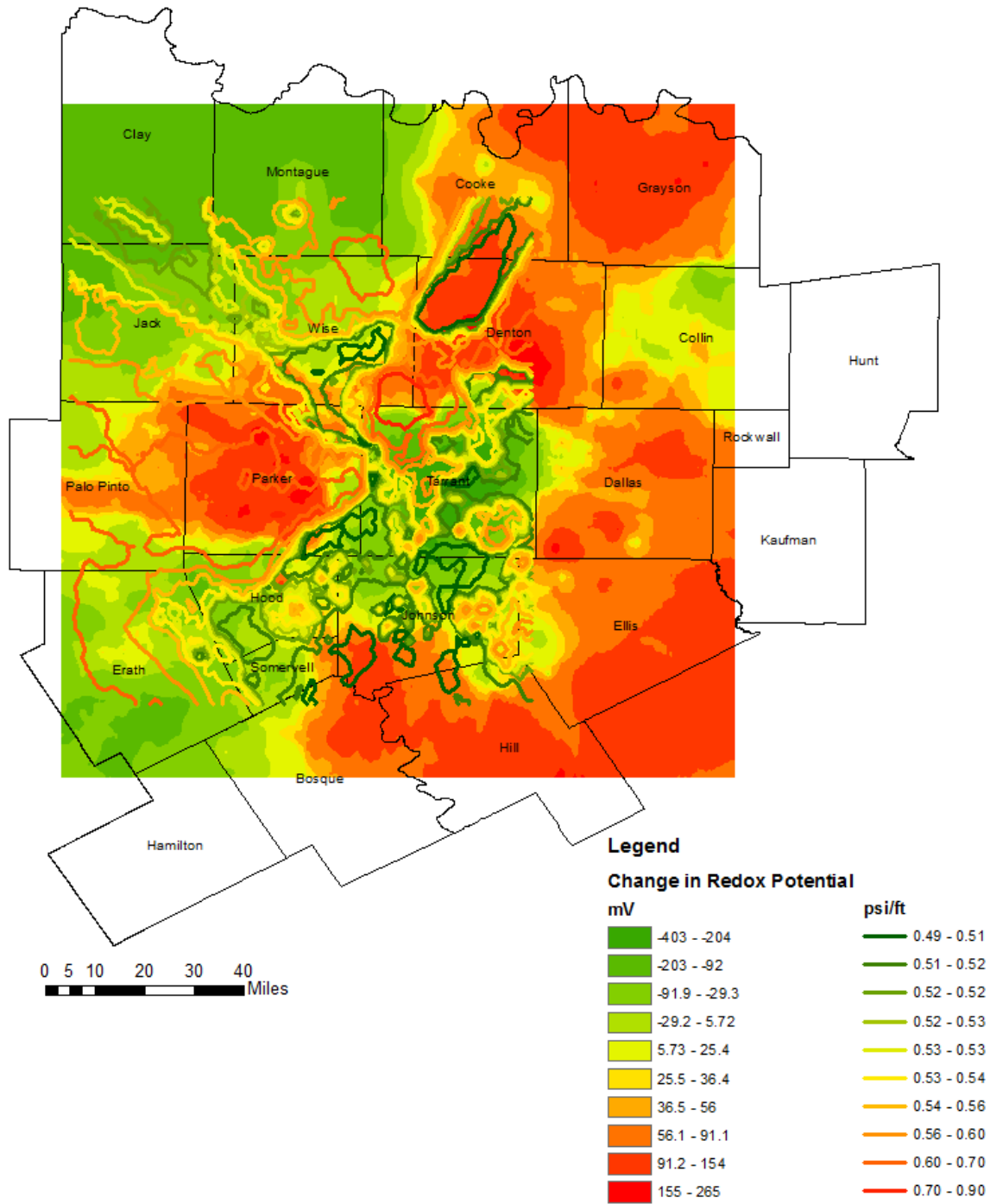


Fig. C- 33: Contour Plot of change in groundwater Oxidation-Reduction Potential concentrations and Barnett Reservoir Pressure Gradient in the study region

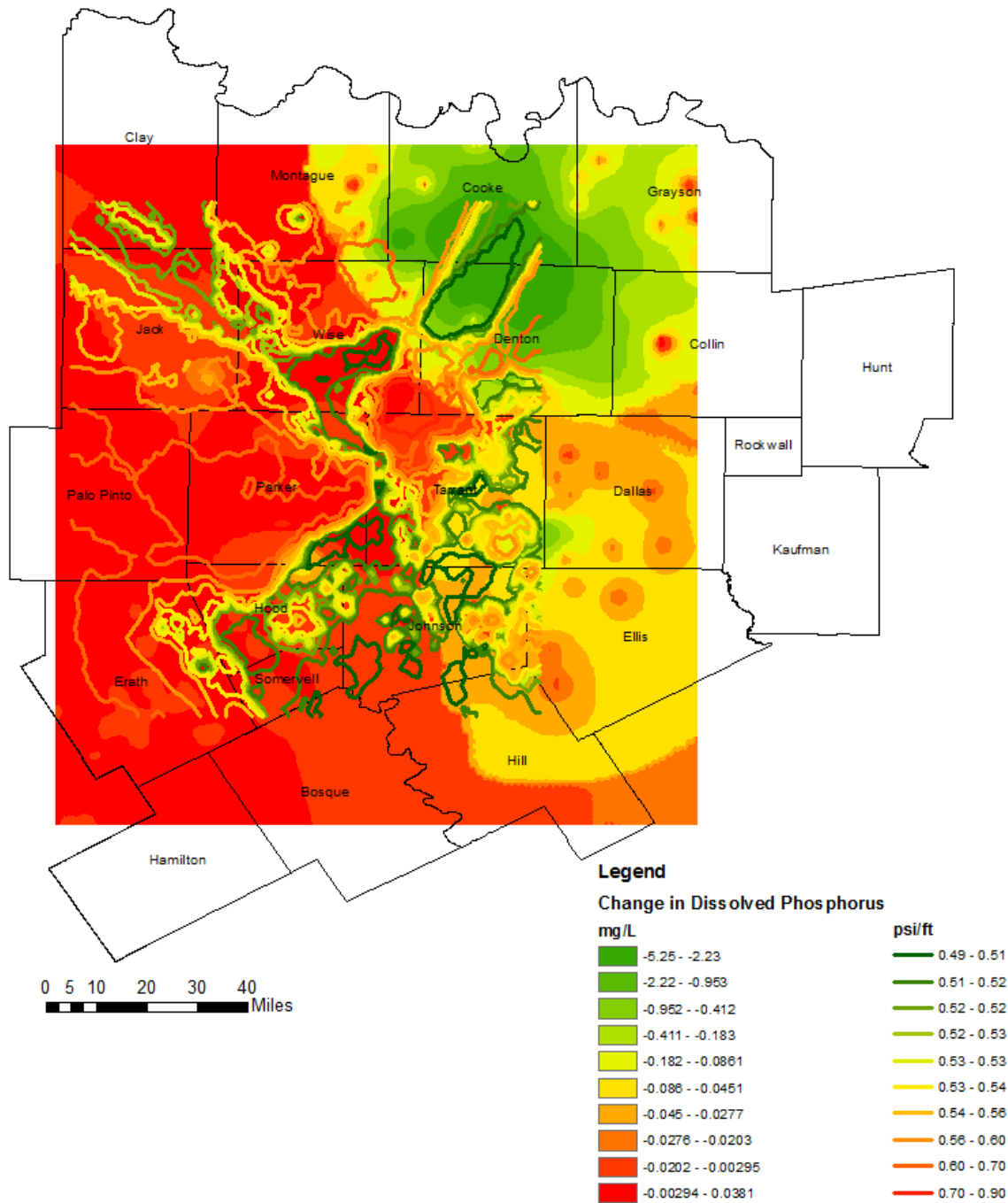


Fig. C- 34: Contour Plot of change in groundwater Dissolved Phosphorus concentrations and Barnett Reservoir Pressure Gradient in the study region

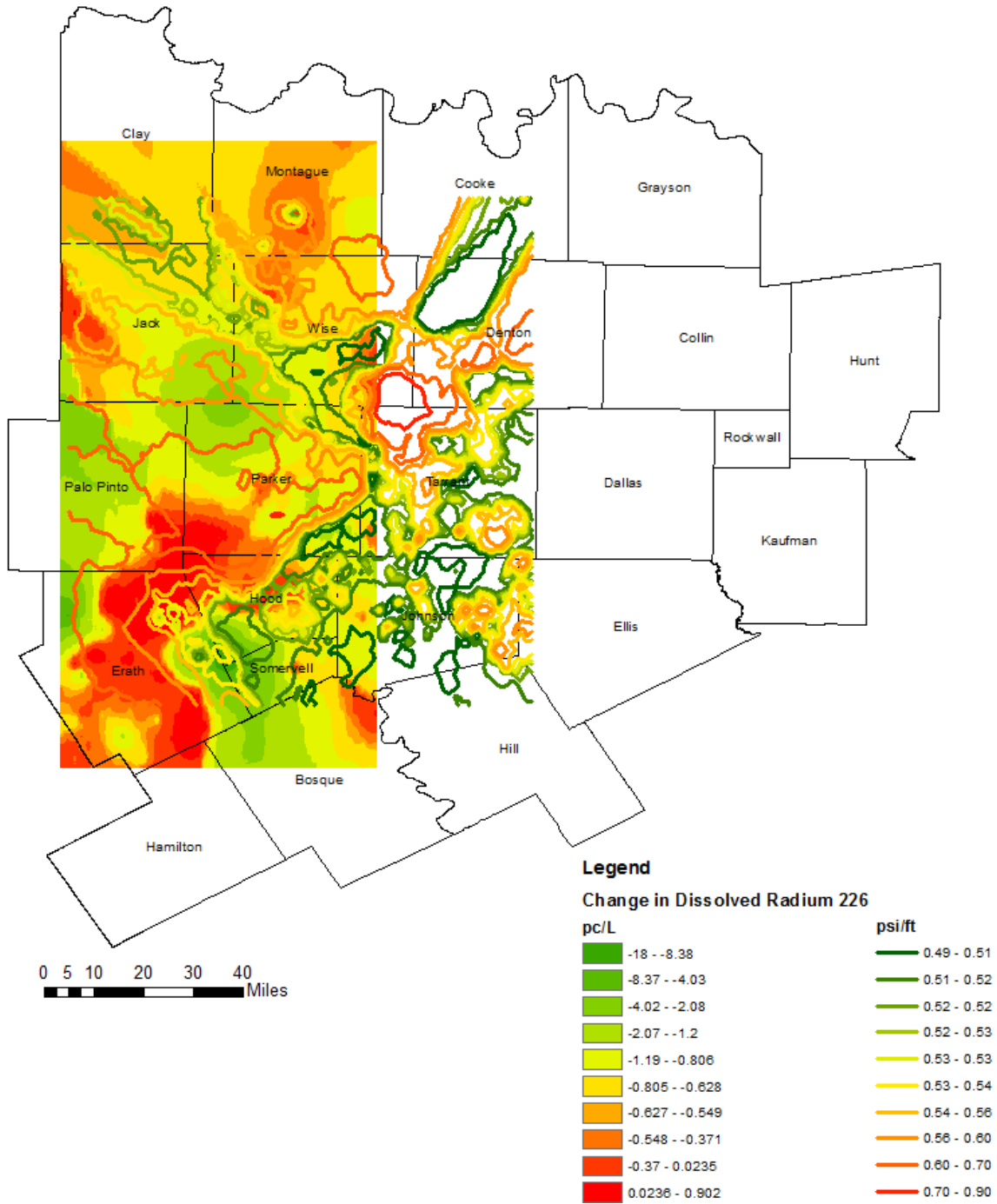


Fig. C- 35: Contour Plot of change in groundwater Dissolved Radium 226 concentrations and Barnett Reservoir Pressure Gradient in the study region

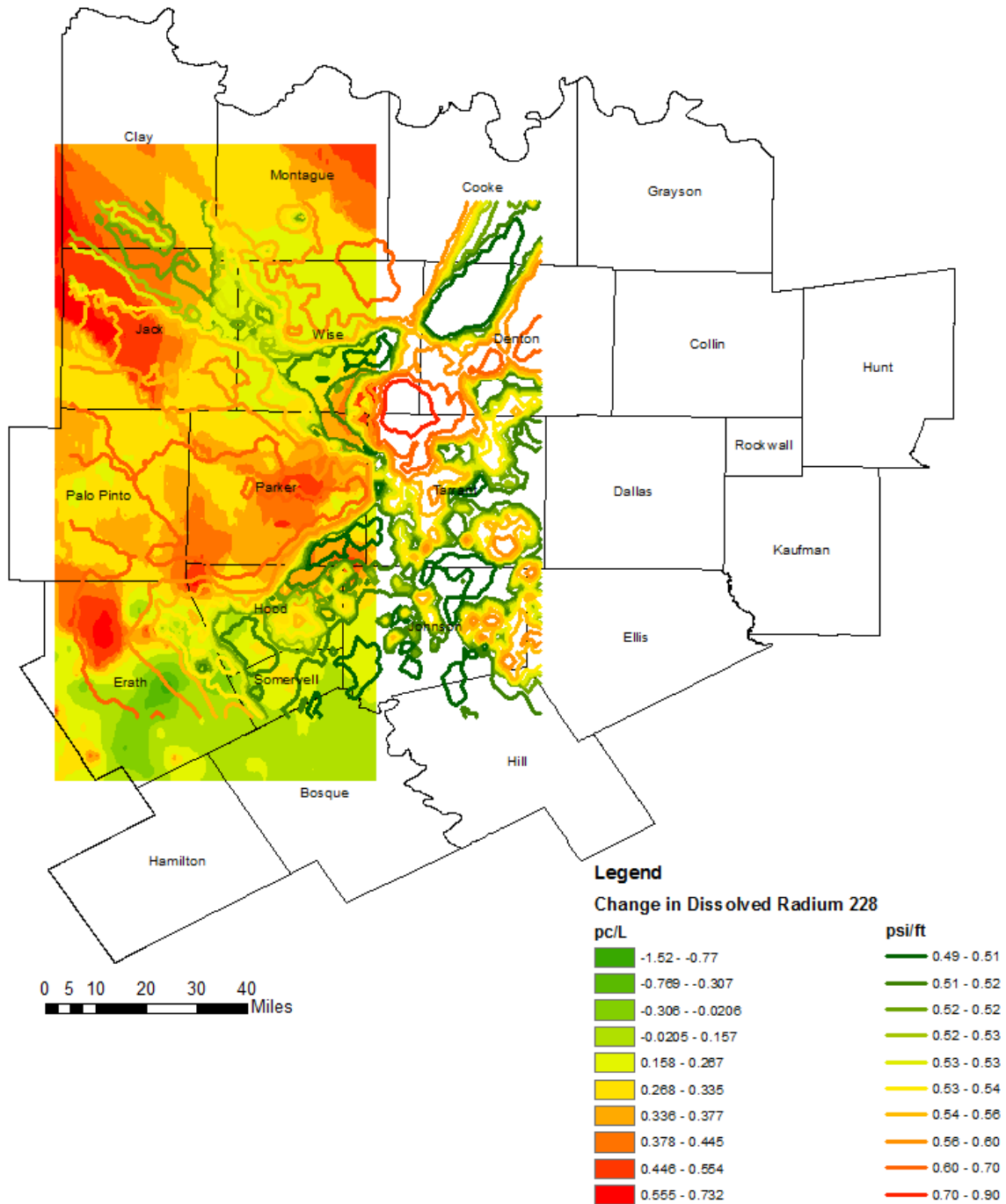


Fig. C- 36: Contour Plot of change in groundwater Dissolved Radium 228 concentrations and Barnett Reservoir Pressure Gradient in the study region

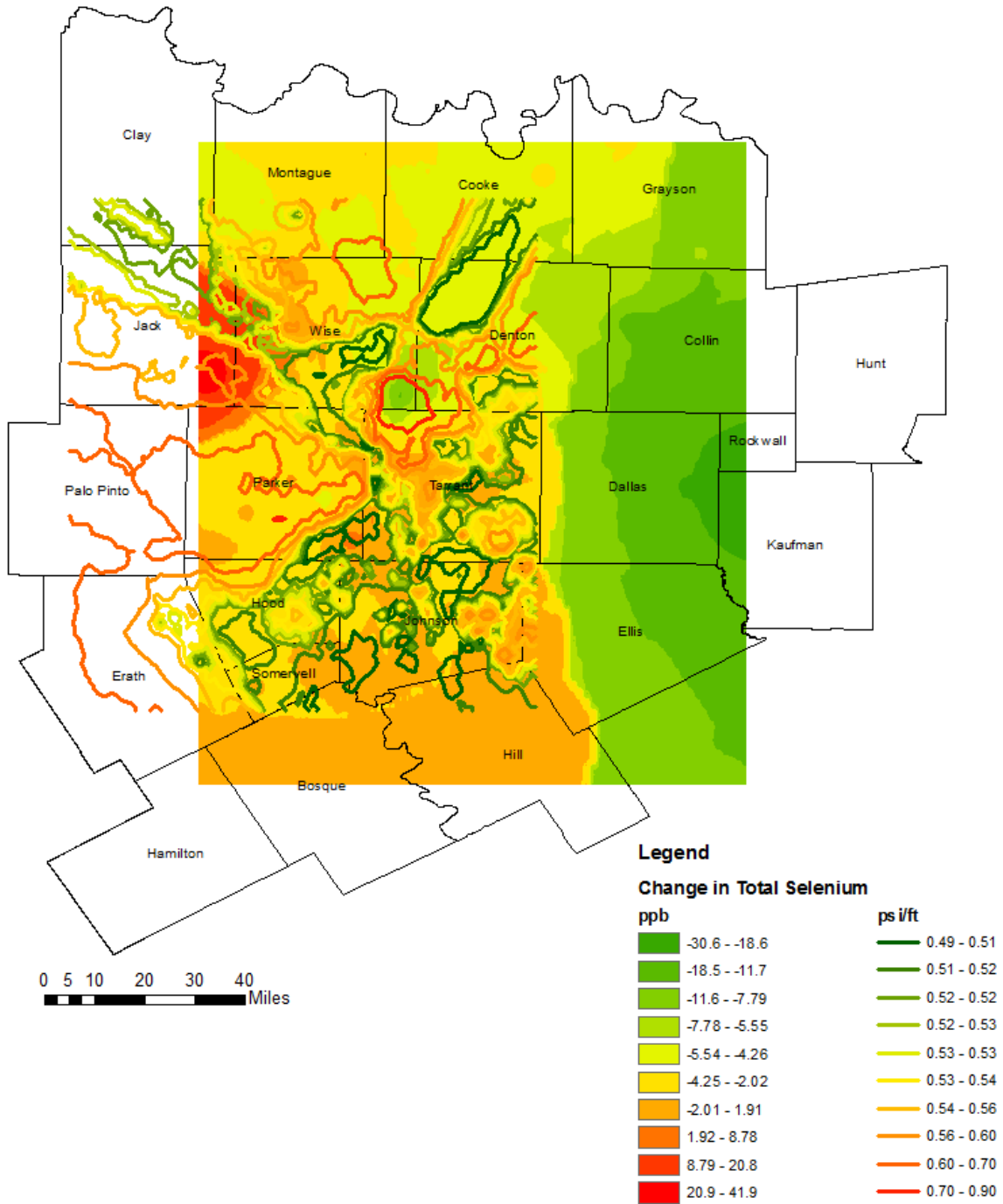


Fig. C- 37: Contour Plot of change in groundwater Total Selenium concentrations and Barnett Reservoir Pressure Gradient in the study region

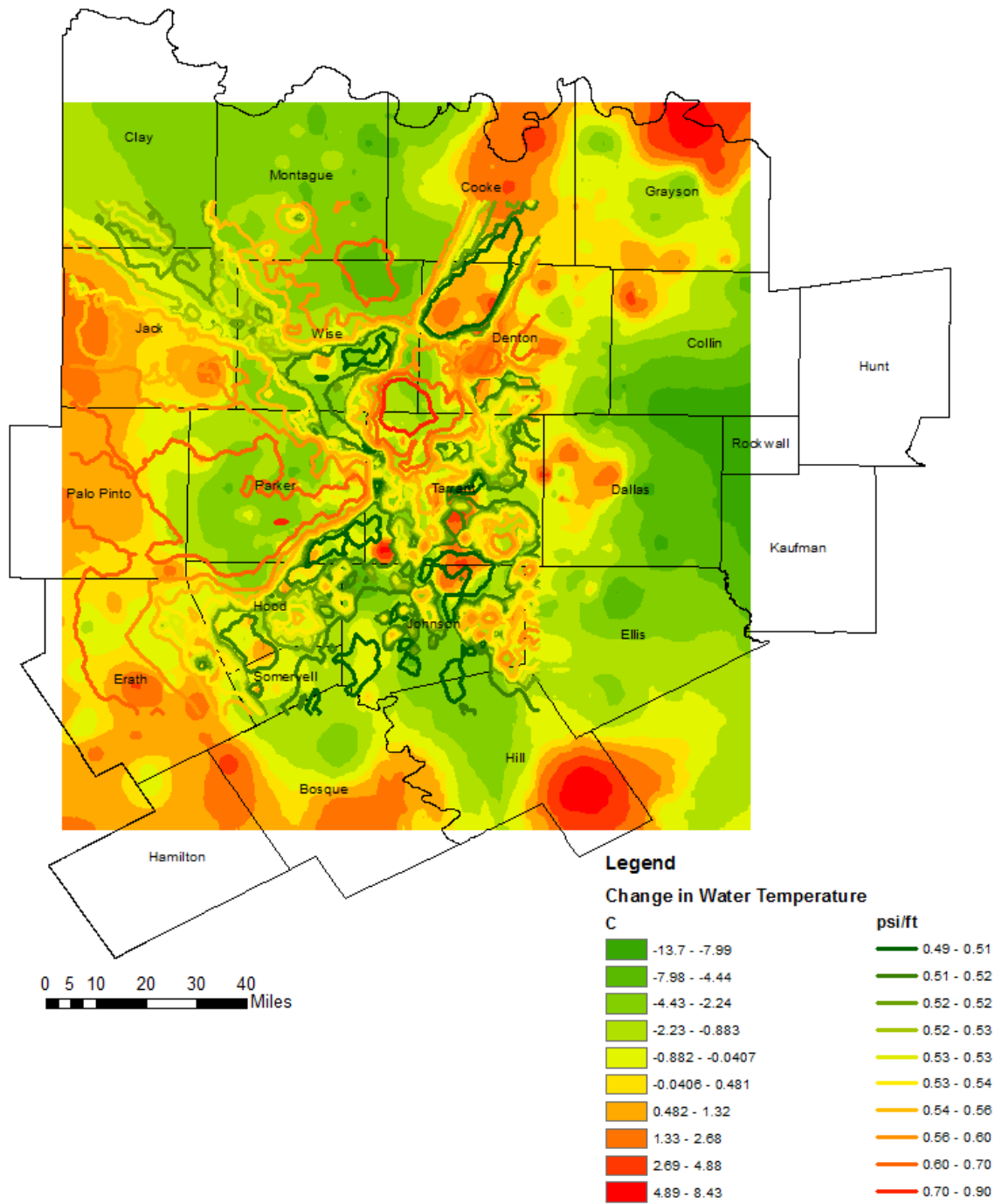


Fig. C- 38: Contour Plot of change in groundwater Temperature concentrations and Barnett Reservoir Pressure Gradient in the study region

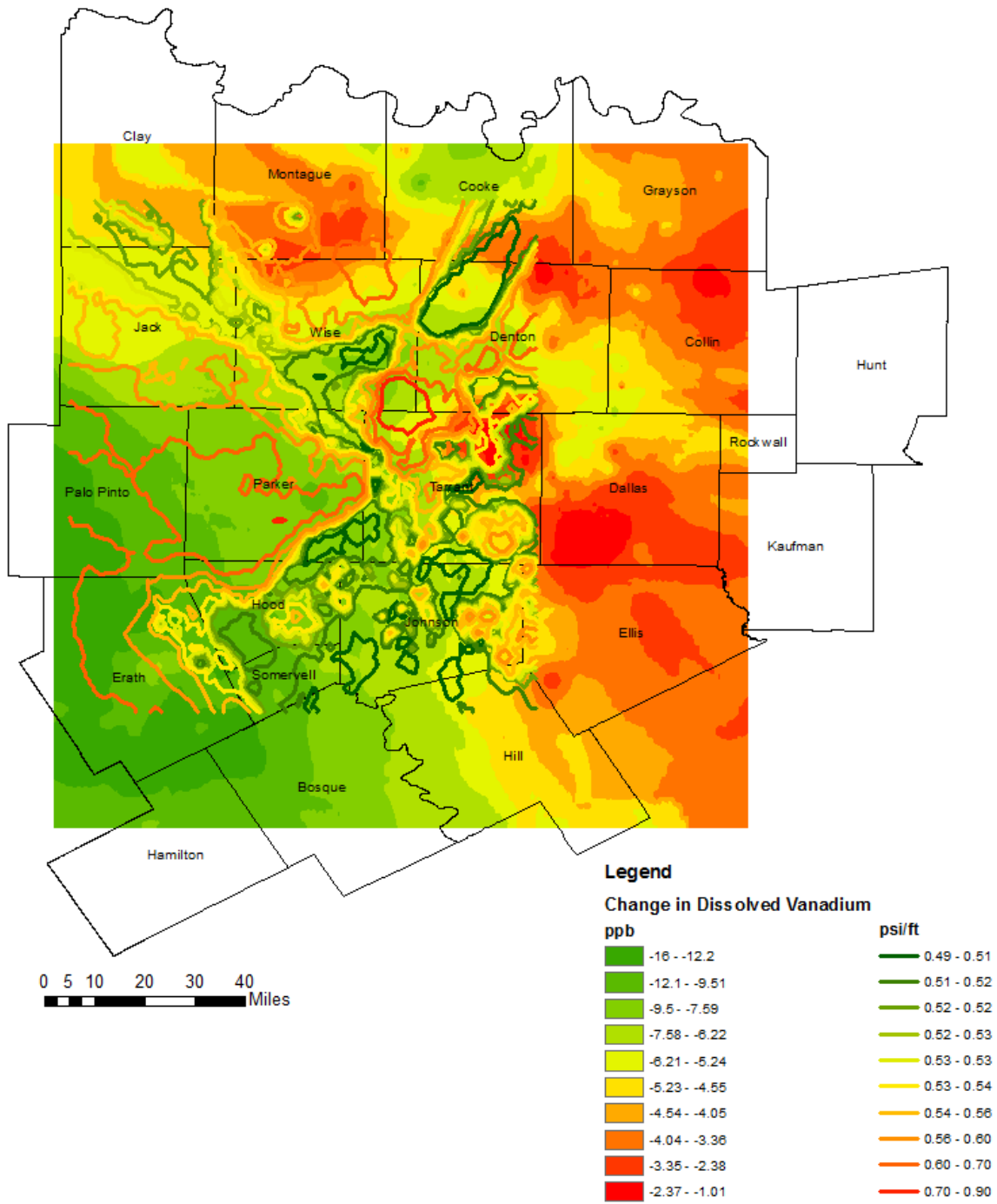


Fig. C- 39: Contour Plot of change in groundwater Dissolved Vanadium concentrations and Barnett Reservoir Pressure Gradient in the study region

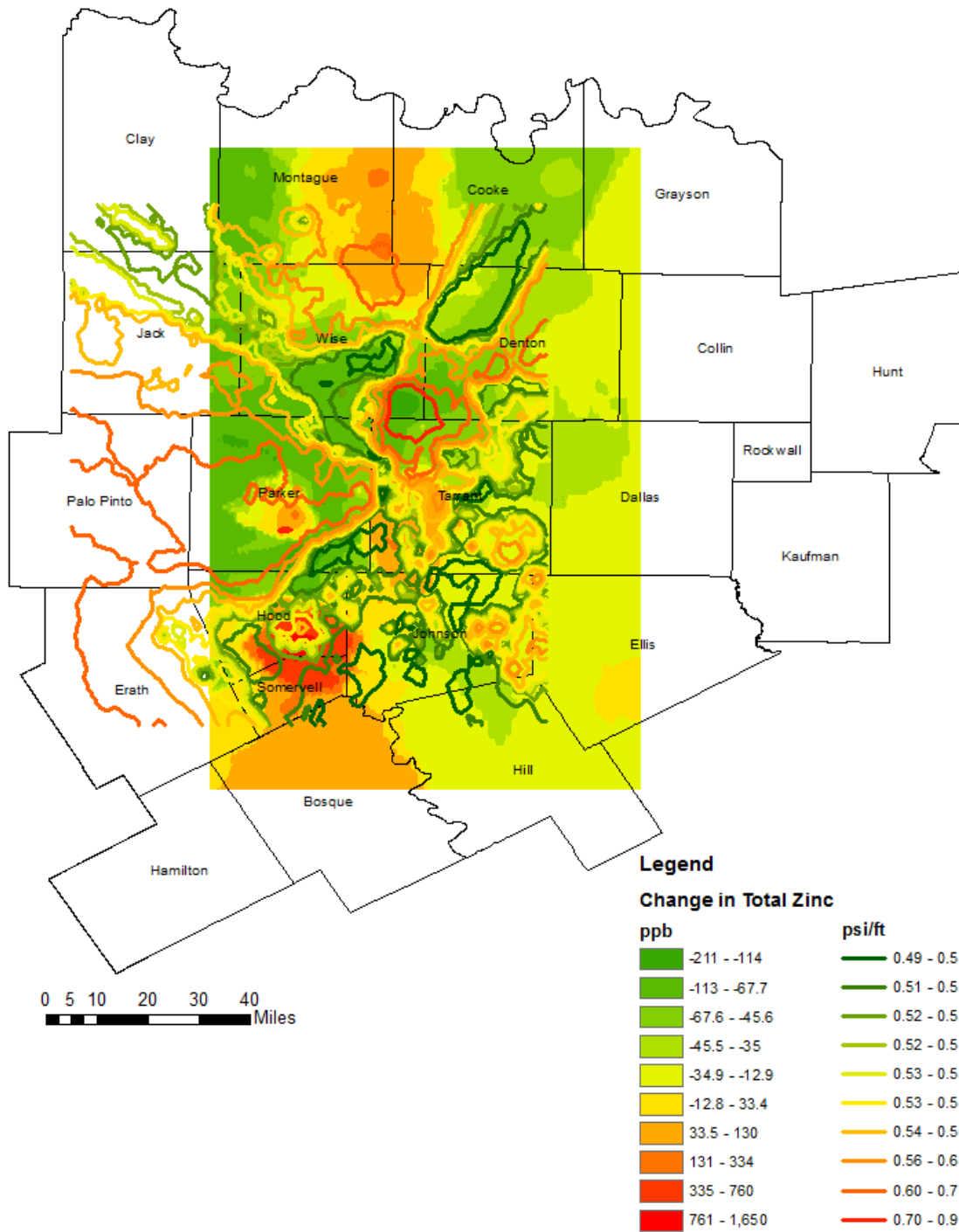


Fig. C- 40: Contour Plot of change in groundwater Total Zinc concentrations and Barnett Reservoir Pressure Gradient in the study region

**APPENDIX D – RELATIVE WATER QUALITY DISTRIBUTIONS
FROM SECTION 5.3**

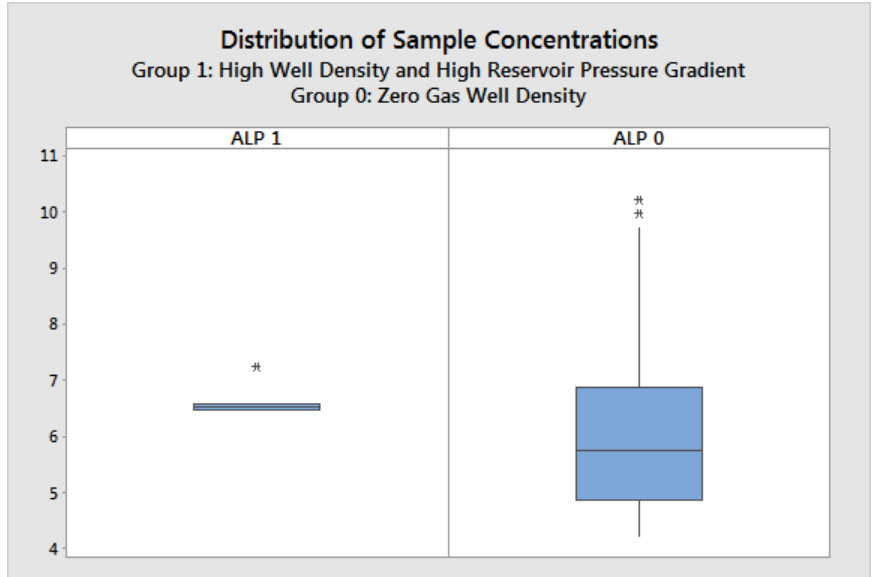


Fig. D- 1: Relative distribution of Dissolved Alpha concentrations detected in Subgroup 6 (left) and Subgroup 1 (right)

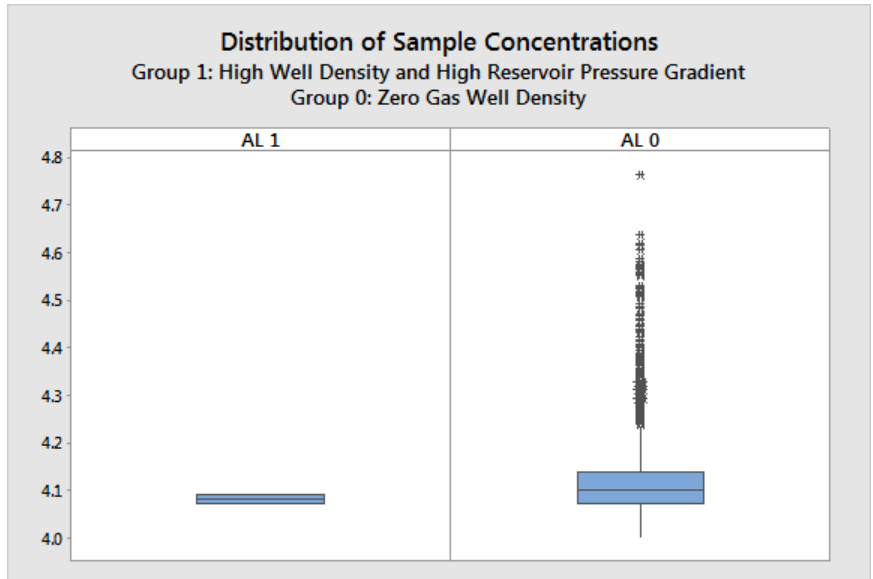


Fig. D- 2: Relative distribution of Dissolved Aluminum concentrations detected in Subgroup 6 (left) and Subgroup 1 (right)

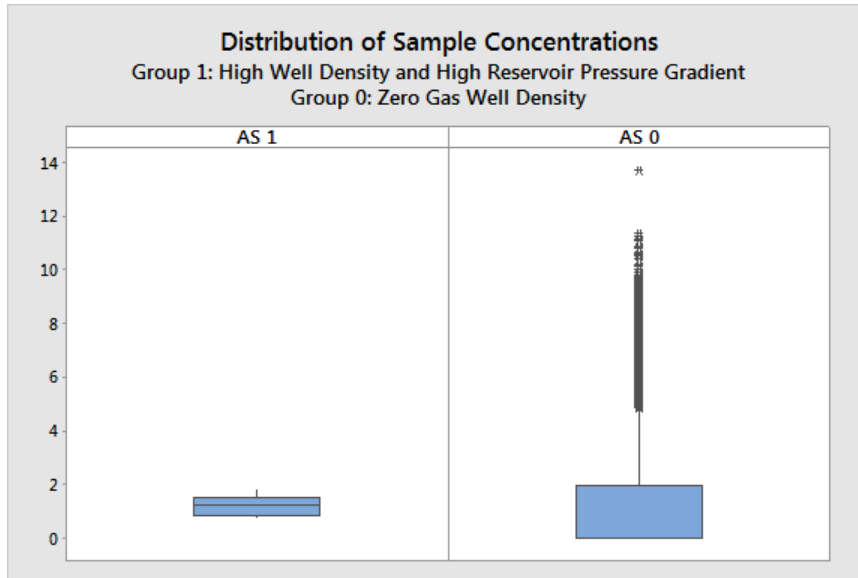


Fig. D- 3: Relative distribution of Total Arsenic concentrations detected in Subgroup 6 (left) and Subgroup 1 (right)

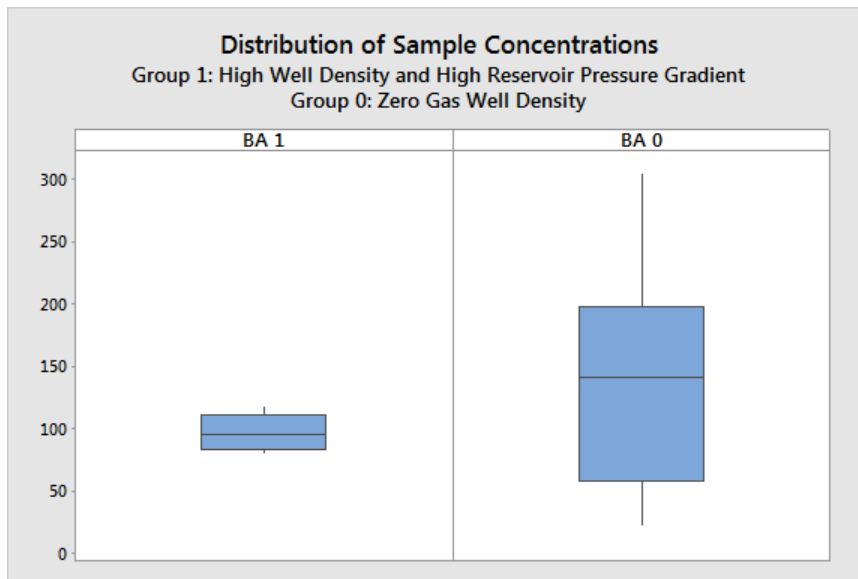


Fig. D- 4: Relative distribution of Total Barium concentrations detected in Subgroup 6 (left) and Subgroup 1 (right)

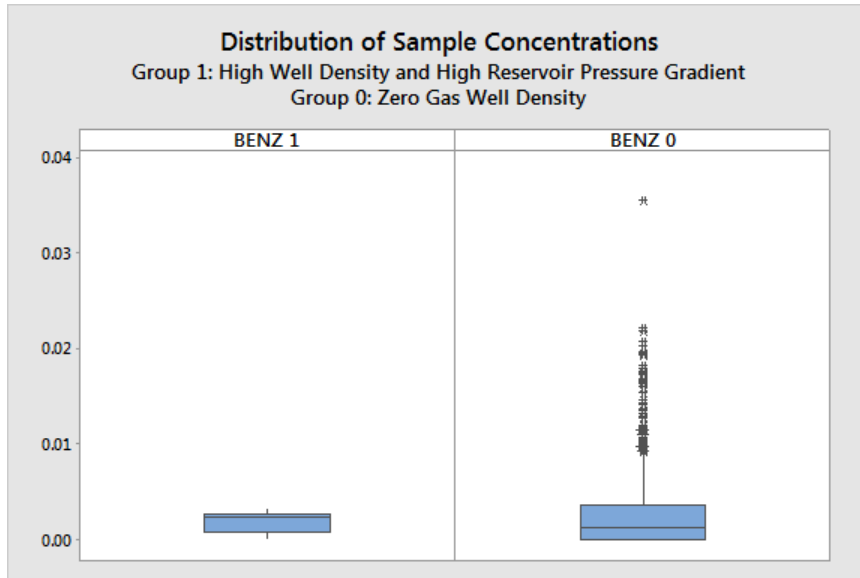


Fig. D- 5: Relative distribution of Total Benzene concentrations detected in Subgroup 6 (left) and Subgroup 1 (right)

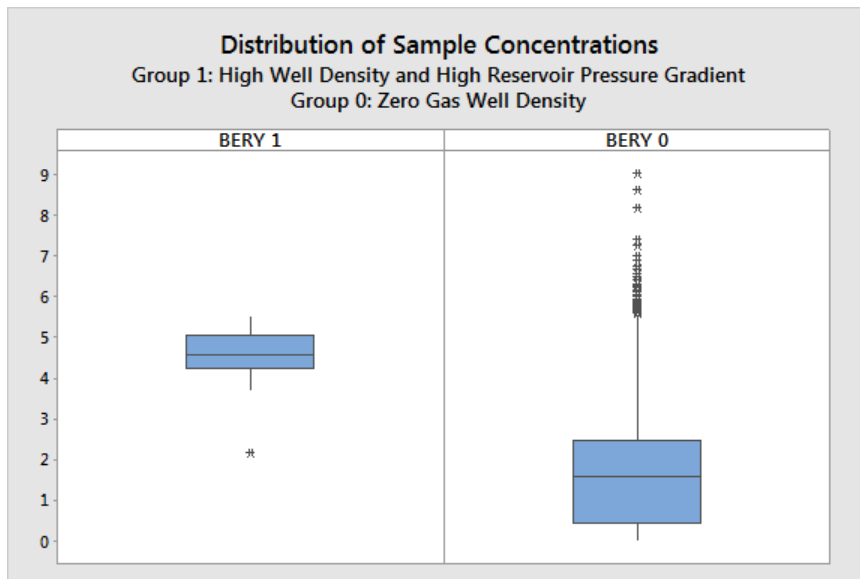


Fig. D- 6: Relative distribution of Total Beryllium concentrations detected in Subgroup 6 (left) and Subgroup 1 (right)

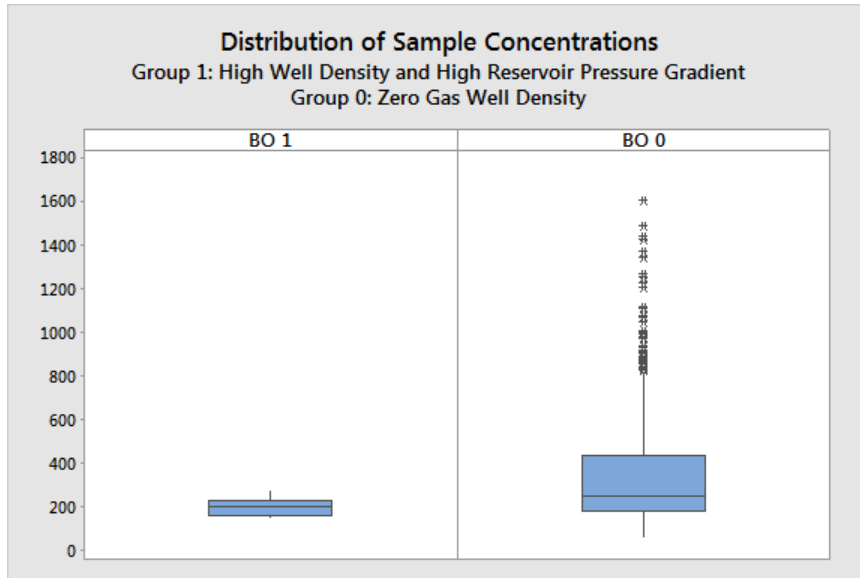


Fig. D- 7: Relative distribution of Dissolved Boron concentrations detected in Subgroup 6 (left) and Subgroup 1 (right)

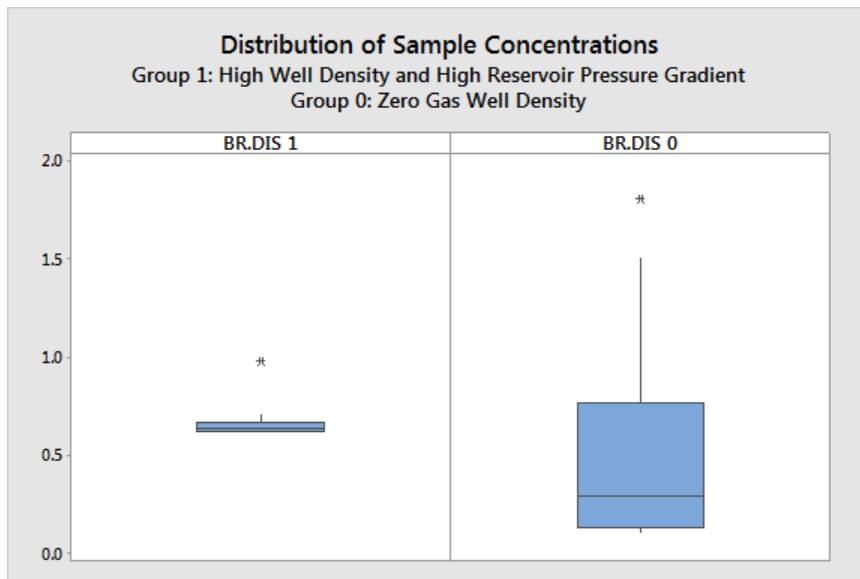


Fig. D- 8: Relative distribution of Dissolved Bromide concentrations detected in Subgroup 6 (left) and Subgroup 1 (right)

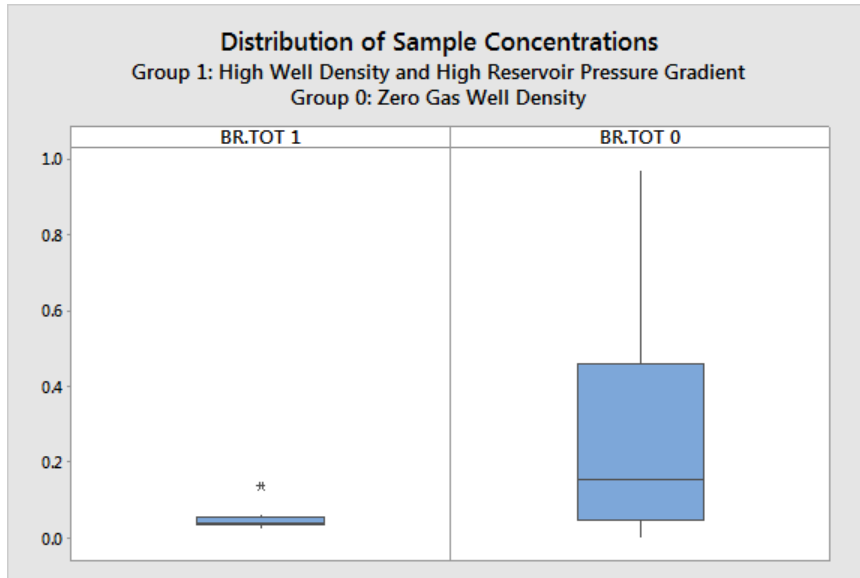


Fig. D- 9: Relative distribution of Total Bromide concentrations detected in Subgroup 6 (left) and Subgroup 1 (right)

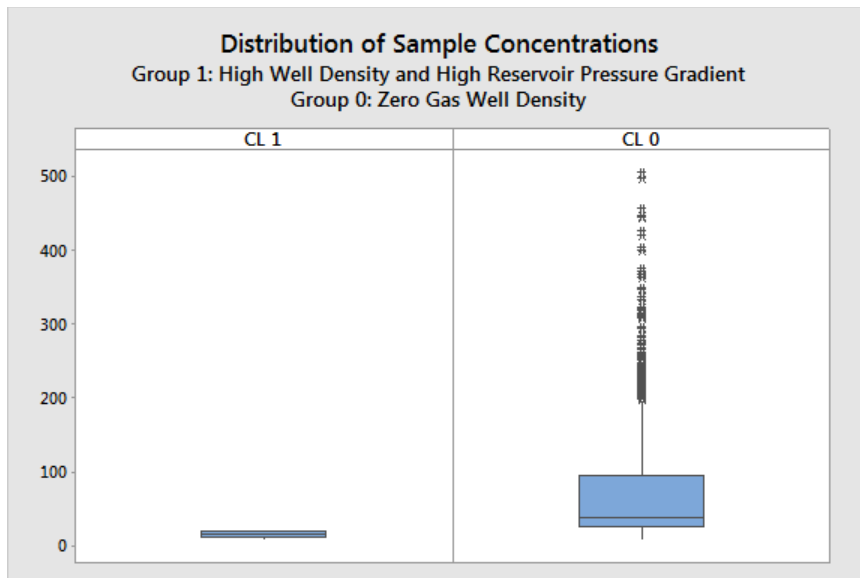


Fig. D- 10: Relative distribution of Total Chloride concentrations detected in Subgroup 6 (left) and Subgroup 1 (right)

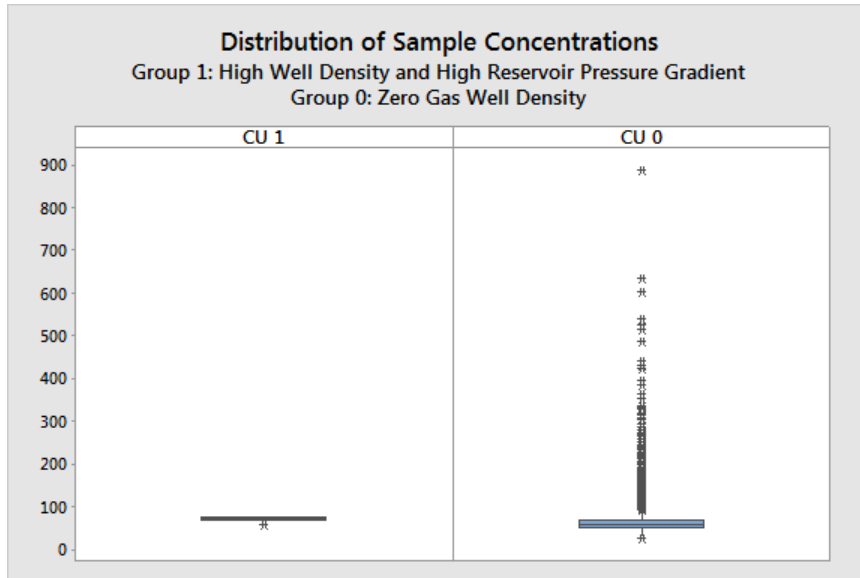


Fig. D- 11: Relative distribution of Total Copper concentrations detected in Subgroup 6 (left) and Subgroup 1 (right)

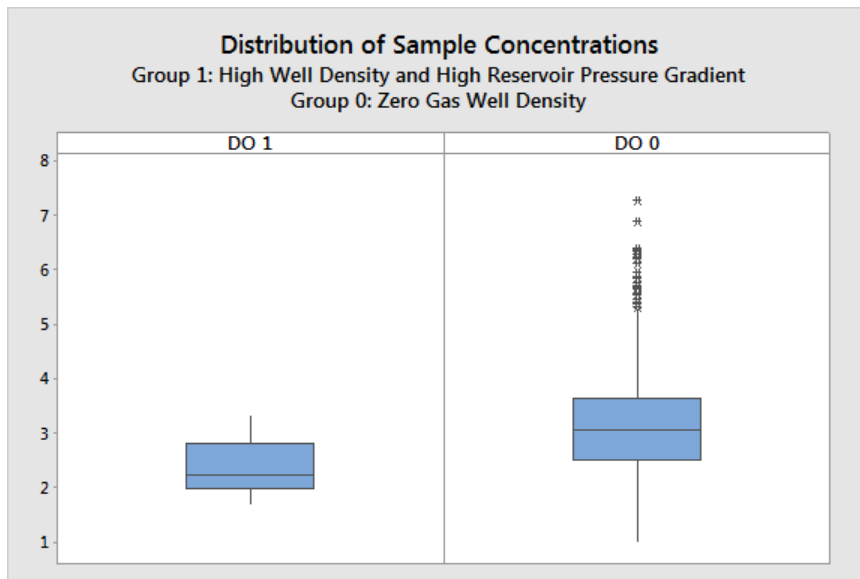


Fig. D- 12: Relative distribution of Dissolved Oxygen concentrations detected in Subgroup 6 (left) and Subgroup 1 (right)

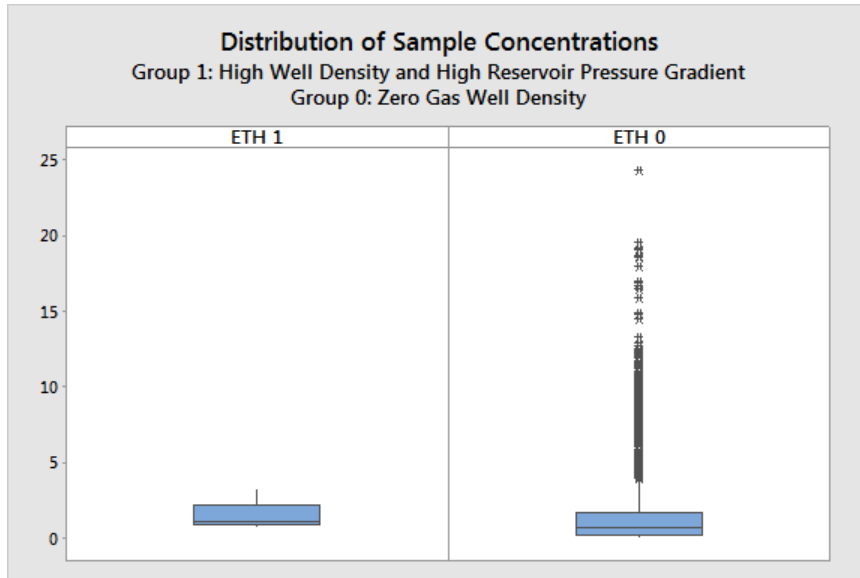


Fig. D- 13: Relative distribution of Total Ethanol concentrations detected in Subgroup 6 (left) and Subgroup 1 (right)

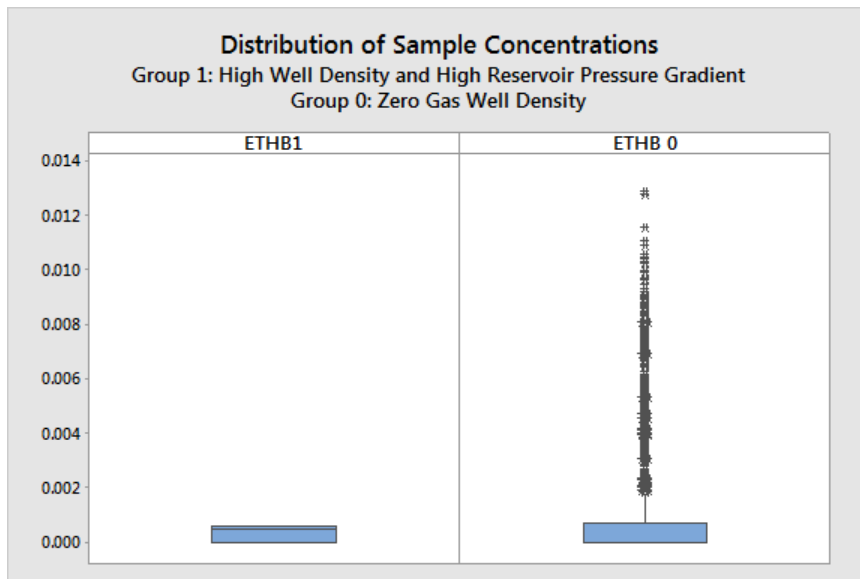


Fig. D- 14: Relative distribution of Total Ethyl Benzene concentrations detected in Subgroup 6 (left) and Subgroup 1 (right)

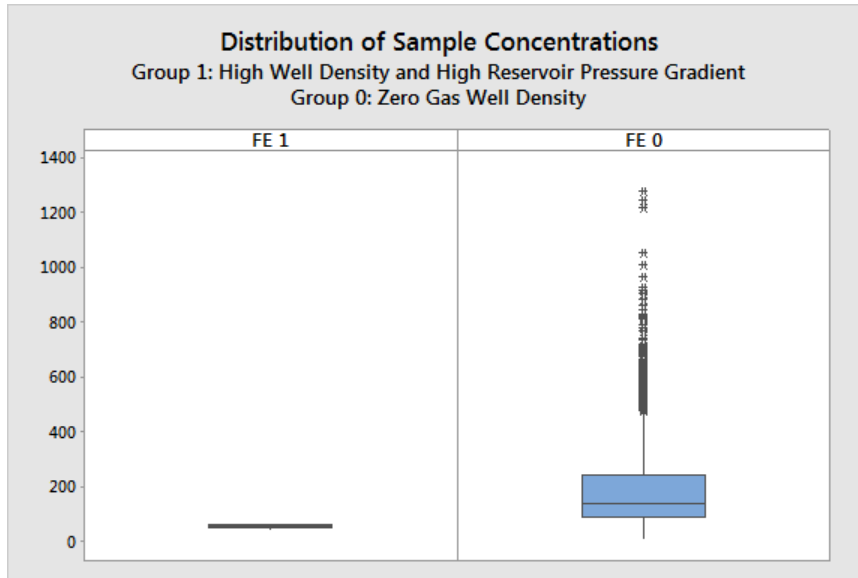


Fig. D- 15: Relative distribution of Total Iron concentrations detected in Subgroup 6 (left) and Subgroup 1 (right)

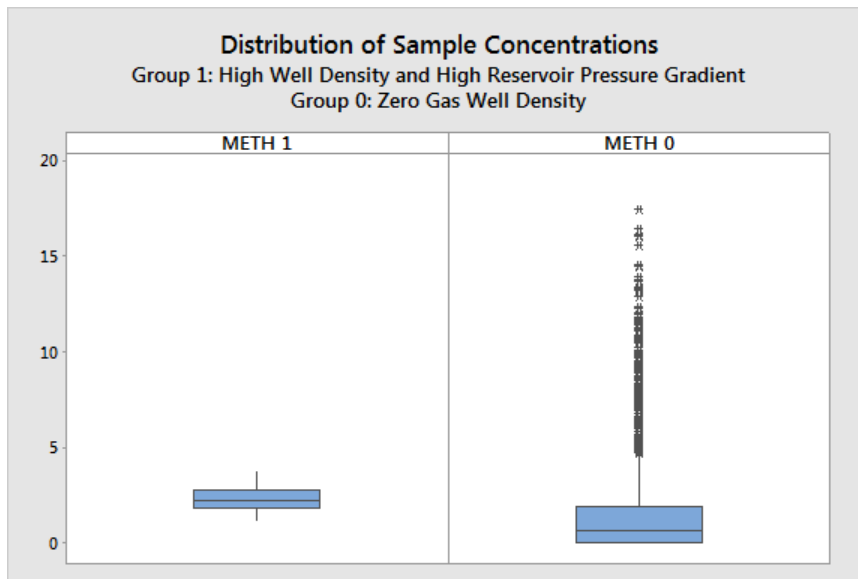


Fig. D- 16: Relative distribution of Total Methanol concentrations detected in Subgroup 6 (left) and Subgroup 1 (right)

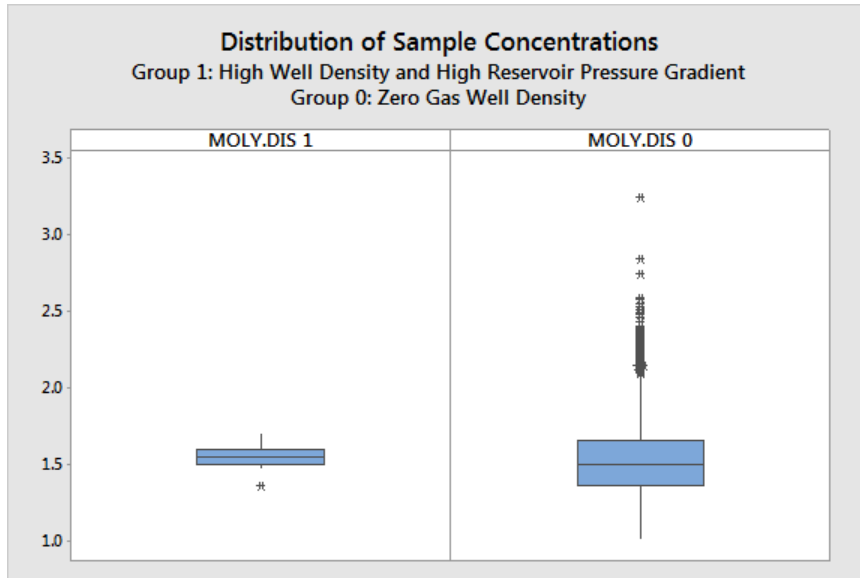


Fig. D- 17: Relative distribution of Dissolved Molybdenum concentrations detected in Subgroup 6 (left) and Subgroup 1 (right)

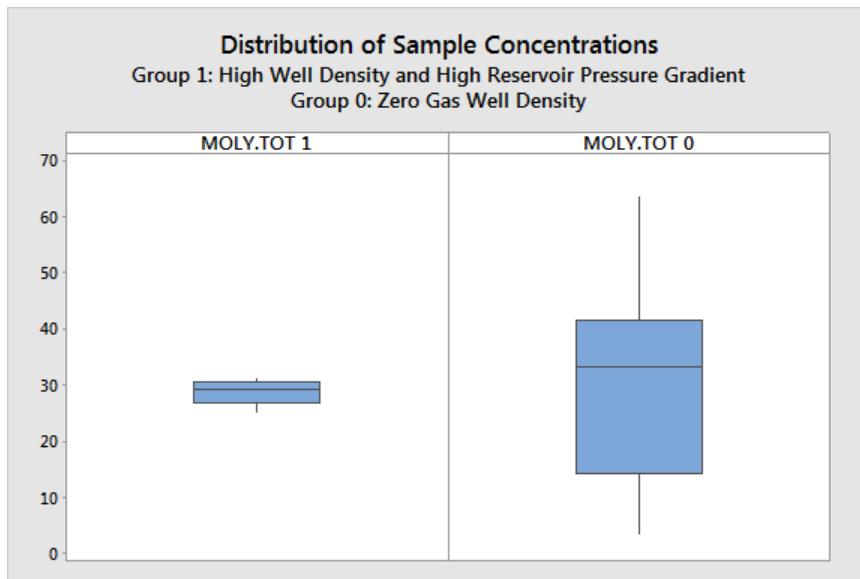


Fig. D- 18: Relative distribution of Total Molybdenum concentrations detected in Subgroup 6 (left) and Subgroup 1 (right)

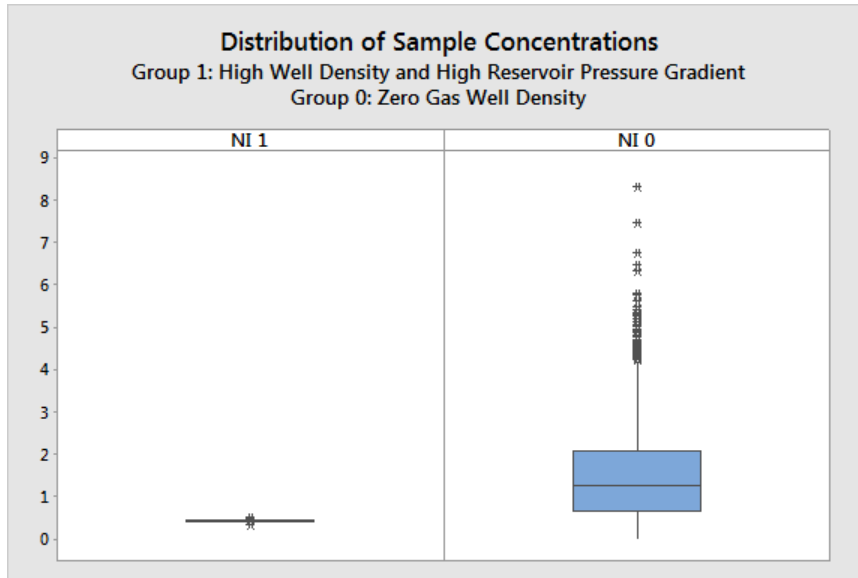


Fig. D- 19: Relative distribution of Total Nickel concentrations detected in Subgroup 6 (left) and Subgroup 1 (right)

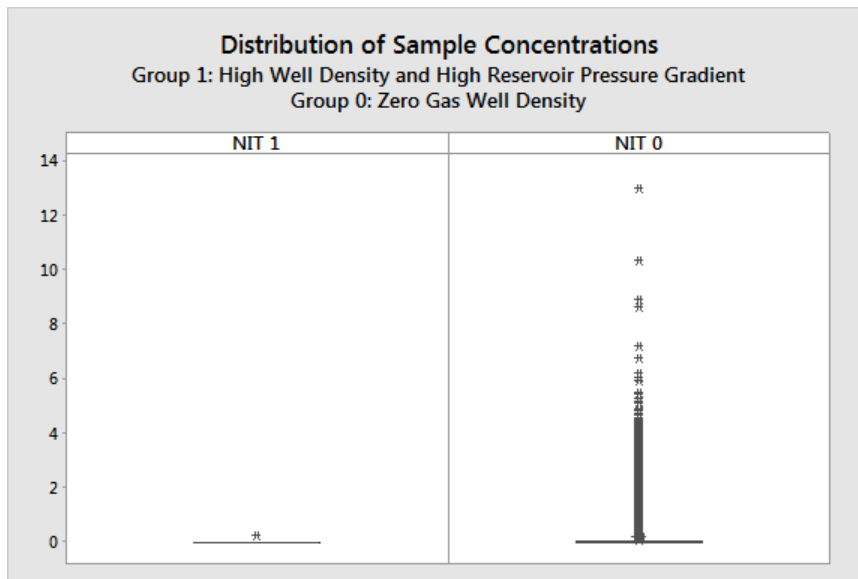


Fig. D- 20: Relative distribution of Total Nitrate concentrations detected in Subgroup 6 (left) and Subgroup 1 (right)

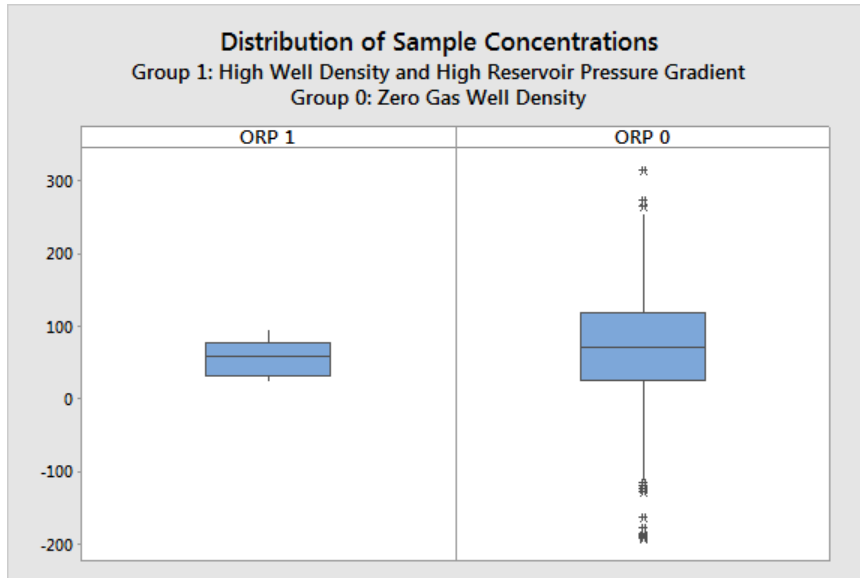


Fig. D- 21: Relative distribution of Oxidation-Reduction Potential detected in Subgroup 6 (left) and Subgroup 1 (right)

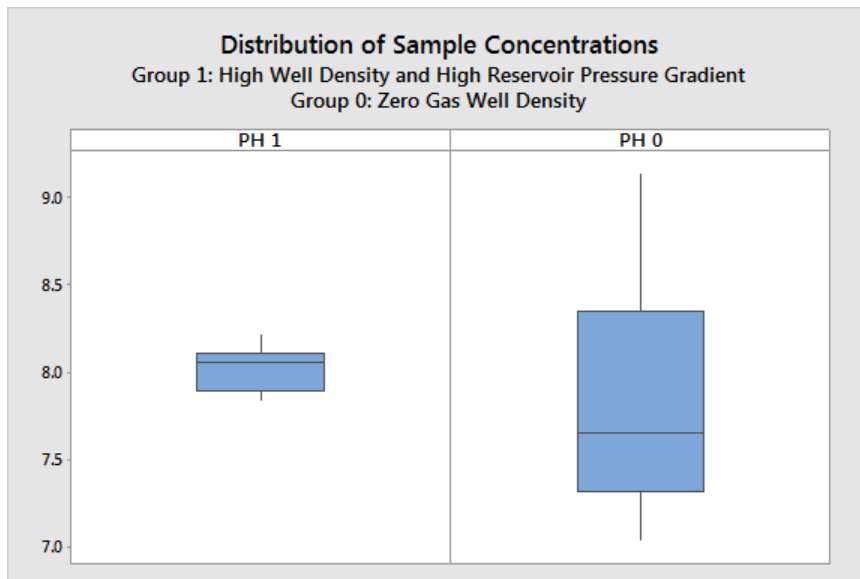


Fig. D- 22: Relative distribution of pH detected in Subgroup 6 (left) and Subgroup 1 (right)

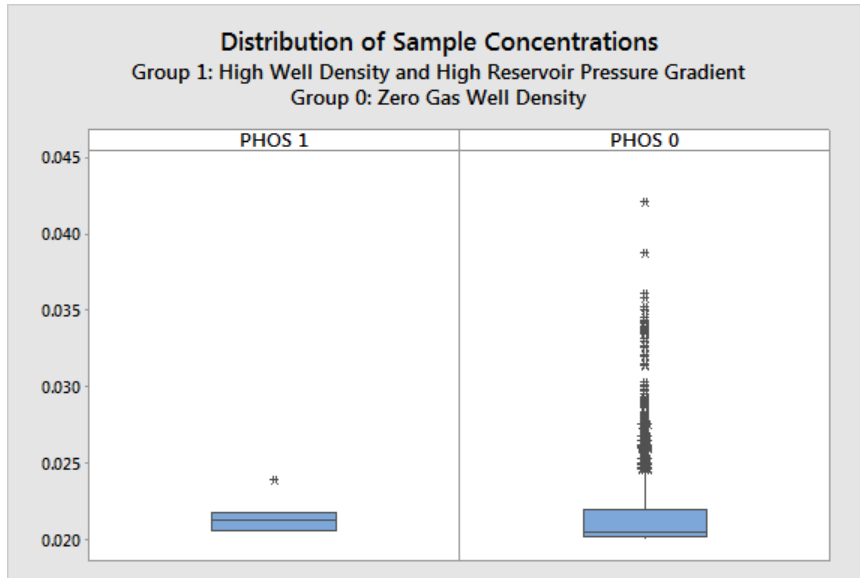


Fig. D- 23: Relative distribution of Dissolved Phosphorus concentrations detected in Subgroup 6 (left) and Subgroup 1 (right)

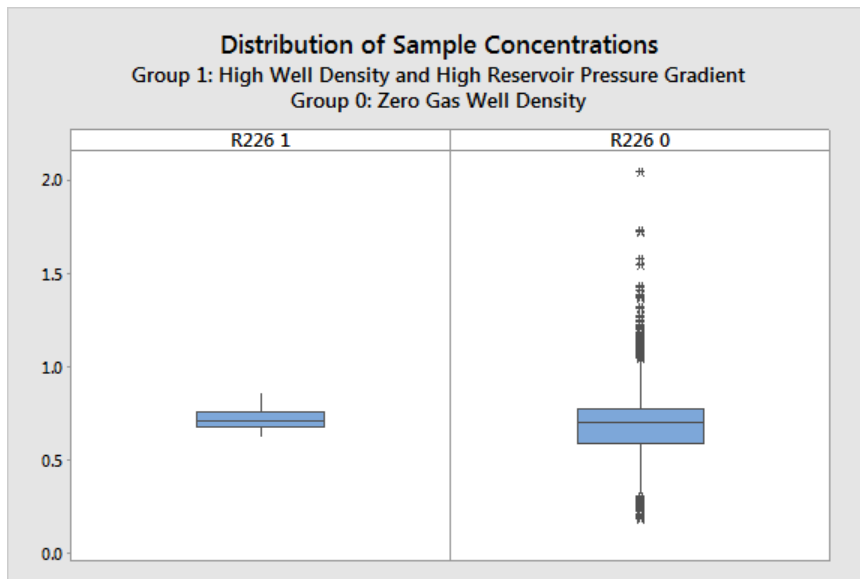


Fig. D- 24: Relative distribution of Dissolved Radium 226 concentrations detected in Subgroup 6 (left) and Subgroup 1 (right)

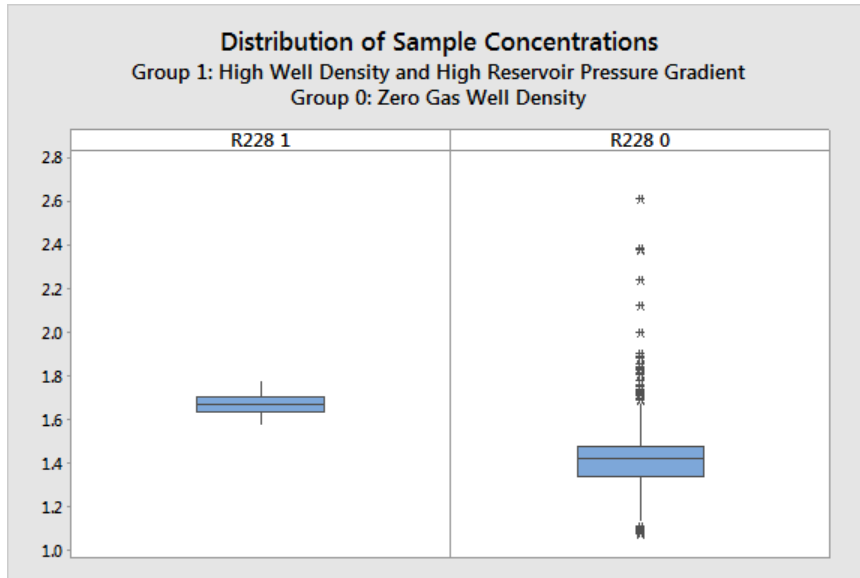


Fig. D- 25: Relative distribution of Dissolved Radium 228 concentrations detected in Subgroup 6 (left) and Subgroup 1 (right)

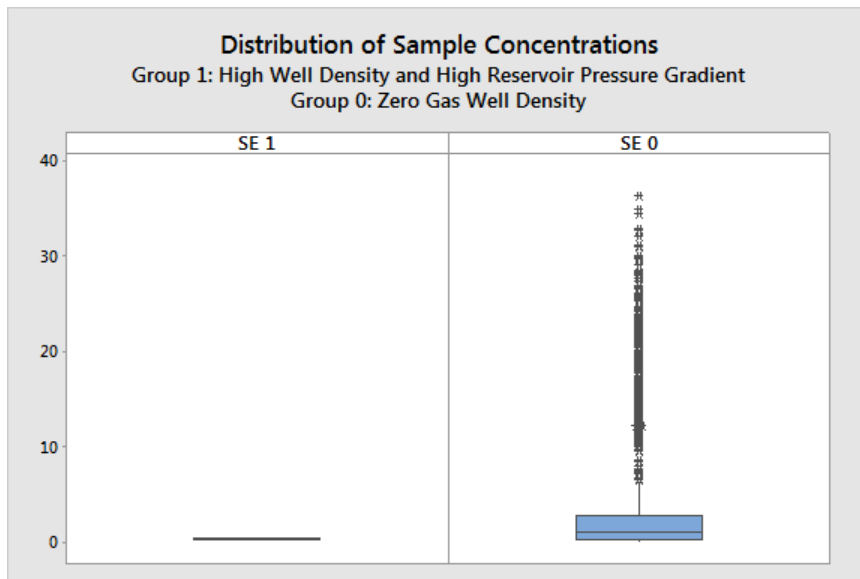


Fig. D- 26: Relative distribution of Total Selenium concentrations detected in Subgroup 6 (left) and Subgroup 1 (right)

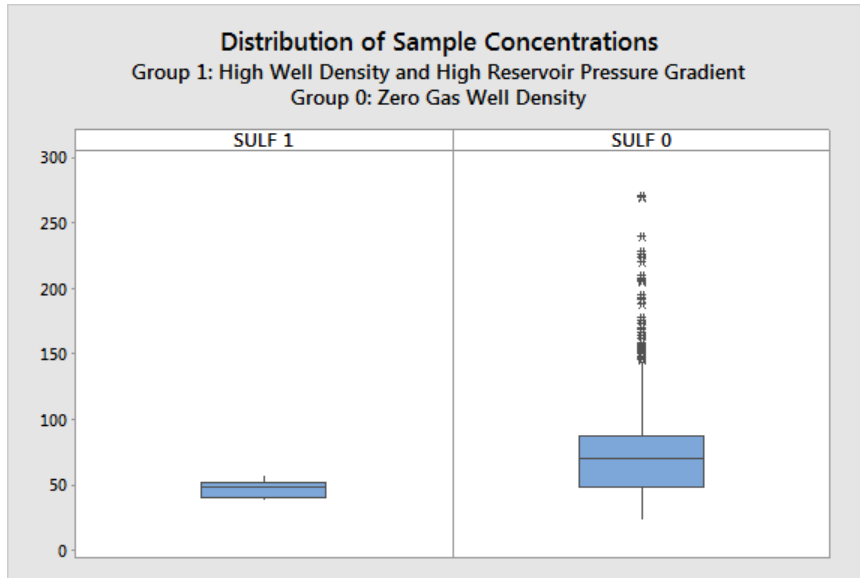


Fig. D- 27: Relative distribution of Total Sulfate concentrations detected in Subgroup 6 (left) and Subgroup 1 (right)

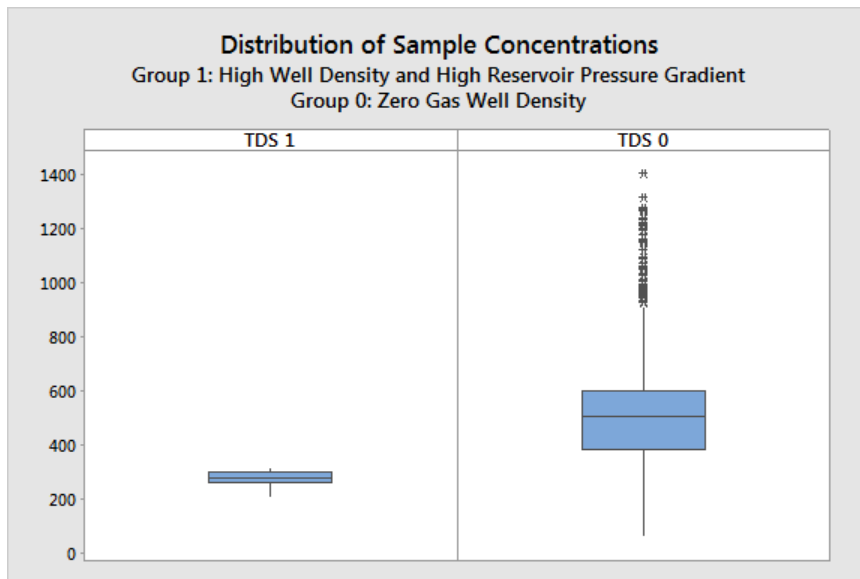


Fig. D- 28: Relative distribution of Total Dissolved Solids concentrations detected in Subgroup 6 (left) and Subgroup 1 (right)

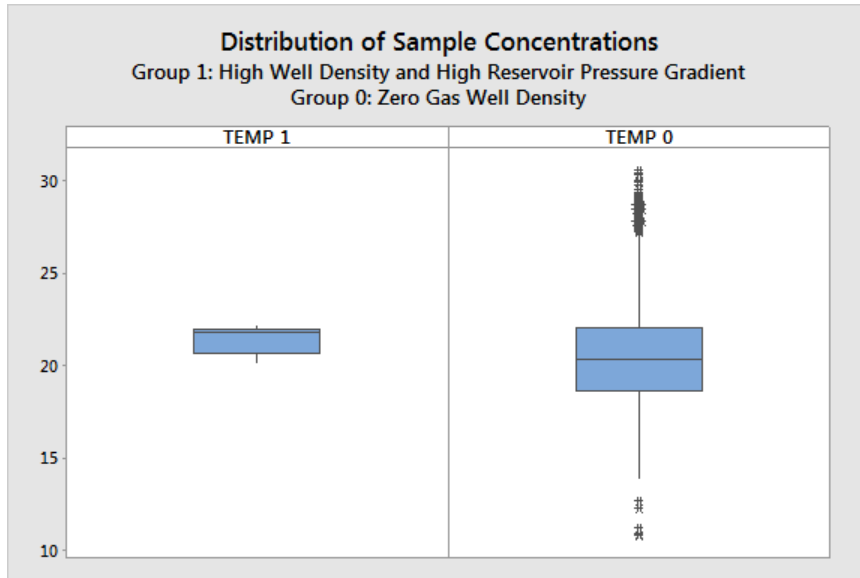


Fig. D- 29: Relative distribution of Water Temperature detected in Subgroup 6 (left) and Subgroup 1 (right)

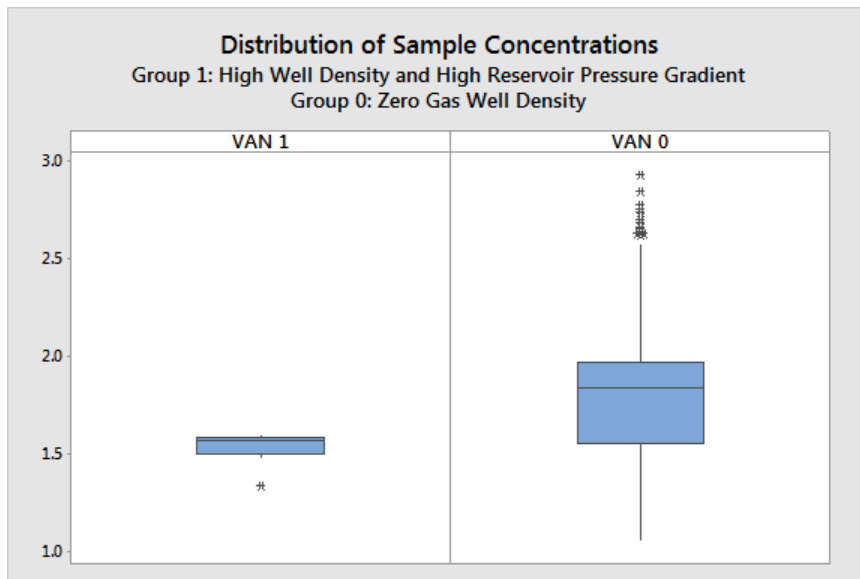


Fig. D- 30: Relative distribution of Dissolved Vanadium concentrations detected in Subgroup 6 (left) and Subgroup 1 (right)

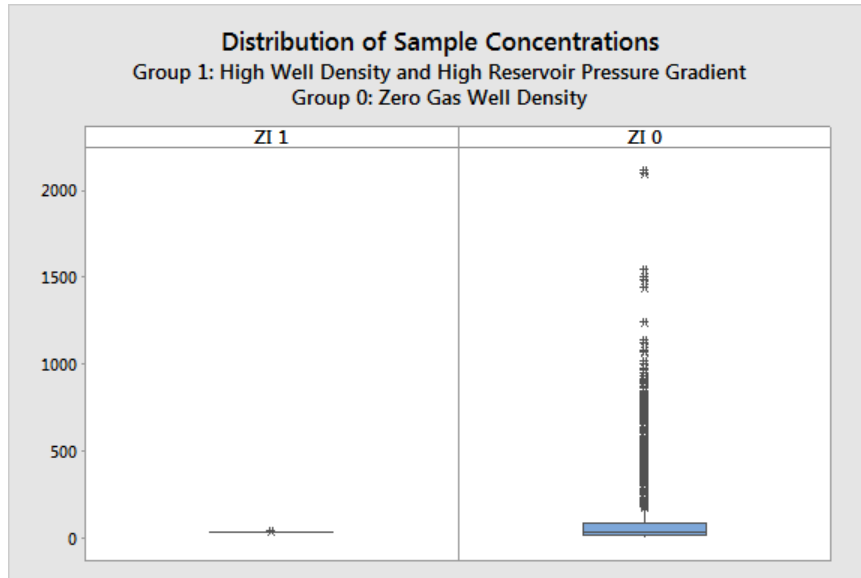


Fig. D- 31: Relative distribution of Total Zinc concentrations detected in Subgroup 6 (left) and Subgroup 1 (right)

